REAL-TIME FLOOD FORECASTING MODEL INTERCOMPARISON AND PARAMETER UPDATING USING RAIN GAUGE AND WEATHER RADAR DATA

by:

SOHRAB HAJJAM, B.Sc, M.Sc (Eng.)

Telford Research Institute
Department of Civil Engineering
Faculty of Engineering
University of Salford, Salford, UK

Submitted in Partial Fulfilment for the Degree of
Doctor of Philosophy, 1997

Dedication

This thesis is gratefully dedicated to my fellow countrymen, the people of Iran, who funded my period of study

TABLE OF CONTENTS

LIST OF FIGURES

LIST OF TABLES

LIST OF ABBREVIATION

ANNs	Artificial Neural Networks
AF	Radar Assessment Factor
API5	Five Day Antecedent Precipitation Index
API30	Thirty Day Antecedent Precipitation Index
APR	Average Pulse Response
ARMA	Auto Regressive Moving Average
ATF	Average Transfer Function
CAPPI	Constant Altitude Plan Position Indicator
CLS	Constrained Linear System
CPTF	Conceptually Parametrised Transfer Function
CWI	Catchment Wetness Index
DPRTF	Dynamic PRTF
DWRP	Dee Weather Radar Project
ERM	Empirical Regressive Model
FDAP	Five Day Antecedent Precipitation
FRONTIERS	Forecasting Rainfall Optimised using New Techniques of Interactively Enhanced rainfall
GA	Genetic Algorithm
GAPI	Rainfall-runoff model with Gamma distributed API
GPRTF	Group PRTF model
GTF	Group TF model
HFS	Hydrologic Forecast System
HGA	Hybrid Genetic Algorithm
IEM	Isolated Event Model
I-O	Input-Output
ISO	Inflow-Storage-Outflow
KF	Kalman Filter
NAPR	normalised average pulse response
NPR	Normalised Pulse Response
OTF	Ordinary TF model = static TF model
PPI	Radar Plan-Position Indicator
PR	Pulse Response
PR	Percentage Runoff
PRTF	Physically Realisable TF
RHI	Radar Range-Height Indicator

RLS	Recursive Least Squares
RMSE	Root Mean Squares Error
ROLS	Recursive Ordinary Least Squares
SCS	Soil Conservation Service
SMAR	Soil Moisture and Routing Model
SMD	Soil Moisture Deficit
SPR	Standard Percentage Runoff
SPRTF	Static PRTF model
SPWFPP	Short Period Weather Forecasting Pilot Project
SRM	Snowmelt Runoff Model
SSARR	Streamflow System And Reservoir Regulation model
TF	Transfer Function
UBC	University of British Columbia catchment model
UH	Unit Hydrograph
WMO	World Meteorological Organisation
WRIP	Weather Radar Information Processor

Acknowledgements

I would like to thank Professor Ian D. Cluckie and Dr. K. A. Tilford who supervised this project and offered endless encouragement and useful guidance throughout the course of PhD.

I like to thank the Iranian Ministry of Culture and Higher Education for the scholarship (1992-95) and the Overseas Research Student Award Scheme in partially financing of 1994-95's tuition fee.

Thanks must also be given to Dr. Han Dawei who have patiently answered my questions and provided valuable information.

I also express my thanks to Dr. J. Yuan, Dr. B. Austin, Dr. N. Narimanzadeh, Mr. L. Zhang and Dr. R. Griffith for their help during this project. Further thanks go to Dr. K. A. Tilford, who had the tedious task of proof-reading and correcting my drafts.

Finally I express my gratitude to my family, my wife Mahbob and to my sons, Arash and Ashkan for their continued encouragement, patience and understanding.

ABSTRACT

This thesis describes the development of real-time flood forecasting models at selected catchments in the three countries, using rain gauge and radar derived rainfall estimates and time-series analysis.

An extended inter-comparison of real-time flood forecasting models has been carried out and an attempt has been made to rank the flood forecasting models. It was found that an increase in model complexity does not necessarily lead to an increase in forecast accuracy.

An extensive analysis of group calibrated transfer function (TF) models on the basis of antecedent conditions of the catchment and storm characteristics has revealed that the use of group model resulted in a significant improvement in the quality of the forecast. A simple model to calculate the average pulse response has also been developed.

The development of a hybrid genetic algorithm (HGA), applied to a physically realisable transfer function model is described. The techniques of interview selection and fitness scaling as well as random bit mutation and multiple crossover have been included, and both binary and real number encoding technique have been assessed. The HGA has been successfully applied for the identification and simulation of the dynamic TF model. Four software packages have been developed and extensive development and testing has proved the viability of the approach.

Extensive research has been conducted to find the most important adjustment factor of the dynamic TF model. The impact of volume, shape and time adjustment factors on forecast quality has been evaluated. It has been concluded that the volume adjustment factor is the most important factor of the three. Furthermore, several attempts have been made to relate the adjustment factors to different elements. The interaction of adjustment factors has also been investigated.

An autoregressive model has been used to develop a new updating technique for the dynamic TF model by the updating of the B parameters through the prediction of future volume adjustment factors over the forecast lead-time. An autoregressive error prediction model has also been combined with a static TF model. Testing has shown that the performance of both new TF models is superior to conventional procedures.

CHAPTER 1

SYNOPSIS AND INTRODUCTION

1.1 Introduction

The United Nations designated the 1990s as the International Decade for National Disaster Reduction. Flooding is one of the major causes of such disasters (WMO, 1992). Floods represent natural hazards to human beings and livestock and can cause large scale damage to property, agriculture, flora and fauna, the environment, communication networks, etc. Furthermore, floods can cause loss of earnings, services and business disruption. In the United States, floods are responsible for injuries to approximately 75000 people and livestock and result in over $2 billion in property damage every year (Yapo and Sorooshian, 1993). In the 'Great Flood' of 1993 of the United States 50000 homes were damaged, 54000 persons were evacuated and economic losses of $15-20 billion have been estimated (Krzysztofowicz, 1995). It is believed that, in the hundred years between 1870 and 1970, flooding has caused an average of $1500 million worth of damage and more than 5000 deaths in the world per year (Nemec, 1986). Perhaps the flash flood of August 15th 1952, at Lynmouth and Lynton, Devon, was the most well known and catastrophic floods in UK. In total 34 people were killed or went missing, and 93 houses, 28 bridges and 132 vehicles destroyed (Delderfield, 1953). Hagget *et al.*, (1993) have estimated that potential flood damage exceeds £20 million in Greater London and 90000 properties are at risk from flooding in the Thames catchment alone.

At the time of writing more than 80 lives have been lost at a campsite in Northern Spain due to a flash-flood in the Pyrenees.

An hydrological forecast can be defined as the prior estimate of the future state of hydrological phenomena in real-time. Real-time itself is execution of the forecasting procedures using the currently available data. Hence real-time forecasting is different from prediction which is for design purposes (WMO, 1992). A real-time data collection network and telemetering system are prerequisite to any real-time forecasting exercise.

A World Meteorological Organisation (WMO) survey of European hydrological forecasting systems indicated that by far the most common purpose is the forecasting of floods. Over 70% of the systems had forecasting periods of up to a week, with half of them being for 24 hours or less. Therefore the most frequently required forecast was a short-term flood forecast (WMO, 1992). Although flood forecasting has received the continued attention of researchers over the years it still remains one of the unsolved problems of operational hydrology. In addition to flooding, hydrological forecasts can be used to support low flow and water quality studies.

In essence flood forecasting is difficult because it is involved with a complex rainfall-runoff phenomena which is stochastic, non-linear and non-stationary. This thesis presents some aspects of real-time flood forecasting.

1.2 Thesis structure

Chapter 2 consists of three sections. The first section provides a brief literature review and discussion about the classification of flood forecasting models. The second section reviews techniques for the calculation of net rainfall and their complexities. The final section of the chapter provides a review of existing flood forecasting models and describes the models submitted to the WMO 'Simulated Real-time Inter-comparison of Hydrological Models' project. It also presents a detailed discussion of transfer function (TF) rainfall-runoff models which are used in this thesis.

Chapter 3 presents the results of an extended inter-comparison of real-time flood forecasting models, with particular emphasis on the TF models. The data sets and catchments are the same as those of used in the WMO project. A comparative analysis is presented whereby the forecasting results of average TF models both in static and dynamic form are assessed by direct comparison with results from the WMO project models. A relatively new technique for objective comparison, the randomness-dispersion diagram is included and an attempt is made to rank the flood forecasts, both on an event basis and overall.

Chapter 4 presents the research undertaken to extend the capabilities of TF models. The chapter includes a simple technique to calculate average pulse responses. The main body of the chapter is allocated to develop an event classification and grouped calibration procedure. Group models are constructed on the basis of storm characteristics and catchment conditions. The final part of the chapter presents an expert system-based approach for further investigations of the grouped model.

System identification has a major impact on model forecast accuracy, and a range of parameter estimation techniques including neural networks and recursive ordinary least squares algorithm are reviewed in chapter 5. They are also assessed within the specific context of rainfall-runoff modelling.

The research described in chapter 6 is based on the application of a genetic algorithm (GA) approach as a methodology both for the identification and adjustment (updating) of physically realisable TF model parameters. A new combined parameter estimation technique (Hybrid Genetic Algorithm, HGA) has been developed. The effectiveness of HGA is demonstrated, some new aspects of GA are included and the robustness of the HGA is investigated using several case studies.

Neither the models nor the data used in flood forecasting are perfect. Consequently, estimated flows, will rarely, if ever, be exactly equal to observed flows. Therefore, it is necessary to update the model in the light of recent model performance. Updating techniques are investigated in chapter 7. Some newly developed methods to improve updating procedures in TF models (both in static and dynamic form) are proposed and their performance are assessed using several case studies.

The ability of weather radar to measure rainfall intensity with high spatial and temporal resolution has made available an alternative data source for flow forecasting. In chapter 8 radar techniques to measure rainfall intensity are presented. Particular attention is focused on the use of radar derived precipitation data in updating techniques developed in chapter 7.

Conclusions and the main points of the investigation are presented in chapter 9. Areas deserving further research are also outlined. Important information is included in the Annexes at the end of thesis.

CHAPTER 2

HYDROLOGICAL MODELS CLASSIFICATION AND WMO INTER-COMPARISON PROJECT

2.1 Introduction

In order to evaluate the flood forecasting procedures a prior general knowledge of them is necessary. This chapter begins with a brief literature review and discussion about the classification of flood forecasting models. Generally, due to complexities involved in the separation of rainfall to determine effective rainfall, total rainfall is used in most of the models. The second part of the chapter provides a relatively comprehensive review of calculation of net rainfall and their complexities. The final section of the chapter describes the details of the models submitted to the WMO project in title of 'Simulated Real-time Inter-comparison of Hydrological Models' together with a comprehensive discussion of transfer function rainfall-runoff models.

2.2 Flood forecasting models

2.2.1 Introduction

Various kinds of flood forecasting models have been developed. There are so many models that one cannot clearly identify which model is most suitable for a specific hydrological problem. Classification of hydrological flow forecasting models is a complex procedure and different researchers classify flood forecasting models in different ways. The WMO (1975) in a comparison study referred to by Correia and Seytoux (1985) observed that none of the models seemed to perform clearly better than the others although they were significantly different in structure and conceptualisation. It looks very different models may lead to similar result. Some comprehensive reviews of flood forecasting models are due to Reed (1984), Bishop *et al.* (1989), Todini (1988), Anderson and Burt (1985) amongst others.

One criteria which may be used to classify flow forecasting models is on the basis of :

i. Whether they use flood routing procedures.
ii. Whether they attempt to apply a relationship between rainfall and runoff.

Flood routing involves the inference of river level at a downstream station on the basis of stage at a point upstream. Rainfall-runoff techniques relate river flow (model output) to the causal process of rainfall (model input) (Reed, 1984).

A second way of classifying models is according to :

i. Whether they try to model the actual physical processes.
ii. Whether they use the cause and effect relationship between input and output (I-O models).

Physically based models are formed around a simple arrangement of a number of components, each of which represents a simplified version of one process in the system being modelled. The I-O models apply statistical relationship between input (rainfall) and output (discharge) (Anderson and Burt, 1985). In the other words, every model can be divided into two sections (Todini, 1988). The first section consists of prior knowledge that can be referred to as the physical component and the second part is a stochastic component which is included in statistical form and cannot be explained by the degree of *a priori* knowledge.

In addition, the various models may be classified on the basis of whether they are considered to be spatially lumped, semi distributed, or fully distributed. In the lumped system all inputs and characteristics of the basin are considered to be spatially homogeneous and only varying in time. In the distributed system the spatial distribution of the input data is considered and incorporated into the forecasting models. Semi-distributed models partially account for spatial inheteorogenities in input data by subdividing a catchment into smaller units and modelling each with a separate model. Furthermore, models can be implemented on the basis of continuous or isolated-event data (WMO, 1992).

Todini (1988) concluded that one possibility for developing flood forecasting in future is to use simplified models combined with stochastic models of their residuals in order to allow for updating. The details of updating procedures are presented in chapter seven.

2.2.2 Flood routing models

Principles of flood routing have been introduced by Reed (1984), Dooge (1986), Murthy *et al.* (1989), and Moore (1993) amongst others.

Flood routing methods can be classified into four categories namely experience models, correlation models, multiple correlation and river routing models. In the experience methods river flows at one location are estimated by reference to an upstream gauging station using the personal judgement of an experienced duty officer. In correlation methods flow at the downstream station is related to an upstream station. Although both flow and river level can be related, flow correlation method is preferred, because river level is affected by local characteristics of the channel and may vary between the upstream and downstream, whilst the flow grows and decays almost the same pattern as each tributary. Multiple correlation methods follow same pattern as simple correlation methods except that the downstream river level (or flow) is now correlated to two (or more) upstream gauging stations sited on different tributaries. River routing models generally are divided into hydraulic and hydrological methods. Hydraulic methods usually attempt a full numerical solution of the St. Venant equations for progressively varying flow in open channels. Two broad classes of hydraulic methods are kinematic wave and linear diffusion equation methods. Hydrological routing models usually are based on Muskingum family of methods (McCarthy, 1938) and (Reed, 1984).

2.2.3 Rainfall-runoff models

Although some researchers believe that real-time flood forecasts, obtained by channel routing especially in large catchment where the catchment response time is long enough, are more accurate than those obtained by rainfall-runoff models, rainfall-runoff methods are preferred in some cases (Reed, 1984). These cases may be summarised as 1) when a greater forecast lead time is necessary and 2) when an upstream gauging station does not exist (head water basins) (Bertoni *et al.*, 1992).

As previously mentioned, the principle of rainfall-runoff models is to increase the lead time of the forecasts by using rainfall data. Rainfall-runoff flood forecasting models could be investigated through four different categories: unit hydrograph methods, non-linear storage models, transfer function models and conceptual models.

2.2.3.1 Unit hydrograph

The unit hydrograph theory developed by Sherman (1932) remains one of the most practical and widely used tools for making flood estimates as well as forecasts (Chow *et al.*, 1988). The unit hydrograph is a lumped, linear, time-invariant model. The discrete convolution of the unit hydrograph takes the form :

$$y_t = \sum_{i=0}^{N} h_i u_{t-i} \tag{2.1}$$

Where :
y_t = f low forecast for time t (direct runoff).
h_i = hydrograph ordinate at time i.
u_t = effective rainfall at time t.

This represents an infinite series which is arbitrarily truncated to a memory of N. Introducing the backward shift operator, Z, where:

$$z^{-n} u_t = u_{t-n} \tag{2.2}$$

then :

$$H(z) = \sum_{i=0}^{N} h_i z^{-i} \tag{2.3}$$

which leads to the expression:

$$y_t = H(z) u_t \tag{2.4}$$

the equation (2.1) can be written in matrix form as $y = uh$ (equation 2.5)

Plate *et al.*, (1988) quoted unit hydrograph will yield results as good as any physically based model, although this conclusion is debatable. The derivation of the unit hydrograph requires effective rainfall and direct runoff to be identified. Effective rainfall separation methods and their complexities are extensively investigated in section (2.2.4).

$$\begin{bmatrix} y(1) \\ y(2) \\ . \\ y(p) \\ y(p+1) \\ y(p+2) \\ . \\ y(m-1) \\ y(m) \end{bmatrix} = \begin{bmatrix} u(1) & 0 & 0 & . & 0 & 0 \\ u(2) & u(1) & 0 & . & 0 & 0 \\ . & . & . & . & . & . \\ u(p) & u(p-1) & u(p-2) & . & 0 & 0 \\ 0 & u(p) & u(p-1) & . & 0 & 0 \\ 0 & 0 & u(p) & . & 0 & 0 \\ . & . & . & . & . & . \\ 0 & 0 & 0 & . & u(p) & u(p-1) \\ 0 & 0 & 0 & . & 0 & u(p) \end{bmatrix} \begin{bmatrix} h(0) \\ h(1) \\ . \\ h(n) \end{bmatrix} \tag{2.5}$$

In real-time flood forecasting, determination of base flow is less important because the base flow during floods is a small part of the total flow and it is often adequate to assume base flow to be uniform and equal to the runoff at the beginning of the event (Reed, 1984). In addition, the unit hydrograph is less reliable when applied to forecast runoff generated from complex situations such as multiple storms, as well as rain-and-snow storms (Kuhnke and Nguyen, 1977). Further, a large number of parameters have to be estimated. However, the unit hydrograph has some advantages such as simplicity and ease of operation. There are different views related to the catchment area that unit hydrograph theory can be applied to. The Flood Studies Report (NERC, 1975) recommends an upper limit equal to 500 km^2, while Corradini *et al.*, (1986) stated that it can be applied to basins whose area is less than 1000 km^2. Plate *et al.*, (1988) Pointed that for obtaining the accurate results unit hydrographs can be used for areas up to 10-20 km^2.

2.2.3.2 Non-linear storage models

In non-linear storage models, a relationship between outflow, quantity of water stored within the catchment and inflow to storage is used. Two of the best known simplified non linear storage models in the UK are the inflow-storage-outflow model *(ISO)* and the isolated event model *(IEM)*. Reed (1984) summarised the main characteristics of procedures as follows. It is believed that at time t the outflow from the catchment q_t is uniquely related to the quantity of water stored within the catchment, s.

$$q_t = q(s) \tag{2.6}$$

On the other hand, a consideration of the water balance equation along with time delay by lagging the rainfall prior to storage routing L yields:

$$ds / dt = p_{t-L} - q_t \tag{2.7}$$

Equation (2.7) can be rewritten as :

$$dq / dt = (p_{t-L} - q_t) dq / ds \tag{2.8}$$

Net rainfall n_t can be computed by multiplying total rainfall in runoff proportion (*ROP*) according to :

$$n_t = ROP.P_t \tag{2.9}$$

The runoff proportion itself is determined from the initial soil moisture deficit (*SMD*) for example by :

$$ROP = PERC.e^{-PERI.SMD} \tag{2.10}$$

where the *PERC* and *PERI* parameters determine the volume of runoff. It is possible to relate storage to outflow using a routing coefficient *AC* according to :

$$s = AC.q^{1/2} \tag{2.11}$$

Combining equation (2.11) with the continuity equation (2.7) and considering net rainfall yields the differential equation:

$$dq / dt = (n_{t-L} - q_t).2q^{1/2} / AC \tag{2.12}$$

Different non linear storage models can be obtained by choosing different values for *ROP* and *dq/ds*. There are briefly defined by Reed (1984).

2.2.3.3 Transfer function models

Transfer function models (sometimes termed stochastic, black-box or grey-box models) are now quite popular in hydrological systems modelling. They are used to relate output to input. Transfer function models have been applied in both rainfall-runoff and runoff-runoff models. In the former, the input and output are rainfall and runoff respectively, whilst in the latter they are discharge at the upstream and downstream locations respectively. *TF* models are more flexible and involve few parameters and can be formulated in state-space (see section 2.5.1.3). Compared to *UH* in addition to rainfall,

TF introduces a feedback element, in the form of past observed flows. *TF* models are covered in greater detail in section (2.5).

2.2.3.4 Conceptual models

Conceptual models (physics based or deterministic models) use some kind of soil moisture or water balance calculation. Here, physical equations are used to define different components of the models. Furthermore, catchments are represented by a network of nodes so that these models are usually spatially distributed. Conceptual models offer an advantage over transfer function models in better representing the non-linearity of hydrological systems. Conceptual models also require relatively little historical calibration data because initial parameter estimates can be based on available information such as soil type and topography (Hendrickson and Sorooshian, 1990). Another advantage of physically based models is that they provide the users with a better understanding of the hydrologic behaviour of the catchment (Marino and Crawford, 1990).

However, the application of conceptual models is often restricted, for reasons may include:

- large number of parameters
- large field data requirements such as soil moisture, infiltration, and evaporation (Ede and Cluckie, 1985)
- dependence on the skill and expertise of the model builder (Anglian Radar Information Project, 1988)
- lack of versatility (Fernando and Fernando, 1989)
- difficulty in relating theoretical equations to spatially heterogeneous and time-varying systems (Chiew *et al*, 1993)
- overall complexity and computational requirements (Ibbitt *et al*, 1990)

In addition, the large number of parameters means there is no simplified way of using telemeter flow data to improve short-term forecast via an updating procedure.

A typical conceptual model is illustrated in figure (2.1).

2.2.4 Different procedures of effective rainfall computation

The non-linear relationship between rainfall and runoff is due to several reasons including soil profile, infiltration, vegetation cover, antecedent catchment condition, seasonal evapotranspiration rates and climate. Therefore the term of effective rainfall is introduced,

which is linearly related to direct runoff. Effective (net) rainfall is that part of precipitation that produces surface runoff (Linsley *et al.*, 1983). The estimation of the effective rainfall is an important and difficult task in rainfall-runoff modelling. Different procedures for estimating effective rainfall have been suggested by researchers and some of these are described.

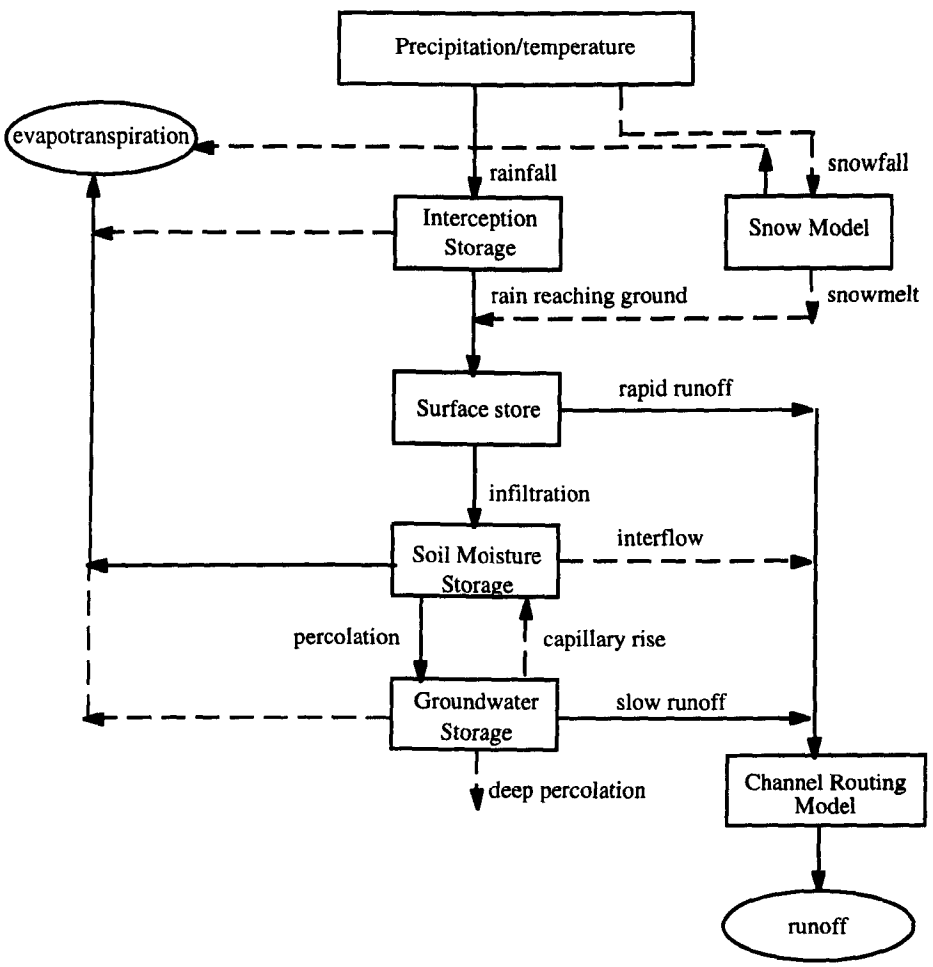

Figure (2.1) Typical structure of a conceptual model (adapted from Reed,1984)

One of the primary approaches used to determine the effective rainfall is the loss rate method. Loss can be related to soil infiltration, evaporation, transpiration, and interception. Loss rate methods themselves can be divided into two different methods: constant loss and variable loss.

In the constant loss rate, a constant and pre-defined loss of rainfall throughout the event is applied (Φ-index) (Reed, 1984). In the variable loss method which is based on Hortonian theory (Horton, 1935) it is accepted that the loss follows a curve which exponentially decreases during the event (infiltration curve). If the rainfall is greater than the infiltration rate then rainfall contributes to direct runoff, otherwise it infiltrates into the

soil (see for example Reed, 1984 and Chow *et al.*, 1988). The drawback of these two methods is that the heterogeneity of soil, vegetation cover and topography of the catchment are neglected. At present, loss rate methods are very rarely used.

The Flood Studies Report (NERC, 1975) introduces two different methods based on proportional loss rates. In these two approaches soil type, land use, topographic slope, rainfall rate, and catchment wetness index are considered. In the first approach, namely constant proportional loss a fixed proportional loss is applied to rainfall. The runoff coefficient *PR* is calculated based on storm depth *p* (mm), catchment wetness index *CWI*, and standard percentage runoff as follow :

$$PR = SPR + 0.22(CWI - 125) + 0.1(P - 10) \tag{2.13}$$

Standard Percentage Runoff *SPR* dependent up on the soil type, topographic slope and land use. Catchment wetness index is calculated according to :

$$CWI = 125 - SMD + API5 \tag{2.14}$$

where :

SMD = Soil moisture deficit (mm)

API5 = 5 - day antecedent precipitation index

In the second approach (variable proportional loss), the percentage runoff varies from time to time according to :

$$PR_t = K \times CWI_t \tag{2.15}$$

K is a rainfall separation parameter which is determined by trial and error using a recursive least squares algorithm in the calibration phase of rainfall-runoff model. As referred to by Reed (1984), Simpson (1980) determined values of K for a number of events and related the variation in K to the initial *CWI* for each event. He concluded that the higher values of initial *CWI* yielded higher values of K.

Another method to determine effective rainfall on daily basis has been suggested by Jakeman and Hornberger (1993) reported by Chiew *et al.* (1993) as follows. Effective rainfall in each time period is calculated by a non-linear relationship:

$$ER_i = Z.R_i.S_i \tag{2.16}$$

Where *ER* (mm) is effective rainfall and *Z* is a factor to guarantee the transformation of rainfall dimension to runoff unit, finally *S* is a catchment wetness index calculated by exponentially decaying weighting of the rainfall:

$$S_i = R_i + (1-\tau_i)^{-1} S_{i-1} \tag{2.17}$$

τ_i is dependent upon temperature and storage on the previous day :

$$\tau_i = \tau \exp.A(20 - Tem_i).\exp(-W.S_{i-1}) \tag{2.18}$$

Where *Tem* is temperature in °C and τ, *A* as well as *W* are model parameters. τ is inversely proportional to the rate of the catchment wetness decline at 20 °C.

In the same way effective rainfall can be obtained by multiplying the measured rainfall by an exponentially weighted index of past rainfall input. The procedure is well illustrated for example by Young and Beven (1994) and Jakeman *et al.* (1990) which can be briefly presented as follows:

This procedure involves three simple operations. The first is a modulation of measured rainfall r_k at time step *k* by a temperature dependent evapotranspiration factor such as:

$${}^{*}r_k = t_m^{-1}(t_m - t_k)r_k \tag{2.19}$$

Where t_m is a reference temperature greater than the recorded maximum for the location in question (overall maximum temperature), t_k is the mean monthly air temperature and r_k is modulated rainfall at time step *k* .

The second operation is presented the antecedent precipitation effects on the soil moisture as :

$$s_k = s_{k-1} + \tau^{-1}({}^{*}r_k - s_{k-1}) \tag{2.20}$$

If a backward shift operator is used, (2.20) can be written as:

$$s_k = \left\{\tau^{-1}/\left[1-(1-\tau^{-1})z^{-1}\right]\right\}^{*} r_k \tag{2.21}$$

Which is a linear equation. t_m and τ are determined by trial and error.

S_k is the soil moisture content (or antecedent precipitation index) and τ is the time constant. It is assumed when there is no rainfall, the soil moisture content decays exponentially. When ${}^*r_k$ is higher than s_{k-1}, there will be a net increase of soil moisture content. The higher τ, the slower the catchment response in soil wetting and drying processes.

Finally in the third step, the effective rainfall u_k is computed by multiplying ${}^*r_k$ by s_k.

$$u_k = c.{}^*r_k.s_k \tag{2.22}$$

c is a normalising factor and chosen in a way such that the volume of effective rainfall u_k is equal to the volume of surface runoff over the calibration period. After a long dry period, s_k because of exponential weighting will reach a low value, and hence, produce less effective rainfall. In contrast when rainfall continues, the soil will be wetter, s_k becomes higher, and consequently more effective rainfall will be produced.

Hino and Kim (1986) introduced an inverse estimation of effective rainfall. They stressed that in the rainfall-runoff model, the past effective rainfall can be estimated from the runoff: true if the system is linear. They divided the main system into several (usually two or three) linear subsystems. If the effective past rainfall is inversely estimated from the runoff data, the future runoff can be forecasted using the estimated effective past rainfall and future forecasted rainfall.

Novotny and Zheng (1989) used the Soil Conservation Service *SCS* empirical formula (see for example Chow, 1988) presented below to calculate effective rainfall R_t:

$$R_t = (P - 0.2S)^2 / (P + 0.8S) \tag{2.23}$$

Where $S = 25400/CN - 254$ (if R and P are in mm) and where P = daily precipitation series and CN is equal to a dimensionless runoff curve number.

The effective rainfall u_k can be defined as the product of the observed rainfall r_k at time step k, and the observed flow $y_{(k-\tau)}$ at time step $k-\tau$ (see for example Tsang *et al.* 1995, Young, 1992 and Young and Beven, 1994). The overall relationship between u_k and y_k is then given by:

$$u_k = r_k y_{k-\tau} \tag{2.24}$$

Where τ is a pure time delay usually considered to be zero. It can be seen that when flow is low, effective rainfall is low as well, while it is high when the flow is high. The main assumption of this method is that the down streamflow of the catchment reflects the soil moisture condition of the catchment. Young and Beven (1994) modified the method by introducing a power function β to the discharge component. Therefore the equation (2.24) can be written as:

$$u_k = r_k(y_{k-\tau})^{\beta} \tag{2.25}$$

The power β is a constant value between zero and one depending upon the catchment wetness condition and the catchment characteristics and can be optimised by trial and error technique during the calibration process. One advantage of this approach is that it does not require on-site measurements of catchment properties.

From above discussion it can be concluded that due to the complexities involved in calculation of effective rainfall, attempts to incorporate effective rainfall in real-time forecasting are generally inappropriate.

2.2.5 Assessment of model development and model suitability

It is difficult to judge which kind of flood forecasting model should be selected for a given area. As mentioned earlier, hydrologists working in flood forecast modelling can roughly be divided into two main groups: those using the physical laws and those using the statistical laws. Usually each group has rejected the methods of the opponents. On one side physicists believe that all knowledge of the physical processes must be used. They also claim that physics based models represent better the non-linearity of hydrological systems. On the other hand, statisticians think that physical problems are too complicated and difficult to run in a real-time mode (Lundberg, 1982). The advantages and disadvantages of each kind of model are discussed mainly in section (2.2.3.4).

A number of references claim that simpler, less data intensive models provide as good or even better forecasts than a more physically based model (see for example Jakeman and Hornberger, 1993 and Manley *et al.* 1980).

Consequently it is impossible to present a definite conclusion in the selection of flood forecasting models. Therefore the remainder of section introduces the characteristics of an appropriate model. A wide range of characteristics will affect the suitable choice of a forecasting methodology for a particular catchment with a specific purpose. These variables may be summarised as follow:

• Accuracy of forecast is most important because if a forecast of a peak flow is in error then a false alarm may be raised. In the other word the predictability of the model should be high.

• For a forecast to be useful, timeliness is important. A system which warns either too late (regardless of accuracy) or too early (and is inaccurate) is undesirable. In practice, a compromise between timeliness and accuracy is made (Tilford, 1987).

• The model should be designed in such a way that users other than the designer are able to apply and to understand it (Ede and Cluckie, 1985). It can be concluded that the model must remain simple enough to understand and use, yet at the same time complex enough to be representative of the characteristics of catchments and event (Anderson and Burt, 1985).

• The model should produce results quickly. This means the time available between the preparation of the forecast and flooding taking place should be long enough (Pearse, 1993).

• The model should be robust. That is, it must be applicable to a wide range of catchment and event types especially when extrapolated beyond the limits of calibration (Dobson, 1993).

• The model should contain the minimum number of parameters. For the physically based models the values of the parameters should be measurable or be related to easily measurable catchment characteristics (Bergstron and Forsman, 1973).

Furthermore, several other factors should be considered including physical characteristics of catchment, availability of data; such as meteorological data; availability of local expertise and computer resources, presence or lack of telemetry network (Bishop and Watt, 1989).

2.3 Historical perspectives, objectives and performance of the WMO project

The importance of effective forecasting of hydrological events has been recognised by most researchers and much activities has been concentrated in this area. The WMO realised the importance of hydrological forecasting a long time ago. During the last twenty five years it has undertaken a series of projects to assess forecasting techniques and has

successfully implemented three projects for the inter-comparison of flood forecasting models (WMO, 1975, 1986, 1992; Serban and Askew, 1991).

Numerical inter-comparison of the performance of the various models has been included in each of these projects. The first project completed in 1974 attempted to compile conceptual models and compare their basic structure, computational requirements and accuracy of simulation (WMO, 1987). The second project implemented during 1976 to 1983 was exactly same as the first one, except that input data included not only rainfall but also snow cover, temperature and the like.

Both projects tested the models more in a simulation mode rather than a forecasting mode and almost all of the models were run without any possibility of updating (Askew, 1989). Therefore it was realised that to include updating procedures, implementation of another project was necessary. The third project was implemented from 1985 to 1992 under the title 'Simulated Real-time Inter-comparison of Hydrological Models' (WMO, 1992).

The main aim of the third project was to compare the abilities of hydrological models to forecast streamflow under real-time conditions. Both rainfall-runoff and snow melt-runoff models were included in the project. Reporting the results of the study and transferring the material prepared to interested countries and organisations were other aims of the project.

The major event of the project the WMO workshop on the Real-time Inter-comparison of Hydrological Models, was held in the Department of Civil Engineering at the University of British Columbia (UBC) Vancouver, from 30 July to 8 August 1987.

The project involved the inter-comparison of fourteen models submitted by eleven countries. Canada submitted two models, Denmark presented two models with the same conceptual component but with two different updating procedures, The United States submitted three models which included one joint model with Switzerland and Czechoslovakia, Hungary, Ireland, Italy, Japan, Romania, and Sweden each submitted one model.

The project was implemented in different stages, including preparation, inter-comparison, and evaluation of the results. The preparatory stage was composed of collection of information relating to models, updating procedures as well as information on data sets necessary for the inter-comparison of models. In the second stage several activities were organised including :

1) In order to model operators could calibrate their models, standard calibration data sets were distributed eight months prior to the workshop.
2) One third of the real-time data as well as detailed instruction on the procedure for inter-comparison were distributed five months before the workshop, provided facilities for model operators to run their models using their computing systems. The results of these stage, defined as warm-up results were submitted at the workshop by each participant.
3) The remaining real-time data were distributed at the workshop under simulated real-time conditions in order to enable the model operators to run their models according to the workshop regulations.

The final stage was composed of analyses evaluation and comparison of the test results, preparation of conclusions and recommendations, and preparation of the final report (WMO, 1992).

Chapter three of this thesis describes the application of transfer function rainfall-runoff models (both static and physically realisable transfer function forms) using the same data sets and catchments as those used in the 1987 inter-comparison. This has enabled the comparison of *TF* model results with those of the fourteen above mentioned models. The *TF* models described have been developed in the Department of Civil Engineering, University of Salford (Tilford, 1990a and 1990b and Han, 1992), and previously at Birmingham University (Owens, 1986, Powell, 1985).

2.4 Introduction of the models submitted to the WMO project

This section introduces each of the models used at the inter-comparison. It should be noted that the different updating procedures utilised by the models are extensively investigated in chapter seven. Only a brief description of these are presented here.

2.4.1 University of British Columbia Catchment model (UBC)

The UBC catchment model was first developed for the Fraser river in British Columbia for daily streamflow forecasting. In addition, it was tested in several other catchments (Quick and Pipes, 1977a).

The UBC model is a deterministic model and mathematically represents the physical processes that control the catchment system. Because it was originally designed for mountainous catchments the model is divided into area-elevation bands. It is assumed that runoff characteristics also tend to be distributed by elevation. The model uses daily

maximum and minimum temperatures and a constant lapse rate for each of them as well as precipitation. The model output is daily streamflow which is obtained from snow melt and rainfall. The main structure of the model is shown in figure (2.2). The model uses unit hydrograph and storage routing techniques. Resultant flow consists of rain, ground water and snow components. The most important variable in the model is the soil moisture deficit. It is calculated from potential evapotranspiration which itself is estimated using maximum temperature. It is accepted that percentage of the basin which contributes to direct runoff is exponentially related to soil moisture (Quick and Pipes, 1976 and 1977a). As can be seen from figure (2.2), the precipitation is distributed into snow or rain according to the maximum and minimum temperatures. The ground water flow component is composed of the slow components of rain and snow melt. The fast component of snow melt is obtained by using a fast unit hydrograph. Similarly using another unit hydrograph the fast component of rain is obtained. The flow at the outlet of the basin is calculated by summing each of the components (Quick and Pipes, 1976 and 1977a and 1977b and Assaf and Quick, 1991). A list of the parameters used in the model and the general specification of this model are presented by Fleming (1975).

In the UBC model both the state variables and output are updated. In the former, manual interaction is used whilst in the latter automated updating is applied (Quick and Pipes, 1977a). Water equivalence of the snow pack as a state variable is updated based on an assessment of cumulative error over the preceding time period. Adjustments are applied on the snow-course data until the cumulative error is brought within normal. An autoregressive model is used to model the errors between the measured and simulated flow (WMO, 1992).

In the most recent version of UBC model, the Kalman filter technique (see sections 5.3.4 and 7.3.2) is used to update the weighting factors of snow component, ground water component, and rain component (Assaf and Quick, 1991).

2.4.2 Soil Moisture and Routing model (SMAR)

SMAR is a lumped, continuous general purpose model applicable to catchments of any shape and size. It is well known that the storage volume $s(t)$ in a reservoir is proportional to its flow $y(t)$ as:

$$s(t) = k.y(t) \tag{2.26}$$

where k is a constant. The rate of storage change ds/dt can be calculated as:

$$ds/dt = \tau.u(t) - y(t) \tag{2.27}$$

where:

s is the storage volume in m^3;

u is rainfall input in mm/h;

$\tau = \alpha\rho A$ (ρ is the percentage runoff over a unit area, A is the catchment area in km^2, and α is a constant to convert the unit of input to m^3s^{-1}).

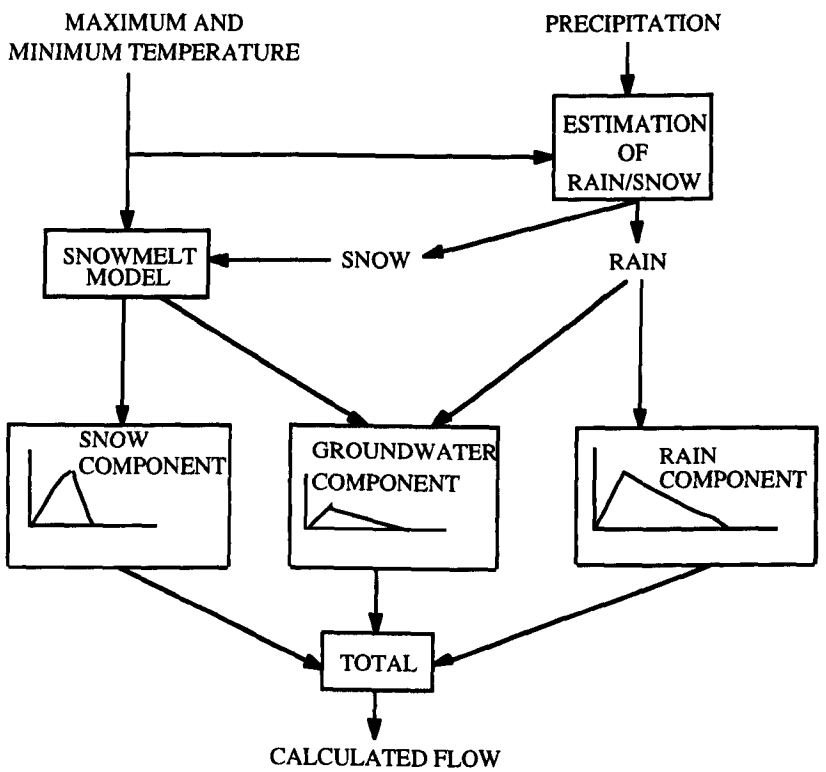

Figure (2.2) A general flow chart of the UBC watershed model (source Assaf and Quick, 1991).

Substitution of equation (2.26) into equation (2.27) yields:

$$dy/dt = 1/k[\tau u(t) - y(t)] \tag{2.28}$$

The pulse response of system can be calculated as (Chow *et al.* 1988):

$$h(t) = \tau/k.e^{-t/k} \tag{2.29}$$

Nash (see for example Nash and Sutcliffe, 1970) generalised the concept as:

$$h(t) = \begin{cases} (\tau(t-l)^{n-1}/k^n\Gamma(n)).e^{-(t-l)/k}; t \geq l+1 \\ 0 \; ; t < l+1 \end{cases} \tag{2.30}$$

where:

$\Gamma(n) = (n-1)$!= Gamma function;
l is the lag time and n is the number of linear storage reservoirs.

In fact the Nash model is derived by routing a lumped unit pulse input through n homogeneous linear reservoir with equation (2.29). It can be seen that it is analogous to the Gamma probability distribution (see also Yuan, 1994).

In the model the following systematic procedure is applied:

1) Assume a simple model.
2) Optimise the parameters and study their stability.
3) Measure the efficiency R^2.
4) Modify the model.

Only the discharge is automatically updated using an autoregressive model which is fitted to the errors between the simulated and measured hydrographs (WMO, 1992).

2.4.3 Rainfall-runoff model with Gamma distributed API (GAPI)

The GAPI model is a lumped model based on gamma distribution function. It is designed for navigation, flood control as well as power generation applications. The model has almost the same structure as SMAR model (see section 2.4.2). The model is divided into area-elevation bands and is restricted to no reservoirs or glaciers in basin. It can be applied to basins with an area between 100 km^2 to 30000 km^2 and time steps of 1 to 24 hours (WMO, 1991). The forecasted discharges are updated automatically using a fifth order autoregressive model which is fitted to the forecasting error. The parameters of the error model are updated as new data become available. Furthermore, modellers stated that the original model parameters can be updated by fitting a new gamma distribution function to new set of API (WMO, 1992).

2.4.4 CEQUEAU model

CEQUEAU is a distributed water balance model for continuous use. It is designed for short-term forecasting and can be used for hydropower, floods and droughts. The model is used for catchment areas in the range 10 km^2 to 100000 km^2. In the model, the basin is subdivided into squares, the area of which depends on the size of the basin and the number of meteorological stations. There are three options for distribution of temperature:

a) A regression relationship between the daily temperature and altitudes of the meteorological station is obtained. The temperature of each square is then calculated using the altitude of the square and above mentioned regression relationship.

b) Thiessen polygons are constructed, and the temperature of each square is represented by the temperature of the nearest meteorological station in the polygon. If the altitude of the square is different from the station, the temperature is modified according to model lapse rates.

c) The temperature is a weighted average of the three nearest stations. If the altitude of square is different from the mean of three stations, the temperature is modified according to the lapse rates are used.

The form of precipitation on each square depends on the temperature of the square. Distribution of precipitation may be defined as the same as either of options *b* and *c* of the previous paragraph. The precipitation is corrected using the lapse rates of the precipitation in the same way as described in *b* and *c* of the previous paragraph. The structure of the model is described in figure (2.3) (WMO, 1986 and 1991).

Both inputs (rainfall and snow melt) and output (discharge) are automatically updated. At each time step the differences between the forecasted and the observed discharge are calculated and named as a model error. If the model error is less than an accepted threshold, no corrections are made on the precipitation and snow melt. If computed error exceeds the threshold error, the precipitation and snow melt are modified, and the procedure iterated until the model error is less than the threshold error.

In order to update output of the model, a first order autoregressive model is fitted to the model error. The predicted error is then added to forecasted output (WMO, 1992).

2.4.5 Constrained Linear System (CLS)

The CLS model is designed for flood warning, flood control and reservoir operation. It is a lumped, continuous model which can be applied to catchments with different shapes and sizes. During a storm, precipitation is divided into two parts. Some of the precipitation infiltrates the ground (the values of infiltration mainly depend on soil system) whilst the remainder produces surface runoff. Some part of infiltrated rainfall finally reappears at the outlet of the catchment. Both the surface flow and ground flow can be considered as a linear system, but the overall relationship between rainfall and runoff is non-linear. In the simplest form of CLS model, the system can be split into two linear systems depending on the value of the antecedent precipitation index. If the value of API is equal to or less than a threshold value, rainfall will then be transformed into runoff by the first linear model. If the soil is wet, that is the API is larger than threshold value, the second linear model is used to transform the rainfall to runoff. Overall flow at any time can be calculated by sum of the output from the two linear systems (Todini, 1978 and Nemec, 1986). The logic of the CLS model is illustrated in figure (2.4).

At each time step when the new precipitation and discharge become available, the ordinates of the unit hydrograph are recalculated. The forecast runoff is updated using the new calculated values of the UH ordinates. The updating procedure is automatic.

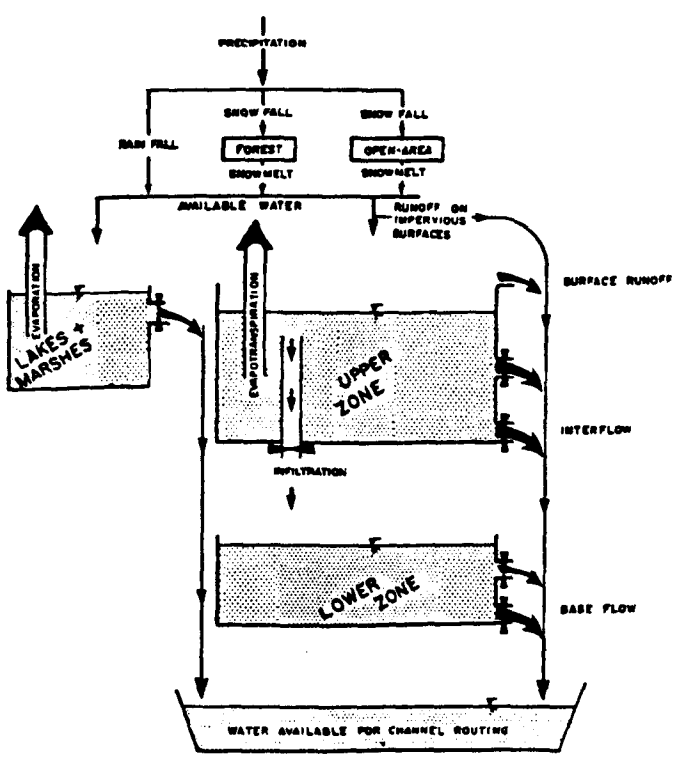

Figure (2.3) Flow chart of CEQUEAU model (source WMO, 1986)

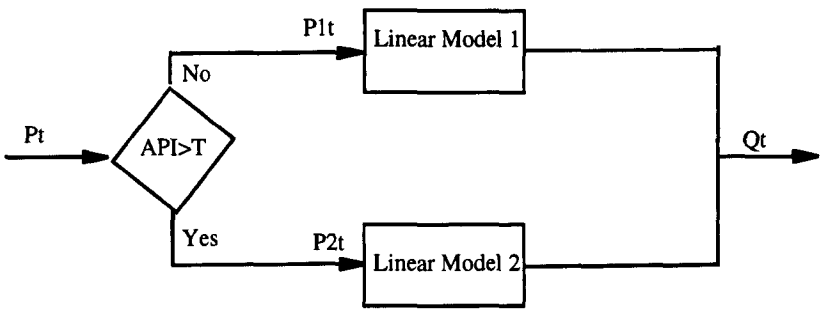

Figure (2.4) CLS model scheme (adapted from Todini, 1988)

2.4.6 HBV model

HBV is a simple conceptual rainfall-runoff model developed at the Swedish Meteorological and Hydrological Institute. It is a lumped model that includes soil moisture storage, an upper zone storage and a lower zone storage. The model time interval used is one day. Data requirements are precipitation and potential evaporation, the latter generally being computed by Penman's formula, using values of total radiation, air temperature, air humidity, wind speed and duration of sunshine. The albedo of the catchment surface also has to be estimated. Evaporation data from evaporimetric pan can be used if available. Finally the streamflow records are used.

The main components of the model are a soil moisture zone and two reservoirs. The soil moisture zone feeds the upper zone storage. Water percolates at a constant rate from the upper to the lower zone storage when available. Runoff is produced in these two storages in proportion to their contents. That part of the lower zones which includes lakes, rivers and outflow areas is affected directly by precipitation and by potential evaporation. When the upper zone storage is not empty, recharge of the lower zone is possible as:

$$NR = PERC - K_2 L_Z \tag{2.31}$$

Where :

NR = net recharge of the lower zone

PERC = percolation

K_2 = storage-discharge constant for the lower zone

L_Z = lower zone storage

Finally discharges from the two reservoirs are added and a simple time-lag procedure between rainfall and runoff is adopted.

The precipitation in the soil moisture zone consists of two parts. One part remains in the soil moisture storage and finally evaporates, whilst the second part enters the upper zone and contributes to runoff or evaporation from the lower zone storage. The value entering the upper zone, Δu_z depends on the soil moisture content. The relation between soil moisture content and the $\Delta u_z / p$ ratio (P= precipitation) is in the form of $(SM / F_c)^{\beta}$ limited to one (*SM* = soil moisture content, F_c = maximum soil moisture content, corresponding to field capacity minus wilting point and β= numerical parameter). This procedure means that after a long dry spell, the contribution of rainfall to runoff is small because the soil moisture content *SM* is low. In contrast after a wet period more rainfall contributes to runoff.

The structure of the HBV model and the relationship between soil moisture content and Δu_z are shown in figures (2.5) and (2.6) respectively (Bergstrom, 1975 and 1978 and Bergstrom and Forsman, 1973).

In addition, several other versions of the HBV model appear in the literature [see for example Gutierrez, 1995].

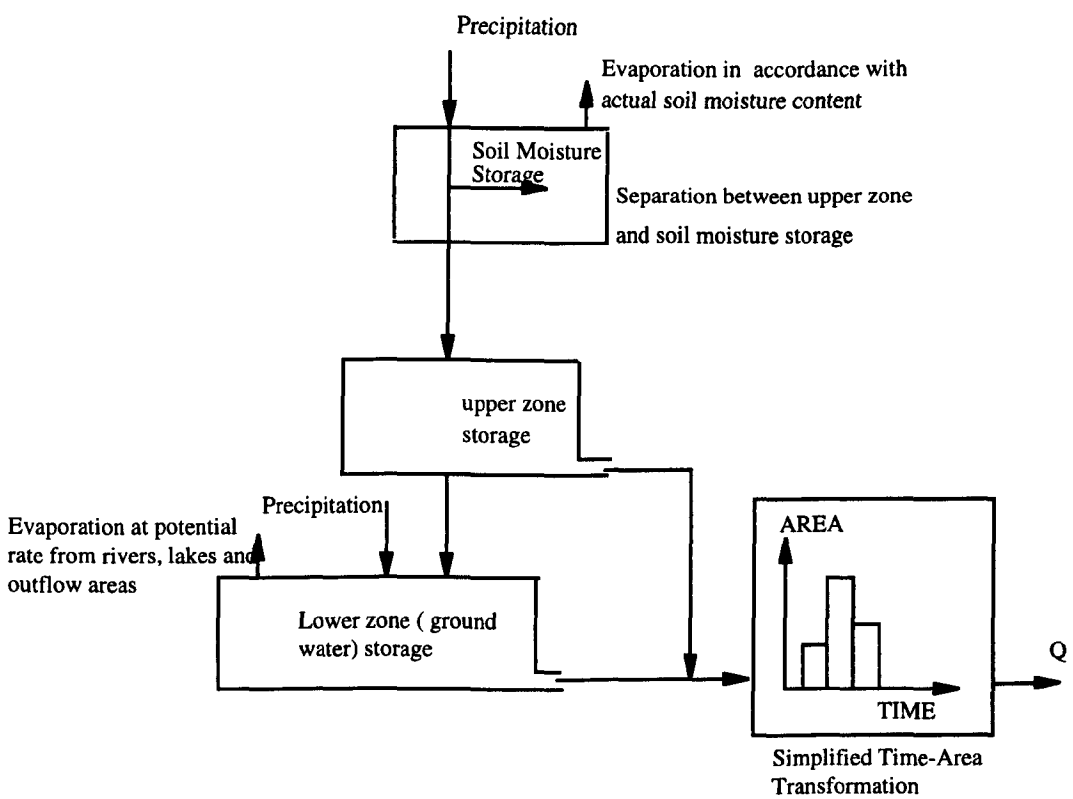

Figure (2.5) The structure of the HBV-2 model (from Bergstrom and Forsman, 1973)

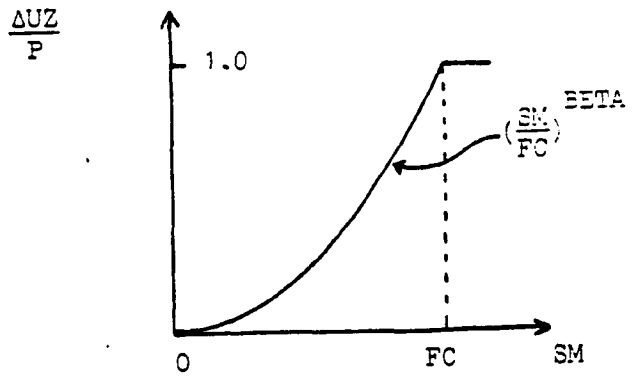

Figure (2.6) The Relationship between soil moisture content and Δu_z in HBV-2 model (from Bergstrom and Forsman, 1973)

To distinguish between rain and snowfall a critical temperature is used in each elevation band (WMO, 1986). Modification of air temperature and precipitation as inputs is done in a manual interactive manner to update the model performance. In addition, the soil moisture states of the simulation model can be manually updated (WMO, 1992).

2.4.7 Streamflow System and Reservoir Regulation (SSARR) model

The SSARR model is a conceptual (mathematical) rainfall-runoff model which comprises of a watershed, river system, and reservoir regulation model. It was developed in 1956 by the U.S. Corps of Engineers for reservoir operation in the Pacific Northwest. It has been used for operational river forecasting on numerous watersheds with a wide range of characteristics and climates including in the Columbia River basin, in the upper Missouri River watershed and in the Alberta flow forecasting Branch (Kuhnke and Nguyen, 1977 and Cundy and Brooks, 1981). The model is able to synthesise the streamflow conditions by continuously evaluating the snow melt and rainfall as well as the characteristics of watershed and rivers and reservoirs. The watershed part of the SSARR model has several multivariable relationship and parameters which create an obstacle for who want to use it (Cundy and Brooks, 1981). Calibration of the SSARR model is mainly a trial and error process of adjusting parameters until, on average, simulated flow matches observed streamflow (Cundy and Brooks, 1981). The original structure of the watershed model is presented in figure (2.7).

The model combines basin runoff techniques which produce surface and subsurface flow with river routing techniques. As can be seen in figure (2.7) base flow, sub-surface flow and surface flow are independently routed into a hydrograph. Several subjective decisions are necessary. Inputs which are on daily basis can be summarised as: observed precipitation and streamflow, forecast precipitation and maximum air temperature. Snow conditions, soil moisture, and solar radiation can be included as inputs or can be computed from other parameters. Outputs consists of surface and sub-surface flow, percentage runoff, snow line elevation, snow water equivalent, soil moisture, river stages and discharge (Nemec, 1986).

In the model used at workshop, the air temperature and precipitation inputs were automatically modified to update the model performance. Other procedures of updating in SSARR model are addressed in the literature [see for example WMO, 1992].

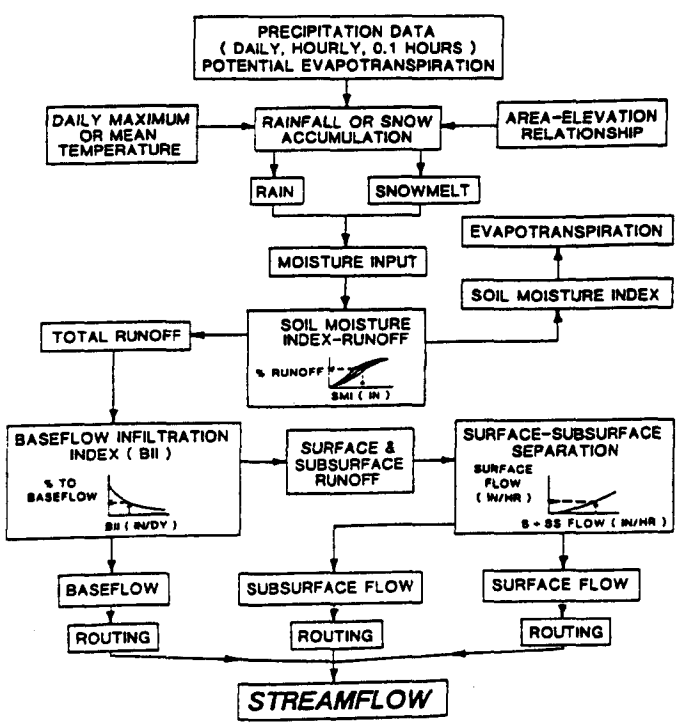

Figure (2.7) Structure of SSARR model (from Cundy and Brooks, 1981)

2.4.8 Hydrologic Forecast System (HFS)

The model used here is the modified Sacramento model, the original version of which was developed in the 1970s (Burnash *et al.*, 1973). It is a conceptual, lumped, discrete-time model suitable for flood forecasting, water supply, low flow forecasting, and water management. The model inputs are mean areal precipitation and mean areal evapotranspiration, and its output is total channel inflow which is composed of direct runoff from impervious areas, surface runoff in cases of excessive rainfall rates, inter flow through the upper soil layers, and ground water flow. The upper soil layers supply water for evapotranspiration, percolation, surface runoff, and inter flow. The lower zone is the source of ground water storage. Figure (2.8) presents the various components of the model, and table (2.1) the model states, inputs and parameters. Further details of the model are presented by (Georgakakos *et al.* 1988 and Georgakakos and Smith, 1990).

In the version used at the workshop, the amount of water available in the model reservoirs (upper zone, tension water, upper zone free water, lower zone supplemental free water, additional impervious area content) and channel conceptual reservoir as indicated in figure (2.8) were directly and automatically updated (WMO, 1992).

2.4.9 NAM System 11 flood forecasting version (NAMS11)

NAMS11 is a mathematical modelling system for real-time flood forecasting . The model is consists of four main elements: A hydrological rainfall-runoff model (NAM), a hydrodynamic model (system) for river routing and reservoir simulation, an updating model, and a data management model for data processing. The model has been applied to more than 50 catchments in different climatic regions throughout the world including part of the 22000 km^2 Damodar River catchment located in Bihar and West Bengal in India, the Bird Creek catchment in the USA, and several other catchments in Borneo, Tanzania, Sri Lanka, Thailand, and Greenland.

NAM is a lumped, deterministic rainfall-runoff model. The model operates by accounting continuously for the moisture content in five different interrelated storages representing physical elements in the catchment. The structure of model is presented in figure (2.9). The input data requirements are precipitation, potential evapotranspiration and temperature (only if snow occurs).

System 11 is based upon a numerical solution of the general one-dimensional 'Saint Venant' equations, that is, conservation of mass and momentum.

Table (2.1) Modified Sacramento model variables (after Georgakakos and Rajaram, 1988)

Symbol	Description
	States:
x_1	upper zone tension water content (mm)
x_2	upper zone free water content (mm)
x_3	lower zone tension water content (mm)
x_4	lower zone primary free water content (mm)
x_5	lower zone secondary free water content (mm)
x_6	additional impervious storage (mm)
	Inputs:
u_p	mean areal precipitation (mm/time interval)
u_e	mean areal evapotranspiration demand (mm/time interval)
	Parameters:
x_1^0	upper zone tension water capacity (mm)
x_2^0	upper zone free water capacity (mm)
x_3^0	lower zone tension water capacity (mm)
x_4^0	lower zone primary free water capacity (mm)
x_5^0	lower zone secondary free water capacity (mm)
d_u	upper zone instantaneous drainage coefficient (1/time interval)
d'	lower zone primary instantaneous drainage coefficient (1/time interval)
d''	lower zone secondary instantaneous drainage coefficient (1/time interval)
ε	parameter in percolation function
θ	exponent in percolation function
p_f	fraction of percolation water assigned to the lower zone free water aquifers
μ	fraction of base flow not appearing in river flow
β_1	fraction of basin that becomes impervious when tension water requirements are met
β_2	fraction of basin permanently impervious
m_1	exponent of the upper zone tension water non-linear reservoir
m_2	exponent of the upper zone free water non-linear reservoir
m_3	exponent of the lower zone tension water non-linear reservoir

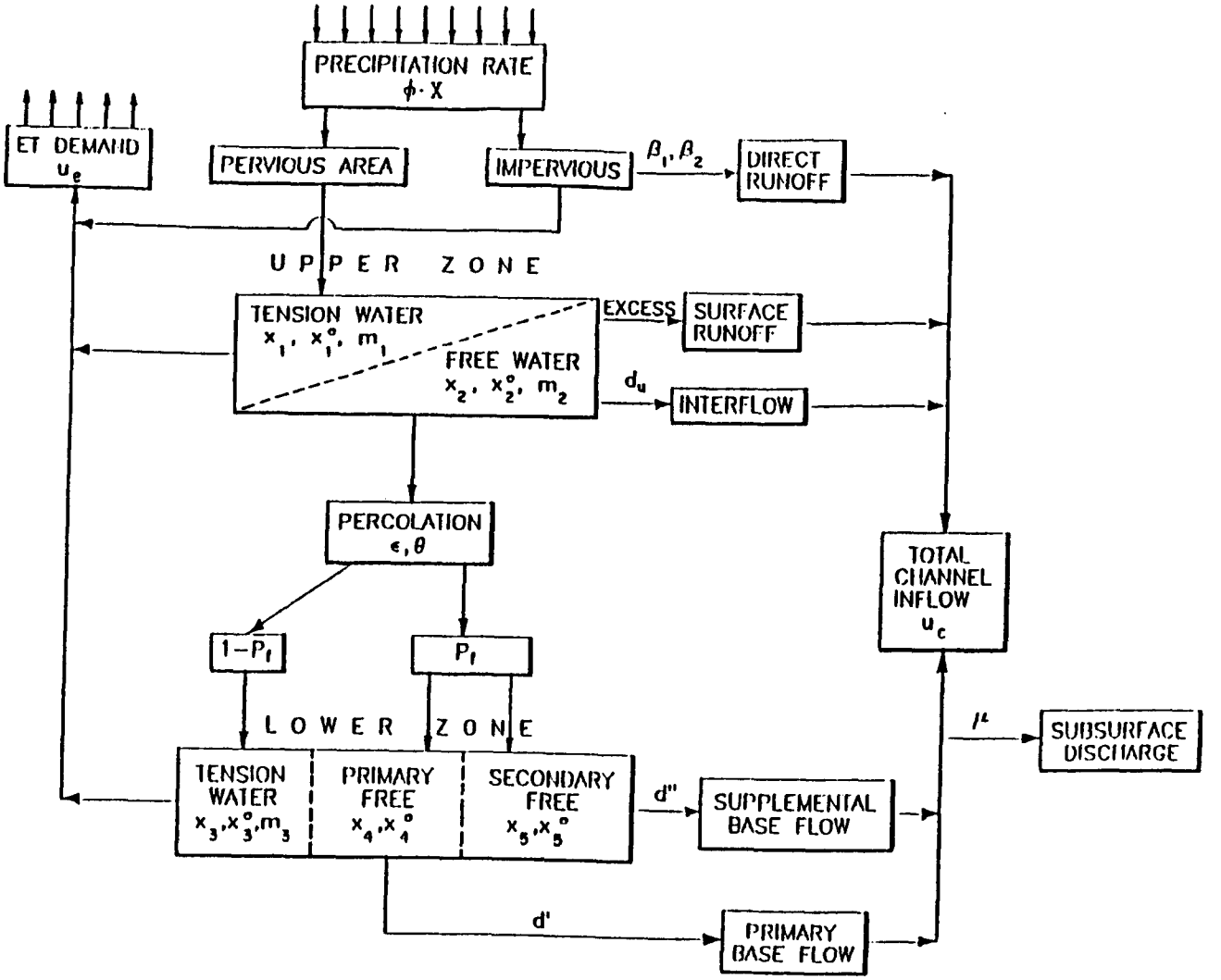

Figure (2.8) Modified Sacramento model's structure (after Georgakakos and Rajaram, 1988)

The updating procedure is based on the predicted error between the computed and measured hydrographs using a first order autoregressive model. Updating is applied manually and automatically. Furthermore, another version of updating has been developed which distinguishes amplitude and phase error. The details of this procedure is presented in chapter seven. The interested reader is also referred to Clausen and Refsgaard (1984), Havno *et al.* (1985), *Rungo et al.* (1989a, 1989b) and Refsgaard *et al.* (1983) for a comprehensive discussion of the model structure and updating procedures.

2.4.10 NAM-KAL man Algorithm (NAMKAL)

The NAM rainfall-runoff model has been reformulated in a state space (see section 2.5.1.3) form incorporating the Kalman filtering algorithm. This version of the NAM

model operates by accounting continuously for the moisture content in four different and interrelated storages representing physical elements in the catchment as indicated in figure (2.10).

The states defining the system are as follows: Water content in surface storage, (*u* in figure 2.10); water content in lower zone storage, (*L* in figure 2.10); water content in ground water storage; water content in routing reservoir no. 1; water content in routing reservoir no. 2; time constant in routing (k_1^{-1} in figure 2.10); parameter in overland flow equation, (*cof* in figure 2.10). The first three states describe the soil moisture conditions, the next two states define the routing into streamflow, and the last two states are related to model parameters. Two serially connected linear reservoirs no. 1 and no. 2 describe the routing. The shape of the hydrograph is determined by the two model parameters *K* and *cof*. The details of mathematical equations including the state-space formulation of NAM model are presented by Refsgaard *et al.* (1983).

The upper zone storage, the lower zone storage, the ground water storage, and routing reservoirs are updated automatically using the extended Kalman filter (WMO,1992).

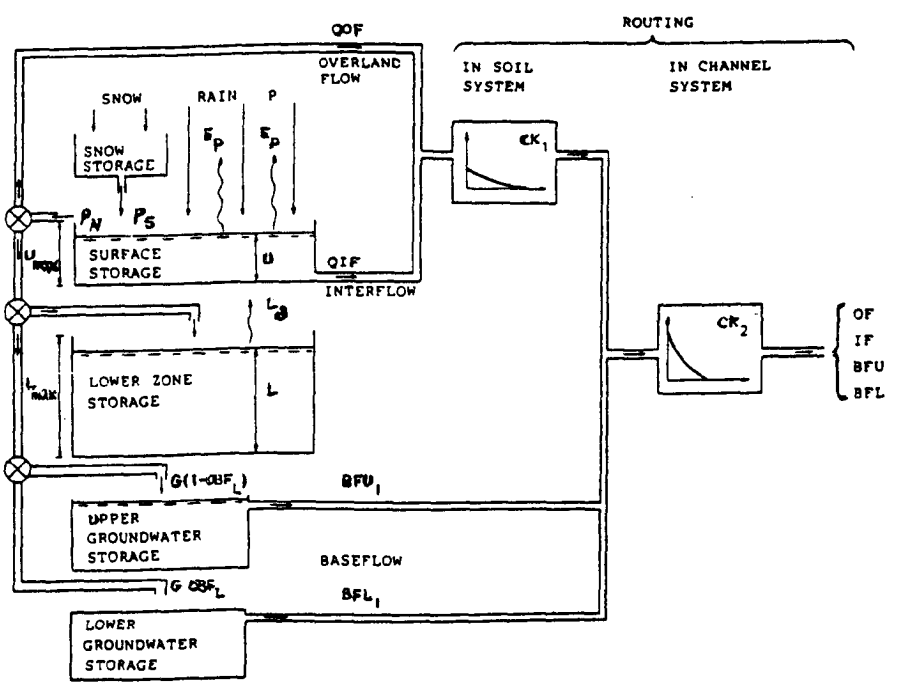

Figure (2.9) Structure of NAM model (adapted from Clausen and Refsgaard, 1984)

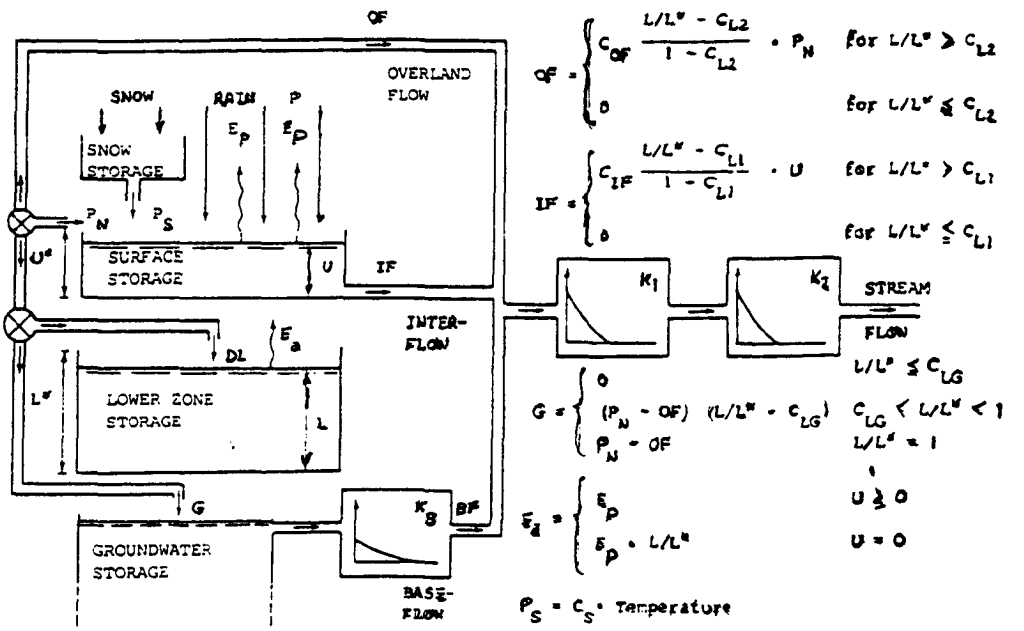

Figure (2.10) Structure of NAMKAL model (after Refsgaard *et al.*, 1983)

2.4.11 TANK model

The TANK model is an implicit moisture accounting model, designed for multipurpose use. Any shape and size of catchment can be used and time steps of less than one day are available. It is based on the hypothesis that runoff and infiltration are a function of the amount of water stored in the ground. Several methods have been examined and the method of the series storage-type model is applied more than others. In the case of Tank in series, the top tank represents surface storage and overland flow, the second, third and fourth Tanks describe intermediate runoff, ground water and base flow respectively. The number of side outlets is arbitrary. The relationship between the storage X and discharge Y is not linear. Infiltration I is proportional to the storage X. The limit of the increase of infiltration is saturation point Hs when I becomes $Is = Hs$ = constant. This principle is valid if there is always a moisture supply to all the tanks (humid regions). The basin is divided in zones according to the distance of the river, the wettest zone being closest to river. The top tank in each zone simulates soil moisture which consists of primary and secondary moisture (Nemec, 1986 and Sugawara, 1961 and Sugawara *et al.*, 1986). Movement is in both directions according to :

$$T_2 = c_0 + c(1 - x_s / c_s) \qquad \text{[infiltration action]} \qquad (2.32)$$

$$T_1 = b_0 + b(1 - x_p / c_p) \qquad \text{[velocity of capillary action]} \qquad (2.33)$$

c_0, c, b_0, b= constants
X_S, X_P = storage of moisture
C_S, C_P = saturation capacity of soil

Evapotranspiration is simple constant of potential one. One example of structure of model is presented in figure (2.11).

A correction coefficient is computed on the basis of the observed discharge then is applied to rainfall and snow melt input to update the performance of the model (WMO, 1992).

2.4.12 VIDRA model

VIDRA is designed for flood control and reservoir operation and is a lumped and continuous model, applicable to small and large catchments. It is applicable in an appropriate selection of Muskingum coefficients. Data requirements include; precipitation, discharge [temperature, snow cover and wind speed (optional) in snow melt-runoff model], basin area and slope, river length and slope, forest cover, and dominant soil texture. The shape of the forecast hydrograph is modified by selecting one of three unit hydrographs which are generated by high, medium, and low intensity rainfall events. The model did not run at the workshop (WMO, 1992).

2.4.13 Empirical Regressive Model (ERM)

ERM is a lumped and continuous model, designed for water management, reservoir regulation, and flood protection. It can be applied to basins with elevation up to 2000 meters above mean sea level and for areas between 100 km^2 to 5000 km^2.

The structure of the transformation model is as follows:

$$Q(N) = Q(N-1) \times \exp(A \times Q(N-1)) + Q_B \times \tan g\left\{\pi / PMPI\left[1 - \exp(B \times P(N-1) + D \times P(N-1)^2)\right]\right\} \qquad (2.34)$$

Where:
Q(N), Q(N-1).....are daily discharge on days, *N, N-1,* .....respectively.

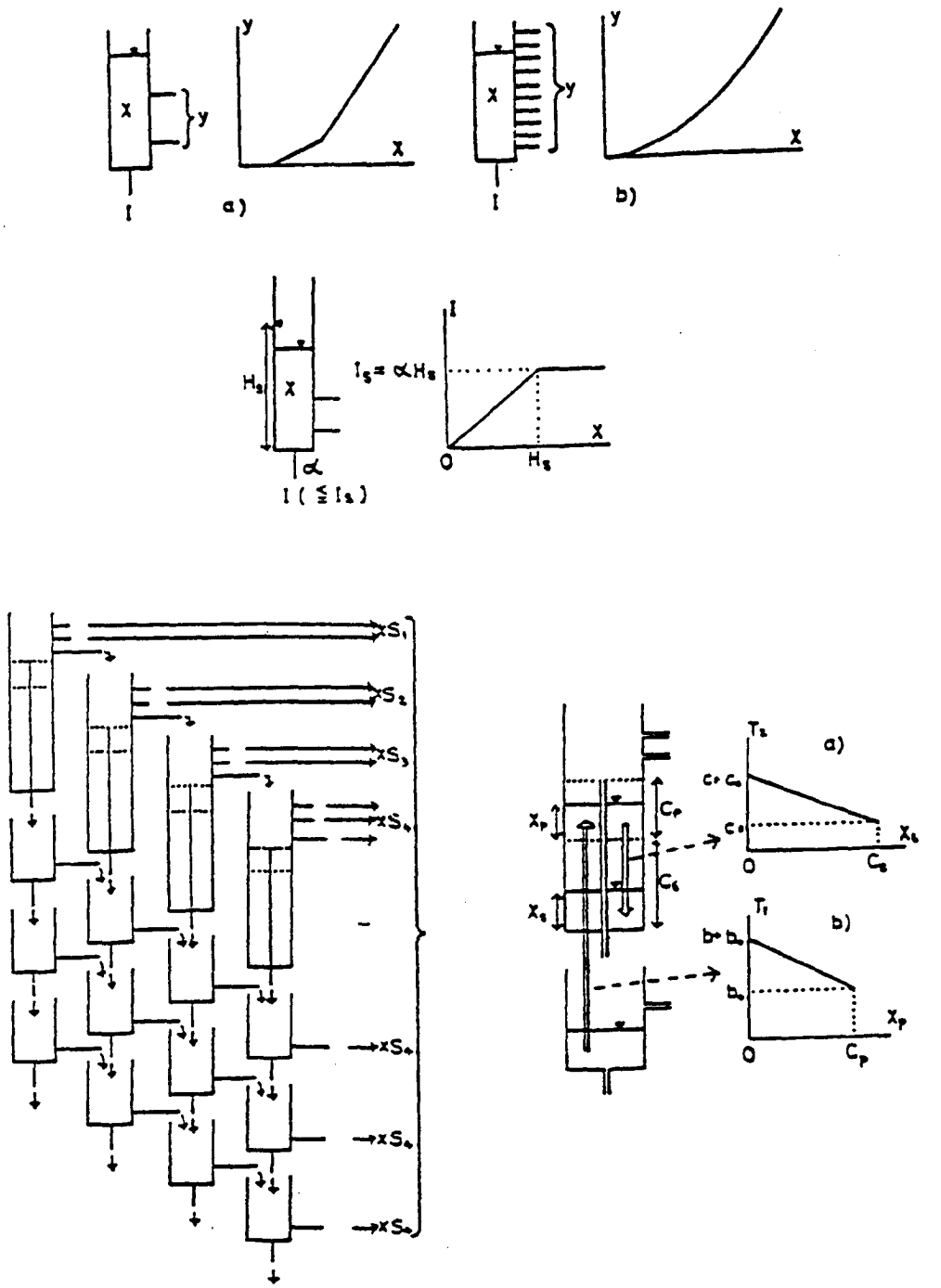

Figure (2.11) TANK model scheme (from Nemec, 1986)

QB discharge on the beginning of the flood wave (index of saturation of the basin), limited by the maximum value of $QB = QL$.
A, PMPI, B, D, and QL are parameters (WMO, 1986).

A base flow indicator of the simulation model is automatically updated as a function of observed discharge. Forecasted discharge is updated by substituting the measured discharge QM_j in the simulation model at time j for the simulated discharge (WMO, 1992).

2.4.14 Snow melt runoff model (SRM)

The SRM model was originally developed and tested on small experimental basins in Europe ranging in size from 2.65 to 43.3 $km^2$and then applied to basin with size between 0.5 km^2 to 64000 km^2. It is a lumped, continuous model which can be used for hydropower, irrigation, water supply, and reservoir operation. Daily discharges can be simulated by the snow melt-runoff model (SRM). Data requirements are just three measured input variables, namely: precipitation, temperature, and snow-covered area. The precipitation and temperature inputs are obtained from a meteorological station and the snow cover is provided from satellite monitoring, aircraft or ground-based measurements, separately for elevation zones.

A simple form equation of (SRM) is:

$$Q_{n+1} = (c_s.a.T_n s_n + c_R \cdot p_n)(A \times 0.01/86400)(1 - k_{n+1}) + Q_n k_{n+1} \qquad (2.35)$$

Where:
Q = average daily discharge ($m^3\ s^{-1}$)
Cs = runoff coefficient for snow
CR = runoff coefficient for rain
a = degree-day factor (cm $°C^{-1}.d^{-1}$) indicating the snow melt depth resulting from a degree day
T = number of degree-days (°C.d) which is obtained from $(T_{Max} + T_{MIn})/2$, T_{Max} and T_{Min} are Maximum and Minimum temperature respectively, if $T_{Min} < 0$, then T_{Min} =0 ℃
S = ratio of the snow-covered area to the total area
P= precipitation contributing to runoff (cm). Critical temperature T_{crit} is used to discriminate between snow and rain. T_{crit} is usually selected to be slightly above the freezing point. This value will vary from basin to basin and seasonally, depending on climatic condition.

A = area of the basin or zone (m^2)
0.01/86400= conversion from cm. $m^2.d^{-1}$ to $m^3\ s^{-1}$
K = recession coefficient indicating the decline of discharge in a period without snow melt or rainfall. On the daily basis K can be calculated from:

$$K_{n+1} = X(Q_n)^Y \tag{2.36}$$

Where X and Y are constants to be determined for the given basin.
n = sequence of days.

The measured variables, T, S, and P, are input to *SRM* on a daily basis. The parameters C_S, C_R, a, T_{crit}, X, Y, and K as well as temperature lapse rate are predetermined for basin and usually input to *SRM* bimonthly (WMO, 1986 and Rango, 1980 and Martine and Rango, 1989). A flow chart for the snow melt runoff model is presented in figure (2.12).

The recession coefficient and hence snow covered extent is updated as a function of observed discharge. The discharge itself is updated by substituting the forecasted discharge with the measured discharge (WMO, 1992).

2.5 Transfer function models in detail

2.5.1 Transfer function model structure

In recent years a large number of stochastic models have been used to represent different aspects of the rainfall-runoff process. The transfer function model suggested by Box and Jenkins (1976) and further explained and applied by Vadaele (1983) has been adapted extensively and are quite popular. The TF models are flexible, involve few parameters, consequently are suitable for real-time applications. Further, they can be formulated in state-space (see section 2.5.1.3). The transfer function model including excess rainfall is a discrete-time equivalent of an approximation of the convolution integral through a unit hydrograph (Jakeman and Hornberger, 1993). It means that the TF models are a statistical framework of unit hydrograph with fewer parameters.

Besides single-input systems, TF models may be used in multi-input systems. For example they can relate river-flow to rainfall, ground water levels and temperature. Further, they have been used for real-time runoff-runoff flood routing (see for example Wilke and Barth, 1991 and Lees et al, 1994 and Cluckie *et al.*, 1989).

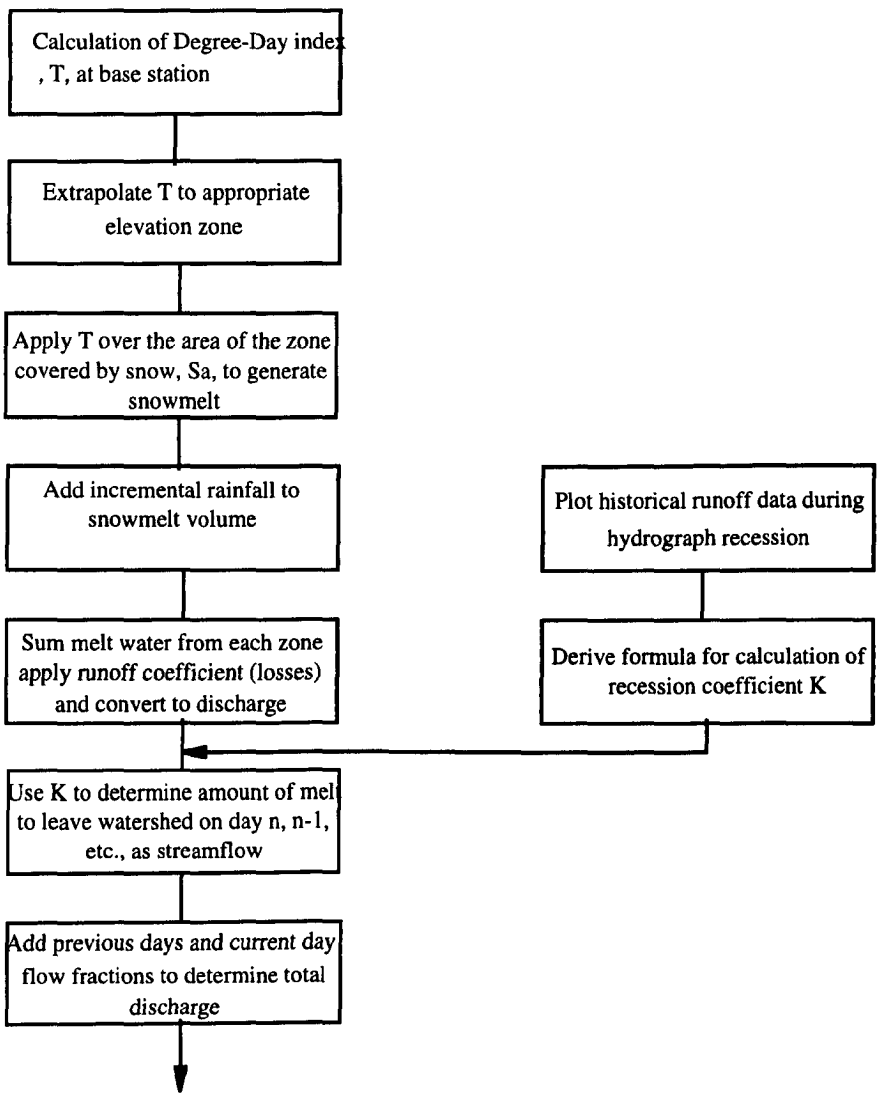

Figure (2.12) Flow chart of SRM model (from Rango, 1980)

Transfer function models have been developed for real-time flood forecasting purpose by researchers working with Professor I. D. Cluckie including Harpin (1982), Owens (1986), Powell (1985), Yu (1989), Han (1991), Tilford (1992), and Yuan (1994). Other researchers who have explored the time series approach include Young and Beven (1994), Moore (1980) and Moore and O'Connell (1978). More recent developments and applications of TF models have been made by Ramos *et al.*, (1995), Jakeman and Hornberger (1993) and Nalbantis (1995). TF models have been applied operationally by the National Rivers Authority, North-West and Wessex Regions (Anglian Radar Information Project, 1988 and WRIP, 1994).

The rainfall-runoff process may be considered as a mathematical transformation whereby a high frequency input signal (rainfall) is modulated to form a low frequency output

(runoff). Transfer function models can represent this kind of transformation. To do this several variants may be considered as follows:

a) A linear relationship between runoff Y_t at current time and rainfall in previous time periods U_{t-1}, U_{t-2},.....can be constructed. If the Y and U is measured in a discrete time period then a linear relationship between them may be written as :

$$y_t = b_1 u_{t-1} + b_2 u_{t-2} + \ldots\ldots\ldots\ldots + b_n u_{t-n} + \zeta_t \tag{2.37}$$

Where:

$b_1, b_2, \ldots\ldots\ldots\ldots, b_n$ are parameters and can be related to ordinates of a finite-memory pulse response.

ζ_t is an error term with zero mean white Gaussian noise and variance $\sigma^2(t)$, representing the effect of model inadequacy, and measurement noise in the Y_t and U_t.

If Y_t and U_t are considered as direct runoff and effective rainfall respectively then this kind of relationship can be refered to as an unit hydrograph. A pure time-delay between rainfall and runoff may be included. It can be concluded that the number of parameters of UH is equal to the numbers of ordinates of UH and are too numerous.

b) A linear relationship between runoff at current time y_t and runoff in earlier time intervals y_{t-1}, y_{t-2}, ...can be written as :

$$y_t = a_1 y_{t-1} + a_2 y_{t-2} + \ldots\ldots\ldots\ldots + a_n y_{t-n} + \zeta_t \tag{2.38}$$

Although this kind of relationship has a natural self-correcting ability when telemetered streamflow is available, the natural lag between the occurrence of rainfall and the response of streamflow is not included, further, the model is not able to determine the time of peak flow.

c) Finally a linear relationship between runoff at current time Y_t and runoff and rainfall in previous time periods those are Y_{t-1}, Y_{t-2} ....., Y_{t-n}, U_{t-1}, U_{t-2}, ...U_{t-m} may be constructed as :

$$\begin{aligned} y_t &= a_1 y_{t-1} + a_2 y_{t-2} + \ldots\ldots\ldots\ldots + a_m y_{t-m} + \\ & b_1 u_{t-1-l} + b_2 u_{t-2-l} + \ldots\ldots\ldots + b_n u_{t-n-l} + \zeta_t \end{aligned} \tag{2.39}$$

Here l is a pure time-delay between rainfall and runoff. Time delay occurs in catchments where flood producing rainfall is consistently confined to an area of the catchment upstream of the river gauging station (O'Connell and Clarke, 1981). Inclusion of a pure time delay means that flood forecasts up to l time steps ahead can be made without recourse to rainfall forecasts (Reed, 1984). This kind of relationship is hereafter called a transfer function (TF) model. $m+n$ is named model order.

By applying the Z- transform as defined for example by Poularikas and Seely (1991) to equation (2.39) and using the backward shift operator (equation 2.2) we get :

$$A(Z)Yt = B(Z)Ut \tag{2.40}$$

giving,

$$Y_t = \frac{B(Z)}{A(Z)}U_t \tag{2.41}$$

$$H(Z) \approx \frac{B(Z)}{A(Z)} \tag{2.42}$$

Where :

$$B(Z) = b_1 z^{-1} + b_2 z^{-2} + \ldots\ldots\ldots\ldots + b_n z^{-n} \tag{2.43}$$

$$A(Z) = 1 - a_1 z^{-1} - a_2 z^{-2} - \ldots\ldots\ldots\ldots - a_m z^{-m} \tag{2.44}$$

A(Z) and B(Z) are related to the auto regressive (AR) and moving average (MA) parts respectively. The Pade' (1982) approximation states that an infinite series can be approximated by division of two finite series (Owens, 1986). Therefore (2.42) can be written as:

$$H(Z) = h_1 z^{-1} + h_2 z^{-2} + \ldots\ldots\ldots\ldots \tag{2.45}$$

The operator H(Z) is called the transfer function of the filter. The weights h_1, h_2.....are called the pulse response function of the system.

It is noted that the equation (2.39) has the advantages of both model (2.37) and (2.38). In addition, as is stated by Box and Jenkins (1976) the ordinates of the pulse response are

directly related to the parameters of (2.39). A general equation to describe the equivalent pulse response function is :

$$h_i = a_1 h_{i-1} + a_2 h_{i-2} + \ldots\ldots\ldots\ldots + a_m h_{i-m} + b_i \qquad \text{for } i \le n$$

$$h_i = a_1 h_{i-1} + a_2 h_{i-2} + \ldots\ldots\ldots\ldots + a_m h_{i-m} \qquad \text{for } i > n \tag{2.46}$$

It can also be seen that equation (2.39) has many fewer parameters than the equivalent UH. The main shortcoming of this kind of relationship is that it uses a linear equation to explain non linear relationships between runoff and rainfall. There are a number of ways in which this can be overcome (see section 7.4).

In order to explain above mentioned formula consider the transfer function model :

$$y_t = 0.52 y_{t-1} + 0.39 u_{t-1} + 0.21 u_{t-2}$$

The pulse response is obtained by a unit input at time $t = 0$. Substituting this input into the transfer function for $t \geq 0$, the pulse response may be calculated :

at time t=0 $\quad h_0 = y_0 = 0$
t=1 $\quad h_1 = y_1 = (0.39 \times 1) = 0.39$
t=2 $\quad h_2 = y_2 = (0.52 \times 0.39) + (0.39 \times 0) + (0.21 \times 1) = 0.41$
t=3 $\quad h_3 = y_3 = (0.52 \times 0.41) + (0.39 \times 0) + (0.21 \times 0) = 0.21$
t=4 $\quad h_4 = y_4 = (0.52 \times 0.21) + (0.39 \times 0) + (0.21 \times 0) = 0.11$

thus,

$$H(Z) = 0.0 + 0.39 z^{-1} + 0.41 z^{-2} + 0.21 z^{-3} + 0.11 z^{-4} + \ldots\ldots$$

The same equation can be also obtained by :

$$H(Z) \approx \frac{B(Z)}{A(Z)} = \frac{0.39 z^{-1} + 0.21 z^{-2}}{1 - 0.52 z^{-1}}$$

It is worth mentioning that the main difference between TF models and regression models is that the error term ζ_t at time t in regression model affects only y_t not y_{t+1}. Whilst in TF the model error continues to affect the system at subsequent times. From this point of view a regression model is static regression whereas a TF model is called a dynamic regression (Olason and Watt, 1986).

Jakeman *et al.* (1990) stated that many conceptual models are special cases of the transfer function model. In the same manner Yuan (1994) developed a conceptually parametrised transfer function model from a Nash model (see section 2.4.2). The Muskingum method of flood routing is a specific case of the TF model namely autoregressive moving average, ARMA (1,1) with zero lag.

2.5.1.1 Steady state gain

In the unit hydrograph, the output volume is in balance with input volume, however, the transfer function using total rainfall has a steady state gain analogous to percentage runoff. When a constant input is applied to a transfer function model, eventually the output will also be constant. The steady-state gain is the ratio of steady output to a constant input of unit magnitude. The steady state gain can be determined directly from the model parameters as shown in equation (2.47) below :

$$SSG = cf\left[\frac{b_1 + b_2 + \ldots\ldots\ldots + b_n}{1 - (a_1 + a_2 + \ldots\ldots + a_m}\right] \tag{2.47}$$

Where cf is a unit conversion. In applying real-time updating the SSG (model percentage runoff) should reflect the variation of percentage runoff during the event. As mentioned previously the (TF) models described here relate flow to total rainfall and a factor Δ is used to compensate for variations in the proportion of rainfall contributing to runoff (see section 2.5.1.5 and 7.4). Other researchers mentioned that total rainfall can also be used in (TF) models (see for example Novotny and Zheng, 1989 and Reed, 1984).

2.5.1.2 Stability

A finite input should produce a finite output, and that the output should decay with time when there is no rainfall. This stability requirement is difficult to formulate. One primary way to express the stability is the condition shown in equation (2.48):

$$\left|\sum_{i=1}^{m} a_i\right| \leq 1.0 \tag{2.48}$$

Work by Han (1991) on physically realisable transfer functions (see section 2.5.2) showed that stability of the pulse response can be ensured if (and only if) the poles (see section 2.5.2.1) are constrained to be on the positive real axis of the Z - plane and outside the unit circle **'x'** on figure 2.13)

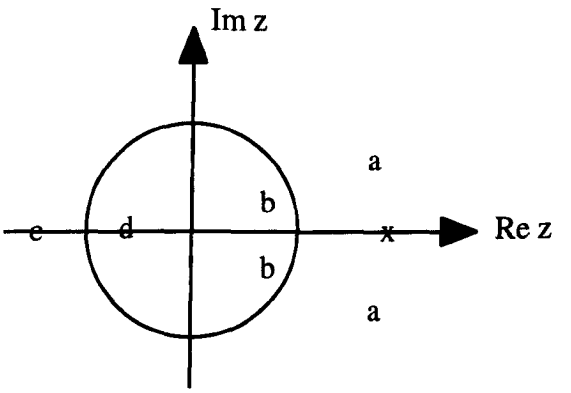

Figure 2.13- Ensuring stability of the pulse response

A pole in any other location can result in an unstable pulse response. A pole outside the unit circle, on the real axis, but negative (**'c'** in figure 2.13) results in a fluctuating pulse response. When the pole location is moved inside the unit circle, **'d'** results in a fluctuating and unstable pulse response. To avoid an unstable pulse response, there should be no complex poles (**'a'** or **'b'**) (in figure 2.13). For more detailed description of the poles and zeros on the transfer function readers should refer to Wyman *et al.*, (1989).

2.5.1.3 State-space formulation

Models given by equation (2.39) can be written as:

$$y(t) = \theta^T(t).R(t) + \zeta(t) \tag{2.49}$$

with the notation:

$$R(t) = (y(t-1), y(t-2), ..., y(t-m), u(t-1-l), u(t-2-l), \\ ....., u(t-n-l))^T \tag{2.50}$$

$$\theta(t) = (a_1(t), a_2(t), ..., a_m(t), b_1(t), b_2(t), ... b_n(t))^T \tag{2.51}$$

Superscript T stands for the transpose of a matrix. In the lack of any information regarding parameter variation, a random walk model can be selected:

$$\theta(t) = \theta(t-1) + w(t) \tag{2.52}$$

where $w(t)$ is white Gaussian noise with zero mean and covariance $R1(t)$, and is independent of $\zeta(t)$.

The above formation, Equation (2.49) and Equation (2.52) is the state space representation, Equation (2.49) is the measurement and Equation (2.51) the state equation. For a comprehensive discussion of state-space technique see for example Kamen (1987).

2.5.1.4 Identification of TF model (model structure)

In order to construct the TF model two questions first should be answered:

1) Given data as the two time series U_k, Y_k for $k=1,2,.....,N$ how can the interval of model as well as the most appropriate structure (i.e. the values of n, m and l) for the model in equation (2.39) be identified.

2) Given the model structure, how can the values of the parameters $(a_1,a_2,.....,a_m,b_1,b_2,.....b_n)$ be estimated (Young, 1986).

The first question is considered here and second question will be examined in the next section and in chapter 5.

A model interval is chosen before the model parameters can be estimated. One way to select the model interval is using the modified form of sample rules proposed by Isermann (1981), and extended to hydrological problems by Powell (1985). In order to obtain the optimum model interval, T_0, the time taken to achieve 90% of the steady state output level, T_{90} should be determined. Powell concluded that T_0 should be between $T_{90}/20$ and $T_{90}/10$. The optimal interval depends on catchment response dynamics and the characteristics of the event, and will consequently vary from catchment to catchment, and even from event to event. Using too small an interval will result in overparameterisation whilst too large an interval will result in too few parameters.

The choice of the most appropriate order is difficult and as mentioned by Tsang *et al.* (1995) it is possible that the 'best' model order obtained during the calibration phase is not suitable for the forecasting phase.

There are several methods which can be used to identify the model order and the time delay of the system, including using the cross-correlation function between input and

output data, Akaike's method (Akaike, 1970), the F-test (Norton, 1986), and Pole-Zero cancellation (Unbehauauen and Gohring, 1974). Owens (1986) reviewed all these methods and suggested the search method described below. Further, Young (see for example Young, 1986) developed a method based on the coefficient of determination (R_T^2) and the error variance. However, the best model in terms of (R_T^2) will generally be of very large order and error variance is less sensitive to under-parameterisation.

The following search technique is a combination of objective statistical criteria and subjective interpretation with physical (hydrological) meaning. The technique is the equal model order search commencing at $n=m=1$. In the search, parameters are sequentially estimated for a 1,1 model then a 2,2 model and so on (usually less than 8) until an increase in model order no longer results in a significant improvement in model accuracy. Once the optimum equal model has been identified, the number of *a* and *b* parameters can be varied and the effect on the model pulse response examined.

It is noted that total reliance on objective statistics is undesirable and should be avoided. Instead, in order to select the best model order a number of complementary evaluation criteria are used including:

- error statistics for the model convolution of the calibration data, together with visual evaluation of simulated and observed flow.
- model pulse response. (The pulse should be 'physically reasonable', that is, a relatively smooth curve without negative ordinates. Oscillations should not be apparent in the pulse response since they indicate over-parameterisation. The pulse response must be also stable.)
- parameter redundancy, that is higher order parameters with small values indicate that a lower model may be adequate.

It is noted that the rainfall parameters largely determine the time and the magnitude of the pulse response peak. The number of *b* parameters (*n)* is approximately the number of time units to the peak of the response. The flow parameters control the response shape, *m* influencing the shape of the rising limb of the hydrograph less than recession part (Collier, 1994). Usually *m* is less than or equal to *n* (Owens, 1986).

2.5.1.5 Parameter estimation and real-time updating

Numerical estimation of model parameters has been extensively researched over the last few decades and is undergoing continued development with existing and new techniques such as Genetic algorithms, and Neural networks. A detailed and comprehensive review

of parameter estimation techniques and their advantages and disadvantages are presented in chapter 5.

Percentage runoff usually varies through the duration of an event, and a model should be able to simulate this. In an attempt to match the percentage runoff (as represented by the model SSG) to the current event percentage runoff, Owens (1986) suggested a rainfall component scaling factor Δ. The form of TF model including the on-line updating is:

$$\hat{y}_t = a_1 y_{t-1} + a_2 y_{t-2} + ... + a_m y_{t-m} + \Delta\left[b_1 u_{t-l-1} + b_2 u_{t-l-2} + ... + b_n u_{t-l-n}\right] \tag{2.53}$$

One-step ahead forecast errors are used to update Δ. Problems arising from the use of Δ along with a full description of different updating procedures are presented in chapter 7.

2.5.2 Physical realisable TF model (PRTF)

Han (1991) developed a 'physically realisable' TF model. This model is a refinement of the basic TF model structure which combines guaranteed stability with improved and more powerful updating characteristics. The PRTF model is introduced in the following sub-sections.

2.5.2.1 Identification of PRTF model

Equation (2.42) can be shown as a cascade factorisation as:

$$H(z) = B(z) \times \frac{1}{A(z)} \tag{2.54}$$

The pulse response function of TF model can then be derived from two parts $B(Z)$ and $\frac{1}{A(z)}$.

Rational functions can provide good approximations to polynomials (see for example Poularikas and Seely, 1991), therefore, the second part of equation (2.54), $\frac{1}{A(z)}$ can be written as:

$$\frac{1}{A(z)} = \frac{(-1)^N \prod_{i=1}^{K} (\beta_i)^{m_i}}{\prod_{i=1}^{K} (z^{-1} - \beta_i)^{m_i}} \tag{2.55}$$

where β is pole location and N is a positive integer representing the total number of poles and m_i is the pole order.

A simplified form of equation (2.55) for the practical use when it is supposed that only one pole is used can be written as:

$$\frac{1}{A(z)} = \frac{(-\beta)^N}{(z^{-1} - \beta)^N} = \frac{z^N}{(z - \frac{1}{\beta})^N} = \frac{1}{S(z^{-1} - \beta)^N} \tag{2.56}$$

where $S = \frac{1}{(-\beta)^N}$

The denominator of equation (2.56) can be extended as:

$$S(z^{-1} - \beta)^N = S\{(z^{-1})^N + N(z^{-1})^{N-1}(-\beta) + \frac{N(N-1)}{2!}(Z^{-1})^{N-2} \times (-\beta)^2 + \ldots$$
$$+ \frac{N(N-1)....[N-(K-1)]}{K!}(-\beta)^K (z^{-1})^{N-K} + ...\} \tag{2.57}$$

The general form of the coefficient of equation (2.57) can be written as:

$$C_n^k = \frac{N(N-1)(N-2).....[N-(K-1)]}{K!} \tag{2.58}$$

The following expressions can be written using equations (2.44), (2.57) and (2.58):

$$S\{\frac{N(N-1)....[N-(K-1)]}{K!}(-\beta)^K\} = S \times C_N^K \times (-\beta)^K = -a_{N-K} \tag{2.59}$$

$$a_i = -S \times c_N^{N-i} \times (-\beta)^{N-i} = -\frac{1}{(-\beta)^N} \times c_N^{N-i} \times (-\beta)^{N-i} = -c_N^{N-i} \times (-\beta)^{-i} \tag{2.60}$$

The pulse response of $\frac{1}{A(z)}$ can then be computed using inverse Z transform of equation (2.56), that is for N=1,

$$\frac{Z}{Z-\frac{1}{\beta}} \Rightarrow h(t) = (\frac{1}{\beta})^t \tag{2.61}$$

where t=1,2,.....

and for N ≥ 2,

$$\frac{Z^N}{(Z-\frac{1}{\beta})^N} \Rightarrow h(t) = \frac{(N-1+t)(N-2+t).....(1+t)}{(N-1)!}(\frac{1}{\beta})^t \tag{2.62}$$

The peak of $h(t)$ can be derived as:

$$\frac{dh(t)}{dt} = 0 \tag{2.63}$$

so for N=2,

$$t_{peak} = \frac{1}{Ln\beta} - 1 \tag{2.64}$$

and if the peak time is given, a desirable β will be:

$$\beta = e^{\frac{1}{t_{peak}+1}} \tag{2.65}$$

For N=3,

$$t_{peak} = \frac{\frac{2}{Ln\beta} - 3 + \sqrt{\left(3 - \frac{2}{Ln\beta}\right)^2 - 4\left(2 - \frac{3}{Ln\beta}\right)}}{2} \tag{2.66}$$

and if the peak time is given, a desirable β will be:

$$\beta = e^{\frac{2t_{peak}+3}{(t^2_{peak}+3t_{peak}+2)}} \tag{2.67}$$

The first part of equation (2.54), $B(Z)$ is related to b_i parameters determined using a Recursive Least Squares (RLS) technique (see section 5.3).

Identification of the PRTF model is straightforward using the equations introduced above. The steps involved can be summarised as following:

1-determine the model order: i.e. the number of a and b parameters (m, n).

2-estimate the initial time to peak t_{peak}.

3-compute β from t_{peak} using equations (2.65) or (2.67) according to the number of a parameters.

4-estimate $a_{(i)}$ from equation (2.60).

5-estimate $b_{(i)}$ using the least squares technique.

6-compute residual error.

7-determine the new t_{peak} according to error.

8-go to 3.

The whole procedure is repeated until the desired results are obtained. The procedure is illustrated by the flowchart in figure (2.14).

2.5.2.2 Modification of PRTF model parameters (dynamic PRTF)

In the real-time operation of a hydrological model, simulated runoff generally differs from the measured runoff. Thus, on-line updating of the model can be used to improve

subsequent forecasts. Catchment hydrograph response variation may be divided into three main types: variations related to volume α, time to peak-shape γ and time delay-τ. The forecasting errors caused by these are summarised in figure (2.15).

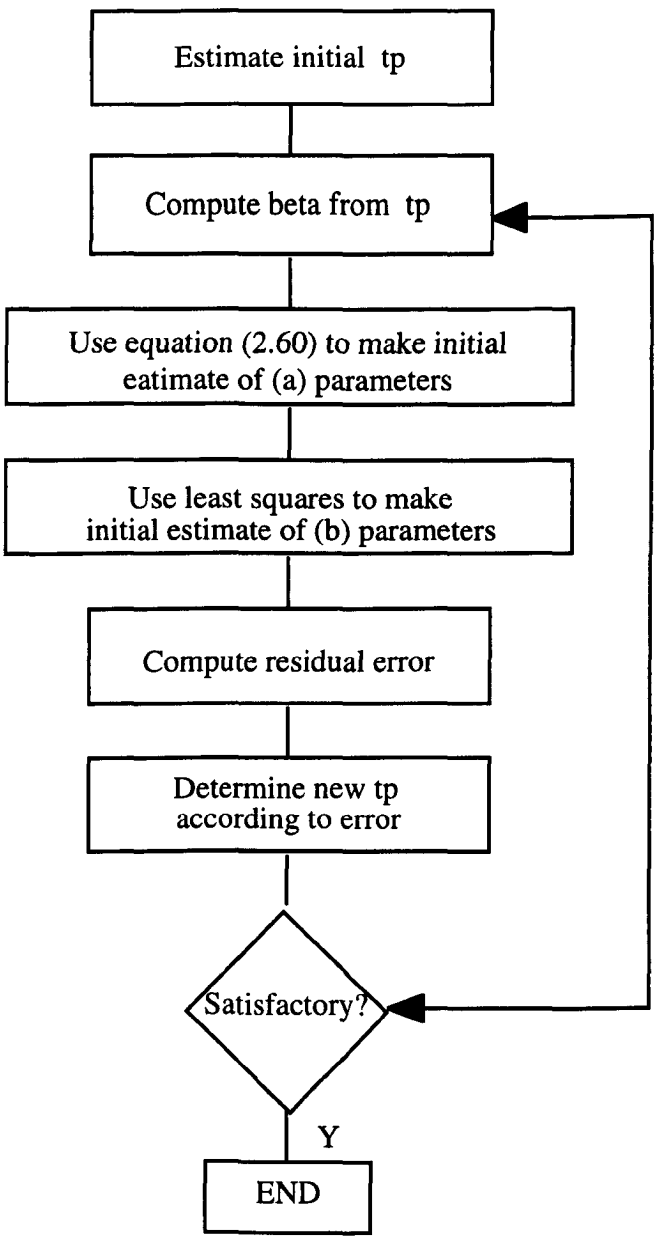

Figure (2.14) Flowchart for model parameter identification (adapted from Han, 1991)

It can be seen that each factor only influences one aspect of the model. Generally speaking, the pulse response *H(Z)* of a PRTF model could be written as:

$$H(z) = f(\alpha,\gamma,\tau,z) \tag{2.68}$$

and the adaptive form of the PRTF model as:

$$Q(t) = \sum_{i=1}^{n} A_i Q(t-i) + \sum_{i=0}^{q} B_i P(t-i) \tag{2.69}$$

It is noted that the model parameters a_i and b_i have been replaced by A_i and B_i as the adaptive model will keep changing its parameters. Q and P are runoff and rainfall respectively.

To include the volume factor, all the b_i parameters are multiplied with a constant factor $(1+\alpha)$, where α is the percentage of volume change. This means that A_i will not be changed but B_i will be changed according to:

$$B_i = (1+\alpha)b_i \tag{2.70}$$

A straightforward way to change the pulse response shape is to replace t_{peak} by $t_{peaknew}$ in equation (2.60). However, one problem here is that the γ factor also alters the volume of the pulse response and thereby conflicts with the α factor. Consequently, it is also necessary to modify the B_i parameters at the same time in order to preserve the original pulse area and hence the mass balance of the system by applying the proportionality of areas:

$$area1 = \frac{1}{(1-\frac{1}{\beta})^N} \tag{2.71}$$

$$area2 = \frac{1}{(1-\frac{1}{\beta_{new}})^N} \tag{2.72}$$

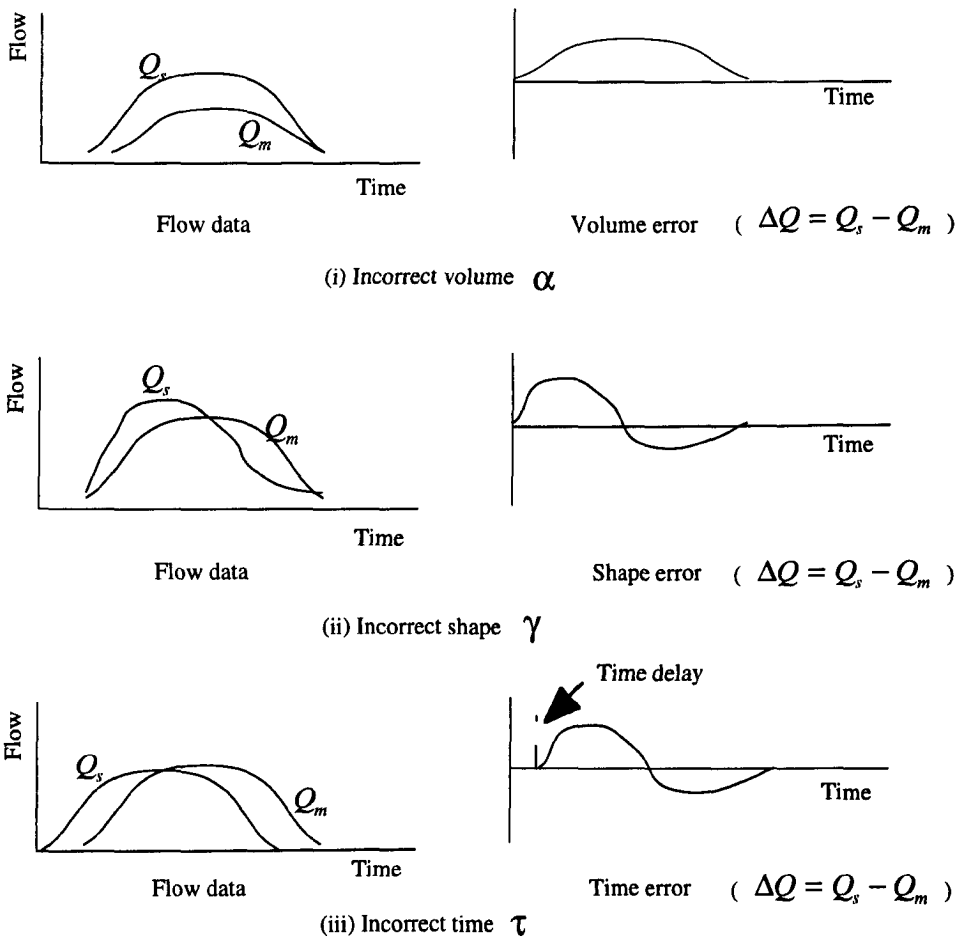

Figure (2.15) TF simulation error by incorrect volume, shape and time (after Han, 1991)

Therefore B_i will be:

$$B_i = (1+\alpha)\frac{area1}{area2}b_i = (1+\alpha)\left[\frac{1-\frac{1}{\beta}}{1-\frac{1}{\beta_{new}}}\right]^N b_i \tag{2.73}$$

The pulse response time of the PRTF model can be simply adjusted by a time shift operator applied to the rainfall terms.

The final form of the adjustable PRTF will be :

$$Q(t) = \sum_{i=1}^{n} A_i Q(t-i) + \sum_{i=0}^{q} B_i P(t-\tau-i) \tag{2.74}$$

$$B_i = \left[\frac{1-\frac{1}{\beta}}{1-\frac{1}{\beta_{new}}} \right]^N (1+\alpha) b_i \tag{2.75}$$

$$A_i = -C_N^{N-i} (-\beta_{new})^{-i} \tag{2.76}$$

Using the above equations and least square techniques, determination of the adjustment factors can be summarised as:

1.-estimate the time delay-suppose an initial time delay, compute simulation error, change time delay and repeat the procedure.

2.-estimate the shape adjustment factor-suppose an initial shape factor, compute simulation error, change shape factor and repeat the procedure as far necessary.

3.-estimate the volume adjustment factor-determine an initial volume factor, compute simulation error, change volume factor and repeat the procedure as necessary.

4.-suppose time delay=0 , go to 1 and repeat the whole procedure two more times.

For more detailed description of the PRTF model readers should refer to Cluckie and Han (1996 a, b, and c).

2.6 Summary

This chapter has presented a general literature review of flood forecasting models, with particular emphasis on the WMO simulated real-time inter-comparison of hydrological models. The basic structure and operational characteristics of the models has been presented in order to provide a foundation for the further improvement of them. Since so many models exist, it is impossible to investigate all of them in detail. Instead, a classification of flood forecasting models has been presented along with a relatively detailed introduction of those models used in the WMO project.

The chapter began with a description of the criteria which may be used to classify flow forecasting models, followed by an introduction to flood routing and rainfall-runoff

models. Different procedures of effective rainfall calculation have been presented illustrating their relative complexity and suggesting why total rainfall is frequently used for real-time applications. Parameters affecting the choice of a suitable model have then been outlined. The chapter continued by introducing different aspects of the WMO project including perspectives, objectives, and performance assessment together with details of the fourteen conceptual flood forecasting models which participated at the workshop.

Finally, transfer function models which are dominant in this thesis have been introduced in detail including their mathematical theory, structure, identification, as well as their advantages and limitations. The transfer function model is a flexible and versatile tool for real-time flood forecasting. It has a simple structure and only requires rainfall and flow data for modelling. TF models are readily updated in real-time and generate acceptable estimates of future discharge. To use the TF techniques detailed understanding of the hydrological system is not necessary.

CHAPTER 3

TRANSFER FUNCTION AND WMO PROJECT MODELS' RESULTS

3.1 Introduction

This chapter presents the results of an extended inter-comparison of real-time flood forecasting models, with particular emphasis on transfer function models. Reed (1984) stated that for assessment of different flood forecasting models, the following points might be considered :

1) different approaches e.g. unit hydrograph, non-linear storage, transfer function and conceptual models.
2) different real-time updating methods.
3) different data sets and catchments.
4) different criteria for model assessment.

In addition, different rainfall forecasting methods and rainfall separation procedures should also be included. Items 1 to 4 of the above list are more or less considered in the present comparison.

Chiew *et al.*, (1993) pointed out that only a few references can be found in literature regarding the comparison of flood forecasting models. They conducted a comparison of six rainfall-runoff modelling approaches to eight catchments throughout Australia which was limited to annual, monthly, and daily flows.

This chapter initially describes the data sets, catchments and assessment criteria applied at the WMO inter-comparison project (and used throughout this thesis). A comparative analysis is then presented whereby the forecasting results of average TF models both in static and dynamic form are assessed by direct comparison with results from the WMO project models. In addition, new techniques for objective comparison are included such as; the randomness-dispersion diagram, and an attempt is made to rank the flood forecasting models, both on an event basis and overall.

3.2 Data sets and catchments

A meeting of experts selected three river catchments from climatologically and geographically varied conditions in three countries. These were Bird Creek, Illecillewaet and Orgeval. The first two basins were chosen because of modellers' experiences with the catchments through previous inter-comparison projects, whilst the later was selected because it is a small fast-response catchment with a good historic data archive. For the purposes of present study both Bird Creek and Orgeval catchments have been considered. The Illecillewaet is disconsidered because the prodominant type is snowmelt which does not include in the TF models.

3.2.1 Bird Creek catchment

The Bird Creek catchment covers an area of 2344 km^2 and is located in Oklahoma (USA) close to the northern State border with Kansas. The outlet of the basin is near Sperry almost ten kilometres north of Tulsa. The catchment is relatively low lying with altitudes ranging from 175m up to 390m above mean sea level at the highest point in the catchment. There are no mountains or large water surfaces to influence local climatic conditions. Some twenty percent of catchment surface is covered by forest whilst the main vegetative cover is grass land. The storage capacities of the soils is very high (Georgakakos and Smith, 1990). The river basin and stream network is shown in figure (3.1).

The catchment receives significant rainfall in most years, and the catchment can be classified as humid although extended periods with very low rainfall can occur. Well defined rainy seasons occur in the spring and summer with rain in the form of showers and thundershowers of convective origin. Snowfall remains on the ground for only a very short time. From the latter part of July to September air temperatures are high (38 °C is common) and as a result significant evapotranspiration occurs during this time. At the same time, relative humidity is low accompanied and southerly breezes are common (Georgakakos *et al*, 1988).

The data set consists of two distinct periods : a calibration period and a verification period. Both comprised of 6-hour values of mean areal precipitation, daily values of mean areal potential evaporation, and 6-hour and daily values of outflow discharge. The rainfall data were derived from a spatial average of 12 rain gauges situated in the catchment area or outside the basin boundaries (see figure 3.1). Five of the stations were hourly recording gauges. The discharge values were obtained from a continuous stage recorder.

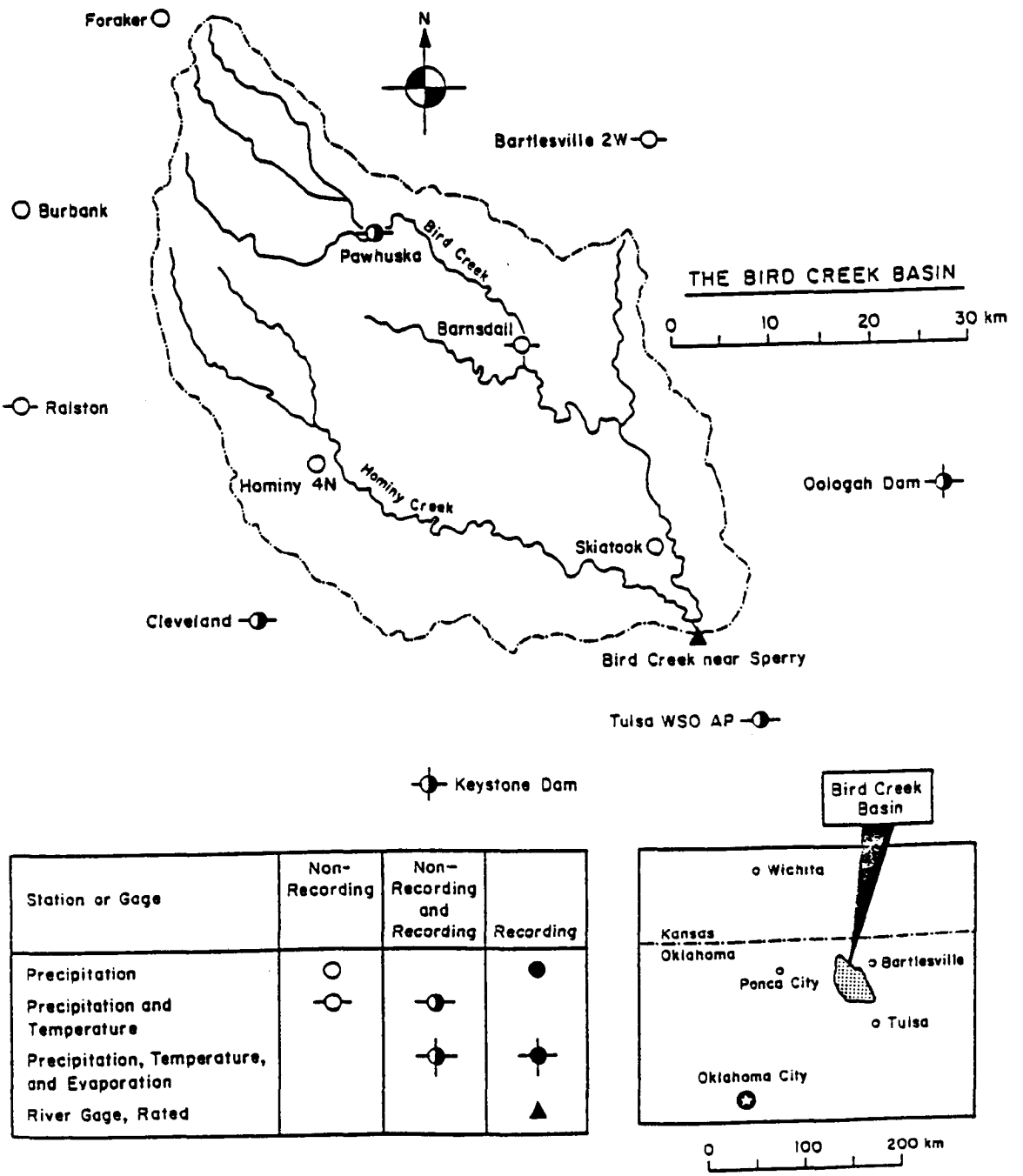

Figure (3.1) The Bird Creek drainage basin (source Georgakakos *et al.*, 1988)

The period used for model calibration spanned the eight-years from October 1955 to September 1963, with an additional independent verification period of data from November 1972 to November 1974. Six hour discharge values were only available for high flow periods while daily discharge values were available for the whole period. During the calibration period the discharge at the basin outlet ranged from 0 to 2540 m^3/sec and the rainfall to 153.8 mm/day and 88.6 mm/6-hour (6.4 mm/hr and 14.8 mm/hr respectively). The highest recorded discharge and rainfall during the verification period were 1506 m^3s^{-1} and 38.2 mm/6-hour (6.4 mm/hr) respectively.

3.2.2 Orgeval catchment

The Orgeval basin is situated 40 km east of Paris in France and is a secondary tributary of the Marne river having first joined the right bank of the Grand Morin river. The drainage area of the Orgeval basin is approximately 104 km^2. The catchment is almost entirely rural, with only one percent of the total surface area being occupied by urban areas and roads. The catchment elevation varies from 70 m at the outflow point to approximately 182 m above mean sea level at the highest point in the catchment. The average elevation is around 148m with the elevation decreasing sharply below 130 m. The land use is mainly arable with 18% forest cover. Approximately 50 percent of the area is suitable for ploughing and for growing crops and has been artificially drained. Because of low permeability the ground water table is very close to the ground surface during wet periods and follows the topography (Askew, 1989). The river basin and stream network is shown in figure (3.2).

The calibration and verification data composed of hourly values of mean areal precipitation and hourly-averaged discharge. The rainfall consisted of a spatial average of three rainfall recording stations (see figure 3.2) situated at elevations of 130m, 146m, and 174m. The periods used for model calibration were the six-years period from October 1972 to September 1978, while the verification events were in the period from December 1978 through July 1980. The hourly-averaged discharge during the calibration period varies up to 21m^3s^{-1}. During this period the highest hourly averaged rainfall was 11.4 mm. The highest hourly averaged discharge and rainfall of the verification period were about 29 m^3/sec and 10.4 mm/hour respectively.

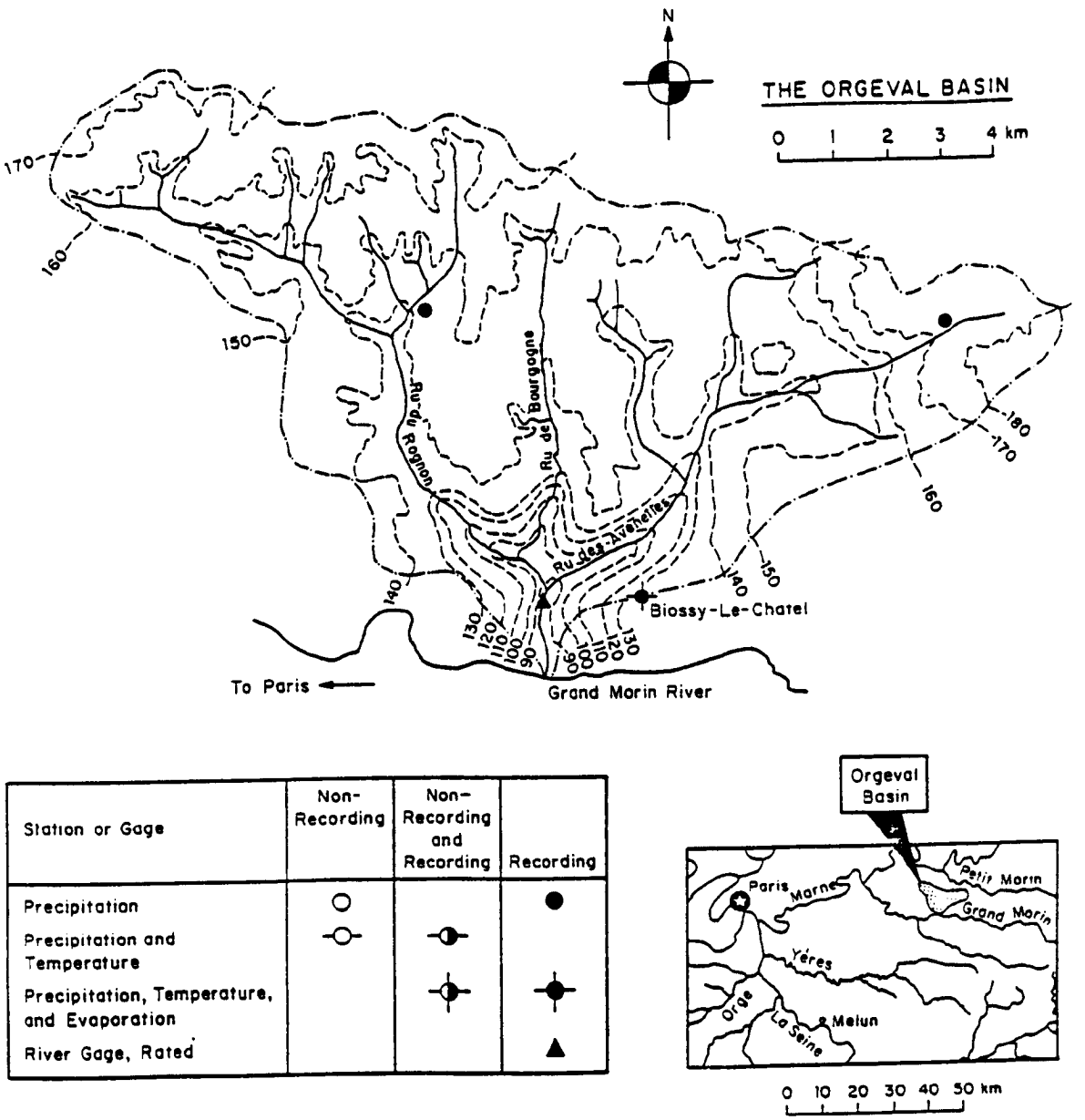

Figure (3.2) The Orgeval drainage basin (source Georgakakos *et al.*, 1988)

3.2.3 Summary information of the catchments

Table (3.1) summaries some of more important characteristics of catchments.

Table (3.1) Summary description of the catchments and data sets

Catchment	Bird Creek	Orgeval
Country	United States	France
Catchment area	2344 km^2	104 km^2
Data interval	1 day	1 hour
Forecast lead time	4 days	9 hours
Forecast prepared	every day	every 3 hours
Predominant type	Rainfall	Rainfall
Flow threshold	262 m^3s^{-1}	12 m^3s^{-1}
Climate	moderate	humid
Topography	Rolling terrain	Flat
Vegetation	Grassland (app. 80%) and forest	Arable (app. 80%) and forest (18%)

3.3 Criteria for model comparison

There are several criteria that can be used to measure model performance and it is not reasonable to use a single measure to judge the performance of a flood forecasting system (Nemec, 1986). Whilst model may forecast peak flows satisfactorily, it may be poor in forecasting low flows. A model may be able to predict flow over longer time periods adequately, but it may not be able to simulate daily streamflows satisfactorily. In fact the criterion chosen depends on the purpose of modelling. A meeting of WMO experts was held to select a range of assessment criteria. It was agreed that the criteria should be most appropriate for testing the ability of a model to provide accurate and timely forecasts of floods, including for the purpose of updating. The Root Mean Square Error (the differences between forecasted and recorded flow) (RMSE) was selected to assess the forecast results. The criteria has the advantage of simplicity and ease of comprehension. Furthermore, it is one of the most commonly used criteria for analysis of forecasting residuals. The criterion puts more weight on large discharges and is useful in reflecting the ability of the models to estimate catchment yields. Probably the major drawback of this criteria is that its dimensionality renders it unsuitable for comparing the forecasting performance of different models with different dimensions, catchments or record lengths. It is noted that RMSE results used along with graphical displays allow a better assessment

of a model's performance. For the purpose of the project the RMSE can be formulated according to :

$$RMSE_n = \left[1/N \sum_{j=1}^{N} (\hat{y}_{n,j} - y_{n,j})^2 \right]^{0.5} \quad (3.1)$$

Where:
n is the lead time;
N is the number of forecasts made, j=1,2,.....,7;
$\hat{Y}_{n,j}$ is the forecasted flow for lead time n for forecast j;
$Y_{n,j}$ is the actual observed flow for lead time n for forecast j;
k is the maximum forecast lead time; and
J is the number of the forecast.

Hence, for each model and each event, $RMSE_1$, ..., $RMSE_j$, ..., $RMSE_k$ were computed. A perfect model will produce an RMSE of zero.

For the purpose of comparison of performance of the *TF* model in this thesis a randomness-dispersion diagram is used in addition to RMSE. The randomness-dispersion diagram (Cavadis and Morindate) is a novel and relatively little used method to evaluate model performance. Here model performance is assessed on the basis of the magnitude and the auto-correlation of the forecast errors. This method is thereby able to consider simultaneously both forecast error properties through the same visual image.

The ordinate of the diagram is the ratio of portmanteau statistic Q (Box and Jenkins, 1976; also Appendix 1) to critical chi-squared (λ^2) value. This ratio is an indicator of the 'randomness' of the forecast error. A value of zero means total randomness whilst a value greater than unity indicates that the auto-correlation of the error for a given confidence level is bigger than zero, the errors are not random and hence the model performance is sub-optimal. Consequently the model may be inappropriate for the data.

The NTD is a variance statistic used to evaluate the magnitude of the forecast errors. A normalising function obtained from a 'naive' model (i.e. flow forecasted for time $t+1$ equals flow observed at time t) is included, thereby providing the ability to compare the performance of the model under evaluation with a naive model. An ideal value is one and a negative value shows that the performance of naive model is better than the model under evaluation. A comprehensive description of the technique along with an example are presented in Appendix 1.

3.4 Procedures of the forecasting adopted

In order to make unbiased assessments of the real-time performance of the models, it is necessary to select individual flood events not used in calibration. For each catchment, six flood events were selected to test the real-time performance of each model. Different scenarios related to future meteorological input, in particular precipitation were considered including perfect foresight, no future precipitation, and average seasonal conditions. Due to difficulties in logically defining the later two scenarios and interpreting the results, perfect foresight of rainfall was used as the future input variable.

Seven forecasts were prepared for each event with a lead time (Tf in figure 3.3) for Bird Creek daily data and for Orgeval hourly data of four days and nine hours respectively. A schematic presentation of procedures applied in real-time forecasting workshop is provided in figure (3.3).

During the simulated real-time test, in order to let the model operators establish initial conditions for the event, precipitation and other input data as well as observed discharge data until the beginning of the day's test event (time $t0$) were disseminated. Furthermore, only input data including precipitation were distributed until the end of the forecast lead time Tf and with forecasts being made by the modellers. Once the forecasts had been submitted to the workshop moderator, another batch of input data were provided up to the end of the next current forecast lead time, that is $T0+T_u+Tf$, starting from $T0+T_u$ where T_u is the state update of one day and three hours for Bird Creek and Orgeval respectively. Along with the input data the observed discharge data for period $T0$, $T0+T_u$ was given, therefore enabling state updates to be made up to and including time $T0+T_u$. Then forecasts were be made for the second forecast period $T0+T_u$, $T0+T_u+Tf$ and so on (WMO, 1992 and Georgakakos and Smith, 1990 and Georgakakos *et al*, 1988).

The graphical results of seven forecasts were presented as shown in figure (3.4) (Orgeval basin). The solid line shows observed discharge data and the shorter lines indicate the results for forecasts made at specific times during the event. For example, the line with the open square is the fourth forecast made at hour 10 for hours 11-20. The last observed discharge value for this forecast was for hour 10 and precipitation data were available to hour 20. A similar presentation of results for each of the six events are provided by each model. The same approach is applied to transfer function models.

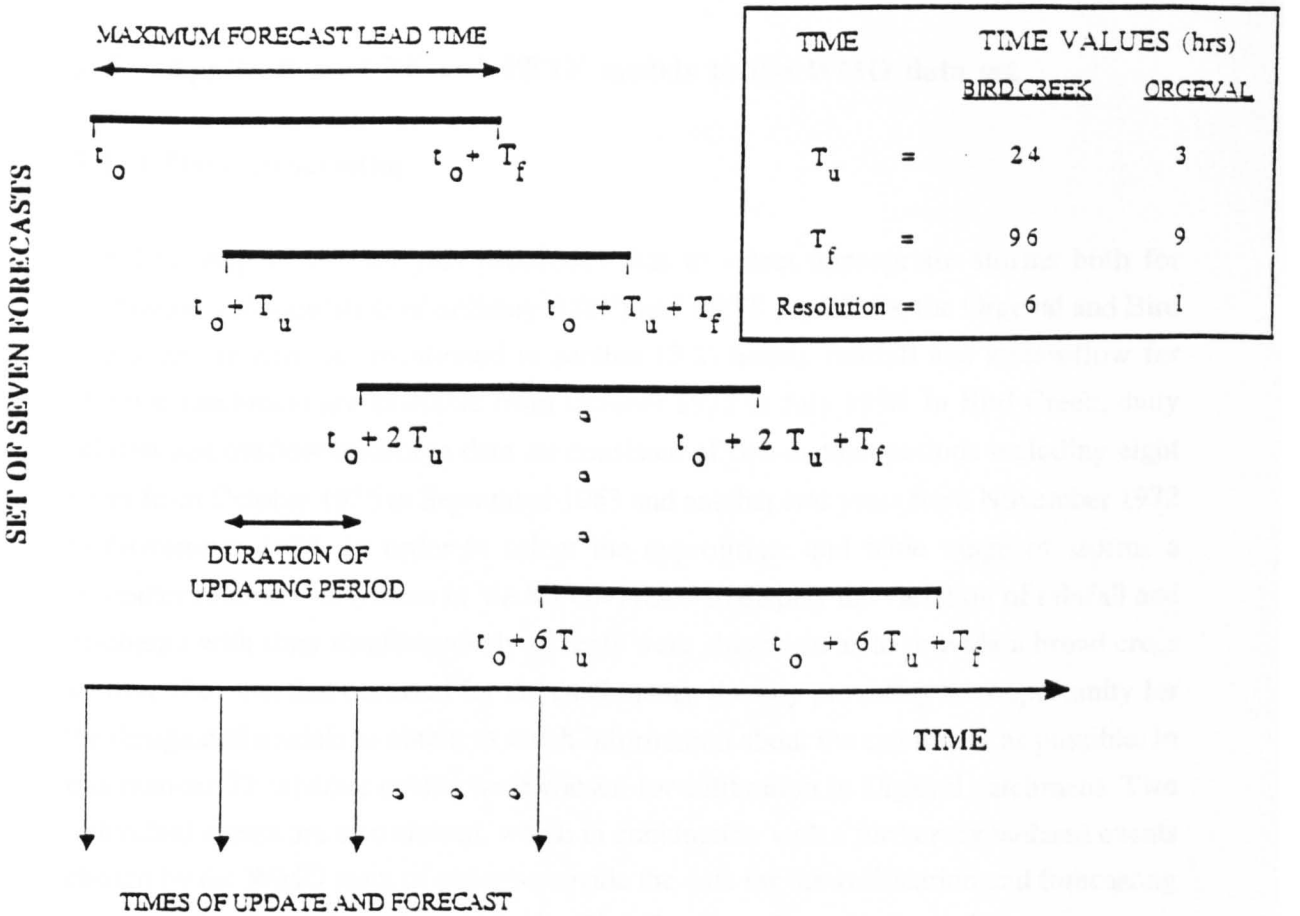

Figure (3.3) Characteristic times in the updating-forecasting sequence for a typical verification event (adapted from Georgakakos *et al.*, 1988)

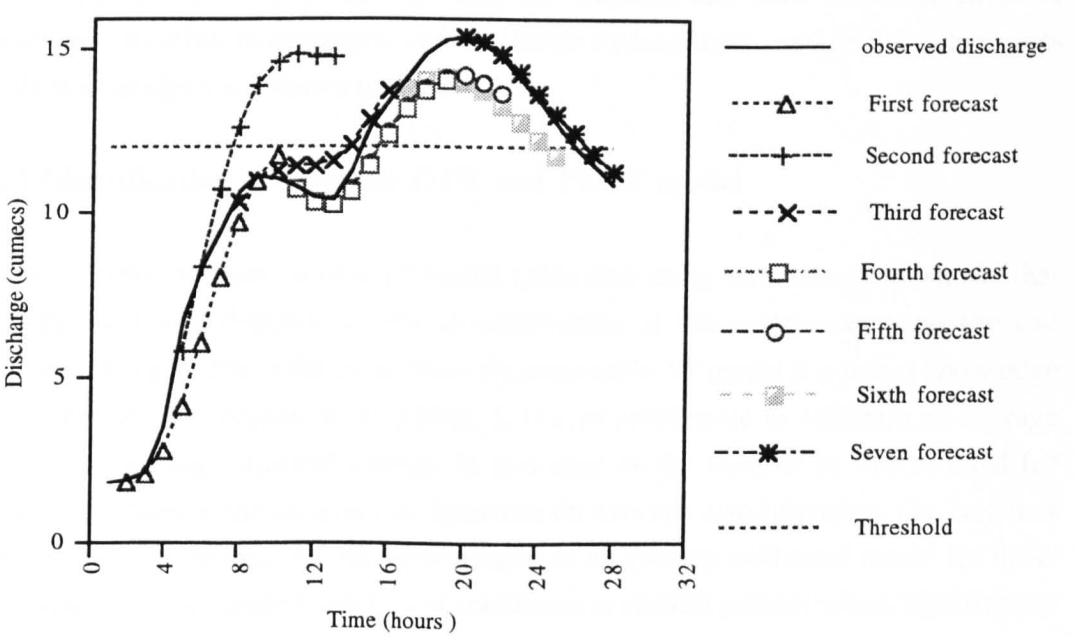

Figure (3.4) Seven multiple step ahead forecasts for a typical verification event (Orgeval catchment).

3.5 Application of TF and PRTF models to the WMO data set

3.5.1 Data processing

The first step in the analysis procedure was to select appropriate storms both for calibration and validation of ordinary (OTF) and PRTF models for the Orgeval and Bird Creek catchments. As mentioned in section (3.2) hourly rainfall and streamflow for Orgeval catchment are available from October 1972 to July 1980. In Bird Creek, daily rainfall and outflow discharge data set consisted of two distinct periods including eight years from October 1955 to September 1963 and another two years from November 1972 to November 1974. In order to select the appropriate and wide range of storms a computer routine was written in VAX FORTRAN to display the variation of rainfall and discharge with time simultaneously. Events were chosen so as to provide a broad cross section of events that occurred for the catchments, thereby providing the opportunity for the designated models to obtain as much information about the catchment as possible. In this manner 32 separate events were chosen for calibration in Orgeval catchment. Two individual events are also chosen, which in conjunction with a further six isolated events chosen by the WMO team of experts provide the data for the verification and forecasting phases in the Orgeval catchment. In the Bird Creek catchment, six notable storm events were selected from the available data for model calibration with a further six independent events for validation and forecasting. The main characteristics of each event are summarised in the tables (3.2) and (3.3) for Orgeval and Bird Creek catchments respectively. Rainfall hyetographs and discharge hydrographs used in the catchments rainfall-flow analysis are shown in Appendix 2.

3.5.2 Identification of average OTF and PRTF model

The pulse response function of a TF model calibrated using only one event shows that catchment response depends on the characteristics of the storm event and the soil conditions. It is possible to define a relatively reasonable TF model if *a priori* knowledge of the event and catchment are available. It is also practicable to calibrate an average model from several historical events. In this case as the number of events used for calibration increases, the accuracy of forecasts on average also improves. On the other hand, it should be stressed that the performance of an average calibrated model for those events which have antecedent catchment conditions or rainfall profiles which significantly differ from the 'norm', falls. Owens (1986) found an average pulse response can be obtained from a sequence of storm events which cover a range of storm type. A similar approach has also been used by other researchers (see for example Wilke and Barth, 1991).

Table (3.2) Main specification of the events studied, Orgeval catchment

Event no.	Start time	End time	Duration (hours)	Maximum rainfall (mm/hour)	Peak flow (cumecs)	Average percentage runoff
	Calibration					
1	01:05/11/73	09:06/11/73	33	7.8	1.5	3.3
2	10:07/12/73	09:09/12/73	48	1.9	2.0	16.9
3	03:13/12/73	07:15/12/73	53	1.2	1.2	19.7
4	19:21/12/73	11:26/12/73	113	2.3	3.5	27.7
5	15:08/01/74	11:11/01/74	69	3.9	4.5	25.8
6	13:28/01/74	21:30/01/74	57	2.5	5.4	26.8
7	06:05/02/74	06:07/02/74	49	2.0	3.7	29.4
8	15:15/03/74	23:22/03/74	177	3.5	6.5	42.0
9	19:18/10/74	13:21/10/74	67	2.8	3.2	13.0
10	01:23/10/74	13:24/10/74	37	1.9	5.0	19.4
11	16:03/11/74	22:04/11/74	31	1.5	1.1	7.6
12	23:21/11/74	19:24/11/74	69	1.3	1.8	24.6
13	13:16/12/74	08:19/12/74	68	1.1	3.7	38.1
14	07:27/12/74	05:29/12/74	47	2.3	2.3	25.5
15	19:07/01/75	08:09/01/75	38	2.1	3.9	24.6
16	14:22/01/75	01:24/01/75	36	1.0	3.1	31.6
17	07:25/01/75	13:26/01/75	31	1.2	2.6	23.9
18	06:27/01/75	14:29/01/75	57	1.6	5.8	39.3
19	06:11/01/78	17:13/01/78	60	3.3	4.7	30.3
20	17:23/01/78	04:26/01/78	60	2.0	11.9	53.9
21	05:28/01/78	24:30/01/78	68	1.4	2.6	21.4
22	18:31/01/78	04:04/02/78	83	2.9	11.7	59.8
23	05:07/02/78	09:08/02/78	29	2.4	3.4	25.3
24	04:16/03/78	14:17/03/78	35	3.6	6.3	31.8
25	18:19/03/78	15:22/03/78	70	3.2	19.5	55.4
26	23:29/03/78	13:31/03/78	39	3.1	9.4	34.7
27	01:19/02/77	17:21/02/77	65	5.1	10.2	36.6
28	24:19/03/75	24:09/04/75	494	1.8	2.8	30.4
29	17:06/05/75	24:12/05/75	152	3.6	5.0	15.4
30	20:29/09/75	24:03/10/75	101	8.0	4.7	12.2
31	21:02/04/77	24:08/04/77	148	3.6	6.0	33.6
32	22:09/05/77	08:15/05/77	120	2.4	3.9	21.0
33	04:11/12/74	19:13/12/74	64	1.2	1.6	20.8
Average	-	-	-	-	-	27.9
	Verification					
1 (wmo1)	01:31/12/78	04:01/01/79	28	4.6	9.5	20.4
2 (wmo2)	01:02/02/79	04:03/02/79	28	1.8	6.4	51.1
3 (wmo3)	10:10/03/79	13:11/03/79	28	1.9	7.5	27.7
4 (wmo4)	11:13/03/80	14:14/03/80	28	3.4	24.4	52.7
5 (wmo5)	17:13/07/80	20:14/12/80	28	10.4	15.0	16.7
6 (wmo6)	10:20/07/80	19:21/05/80	28	5.7	13.6	30.8
7 (v1)	17:15/11/73	11:17/11/73	43	4.4	2.4	11.9
8 (v2)	04:30/11/74	23:01/12/74	44	0.9	3.0	28.4
Average	-	-	-	-	-	30.0

Table (3.3) Main specification of the events studied, Bird Creek catchment

Event no.	Start time	End time	Duration (days)	Maximum rainfall (mm/day)	Peak flow (cumecs)	Average percentage runoff
	Calibration					
1	24/09/59	09/10/59	16	153.8	1731.1	49.5
2	30/04/61	14/05/61	15	50.5	491.8	51.5
3	12/07/61	25/07/61	14	51.3	499.2	31.1
4	11/08/61	19/08/61	9	64.8	440.8	29.4
5	03/09/61	06/09/61	4	65.7	186.0	16.6
6	11/09/61	16/09/61	6	65.3	741.9	59.6
Average	-	-	-	-	-	39.6
	Verification					
1	11/11/72	21/11/72	11	52.1	316.7	39.9
2	03/03/73	13/03/73	11	34.8	332.1	56.8
3	09/04/73	19/04/73	11	57.3	527.7	56.4
4	19/11/73	29/11/73	11	59.6	435.2	43.9
5	07/03/74	17/03/74	11	87.8	1103.1	72.3
6	28/10/74	07/11/74	11	63.3	1287.3	71.2
Average	-	-	-	-	-	56.8

In the WMO workshop a model interval of one hour and one day were selected for Orgeval and Bird Creek catchments respectively. The same model intervals are also used for the present study.

In order to construct an average static TF model for the Orgeval catchment, the search procedure described in section (2.5.1.4) was used. Eight equal order models were considered in the search, from 1,1 to 8,8. The model parameters, model percentage runoff, root mean square error (RMSE), and pulse response characteristics of each structure in each selected event, were considered. The search indicated a 3,3,0 model structure to be the optimum equal order model. The model order reduction technique was then used to reduce the order of the model. The number of a and b parameters were reduced from 3 down to 1. This procedure again confirmed a 3,3,0 structure to be optimal for almost all the events considered. Therefore it is concluded that for the Orgeval catchment a model with (3,3,0) structure is most appropriate.

Some statistical characteristics of the model identification procedure for the Orgeval catchment TF model are presented in table (3.4). Only the pulse responses of the average static TF as an example for investigated model order are shown in figure (3.5). It should be stressed that some ordinates of PR of orders (2.2) and (2.3) are negative.

A similar procedure, especially in varying the rainfall parameters is used to identify the optimal model structure of the PRTF model. Error statistics along with visual

considerations of convoluted rainfall as well as shape of pulse responses culminated in a model with (3,2,0) order, that is a model with three *a* and three *b* parameters.

The same search technique was used to identify a static TF model for the Bird Creek catchment. A TF model of order (1,2,0) is found adequate in almost all the events.

It should be noted that current software (Tilford, 1990a and Han, 1992) have been modified to make them suitable for the WMO workshop data formats.

3.5.3 An investigation of initial Δ values

The initial Δ (see sections 2.5.1.5 and 7.4) value has a major impact on the model forecast accuracy, particularly in the early stages of an event. The minimum and maximum range of Δ usually can be calculated from *0.05/gain* and *1/gain* (an exception would be due to a release of water from storage, for example a sudden thaw releasing melt water into the river system). In order to investigate the different initial Δ, four initial Δ namely $(\Delta_{Min} = 0.05/gain, \Delta_1 = 1, \Delta_{Mean} = 0.525/gain, \Delta_{Max} = 1/gain)$ are considered. It also is important to know whether the initial value of Δ is variable or constant. Thus eight combinations of Δ variant are investigated.

Using the OTF model parameters found during calibration, the one to nine step (hours) ahead forecasts were issued for each of eight Orgeval validation events. Error statistics including $RMSE, Q/\lambda^2_{5\%}$ and NTD_1 for different variants of initial Δ are calculated.

Summarised graphical results of this investigation are presented in figure (3.6). It can be seen that in each category (i.e. $\Delta_{Min}, \Delta_1, \Delta_{Mean}, \Delta_{Max}$) an updated variable Δ provides better forecasts than a constant value. Further, when all three statistics ($RMSE, Q/\lambda^2_{5\%}, NTD_1$) are considered together, $\Delta_{Min\ var\ iable}$ (i.e. initial $\Delta = \Delta_{\text{Minimum}}$ and variable with time) provides the best overall and average choice. However, if only the RMSE results are considered different conclusions can be obtained. This is investigated further in section (4.3.1). As the percentage runoff varies during the event and usually is small at the beginning of the event this conclusion is reasonable. It should be stressed that the results obtained may differ from catchment to catchment.

Table (3.4) Parameters, reconvolution and pulse response statistics of different order models (AOTF model, Orgeval catchment)

	a parameters							
Model order (a,b)	a_1	a_2	a_3	a_4	a_5	a_6	a_7	a_8
(1,1)	0.993							
(2,2)	1.857	-0.867						
(3,3)	2.350	-1.862	0.057					
(4,4)	2.364	-1.946	0.619	-0.044				
(5,5)	2.360	-1.923	0.560	0.022	-0.025			
(6,6)	2.361	-1.914	0.580	-0.089	0.116	-0.061		
(7,7)	2.357	-1.903	0.575	-0.110	0.176	-0.126	0.024	
(8,8)	2.357	-1.899	0.569	-0.106	0.168	-0.077	-0.033	0.023
(2,3)	1.843	-0.853						
(1,3)	0.985							
(3,2)	2.351	-1.864	0.508					
(3,1)	2.400	-1.950	0.540					

Table (3.4) continued

	b parameters							
Model order (a,b)	b_1	b_2	b_3	b_4	b_5	b_6	b_7	b_8
(1,1)	0.146							
(2,2)	0.024	0.058						
(3,3)	0.025	0.032	0.001					
(4,4)	0.022	0.034	-0.011	0.022				
(5,5)	0.022	0.034	-0.011	0.019	0.005			
(6,6)	0.023	0.033	-0.009	0.015	0.017	-0.019		
(7,7)	0.023	0.032	-0.009	0.016	0.016	-0.014	-0.008	
(8,8)	0.023	0.033	-0.010	0.016	0.016	-0.014	-0.009	0.000
(2,3)	0.024	0.046	0.020					
(1,3)	0.015	0.067	0.178					
(3,2)	0.025	0.033						
(3,1)	0.004							

Table (3.4) continued

	Model characteristics			
Model order (a,b)	Gain (%)	run off (%)	RMSE (m^3 /sec)	Peak time of pulse response (hours)
(1,1)	67.90	28.14	0.234	1
(2,2)	29.20	28.14	0.080	12
(3,3)	37.41	28.14	0.066	8
(4,4)	37.80	28.14	0.066	9
(5,5)	37.63	28.14	0.066	9
(6,6)	35.32	28.14	0.065	8
(7,7)	35.35	28.14	0.065	8
(8,8)	35.78	28.14	0.065	8
(2,3)	30.52	28.14	0.079	11
(1,3)	59.00	28.14	0.204	3
(3,2)	37.33	28.14	0.066	8
(3,1)	35.20	28.14	0.068	8

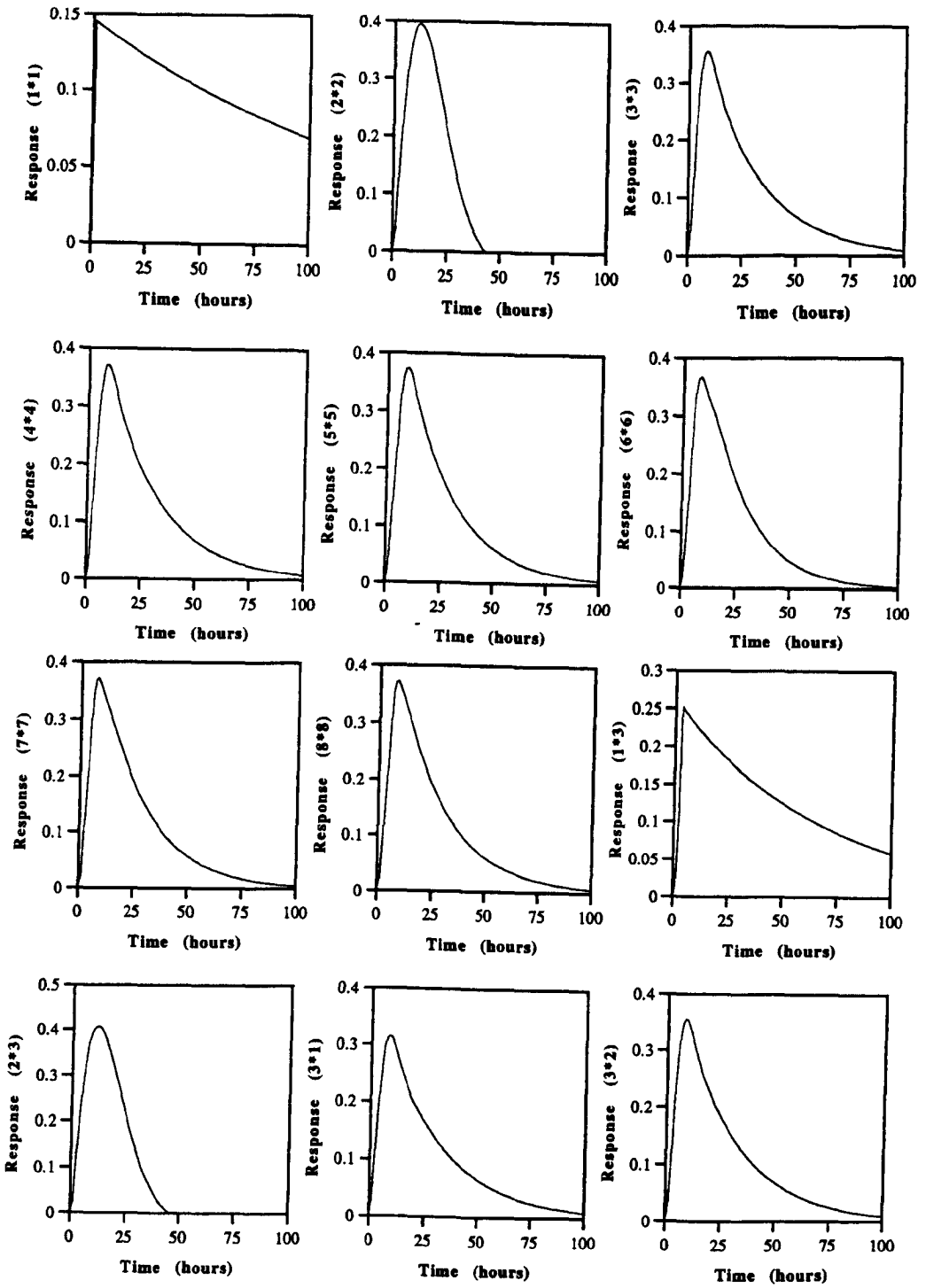

Figure (3.5) pulse response for average static TF, different orders, Orgeval catchment.

In an attempt to relate the initial Δ value to initial flow, the variation of base flow versus percentage runoff in all the investigated events are examined. The result of this study, presented in figure (3.7), indicates that no strong positive relationship between initial flow and percentage runoff is apparent. Owens (1986) also failed to find a well-defined relationship between base flow and average percentage runoff for a number of events for catchments in North West England but stated the possibility of identifying this kind of relationship if more event data were available. However, despite these comments it will be seen in section (4.3.1) that some reasonable relationship between base flow and percentage runoff and hence initial Δ value can be extracted through a classification of events.

3.5.4 Results of OTF and PRTF models

In this section, forecasting results from average OTF and PRTF models (both in static and dynamic form) derived from the WMO project data are presented graphically for the Orgeval catchment. The results of the average OTF models are also given for the daily data of the Bird Creek catchment. The RMSE results of the OTF and PRTF models and other models also first presented for each step ahead forecast, and a comparison is then made to evaluate the relative performance of the different models. In addition to the RMSE, the portmanteau statistic Q and the NTD criterion are also presented for different TF models for the Orgeval catchment.

3.5.4.1 Ordinary TF model results in Orgeval catchment

Using the OTF model parameters found in the calibration phase, one to nine steps (hours) ahead forecasts are issued at times 1, 4, 7, 10, 13, 16 and 19 for each of the six test events. The RMSE for each step ahead forecast for all of the models in the inter-comparison project and the TF models are provided in tables (3.5) to (3.10) for events 1 to 6 respectively. In addition, the NTD and portmanteau statistics for the TF models only are also provided in the same tables. Furthermore, a model performance ranking table has also been provided for each event on the basis of the RMSE statistics. Ranking , have been provided for 1 step ahead, and 9 step ahead forecasts, and also for all the forecasts taken as a whole (average). Average rank of a given model is obtained by averaging its ranks on the whole step aheads. Some notable results are discussed below. Hydrographs and hyetographs both for the events and pre-events are shown in appendix 2. For the sake of conciseness graphical forecasts are given in section 4.3.1.

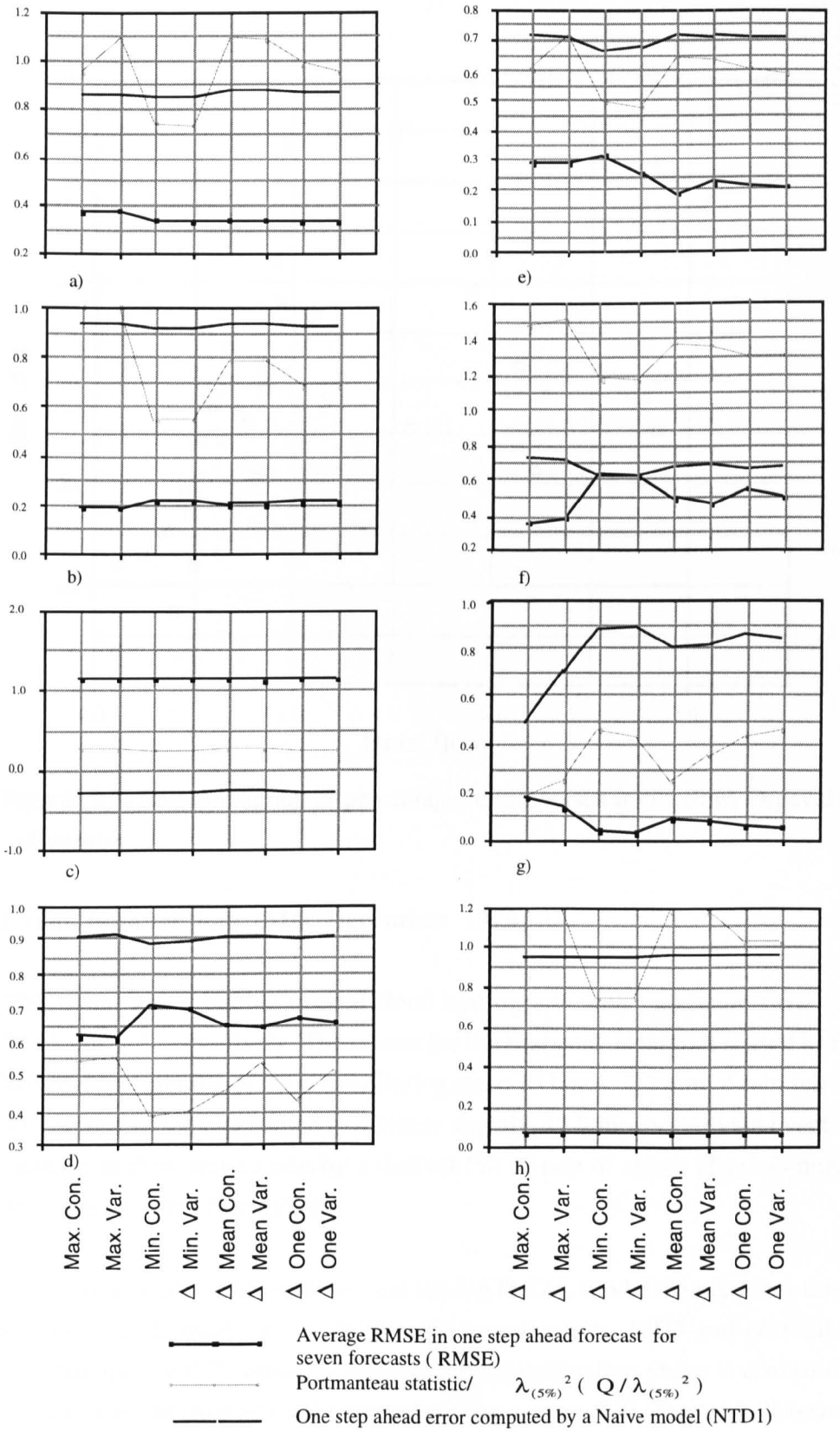

Figure (3.6) Comparison of RMSE, $Q/\lambda^2_{5\%}$, and NTD1 with different initial Δ in several events, Orgeval catchment. a) WMO1, b) WMO2, c) WMO3, d) WMO4, e) WMO5, f) WMO6, g) V1, h) V2

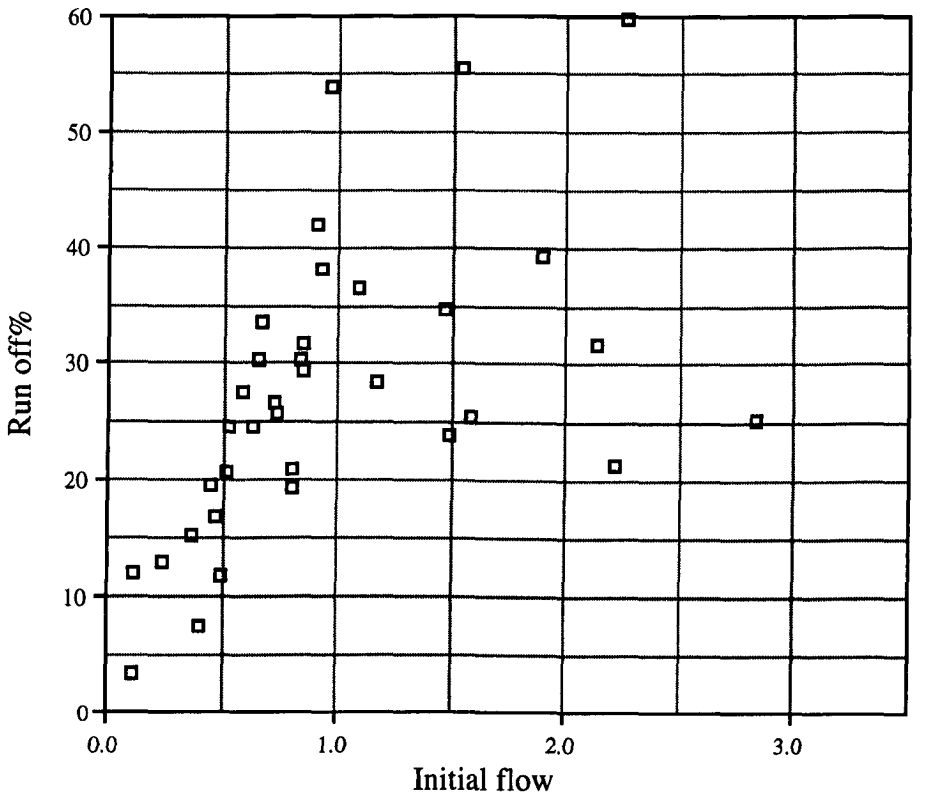

Figure (3.7) Scatter diagram of percentage runoff versus initial flow, Orgeval catchment. (33 events)

Event number one (31st December 1978)

This event was a double peaked flood hydrograph with maximum flow of 7.23, and 14.61 $m^3 s^{-1}$ respectively. The reason for the first peak is rainfall started to fall 15 hours before the beginning of the event. During these 15 hours, 1.5 mm of rain fell in each hour on average. Discharge started to increase slightly, 12 hours prior to the event. The second increase in flow was caused by a distinct fall of rain of about 11-hours duration with a peak intensity of 4.6 mm/hour.

The values in table (3.5) indicate that the NAMKAL model clearly gives the best results and the TANK model gives, by far, the worst results. NTD and portmanteau values confirm that the OTF model constructed in the calibration phase is also suitable for this validation event (reason can be extracted from section 3.3). The table also shows that the forecasting capability of the OTF model decreases with increasing lead time; the rank of the model falling from 7 in first step ahead to 12 both on average and nine steps ahead forecast. In addition, OTF model's RMSE are smaller than those of average model in first and second step ahead forecast, but larger than average of the models for the longer lead

times. This is probably because calibration minimises convolution errors of one step ahead errors.

Event number two (2nd February. 1979)

This is a relatively low flow event (maximum flow is 10.25 $m^3 s^{-1}$), which fails to reach threshold level status. The single peaked hydrograph is caused by a relatively long period (about 20 hours) of rainfall starting 11 hours prior to the event. Total rainfall prior to the event was about 10 mm. The water level started to increase about 5 hours before the beginning of the event.

Table (3.6) indicates that the model found in calibration phase is also applicable for this validation event. Once again the absolute and relative RMSE of OTF model increase with lead time, so that the RMSE of the OTF model are less than those of average of all models up to three steps ahead but they are larger for longer lead times. The rank of the OTF model is 5 for one step ahead forecasts but overall and for nine steps ahead is 12th and 13th respectively.

Table (3.6) also shows that the HBV model in contrast to event number one produces the best result, while the TANK model once again gives by far, the worst result.

Event number three (10th March 1979)

The event is unique in that it is the only one where the discharge falls sharply 10 hours prior to beginning of the event. The decrease in discharge was continued even 10 hours after the start of the event. It was a single peaked flow hydrograph with a maximum flow of 12.94 $m^3 s^{-1}$. The increase in flow was caused by falls of rain of 15- hours duration.

According to table (3.7) the RMSE of the OTF model are the largest for all forecasts. Reference to the characteristics of this event (such as percentage runoff 27.66%) show there is not a significant difference between this event and other events except for a sharp fall in flows at the start of the event. One possibility was thought to be inappropriate selection of initial Δ, but as figure (3.6c) shows, selection of any initial Δ leads to similar RMSE. Further investigation revealed the cause to be due to incorrect pre-event flow data being used by the model for this particular event.

Table (3.7) shows that the event is also unique in that it is the only one where the performance of a simple naive model is superior to the transfer function model (as indicated by the NTD < 0). This criteria indicates that the model found in the calibration

phase is not appropriate for this event. Indeed amongst the 32 calibration events there are no other events where the initial discharge decreases with time. Such a situation (decrease of discharge in the start of event for such a long time) will not occur in reality. It can be said that the start of the event is in fact at time 9. Therefore probably this is the main reason for a very poor quality of the forecasts.

Table (3.7) shows that the SSARR model presents the best result on average.

Event number four (13th March 1980)

This is a large single peaked event with the maximum observed flow of 28.79 m^3s^{-1} resulting from a long duration of rainfall falling on a catchment wetted by heavy rainfall during 13 hours prior to the event. The discharge started to increase 7 hours before the beginning of the event.

Table (3.8) indicates that the calibration model is appropriate for this verification event. As with previous events the forecasting accuracy of the OTF model decreases with lead time, so that the rank of OTF model in first step ahead is 3 but it falls to rank 9 and 12 on average and for the nine step ahead forecasts respectively. In addition, the OTF model's RMSE are smaller than those of average models for first and second step ahead forecasts but larger than the models' average for the bigger lead times.

The UBC and TANK models produce the best and the worst results respectively.

Event number five (13th July 1980)

This event has at least three peak flood hydrographs with maximum flows of 14.56, 15.32, and 13.08 m^3s^{-1} respectively. Rain started to fall almost 15 hours prior to beginning of the event and continued 9 hours after start time of the event. Water level started to increase 7 hours before the start time of the event. Although the amount of rainfall exceeds many of the other events, the value of maximum flow is less (average percentage runoff is 16.70%). The reason for this is that the first spell of rain served to satisfy the catchment soil moisture deficit which had accumulated through July. The third increase in flow was caused by falls of rain of about 5-hours duration.

Table (3.5) Root Mean Square Error for each model, Orgeval catchment event number 1

Step ahead forecast	TF	SPRTF	DPRTF	UBC	CEQUEAU	GAPI	SMAR	CLS	HBV	TANK	SSARR	HFS	NAMS11	NAMKAL
1	0.33	0.30	0.42	0.38	0.33	0.26	0.20	0.27	0.18	3.24	0.49	0.38	0.34	0.10
2	0.75	0.65	0.71	0.66	0.55	0.51	0.45	0.48	0.32	3.37	0.82	0.53	0.54	0.27
3	1.30	1.13	0.97	1.00	0.87	0.73	0.89	0.72	0.78	3.49	1.42	0.86	0.76	0.57
4	1.75	1.60	1.22	1.39	1.18	0.93	1.28	1.03	1.29	3.67	2.08	1.20	0.98	0.76
5	2.15	2.04	1.39	1.68	1.28	1.21	1.64	1.27	1.89	3.68	2.55	1.31	1.21	0.86
6	2.54	2.45	1.50	1.96	1.27	1.39	1.97	1.36	2.56	3.75	2.84	1.34	1.32	0.82
7	2.99	2.91	1.67	2.33	1.27	1.53	2.33	1.40	3.23	4.00	3.02	1.42	1.40	0.88
8	3.45	3.38	1.89	2.62	1.20	1.80	2.70	1.51	3.94	4.20	3.02	1.37	1.55	0.89
9	3.80	3.73	2.06	2.89	1.14	1.99	3.00	1.55	4.55	4.32	2.91	1.32	1.63	0.85
NTD1	0.85	0.82	0.56											
Q/λ^2	0.73	0.88	1.68											

Model rank (from best to worst)

One step ahead	NAMKAL	HBV	SMAR	GAPI	CLS	SPRTF	TF	CEQUEAU	NAMS11	HFS	UBC	DPRTF	SSARR	TANK
Average	NAMKAL	CLS	GAPI	CEQUEAU	NAMS11	HFS	SMAR	DPRTF	HBV	UBC	SPRTF	TF	SSARR	TANK
Nine steps ahead	NAMKAL	CEQUEAU	HFS	CLS	NAMS11	GAPI	DPRTF	UBC	SSARR	SMAR	SPRTF	TF	TANK	HBV

Table (3.6) Root Mean Square Error for each model, Orgeval catchment event number 2

Step ahesd forecast	TF	SPRTF	DPRTF	UBC	CEQUEAU	GAPI	SMAR	CLS	HBV	TANK	SSARR	HFS	NAMS11	NAMKAL
1	0.21	0.23	0.38	0.26	0.16	0.25	0.18	0.21	0.17	1.56	0.20	0.41	0.33	0.37
2	0.47	0.49	0.73	0.49	0.37	0.55	0.37	0.41	0.28	1.80	0.43	0.51	0.56	0.63
3	0.75	0.77	1.03	0.69	0.58	0.74	0.58	0.57	0.33	2.12	0.69	0.55	0.78	0.87
4	1.10	1.10	1.34	0.91	0.79	0.86	0.86	0.77	0.40	2.51	1.05	0.65	1.01	1.09
5	1.43	1.39	1.61	1.10	0.94	0.94	1.12	0.94	0.47	2.90	1.38	0.73	1.20	1.26
6	1.74	1.65	1.82	1.24	1.02	0.92	1.32	1.05	0.51	3.22	1.67	0.77	1.34	1.40
7	2.09	1.96	2.06	1.42	1.13	0.85	1.56	1.19	0.57	3.44	1.98	0.84	1.50	1.54
8	2.39	2.24	2.26	1.60	1.26	0.79	1.77	1.33	0.63	3.59	2.22	0.91	1.67	1.68
9	2.59	2.43	2.41	1.73	1.35	0.80	1.90	1.42	0.61	3.71	2.36	0.94	1.80	1.79
NTD1	0.91	0.88	0.39											
Q/λ^2	0.54	0.85	4.90											

Model rank (from best to worst)

One step ahead	CEQUEAU	HBV	SMAR	SSARR	TF	CLS	SPRTF	GAPI	UBC	NAMS11	NAMKAL	DPRTF	HFS	TANK
Average	HBV	CEQUEAU	HFS	CLS	GAPI	SMAR	UBC	SSARR	NAMS11	NAMKAL	SPRTF	TF	DPRTF	TANK
Nine steps ahead	HBV	GAPI	HFS	CEQUEAU	CLS	UBC	NAMKAL	NAMS11	SMAR	SSARR	DPRTF	SPRTF	TF	TANK

Table (3.7) Root Mean Square Error for each model, Orgeval catchment event number 3

Step ahead forecast	TF	SPRTF	DPRTF	UBC	CEQUEAU	GAPI	SMAR	CLS	HBV	SSARR	HFS	NAMS11	NAMKAL
1	1.10	0.72	0.43	0.54	0.39	0.17	0.22	0.22	0.28	0.18	0.60	0.37	0.21
2	2.21	1.34	0.78	1.03	0.67	0.35	0.41	0.40	0.41	0.31	0.69	0.50	0.33
3	3.18	1.93	1.15	1.60	0.97	0.62	0.78	0.66	0.62	0.49	0.77	0.72	0.52
4	3.97	2.47	1.52	2.18	1.31	0.98	1.19	0.94	0.82	0.67	0.90	1.01	0.75
5	4.55	2.96	1.78	2.66	1.51	1.21	1.56	1.12	0.92	0.73	0.91	1.16	0.90
6	4.98	3.44	2.03	3.17	1.72	1.44	1.96	1.31	0.99	0.82	0.93	1.33	1.05
7	5.29	3.89	2.29	3.68	1.96	1.75	2.38	1.53	1.12	0.96	1.02	1.56	1.28
8	5.41	4.21	2.42	4.09	2.09	1.96	2.69	1.65	1.18	1.00	1.03	1.66	1.42
9	5.45	4.49	2.54	4.51	2.21	2.18	2.99	1.74	1.24	1.09	1.03	1.78	1.56
NTD1	-0.29	0.45	0.49										
Q / λ^2	0.22	0.42	7.21										

Model rank (from best to worst)

One step ahead	GAPI	SSARR	NAMKAL	SMAR	CLS	HBV	NAMS11	CEQUEAU	DPRTF	UBC	HFS	SPRTF	TF
Average	SSARR	NAMKAL	HBV	HFS	CLS	GAPI	NAMS11	SMAR	CEQUEAU	DPRTF	UBC	SPRTF	TF
Nine steps ahead	HF	SSARR	HBV	NAMKAL	CLS	NAMS11	GAPI	CEQUEAU	DPRTF	SMAR	SPRTF	UBC	TF

Table (3.8) Root Mean Square Error for each model. Orgeval catchment event number 4

Step ahead forecast	TF	SPRTF	DPRTF	UBC	CEQUEAU	GAPI	SMAR	CLS	HBV	TANK	SSARR	HFS	NAMS11
1	0.69	0.76	1.19	0.52	0.62	0.70	0.97	2.20	0.77	2.92	1.05	0.92	0.69
2	1.47	1.59	2.20	0.94	1.14	1.08	1.00	1.84	1.22	3.65	2.39	1.59	1.09
3	2.41	2.52	3.17	1.30	1.61	1.44	1.28	3.41	1.69	4.83	3.75	2.09	1.44
4	3.49	3.54	4.08	1.70	2.16	1.94	1.85	3.11	2.19	5.40	4.92	2.60	1.80
5	4.46	4.39	4.73	2.03	2.65	2.42	2.26	2.14	2.53	6.44	5.93	3.01	2.11
6	5.41	5.19	5.35	2.26	3.05	2.86	2.59	2.58	2.73	7.68	6.57	3.26	2.39
7	6.36	6.03	5.93	2.50	3.47	3.40	2.86	3.03	2.84	8.03	6.77	3.53	2.69
8	7.31	6.87	6.49	2.71	3.86	3.85	3.07	2.69	2.88	8.44	6.55	3.81	2.93
9	8.21	7.70	7.06	2.89	4.21	4.24	3.12	3.07	2.85	8.88	5.99	4.09	3.12
NTD1	0.89	0.87	0.42										
Q/λ^2	0.39	0.78	3.55										

Model rank (from best to worst)

One step ahead	UBC	CEQUEAU	TF	NAMS11	GAPI	SPRTF	HBV	HFS	SMAR	SSARR	DPRTF	CLS	TANK
Average	UBC	NAMS11	SMAR	HBV	GAPI	CEQUEAU	CLS	HFS	TF	SPRTF	DPRTF	SSARR	TANK
Nine steps ahead	HBV	UBC	CLS	SMAR	NAMS11	HFS	CEQUEAU	GAPI	SSARR	DPRTF	SPRTF	TF	TANK

Table (3.9) indicates that the calibrated model is appropriate to this event. With respect to forecast RMSE, the best model differs according to the number of steps ahead. While the TANK model gives the worst results for all step ahead, the OTF model presents the best results for one and two step ahead forecasts although its ranking falls to rank 6 overall and 8 for nine step ahead forecasts respectively. On the other hand, OTF model's RMSE are lower than those of average models up to 5 step ahead forecasts but higher for the other lead times.

Event number six (20th July 1980)

The event occurring on the 20th July 1980 had a double peaked flood hydrograph with maximum flows of 11.18 and 15.45 m^3s^{-1} respectively. The increase in flows was caused by two distinct falls of rain each of about 10-hours duration. Despite the relatively large amount of rain, the increase in discharge is not comparable with other events, notably with event number three. As with event 5, this probably is because of the soil moisture deficit.

Table (3.10) indicates that the best model differs for different step ahead forecasts. The best model on average is the SMAR model, and again the TANK model produces the worst results for all steps ahead. The rank of the OTF model is second best for one step ahead, but falls to 10^{th} and 12^{th} for average and nine step ahead forecasts respectively. The OTF model RMSE's are smaller than those of average and up to three steps ahead but are larger than average compared to the other models in the other lead times.

Finally although the portmanteau statistic is a little greater than 1, the table confirms the suitability of OTF model found in calibration phase for forecasting.

3.5.4.2 Ordinary TF model results in Bird Creek catchment

As mentioned in section (3.5.2) a (1,2,0) model is identified in the calibration phase using the daily data of the catchment. In this section the same model is used to issue one to 4 step (days) ahead forecasts at times 1, 2, 3, 4, 5, 6 and 7 for each of the six test events. Here graphical forecasts as well as RMSE results of the OTF are presented. (The event hydrographs and hyetographs are shown in appendix 2).

Table (3.9) Root Mean Square Error for each model, Orgeval catchment event number 5

Step ahead forecast	TF	SPRTF	DPRTF	UBC	CEQUEAU	GAPI	SMAR	CLS	HBV	TANK	SSARR	HFS	NAMS11	NAMKAL
1	0.26	0.83	1.40	1.57	1.42	0.79	0.97	2.01	1.77	3.76	1.17	1.35	1.31	0.96
2	1.18	1.73	2.57	2.66	2.15	2.02	2.00	3.38	3.09	4.53	1.64	2.89	1.89	1.33
3	2.23	2.39	3.11	3.50	2.97	2.24	2.46	5.26	3.58	6.04	2.04	5.07	2.55	1.79
4	3.91	3.60	3.83	4.49	4.04	2.21	3.32	7.58	4.11	8.72	3.01	7.08	3.09	2.59
5	5.43	5.27	4.91	5.46	4.65	2.82	4.74	9.09	5.21	10.22	3.85	8.17	3.82	3.19
6	6.10	5.88	5.06	5.87	5.55	3.11	5.04	10.26	5.33	11.77	3.38	9.45	3.99	3.69
7	6.16	5.97	4.97	6.13	6.63	3.21	4.93	11.02	4.84	13.67	2.25	10.47	3.91	4.17
8	6.50	6.53	5.21	6.48	7.11	3.46	5.22	11.65	4.78	14.54	1.70	10.47	3.96	4.56
9	6.36	6.57	5.27	6.77	7.63	3.71	5.18	11.90	4.44	15.24	1.10	10.13	3.91	4.87
NTD1	0.68	0.65	0.39											
Q/λ^2	0.47	0.40	2.72											

Model rank (from best to worst)

One step ahead	TF	GAPI	SPRTF	NAMKAL	SMAR	SSARR	NAMS11	HFS	DPRTF	CEQUEAU	UBC	HBV	CLS	TANK
Average	GAPI	SSARR	NAMKAL	NAMS11	SMAR	TF	SPRTF	DPRTF	HBV	CEQUEAU	UBC	HFS	CLS	TANK
Nine steps ahead	SSARR	GAPI	NAMS11	HBV	NAMKAL	SMAR	DPRTF	TF	SPRTF	UBC	CEQUEAU	HFS	CLS	TANK

Table (3.10) Root Mean Square Error for each model, Orgeval catchment event number 6

Step ahead forecast	TF	SPRTF	DPRTF	UBC	CEQUEAU	GAPI	SMAR	CLS	HBV	TANK	SSARR	HFS	NAMS11	NAMKAL
1	0.61	0.86	1.11	0.99	0.76	0.73	0.73	0.58	1.22	3.74	1.04	0.65	0.71	0.61
2	0.97	1.40	1.58	1.42	1.01	1.15	0.92	0.91	1.61	4.14	1.61	0.96	0.94	0.96
3	1.38	1.88	1.93	1.75	1.20	1.51	1.06	1.22	1.79	4.62	2.00	1.37	1.20	1.21
4	2.45	2.87	2.62	2.39	1.46	1.74	1.42	1.98	2.40	4.87	2.65	1.59	1.77	1.52
5	3.24	3.62	2.89	2.62	1.51	1.93	1.62	2.51	2.56	5.33	3.00	1.84	1.87	1.72
6	3.78	4.13	2.99	2.68	1.59	2.09	1.83	2.84	2.53	5.85	3.00	2.22	2.02	1.91
7	4.31	4.56	3.04	2.70	1.61	2.15	1.86	3.07	2.44	6.03	2.84	2.34	2.04	2.01
8	4.68	4.80	2.93	2.49	1.42	2.01	1.78	3.23	2.21	6.31	2.70	2.38	1.94	1.96
9	4.80	4.89	2.77	2.20	1.27	1.92	1.90	3.24	1.98	6.75	2.62	2.57	1.88	1.97
NTD1	0.63	0.65	0.42											
Q/λ^2	1.16	0.69	1.84											

Model rank (from best to worst)

One step ahead	CLS	TF	NAMKAL	HFS	NAMS11	SMAR	GAPI	CEQUEAU	SPRTF	UBC	SSARR	DPRTF	HBV	TANK
Average	SMAR	CEQUEAU	NAMKAL	NAMS11	HFS	GAPI	CLS	UBC	HBV	TF	DPRTF	SSARR	SPRTF	TANK
Nine steps ahead	CEQUEAU	NAMS11	SMAR	GAPI	NAMKAL	HBV	UBC	HFS	SSARR	DPRTF	CLS	TF	SPRTF	TANK

Event number one (11th November 1972)

This is a double peaked flood hydrograph with maximum flow of 322.82, and 43.68 m^3s^{-1} respectively. The first peak derives from rain falling for two days prior to the peak totalling 60 mm and causing the discharge to increase from negligible flow to 322.82 m^3 s^{-1}. The second increase in flow was caused by a fall of rain of four days duration with a maximum of 14.6 mm day.

The diagram in figure 3.8 (top) shows that the first forecast is in close agreement with the observed flow for both rising and recession limbs and that the magnitude and time of peak forecasted are reasonably well. The second to fourth forecasts fit the first descending limb perfectly. The fifth forecast is reasonably accurate for the first three steps but overestimates the second rising limb. The sixth and seventh forecasts both overestimate the actual flow. Overall the OTF model produces acceptable forecasts with good agreement between observed and forecasted discharges. At the same time as shown in figure 3.8 (bottom) the RMSE for one and two step ahead forecasts are the smallest of all models. The OTF model ranks first both for one step ahead forecasts and on average. In order to calculate the average RMSE without extreme values, two models with the biggest and lowest RMSE are eliminated and the average RMSE is calculated based on the RMSE of the remaining models.

Event number two (3rd March 1973)

This event has a three peak hydrograph with maximum flows of 219.17, 353.96, and 390.67 m^3 s^{-1} respectively. The first peak was due to rain falling three days previously, whilst both the second and third peaks were attributable to rain occurring just one day before. It is interesting to note that in each case the total amount of antecedent rainfall is the same, and the peak discharges are very similar in both cases.

Figure 3.9 (top) shows that the first two forecasts parallel the observed discharge, and successfully predict the peak time, although the peak flow is underestimated. The same situation exists for the third forecast, although it overestimates the fourth turning point a little more. The fourth forecasts exceed the actual recession limb whilst underestimating the observed flow at the latest steps. The fifth forecast exceeds the recession limb at the two first steps, but is lower than the final rising limb at the two last steps. The sixth and seventh forecast both underestimate actual flow. Although the OTF model results are not as good as those of event one, they are still acceptable, being more or less average (see figure 3.9 bottom). The GAPI model gives the biggest RMSE. The rank of OTF model in all of the models for one step ahead forecasts is third.

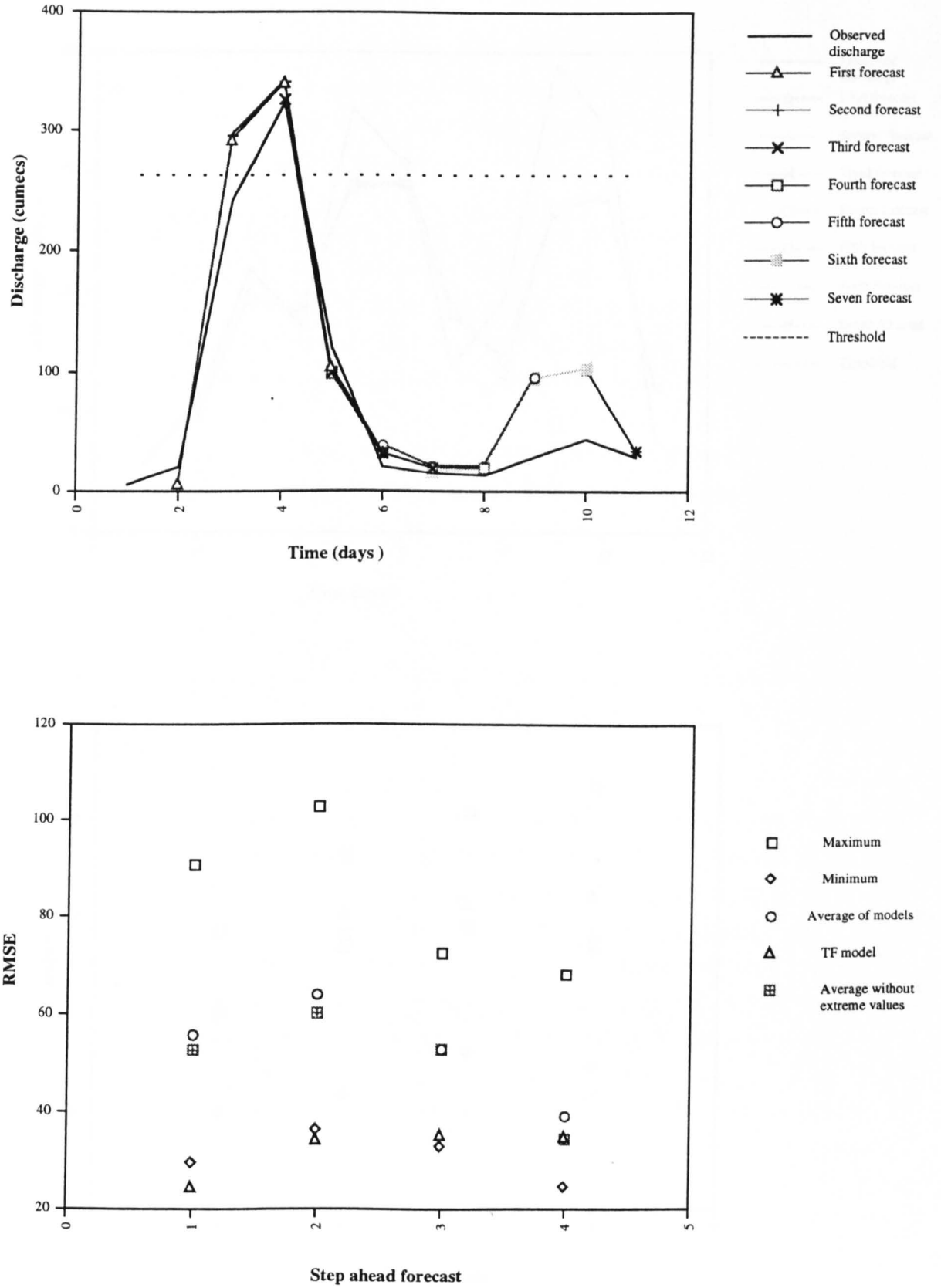

Figure (3.8) Seven multiple step ahead OTF forecasts (top), comparison of RMSE of different models (bottom) Bird Creek catchment, event no. 1 .

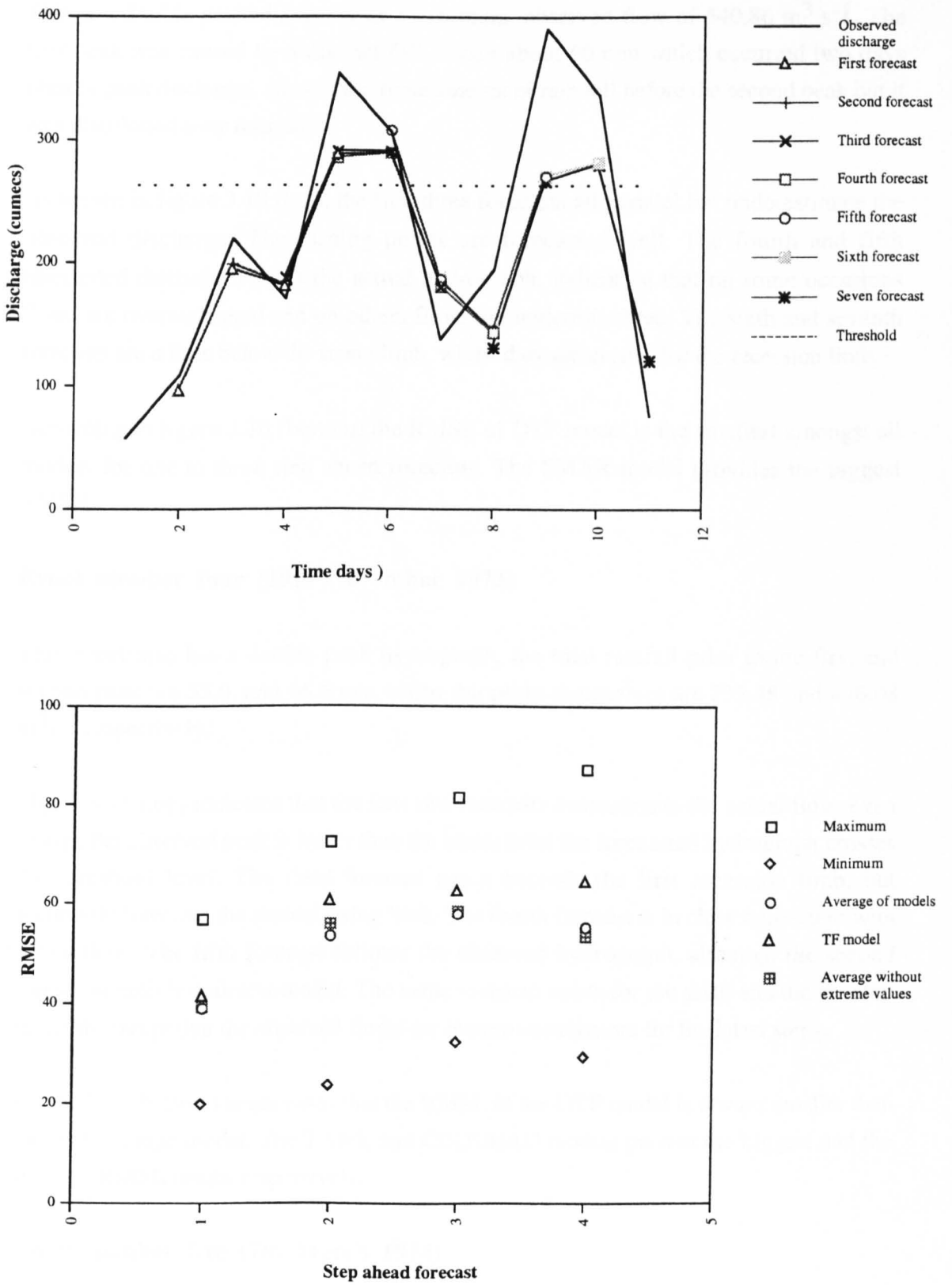

Figure (3.9) Seven multiple step ahead OTF forecasts (top), comparison of RMSE of different models (bottom) Bird Creek catchment, event no. 2.

Event number three (9th April 1973)

This is a double peaked event with a maximum observed flow of 540.86 $m^3 s^{-1}$. The first peak was caused by a distinct fall of rain about 60 mm which occurred two days prior to peak discharge. Almost the same amount of rain fell before the second peak but it was distributed over four days.

As shown in figure 3.10 (top), the first three forecasts all parallel but underestimate the observed discharge. The turning points are forecasted well. The fourth and fifth forecasted discharges cross the actual hydrograph, indicating that on some occasions flows are overestimated and on others flows are underestimated. The sixth and seventh forecasts are a little below the rising limb, whilst they are greater for the recession limb.

According to figure 3.10 (bottom) the RMSE of OTF model is the smallest amongst all models for one to three step ahead forecasts. The SMAR model provides the biggest RMSE.

Event number four (19th November 1973)

This event also has a double peak hydrograph, the total rainfall prior to the first and second peak are 55.0, and 66.6 mm whilst the peaks themselves are 232.48 and 436.08 $m^3 s^{-1}$ respectively.

Figure 3.11 (top) indicates that the first two forecasts overestimate the actual flow, even though the observed peak is lower than the alarm level the forecasted hydrograph crosses the threshold level. The third forecast again exceeds the first recession limb, but accurately forecasts the second rising limb. The fourth forecast is in close agreement with actual flow. The fifth forecast follows the observed hydrograph, although the second recession limb is underestimated. The same scenario exists for the sixth and the seventh forecasts except that the observed flows are overestimated more for the latest steps.

Figure 3.11 (bottom) emphasises that the RMSE of the OTF model is always smaller than those of average model. The TANK and CEQUEAU models present the biggest and the smallest RMSE results respectively.

Event number five (7th March 1974)

This event has a large single peaked flood hydrograph with maximum flow of 1110.03 $m^3 s^{-1}$ resulting from a three days rainfall totalling 139.9 mm.

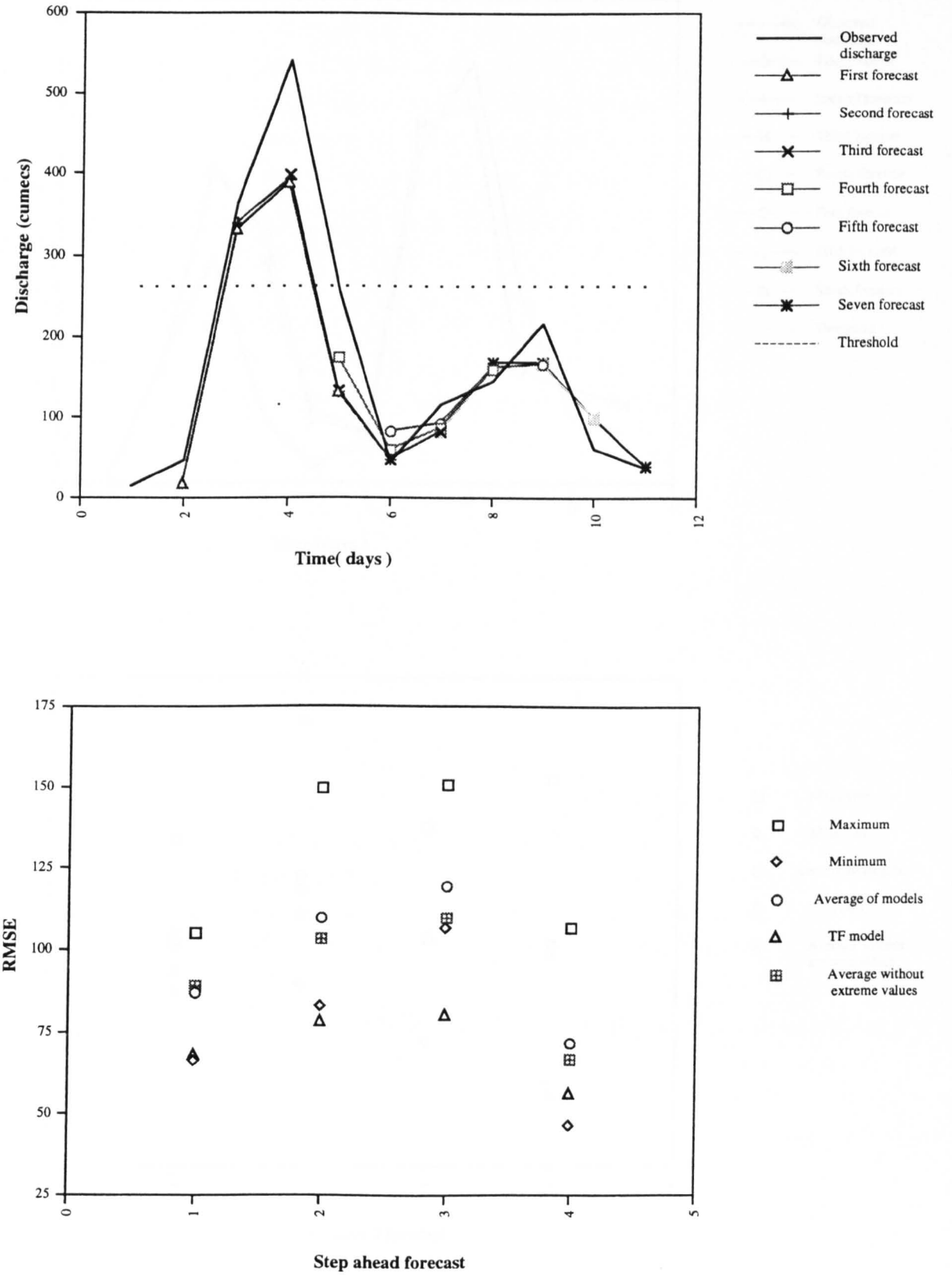

Figure (3.10) Seven multiple step ahead OTF forecasts (top), comparison of RMSE of different models (bottom) Bird Creek catchment, event no. 3.

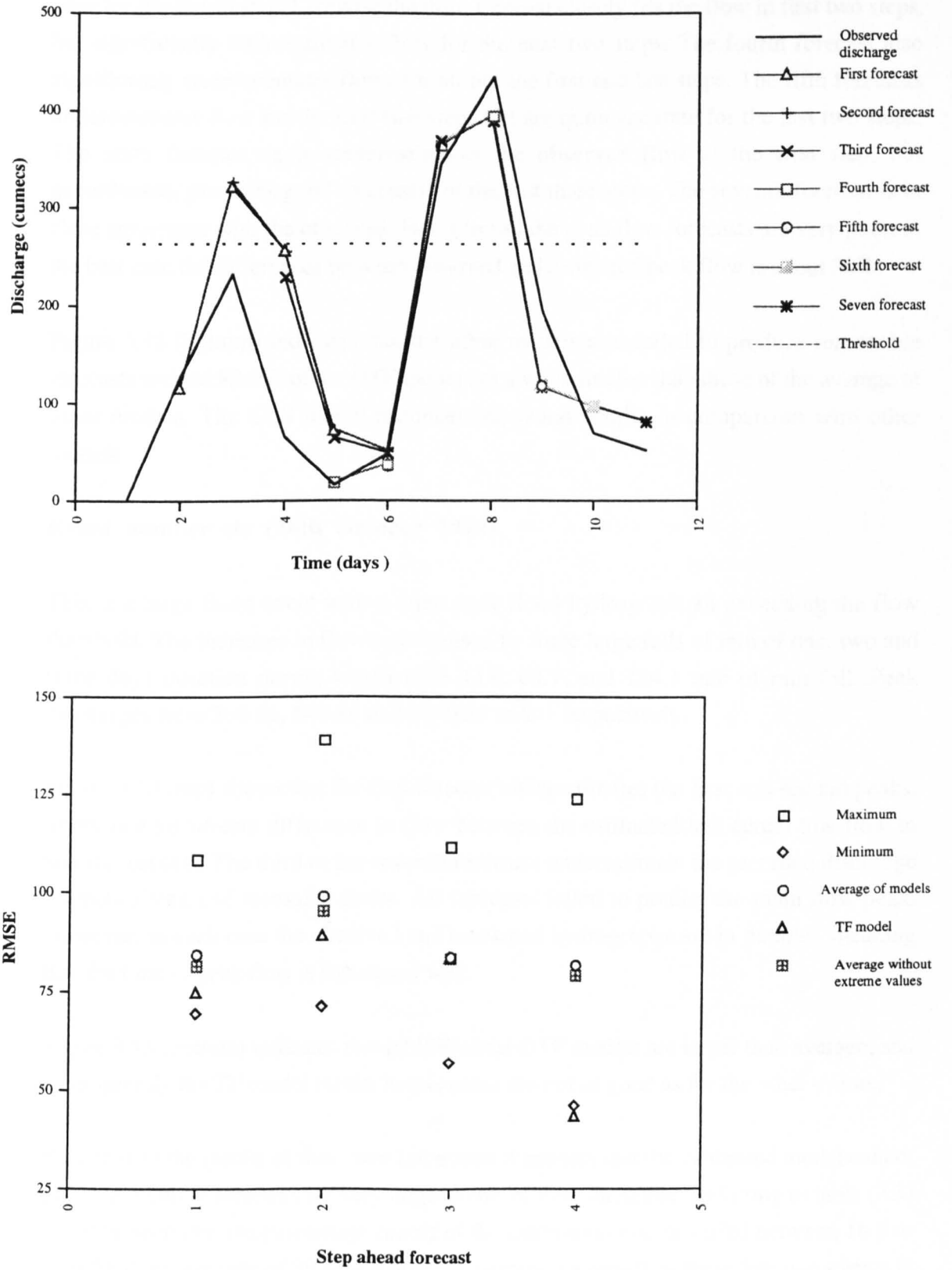

Figure (3.11) Seven multiple step ahead OTF forecasts (top), comparison of RMSE of different models (bottom) Bird Creek catchment, event no. 4.

According to figure 3.12 (top) the first forecast closely corresponds to the observed flow. The second forecast is in agreement with actual flow for the first three steps but is very poor for the fourth step. Likewise the third forecast closely fits the flow in first two steps, but significantly underestimates flow for the next two steps. The fourth forecast also significantly underestimates flows for all but the first and last steps. The fifth forecasts underestimates flow for the first two steps but are quite accurate for the last two steps. The sixth forecast again underestimates the observed flow at the first step, but nevertheless, produces good forecasts for the last three steps. The seventh forecast is in close agreement with the observed flow. Overall the peak flow forecasts are very poor; in the best case the differences between observed and estimated peak flow is about 30%.

Figure 3.12 (bottom) indicates that the other models also failed to produce reasonable forecasts and the RMSE of the OTF model are always smaller than those of the average of other models. The CLS model produces the worst results in comparison with other models.

Event number six (28th October 1974)

This is a large flood event with a three peak flood hydrograph all exceeding the flow threshold. The increases in flow were caused by three large falls of rain of one, two and three days duration during which time 33.6, 60.7, and 124.1 mm of rain fell. Peak discharges were 308.66, 540.86 and 1370.55 m^3s^{-1} respectively.

Figure 3.13 (top) shows that the first forecast underestimates the first and second peaks. There is a significant difference in flow between the estimated and actual low flow in second forecast. The third to the seventh forecasts underestimate the recorded discharge for both rising and recessing limbs. All forecasts failed to predict the main flow peak. However, in each case the observed and estimated hydrographs are in parallel, meaning that the time of peak flow is forecasted well.

Figure 3.13 (bottom) indicates that RMSE of the OTF models are larger than average, and consequently the TF model results in this event are not as good as for the other events.

Referring to the results of these two last events it appears that the calibrated model cannot produce accurate forecasts for very large events of this catchment. Referring to table (3.3) it can be seen that the percentage runoff of the calibration events varied between 16.6 to 59.6 (with an average of 39.6%) whilst the percentage runoff of these last two events is 72.3 and 71.2% respectively and are too far from the average percentage runoff of the calibration events. However, amongst the five models presented forecasting results for all

six events of the Bird Creek catchment, on the average, the rank of TF model is the second best both in one step ahead forecast and in average of all step ahead forecasts.

3.5.4.3 Summary of observations relating to ordinary transfer function models and WMO project models

The following general comments are made in relation to the application of average OTF model for the Orgeval and Bird Creek catchments.

The absolute forecast error increases with lead time for all 14 models evaluated. However, the relative increase of the RMSE in different models is not similar. The OTF, and SMAR models usually perform better for short lead times and when the lead time is increased the relative RMSE of these two models also increases. For the TF model it may be said that, it is because the one step ahead forecast error is considered to select the best calibration model. In contrast, the relative performance of the HBV, NAMS11, HFS, SSARR, and UBC models improves with lead time. Thus, whilst a given model may be ranked sixth in the primary steps its ranking may improve to two for the longer lead times. The same general conclusion does not apply to the remaining models.

There is no consistent pattern in the performance of the models on an event basis. A given model may rank first in one event and last in others. Therefore, no comment can be made concerning that a particular model always presents the best results. However, it appears that the TANK model usually presents the worst results for the Orgeval catchment, probably it may be because of miscalibrating of the model.

An increase in model complexity does not necessarily lead to an increase in forecast accuracy. It may be said that the accuracy of the forecasts is highly dependent on the updating method.

It appears that the calibrated TF model cannot produce accurate forecasts for very large events with a large percentage runoff in Bird Creek catchment. This is because the average percentage runoff of the calibration events (39.6%) is too far from the events with large percentage runoff (more than 70%). Therefore, it looks in large events, calibrated model obtainable from event with large percentage runoff will improve the quality of the forecasts.

Transfer function models can satisfactorily simulate the discharge in the catchments in most cases, as this model directly relates discharge to rainfall.

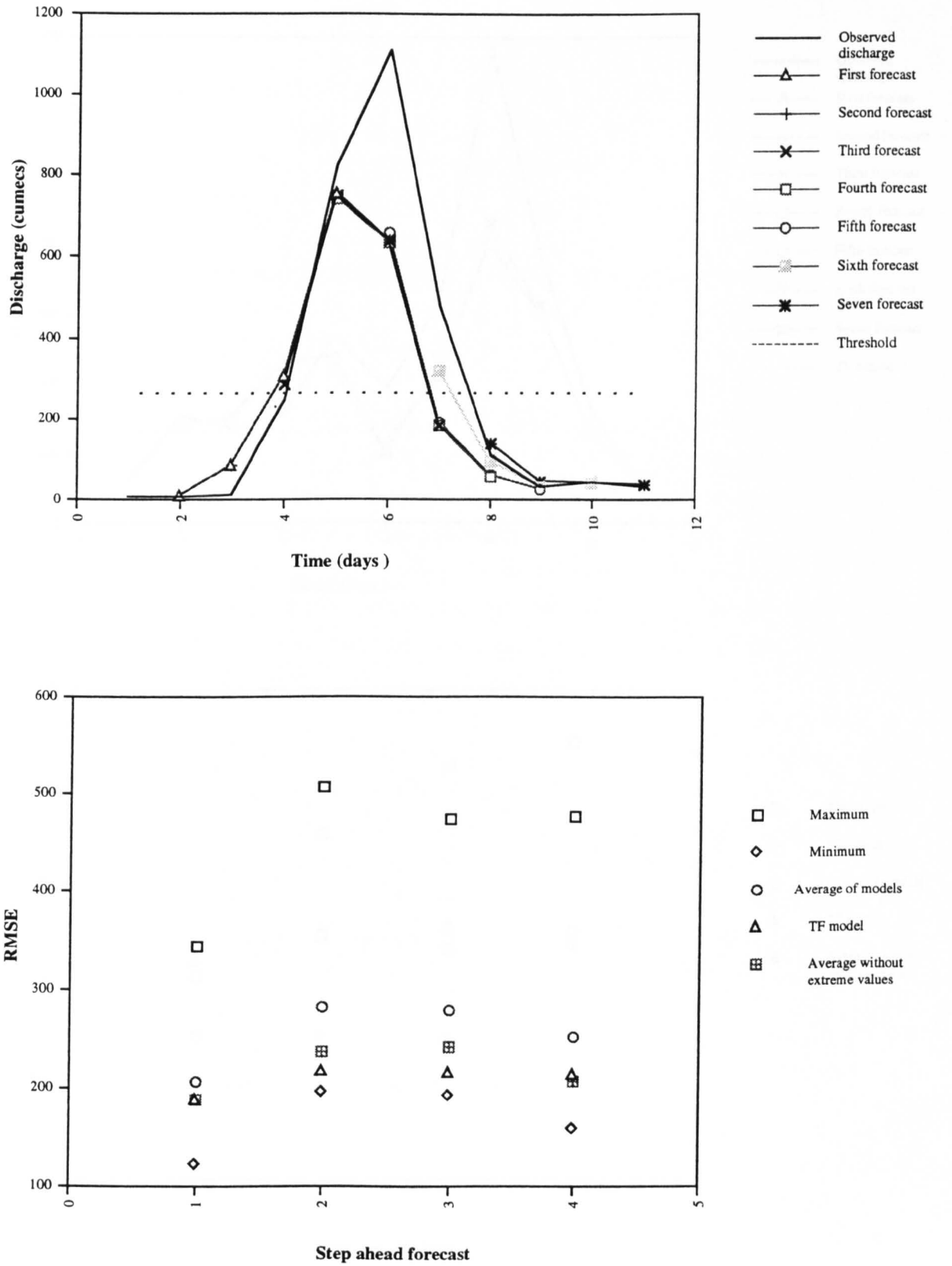

Figure (3.12) Seven multiple step ahead OTF forecasts (top), comparison of RMSE of different models (bottom) Bird Creek catchment, event no. 5.

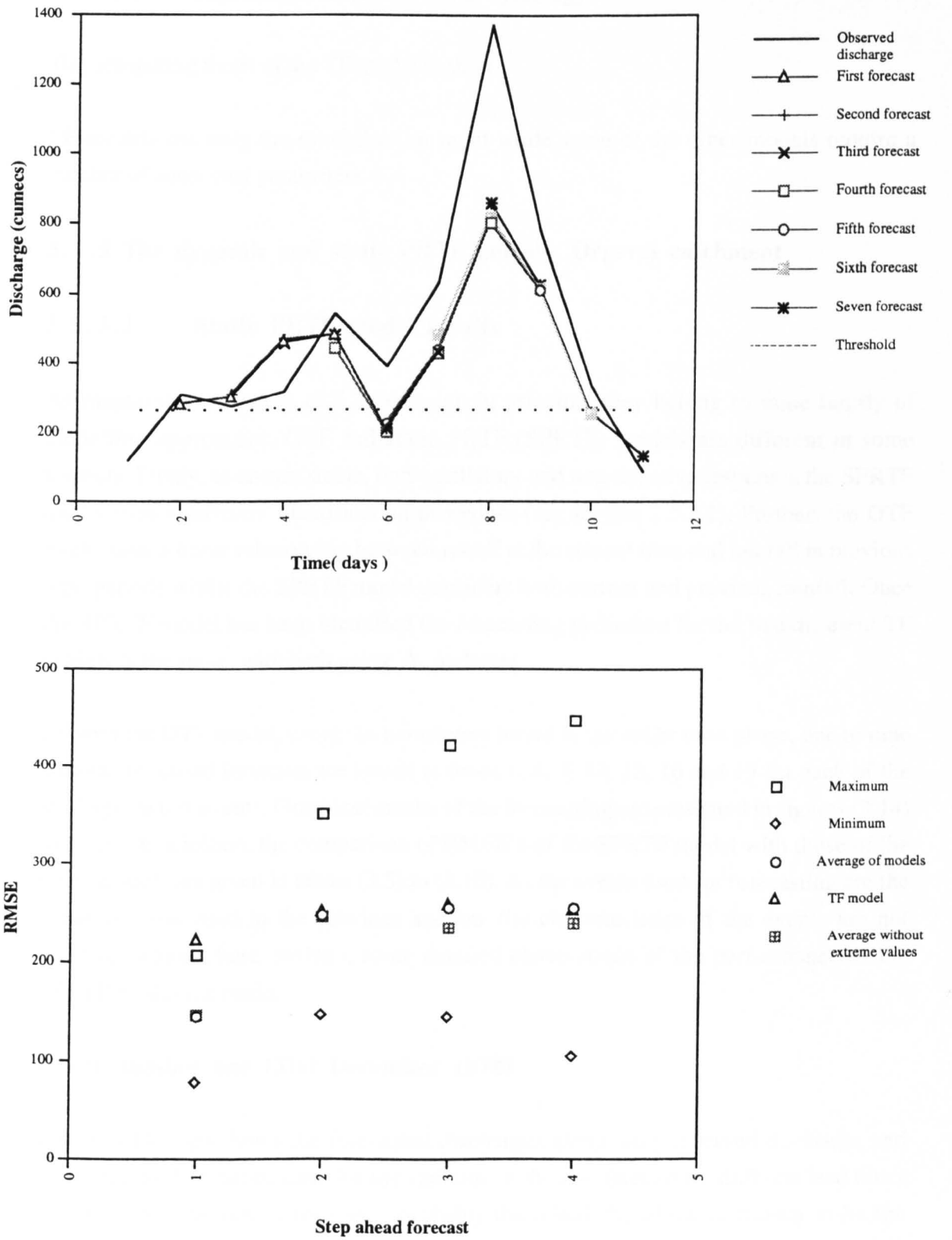

Figure (3.13) Seven multiple step ahead OTF forecasts (top), comparison of RMSE of different models (bottom) Bird Creek catchment, event no. 6.

Transfer function models can be easily used and require minimal training in modern estimation theory, whereas the application of the some of the other models requires detailed knowledge both in modelling and in hydrology.

The computing times of the TF model is short.

TF models use only the rainfall as an input while some of the other models require a number of additional parameters.

3.5.5 The dynamic and static PRTF models: Orgeval catchment

3.5.5.1 Static PRTF model results

As mentioned in section (2.5.2) although in principle they belong to same family of modelling approaches, OTF and static PRTF (SPRTF) models are different in some respects. Firstly, to ensure stable, non-oscillatory and non-negative responses the SPRTF model uses a different identification procedure (see section 2.5.2.1). Further, the OTF model uses a linear relationship between runoff at the current time and rainfall in previous time periods whilst the SPRTF model considers both current and previous rainfall. Once the SPRTF model has been identified the forecasting procedure for the two different TF models is the same, with both using Δ updating.

As with the OTF model, using the parameters found in the calibration phase, one to nine step (hour) ahead forecasts are issued at times 1, 4, 7, 10, 13, 16 and 19 for each of the six Orgeval test events. Graphical results of the forecasting are presented in figures (3.14) to (3.16). In addition, the comparison of RMSE's of the SPRTF model with those of the other models are given in tables (3.5) to (3.10). As the events used for forecasting are the same as those used in the previous section, the characteristics of the events are not mentioned again here. Instead, some detailed observations of the performance of the SPRTF model are made.

Event number one (31st December 1978)

Figure 3.14 (top) shows the forecasted discharges along with observed discharge and threshold level. It can be seen that the variation of the first forecast for different lead times is very slow. The reason for this is probably the initial Δ, which is chosen to be the smallest one at the beginning of the each event. Although as concluded in section (3.5.3) the use of smallest Δ as the initial Δ, overall and average may be the best choice when three criteria considered together, but as it has been seen in this event the use of

$\Delta_{minvariable}$ produced a very poor forecast for first forecast when only the RMSE criterion is considered (this is the case for other events). From figure (3.14) it can be seen that if the first forecast is disregarded the ranking of the TF model will improve considerably. The second forecast overestimates the discharge. The third forecast is in agreement with observed discharge up to four steps ahead, but fails to predict the rising limb for other steps. The fourth forecast is totally wrong. The fifth forecast more or less fits the observed discharge at least up to 3 step ahead and is able to predict reaching of the threshold reasonably well. Although this forecast provides a good prediction of the time of peak flow 9 hours in advance, values of observed discharge from the fourth step ahead are underestimated. The sixth forecast parallels the observed discharge but underestimates the actual flows. In contrast, the seventh forecast overestimates the recession limb.

The NTD1 and portmanteau statistics in table (3.5) both indicate that the calibration model is appropriate for this event. Further, the RMSE of the SPRTF are smaller than those of average of other models up to three steps ahead, but are bigger for the remaining steps As with the OTF model, the absolute values of the RMSE of the current model increases with lead time, but the relative increase is less than those of the OTF model.

Event number two (2nd February 1979)

The NTD and portmanteau statistics (table 3.6) show that the calibrated model can be used for this event. Figure 3.14 (bottom) shows that the first three forecasts fail to predict the ascending limb, but the second and the third forecast are able to show the time of peak flow relatively well 8 hours in advance. The estimated discharge at the fourth forecast only fit the observed data up to two steps ahead. Fitness of estimated and actual flow in the sixth and seventh forecast are perfect.

Again here the absolute and relative RMSE of model increases with lead time, but as with event one the relative increase of RMSE in comparison with the OTF model is smaller.

Event number three (10th March 1979)

Figure 3.15 (top) shows the seven forecasts of this event. Unlike previous events the discharge falls sharply prior to start of the event and continues to decrease hours after this time. The first forecast increases very rapidly with time, despite the fact that the six other forecasts are in close agreement with actual flow, the large differences between estimated and observed flow for the first forecast causes the SPRTF model to be worst model overall. The values of the second and the third forecast closely fit observed flow at least up to four steps ahead but fail to adequately represent the rising limb. The fourth forecast

significantly underestimates the actual values. Although the fifth forecast follows the same pattern as the observed values, it also underestimates the discharge. The sixth forecast clearly fits the actual values up to three steps ahead and then overestimates the recession limb. Finally the seventh forecast also overestimates the observed values of discharge.

Table (3.7) indicates that the RMSE's of the SPRTF model are always larger than the other models and are only comparable with its OTF counterpart.

Event number four (13th March 1980)

Figure 3.15 (bottom) shows the forecasted and observed discharges and threshold level. It can be seen that the second forecast is in close agreement with observed discharges up to four steps ahead and is able to forecast the reaching of the threshold. The third and fourth forecasts underestimate the discharge. The fifth forecast parallels but underestimates the actual flow. The time of the peak value is forecasted very well. Finally the sixth and the seventh forecasts estimate the recession limb reasonably well.

As with the OTF model the forecasting accuracy of the SPRTF decreases with lead time (see table 3.8). The rank of SPRTF is 6^{th} amongst the events evaluated in first step ahead but it falls to 10^{th} and 11^{th} for average and nine steps ahead forecast performance respectively.

Event number five (13th July 1980)

As shown in figure 3.16 (top) the second forecast predicts the threshold exceedance three hours in advance but underestimates the main rising limb. On the other hand, the third forecast overestimates the observed discharge. The fourth forecast parallels but overestimates the recession limb of the observed hydrograph. In contrast, although the fifth forecast follows the ascending limb, it underestimates the observed flow. The sixth forecast closely follows actual flow up to four steps ahead but the errors are large for longer lead times. The final forecast fails to predict both the final rising and recession limbs.

As regards RMSE, table (3.9) indicates that the performance of SPRTF model for all steps ahead is better than those of the average models. As with the other events, the forecasting capability of the SPRTF model decreases with lead time.

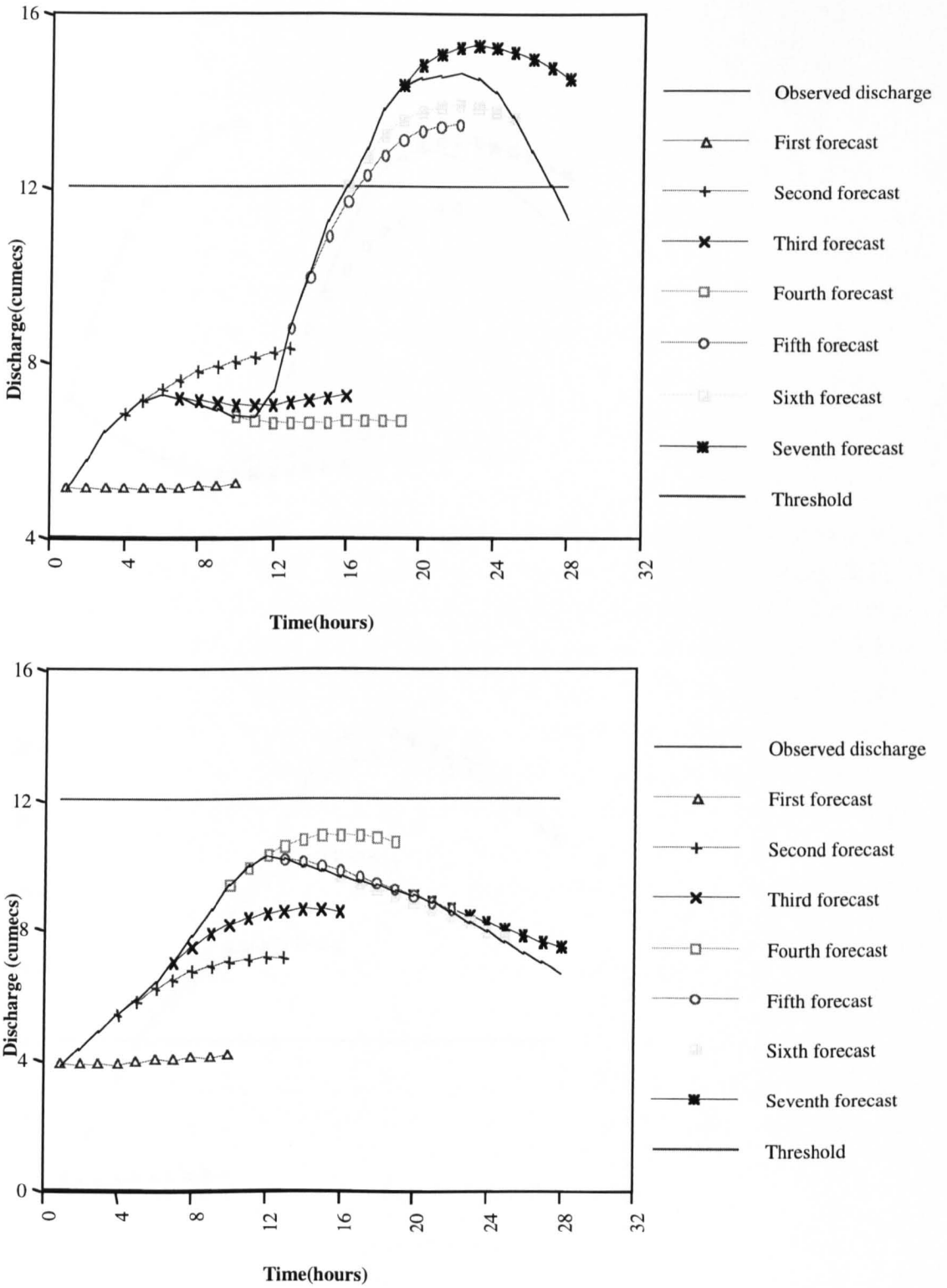

Figure (3.14) Seven multiple step ahead forecasts by SPRTF model for the Orgeval catchment (top, event 1; bottom, event 2).

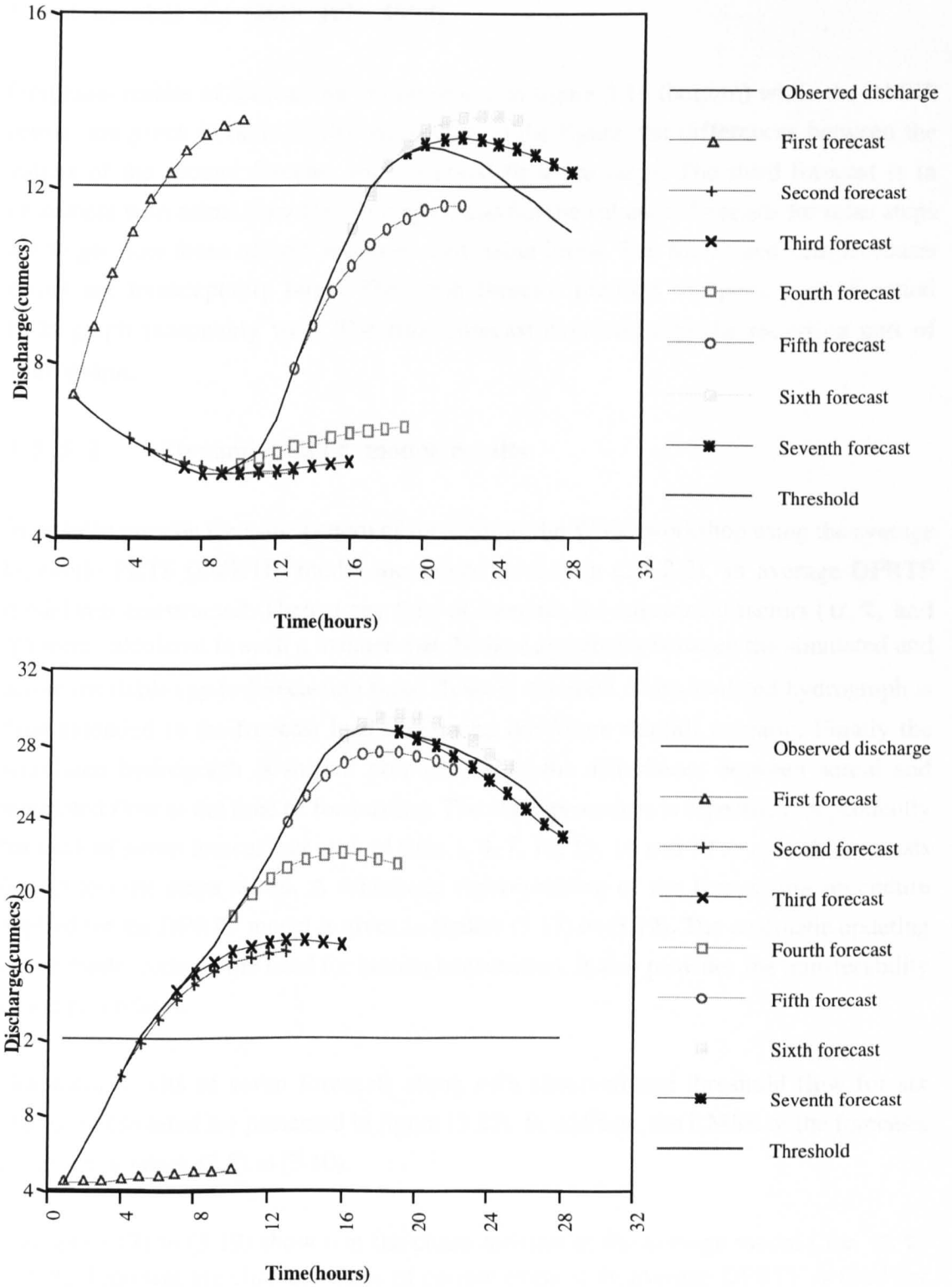

Figure (3.15) Seven multiple step ahead forecasts by SPRTF model for the Orgeval catchment (top, event 3; bottom, event 4).

Event number six (20th July 1980)

Graphical results of forecasting are presented in figure 3.16 (bottom) while the RMSE results are given in table (3.10). According to the figure, the differences between the values of the second forecast and observed flow are large. The third forecast is in agreement with actual flow for two steps ahead but the values of forecasts for other steps are larger than those of both recession and rising limbs. The fourth and fifth forecasts errors are unacceptably large. The sixth forecast predicts the peak part of actual hydrograph reasonably well. The final forecast overestimates the recession part of hydrograph.

3.5.5.2 Dynamic PRTF model results

In order to provide the same pattern of forecasts as the WMO workshop using the average Dynamic PRTF (DPRTF) model mentioned in section (2.5.2.2), an average DPRTF model was constructed. Then at any time of forecast, the adjustment factors (α, τ, and γ) were calculated in such a manner that the best agreement between the simulated and actual available (up to forecasting time) flows is obtained. The simulated hydrograph is then extended to the forecast lead time using the future rainfall scenario. Finally the simulated hydrograph is shifted proportional to the differences between actual and simulated flow at the time of forecasting. The same procedure is repeated independently for each of seven forecasts at each of time 1, 4, 7, 10, 13, 16 and 19 to provide forecasts for up to nine steps ahead. A schematic representation of the forecasting procedure applied for the DPRTF model is given in figures (3.17) to (3.19). The automatic updating of the model reduces the need for human intervention. It also provides the transferability of the procedures.

Graphical results of seven forecasts along with observed and threshold flow for six events investigated are presented in figure (3.20). In addition, the RMSE of the forecasts are given in tables (3.5) to (3.10).

Figures (3.17) to (3.19) show that the characteristics of the average model (i.e. α, τ, and γ) dominate the characteristics of current event if an average DPRTF is used for forecasting because duration of the current event is very short compare with very long period of average model data. Therefore, if the condition of the current event differs significantly from the average condition the quality of forecast will fall.

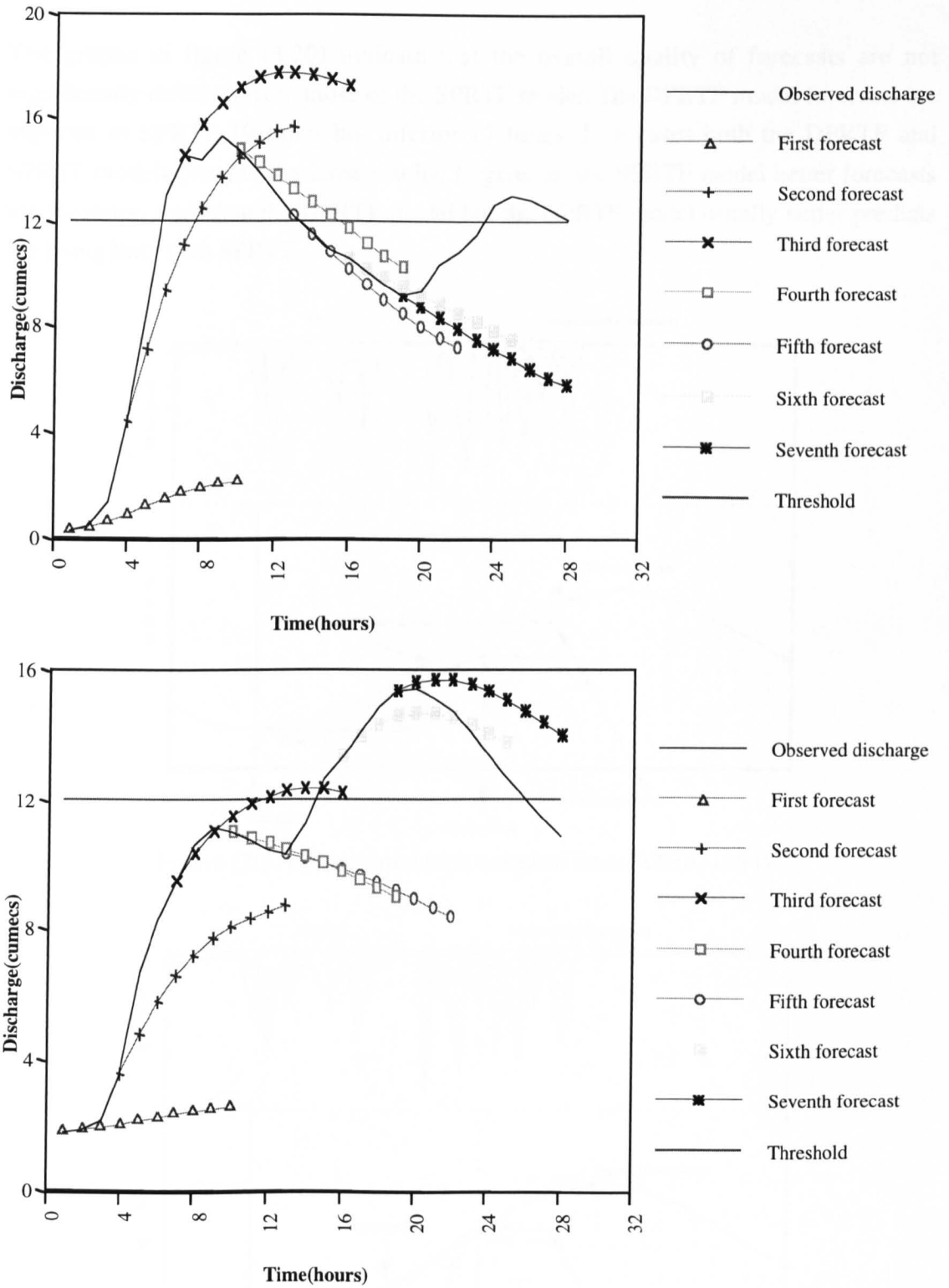

Figure (3.16) Seven multiple step ahead forecasts by SPRTF model for the Orgeval catchment (top, event 5; bottom, event 6).

The graphs in figure (3.20) indicate that the overall quality of forecasts are not significantly different from those of the SPRTF model. The DPRTF model forecasts are superior to SPRTF 19 times but inferior 17 times. In 6 cases both the DPRTF and SPRTF models provide the same results. In general, the SPRTF model better forecasts the recession limb than the DPRTF model but the DPRTF model usually better predicts the rising limb than SPRTF.

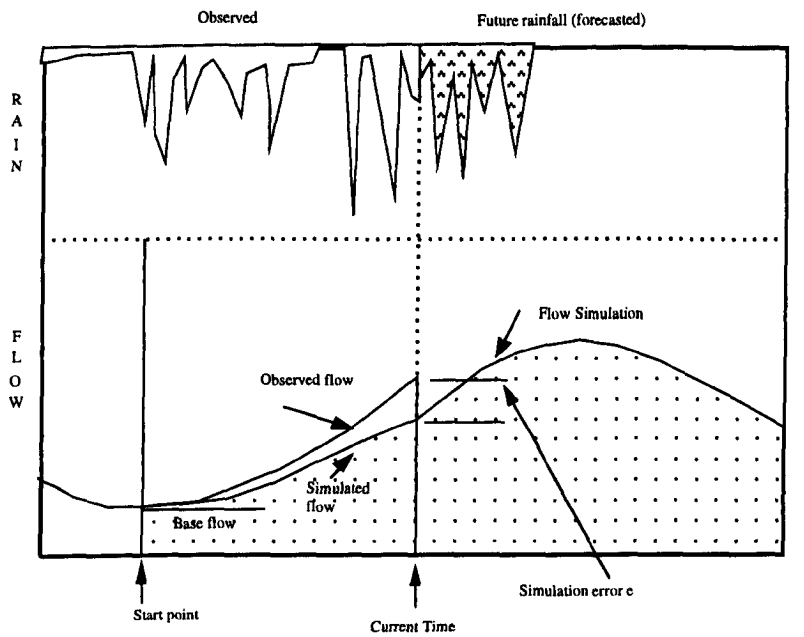

Figure (3.17) Flow simulation (adapted from WRIP, 1994)

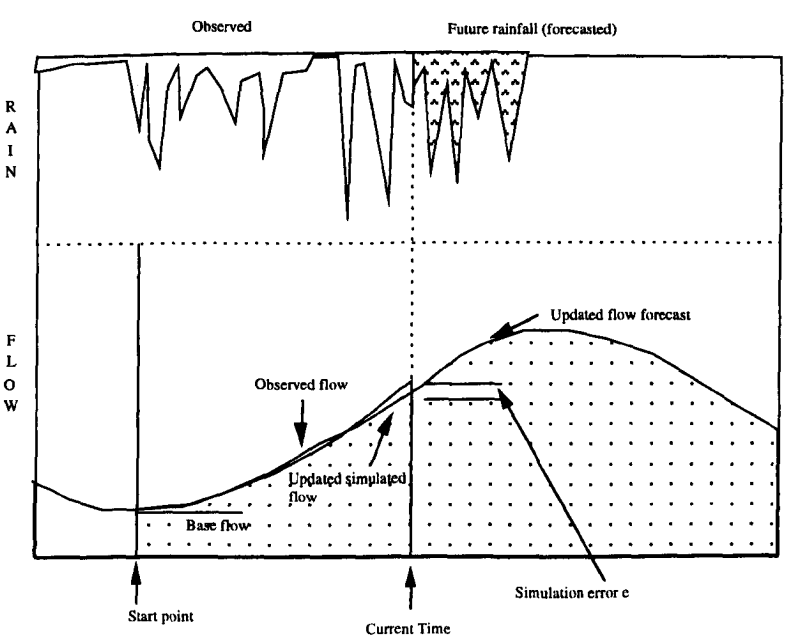

Figure (3.18) Flow simulation after TF model updating (adapted from WRIP, 1994)

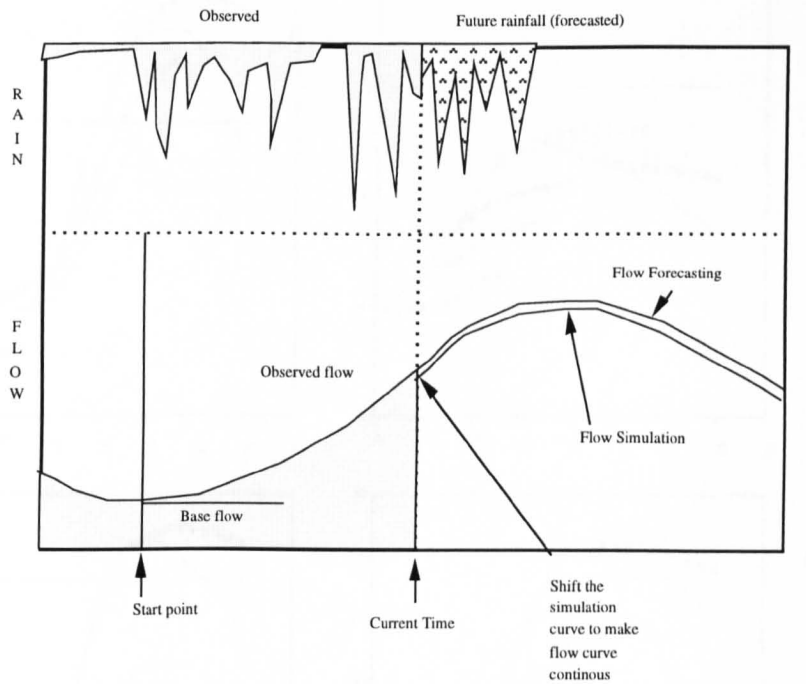

Figure (3.19) Flow forecasting based upon flow simulation (adapted from WRIP, 1994)

3.5.5.3 Summary of observations relating to PRTF model

With respect to RMSE results for all six events forecasted by SPRTF model it can be concluded that as with the OTF model the relative and absolute values of RMSE increase with lead time. Therefore performance of the SPRTF model in lower steps is better than for larger lead time. In comparison, the OTF model forecasts both for one step ahead and on average are superior to the SPRTF forecasts. In contrast, the model produces better forecasts than the OTF model's for the longer lead times, especially 9-hours ahead.

The forecast quality of the DPRTF model is not significantly different from the average static transfer function model.

As the use of $\Delta_{minvariable}$ as initial Δ usually produces poor forecasts in first forecast, if the first forecast of each event under evaluation is disregarded the ranking of the SPRTF model will improve remarkably.

As it mentioned in section (3.5.4.3) there is no consistent pattern in the performance of the models on an event basis. In table (3.11) the RMSE results of ATF models are compared with those of WMO project models. Note as the TANK and NAMKAL models did not attempt to model all the events, they are not considered in ranking comparison.

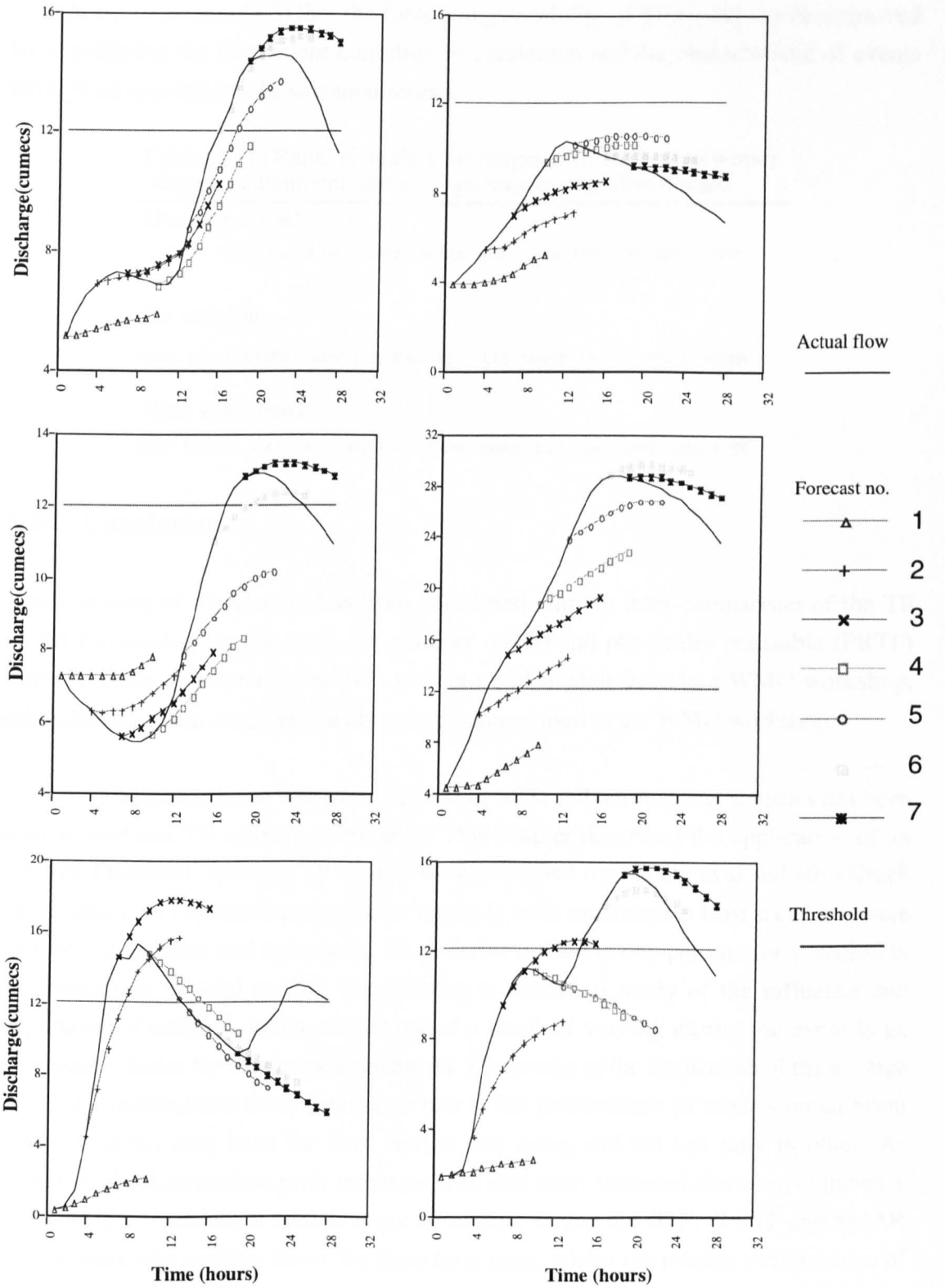

Figure (3.20) Seven multiple step ahead forecasts by DPRTF model, Orgeval catchment (Top left event 1, Top right event 2, Middle left event 3, Middle right event 4, Bottom left event 5, Bottom right event 6)

It is shown in section (4.3) that the forecasting capability of TF model can be improved by considering the antecedent condition of catchment and the characteristic of events through an appropriate classification scheme.

Table (3.11) Rank of models investigated (from best to worst) , Orgeval catchment and average transfer function models.

One step ahead:

GAPI TF SMAR CEQUEAU NAMS11 SSARR SPRTF CLS HBV UBC HFS DPRTF

On average:

GAPI SMAR NAMS11 HBV CEQUEAU HFS CLS SSARR UBC TF DPRTF SPRTF

Nine step ahead:

HBV NAMS11 GAPI HFS CEQUEAU SSARR SMAR CLS UBC DPRTF SPRTF TF

3.6 Conclusion

Major section of the chapter has been concerned with an inter-comparison of the TF model forecasting results (both for ordinary (OTF) and physically realisable (PRTF) forms in static and dynamic modes) with those of models used in a WMO workshop, using the same data sets, catchments and procedures used in the WMO workshop.

A cross-validation scheme consisting of RMSE, NTD and portmanteau statistics has been used to evaluate TF model performance. This chapter described the application of an average TF model. Average TF models were identified for the Orgeval and Bird Creek catchments either for static and dynamic forms. In each catchment at least six events were used for verification and forecasting. A Δ factor is used to compensate for variation in the proportion of total rainfall contributing to runoff. A study of the influence and importance of initial Δ indicated that use of a small Δ varying during the event is an appropriate choice for the Orgeval catchment. The results of the application of the average TF model indicate that there is no strict rule in the performance of models on an event basis. A model may have the first rank in one event and the last rank in other. As expected, absolute forecast error increases with lead time. However, the relative increase of the RMSE for different models is not consistent, so that the OTF, SPRTF and SMAR models generally perform better for short time steps, whilst the relative performance of the HBV, NAMS11, HFS, SSARR, DPRTF and UBC models increases with lead time. If only the performance of the OTF and SPRTF are concerned, the quality of forecasts in OTF model both in one step ahead and on average are superior to SPRTF. In contrast the SPRTF model provides better forecast than those of OTF for longer lead times. With respect to comparison of the performance of static and dynamic form of TF models, it is

concluded that there is not a significant difference between the quality of the forecasts derived from the static and dynamic TF models.

CHAPTER 4

FURTHER DEVELOPMENT OF TF MODELS

4.1 Introduction

This chapter begins with an introduction to a simple technique to calculate average pulse responses. Further research has been done to extend the capabilities of TF models through an event classification and grouped calibration procedure. Group models are constructed on the basis of storm characteristics and antecedent catchment conditions. This study is followed by an evaluation of single event TF models. Finally an overall comparison of average, grouped, and single event TF models as well as the WMO project models is presented. In the last part of the chapter an expert system-based approach for the further investigation of the grouped model is proposed.

4.2 Improving TF model simulation

Sometimes there is a need to estimate a single average pulse response (APR) from several pulse responses associated with a number of events. This section deals with the evaluation of different approach of calculating APR.

4.2.1 A simple model to calculate the average pulse response

One way of calculating the APR is to combine all the events into one continuous data set and calculate the corresponding pulse response (method 1). A second estimate can be obtained through a simple ordinate averaging technique: however, such an approach produces a flattened pulse response (method 2). A further novel approach is to estimate the average pulse response using a simple model of average characteristics (method 3).

The proposed model computes the average of the time to peak, the peak, and the width of the pulse response at the 10, 20, 30, 40, 50, 60, 70, 80, and 90% of the peak; and then draws a curve with unit volume through the resulting points. The details are summarised below.

The first step is to calculate the pulse response ordinates of several events using the a and b parameters found in the model identification phase. Since each event has its own

percentage runoff (PR) it is necessary to normalise each PR to provide unit volumes. The peak and the time to peak of each normalised PR (NPR) are calculated. The peak and time to peak of normalised APR (NAPR) is simply calculated by averaging the peak and time to peak of all events. To find other points of the NAPR the following procedure is applied.

Using a simple interpolation programme (also see Fritsch and Bultland, 1984 and Numerical Algorithm Group, 1990) the start time, the end time and its corresponding width of pulse response at the 10, 20,....., and 90% of the peak for each event are calculated. The mean width of a specified percent of the peak on the whole events is calculated simply by averaging the width of the same specified percent of the peak on the different events. This mean width is then used for the average pulse response. To find the start time and end time of a specified percent of the peak on the APR the following procedure is applied.

First, the differences between the start time and time to peak in a specified percent of the peak in the individual event is calculated. This difference then is divided by the width of the same specified percent of the peak. A similar computation is applied to the end time. The sum of these two ratios is unity. The mean ratio of the all the event is then calculated by averaging the ratios of the different events in the specified percent of the peak. Finally, the resulting ratios are applied to the mean time to peak calculated in the previous steps. At this stage, the properties of twenty points of average pulse response have been calculated ranging from 0 to 100 percent of the peak. The ordinates of the NAPR are calculated using the same interpolation program. Adjustment is applied to the resultant ordinates to provide a unit volume for the NAPR. Finally the NAPR are denormalized to calculate the ordinates of average pulse response of the all events.

Figure (4.1) illustrates the relationship between the pulse response function, input and output of a hypothetical example, computing of convolution amounts is straightforward.

4.2.1.1 Comparison of APR achieved from three different methods

Two events from the Orgeval catchment are used to evaluate the performance of the three different APR determination procedures. A graphical comparison of the resulting pulse responses and convoluted rainfall are presented in figures (4.2) and (4.3) respectively. Meanwhile some characteristics of the initial and resultant pulse response and RMSE of convoluted rainfall are given in table (4.1). It can be seen that overall, the use of the proposed method has proved to be encouraging. Although it needs more investigation, this method may be worth consideration.

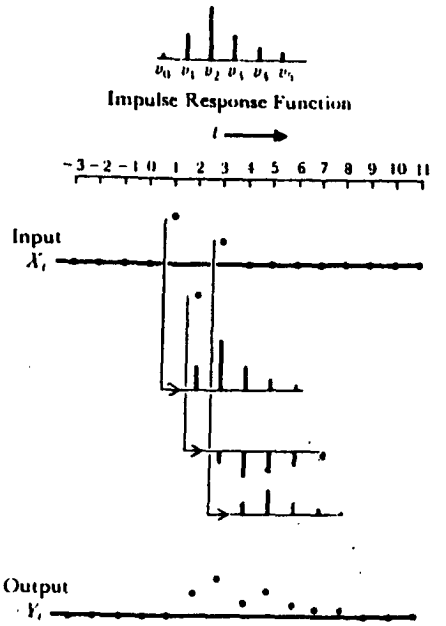

Figure(4.1) Linear transfer from input X to output Y (adapted from Box and Jenkins, 1976)

Table (4.1) Summary description of the characteristics of different methods of calculation of average pulse response

	a1	a2	a3	b1	b2	b3	pulse response tpeak	pulse response peak	RMSE of reconvolution
Event 1	1.935	-0.979	0.040	0.005	0.022	0.004	18	0.213	-
Event 2	1.533	-0.689	0.125	0.005	0.299	0.006	4	0.514	-
Method1	1.936	-1.141	0.194	0.001	0.153	-0.058	7	0.330	0.553
Method2	-	-	-	-	-	-	5	0.304	0.525
Method 3	-	-	-	-	-	-	11	0.309	0.536

4.3 Improving TF model forecasting performance- A group model approach

As mentioned in section (3.5.2) the pulse response function derived from a sequence of storms reflects the average catchment response to those storms. However, every event has its own distinguishing features according to antecedent conditions of catchment and storm characteristics. This implies that if a sequence of storms with similar characteristics are selected for calibration, the resultant average TF (ATF) may provide better forecasting performance for future events with similar characteristics. Thus, a suite of several ATFs could be constructed, and used to forecasting flows for events whose characteristics closely matched.

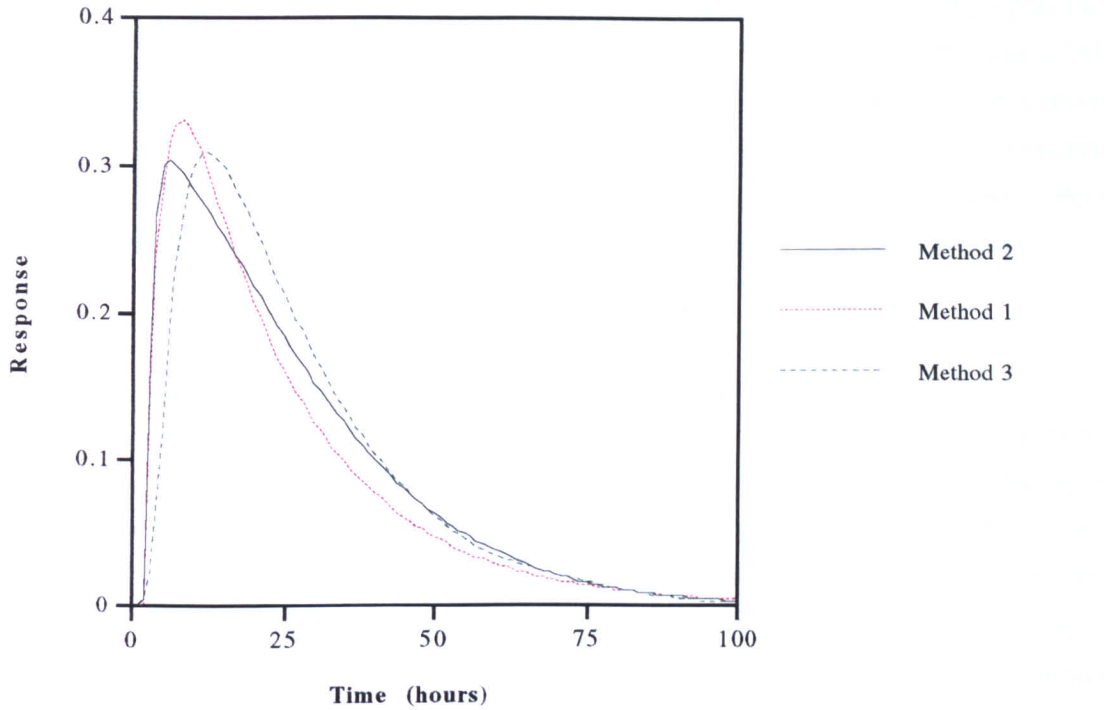

Figure (4.2) Comparison of average pulse response obtained from three methods.

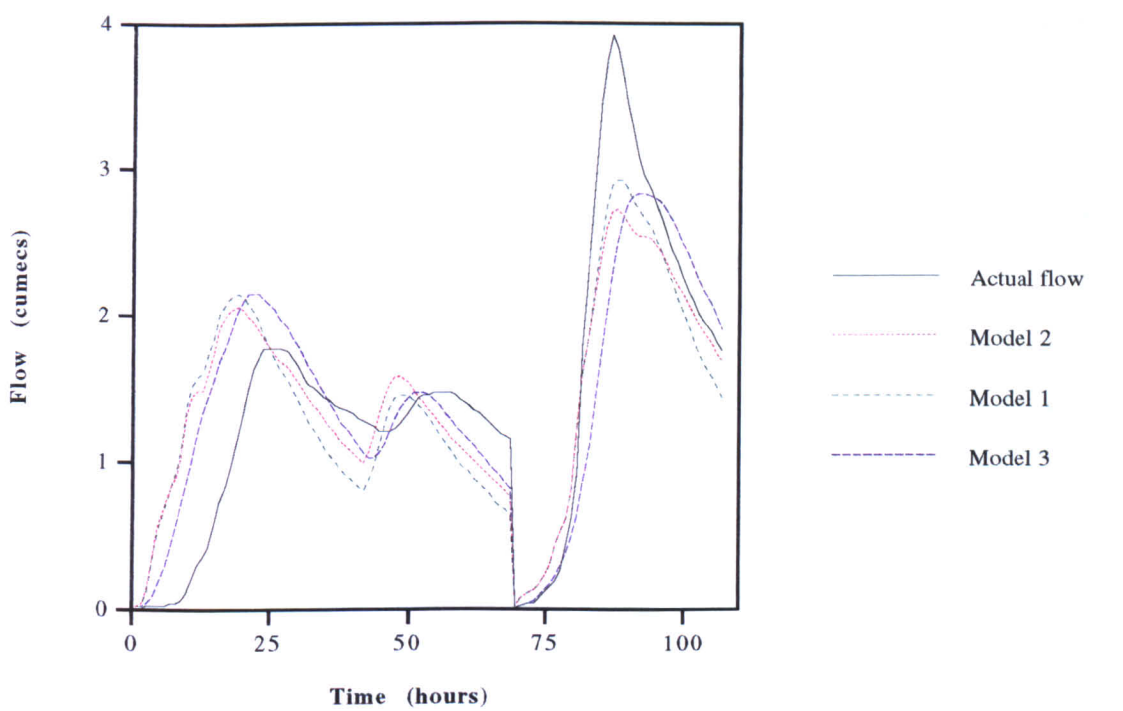

Figure (4.3) Comparison of actual flow and reconvoluted flow obtained from different methods

In such a manner, Viner (1992) classified storms into three groups depending upon the gradient of the rising limb of an individual storm's pulse response (PR). He concluded that the 'higher gradient event' could be related to higher intensity flashy rainfall events often corresponding to higher intensity showers. Similarly, the lower gradient events were often seen to correspond to low intensity, long duration rainfall often associated with low intensity frontal type precipitation. Finally an intermediate group was also found where no dominant precipitation type could be identified.

The quantity of runoff from a storm depends on the storm characteristics and the moisture conditions of the catchment at the beginning of the storm. Therefore, this section develops a storm classification scheme based not only upon storm characteristics but also the catchment antecedent condition. The classification approach developed utilizes variables that can be easily available in real-time in the hope that a significant improvement in real-time flow forecasts can be realised. In order to implement this study, all 32 Orgeval events used in construction of an average TF (section 3.5.2) were considered. Further, another individual event as well as eight verification events also are included.

In order to classify events according to the PR gradient, a model with same order was calibrated for each event. The ordinates of pulse response function of each event were then calculated. For the purpose of direct comparison the steady state gain of the model was kept constant.

Events were divided into three groups according to the gradient of the rising limb of the pulse response. A listing of each group is given in table (4.3) and figures (4.6) and (4.7). Although 41 distinct events were available from the WMO data set compared to the 24 available to Viner it has not been possible to produce the same definite conclusions as him regarding the relationship between the gradient of the PR and precipitation type. Despite this it was decided to include a gradient classification to evaluate the probable role of the gradient of PR on the quality of forecasts.

There are several methods for determining the antecedent moisture conditions of a catchment ranging from direct measurements (e.g. Lysimeters (Shaw, 1994)) to mathematical estimation (e.g. antecedent precipitation index, Linsley *et al.*, 1983). Since the aim of the current investigation is to provide an index of the antecedent moisture condition for classification of catchment wetness, a simple method introduced by the US Soil Conservation Service (SCS) has been used.

The SCS established three antecedent moisture conditions in computing abstractions from storm rainfall (Wanielista, 1990). The three conditions relate to five day antecedent precipitation as shown in table (4.2). It should be stressed that the actual initial moisture of catchment depends on the type of soil, topography, vegetation, season, climatological conditions, etc. Therefore this classification only approximates the moisture condition of the catchment and is best considered as an indicator of the initial moisture of the catchment.

Table (4.2) (after Wanielisa, 1990) based on an analysis of 41 events

Condition	Description	Five Day Antecedent Precipitation (FDAP)
1	A condition of drainage basin soils where the soils are dry but not to wilting point (Lowest runoff potential)	<12.7 mm.
2	The average case (Average runoff potential)	12.7 to 38.1 mm.
3	When heavy rainfall or light rainfall with low Temperature have occurred producing high runoff potential	>38.1 mm.

The five day antecedent precipitation (FDAP) in two different periods with same daily amount of rainfall but with reverse order is the same. Therefore, five day and thirty day antecedent precipitation indices (API5, API30) were also calculated for all the events evaluated. In order to classify the values of API5 and API30 as indicated in figures (4.4) and (4.5) relationships between these values and FDAP were constructed. Then the values of API5 and API30 each were classified into three group using same relationships and FDAP boundaries.

Different data sets can be chosen either by individual or joint consideration of characteristics. As mentioned earlier, the final purpose of this study is to use the group calibrated model for forecasting eight verification events. Therefore, as shown in figures (4.6) and (4.7) some groups obtained from a consideration of either individual or combined characteristics are not appropriate for the current study. As a result, and according to table (4.3), thirteen different groups have been derived to construct different average transfer function models. Note that the group D and group E are obtained from five day antecedent precipitation index classification.

Table (4.3) Details of classification used in group investigation

Groups ' name	Calibration series	verification series	MO	MPR	APR	PTPR	Base flow runoff relationship
II	10,14,17,18,21,22,25,26	wmo2,wmo4,v2	3,1	53.9	34.9	8	-
III	1,13,15,23,24,30	wmo1,wmo3, wmo5 ,wmo6,v1	3,2	19.6	22.6	6	-
A	1,2,3,4,5,6,7,8,9,11,12,13, 14,15,16,17,19,20,26,27, 28,29,31	wmo2,v2	3,2	34.0	26.7	8	R=18.3+10.4B
B	10,18,21,22,23,24,25,30, 32	wmo3,wmo4, wmo5 ,wmo6,v1	3,3	43.1	31.7	8	R=15.5+9.0B
AII	1,9,v2,14,17,26	wmo2,v2	3,3	20.4	21.5	9	R=6.1+15.2B
BII	10,18,21,22,25,32	wmo4	3,3	53.2	36.0	8	R=12.7+14.7B
BIII	v1,23,24,30	wmo3,wmo5, wmo6, v1	3,3	22.5	20.3	6	R=11.0+6.6B
D	2,3,4,6,7,8,11,12,13,14,15 ,16,17,19,20,26,28,29	v2	3,2	36.3	27.9	9	R=17.7+12.0B
E	1,5,9,10,18,21,22,23,24,25 ,27,30,31,32	wmo1,wmo2, wmo3,wmo4, wmo5,wmo6, v1	3,3	37.1	28.4	8	R=14.6+10.6B
X	2,3,4,5,6,7,8,12,13,14,15, 16,17,18,19,20,28,29	v2	3,3	37.5	29.2	9	-
Y	1,9,10,11,21,22,23,24,25, 26,27,30,31,32	wmo1,wmo2, wmo3,wmo4, wmo5,wmo6, v1	3,1	35.8	26.8	8	R=12.8+11.4B
XII	14,17,18	v2	3,3	44.7	29.6	9	-
YIII	1,23,24,30	wmo1,wmo3, wmo5,wmo6,v1	3,2	18.6	18.2	6	R=7.8+8.0B

APR = Average percentage runoff, MPR = Model percentage runoff, PTPR = Peak time of pulse response, MO = Model order

4.3.1 Ordinary TF group model results

In order to carry out the group model classification study the same methodology as described in section (2.5.1.4) was used. For each of the grouped time series a search procedure was applied and models of increasing order, ranging from 1:1 through 8:8 were constructed and the pulse response functions as well as convoluted rainfall and error statistics compared. Once the appropriate equal order models were selected, the model order reduction technique was used and the ideal model for each group selected. Some characteristics of the grouped models are presented in table (4.3).

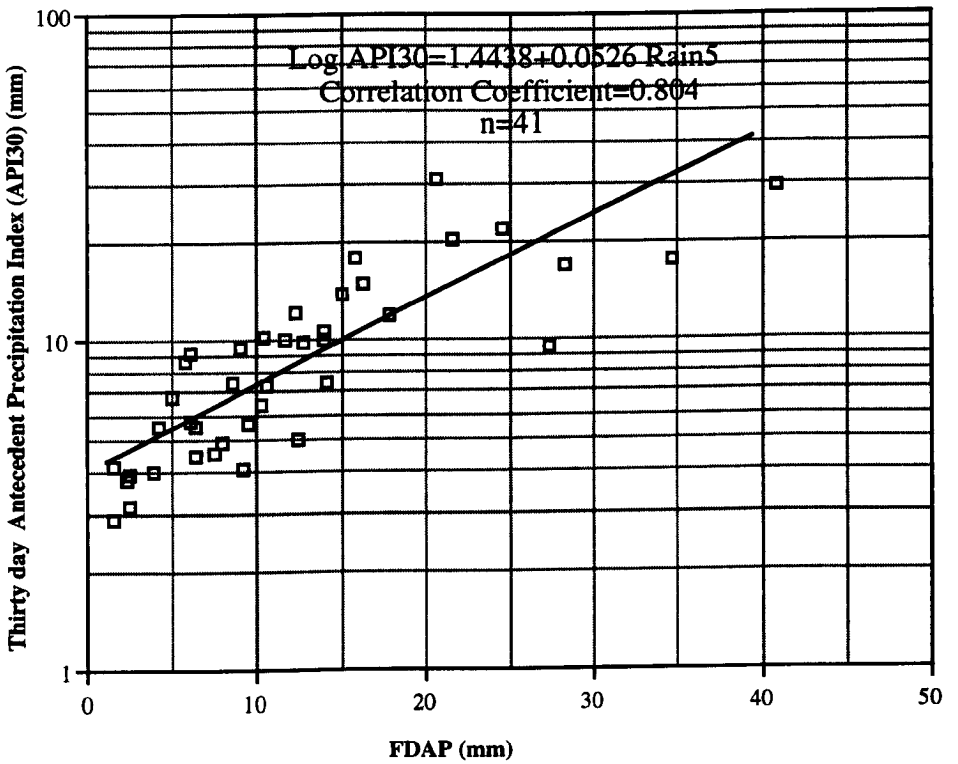

Figure (4.4) Thirty day antecedent precipitation index, five day antecedent precipitation relationship, Orgeval catchment.

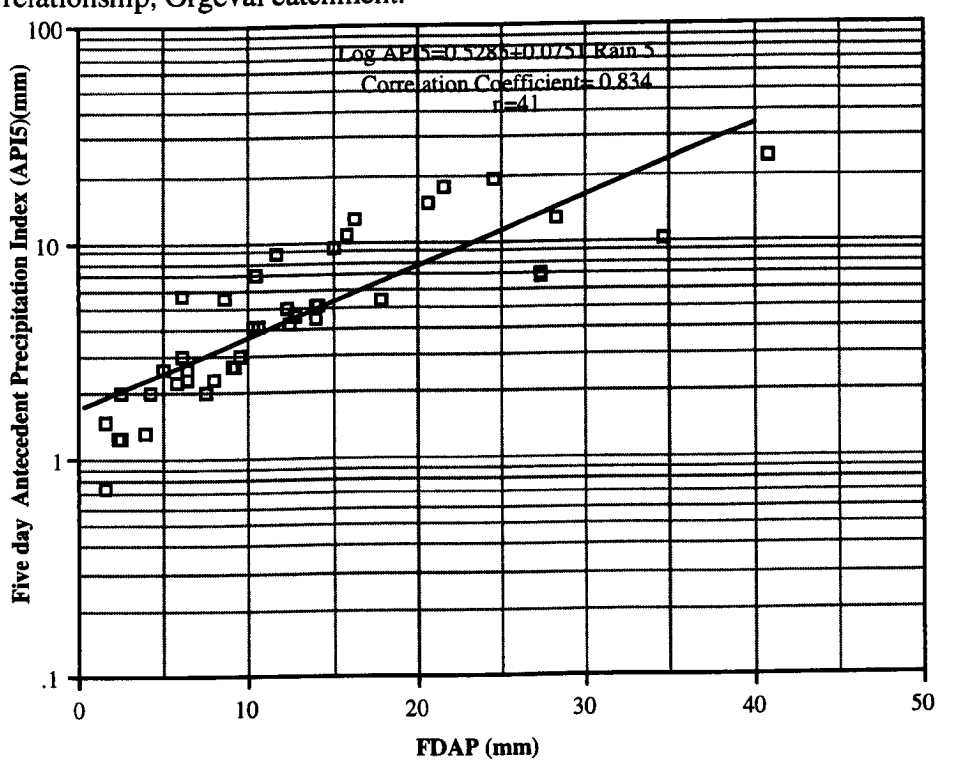

Figure (4.5) Five day antecedent precipitation index, five day antecedent precipitation relationship, Orgeval catchment.

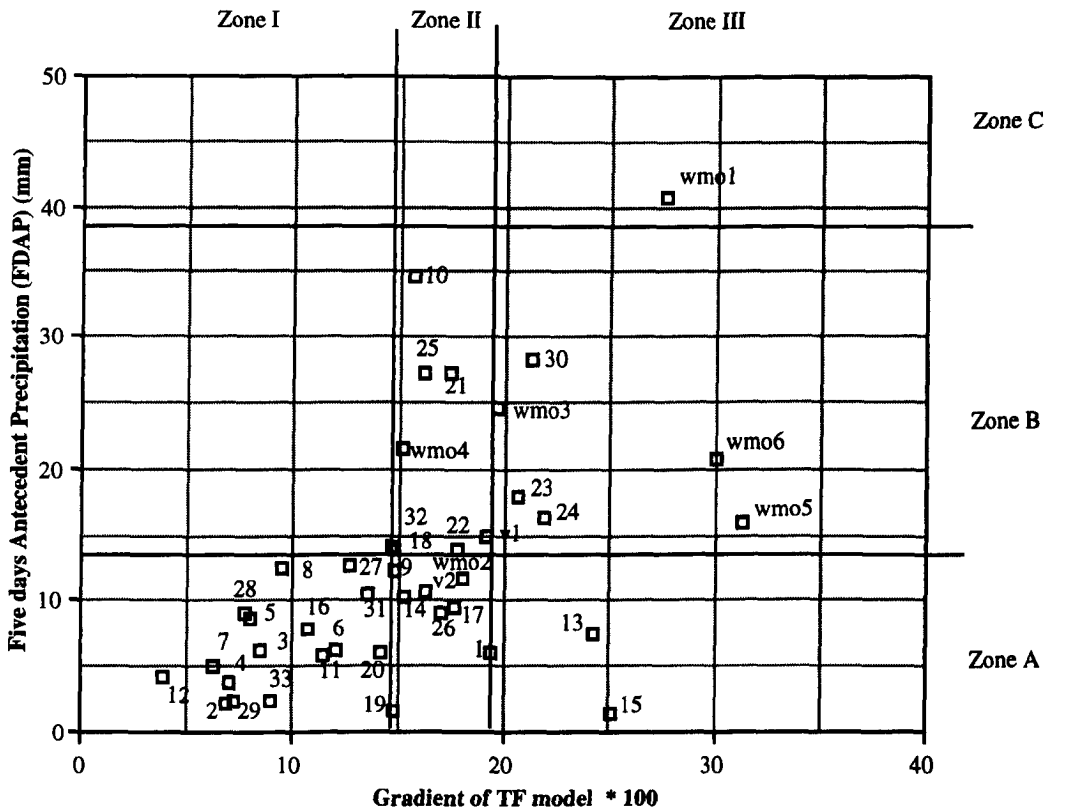

Figure (4.6) Classification of selected events according to five day antecedent precipitation and gradient of the pulse response, Orgeval catchment.

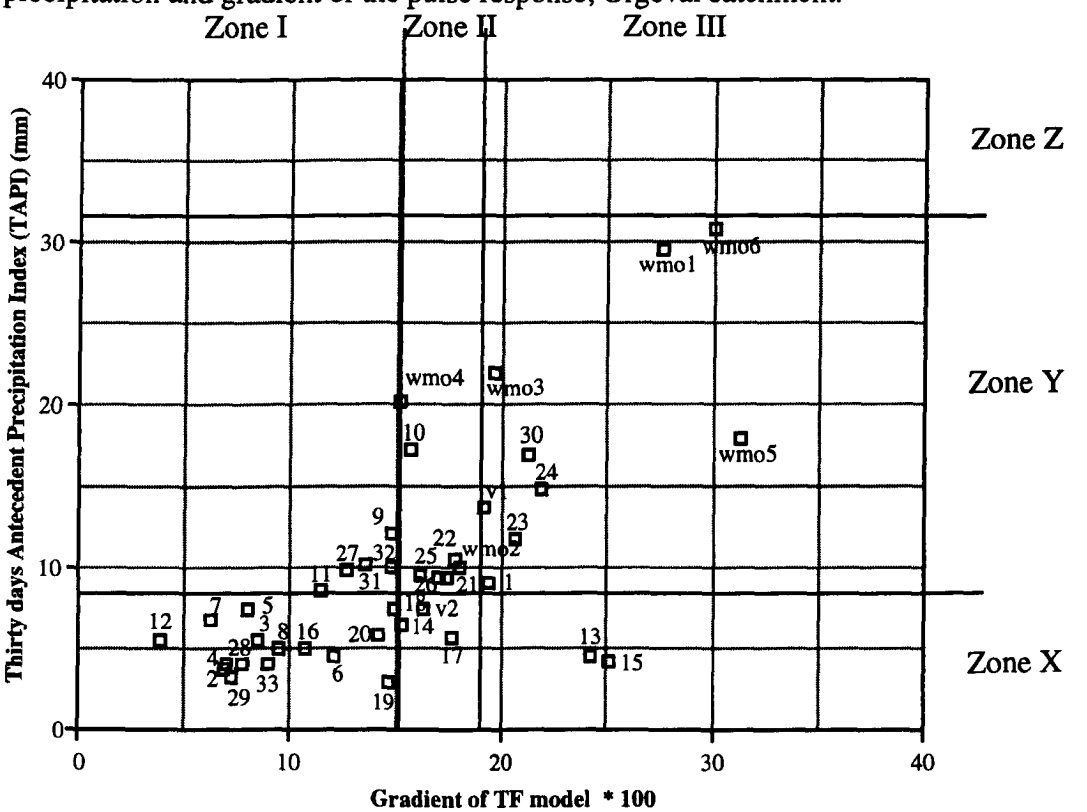

Figure (4.7) Classification of selected events according to thirty day antecedent precipitation index and gradient of the pulse response, Orgeval catchment.

The models calibrated for each of the thirteen groups were compared to the previous average transfer function (ATF) model. Verification events include the same six events which were used in section (3.5.4) together with another two events (15th November 1973, 30th November 1974) both of which are introduced later in this section. For the assessment of the performance of the models, the rainfall of each verification event was inputted into the given group model and the forecasted flows for one to nine steps ahead at each hour were calculated. Note that here, for better assessment of the models, the number of forecasts is increased from seven to the duration of each event (hours).

It was mentioned in section (3.5.3) no obvious relationship existed between percentage runoff and base flow for the 32 events as a whole although the possibility of a grouped relationship was introduced. Figure (4.8) indicates that the extraction of such a relationship in some of the groups investigated is possible. The equations relating runoff to base flow for each event group are presented in table (4.3), and where applicable, these were used to estimate the initial Δ for use in forecasting.

In order to evaluate the performance of the models, a direct subjective comparison was made of the forecasted hydrographs as well as an objective comparison of the RMSE of the flow forecasts at each time step ahead. This approach has been applied to all verification events and all groups where relevant.

Only the best forecasting performances for each verification event are presented graphically. In order to allow a direct comparison with the forecasts produced in figures (3.14) to (3.16) and (3.20) only the same seven forecasts are included. Further, in each verification event, grouped forecasted flow hydrographs for one, four and nine hours ahead are compared to those forecasts produced by the ATF model. Finally for objective comparison the RMSE's of each event-case obtained from all the forecasts, together with the randomness-dispersion diagram (see appendix 1) are presented. The following paragraphs describe the symbols used in these figures giving a brief outline of the methodology used to compare the performance of different models. Thirteen cases are included in each figure represented by letters A to M.

In section (3.5.3) when $\Delta_{\text{minvariable}}$ was selected as the initial Δ, it was noted that if only the RMSEs are considered, the best initial Δ may be different. Here, for comparison, this initial Δ (Δ_{best}) is also used. Letter A represents the performance of ATF model resulting from all 32 events using Δ_{best} as the initial Δ. As with $\Delta_{\text{minvariable}}$, Δ_{best} is time variant. Letter B is allocated to the performance of the ATF model in which the initial Δ is $\Delta_{\text{minvariable}}$

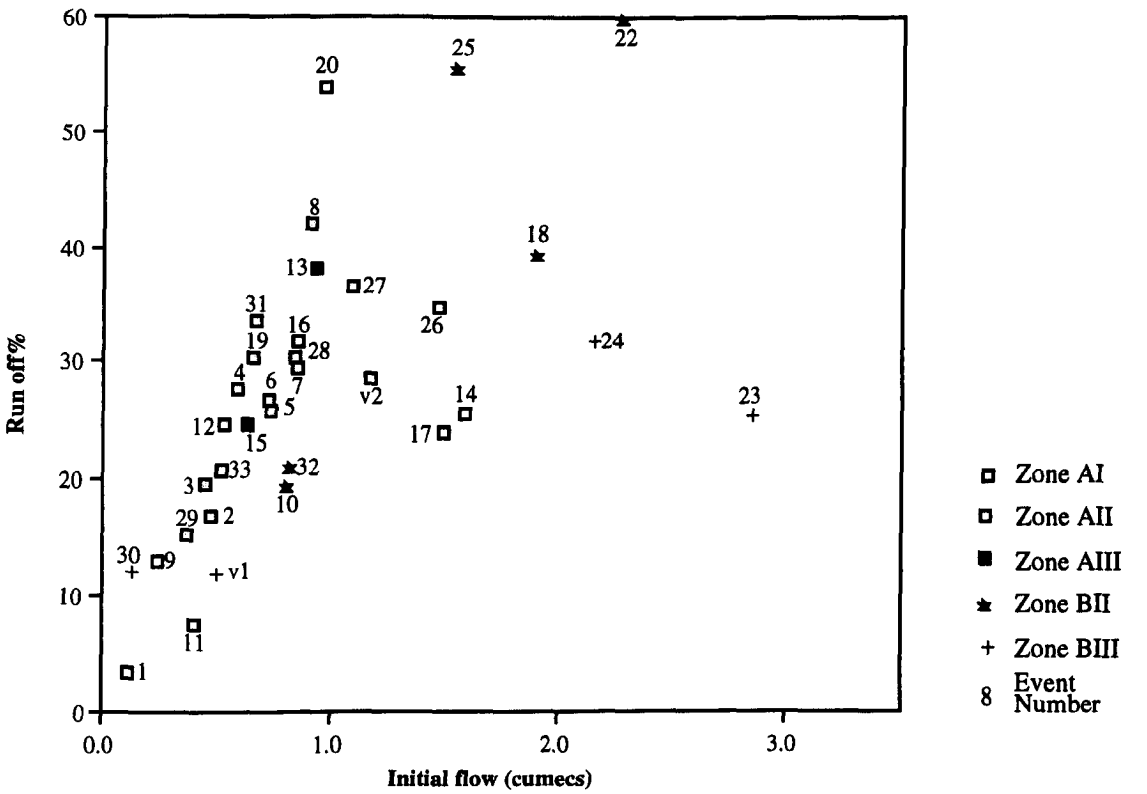

Figure (4.8) Percentage runoff and initial flow relationship in different classified zones.

Letter C represents the performance of a group obtained from five day antecedent precipitation. Initial Δ is the smallest one and time variant. Letter D is related to the same group of models but the initial Δ is now calculated from the runoff and base flow relationship. Δ is again time variant.

Letter E is concerned the ability of the thirty day antecedent precipitation index time series group, with the smallest Δ and variable with time. Letter F is the representative of the same group except the initial Δ is estimated from the runoff and base flow relationship.

Letter G is related to a group consisting of the classified gradient of the pulse response. Initial Δ is again the lowest one and time variant. Note that here it was not possible to construct a relationship between runoff and base flow.

Letter H is the representative of a group obtained from the thirty day antecedent precipitation index and gradient of the pulse response data sets. The smallest Δ is selected as the initial Δ. Letter I is used to show the forecasting performance of same group but the initial Δ is calculated from runoff and base flow dependency.

Letter J is selected to introduce the forecasting ability of a group which is composed of events with similar classified five day antecedent precipitation indices. The value of initial Δ is the lowest. Letter K represents the same group but the initial Δ is estimated from the runoff and base flow relationship. Finally letter L is selected to represent the performance of a group obtained from five day antecedent precipitation and gradient of the pulse response data sets. Initial Δ is again the lowest one and variable with time. Finally letter M is for forecasting ability of same group except initial Δ is estimated from runoff and base flow equation.

Randomness-dispersion diagrams of each event group are presented at the top left of each graph. Some of the more notable results of the group evaluation for each eight verification event are described below.

Event number one (31st December 1978)

The graphs in figure (4.9) compare the RMSE's of the flow forecasts produced by the grouped models (GTF) and the original ATF model along with the randomness-dispersion diagram. For this event 7 out of the 13 cases listed previously can be evaluated. As an example, and because the FDAP of the event has a unique value, the evaluation of FDAP and its combination with other groups is not possible.

Compared to the performance of $\Delta_{\text{minvariable}}$ in different groups only the API5 outperforms the average model. At the same time in each model when initial Δ is extracted from the runoff-base flow equation, the model performed better. Figure (4.9) also indicates that at least from an RMSE point of view, the average model which used the best Δ provides the best result. However, firstly because of shortage of models evaluated and secondly because determination of the Δ best is not possible prior to analysis of the event, the extension of this conclusion is neither applicable nor useful for real-time application. The group which consisted of the API30 provides the second best forecasts, nevertheless, and as with the average model, its portmanteau statistic is greater than one. The group model which is composed of API5, from the RMSE point of view performs the third best model and is the first valid model both from portmanteau and RMSE statistics points of view together.

Figure (4.10) shows the forecasting results of the best group model in which only the same seven forecasts as figures 3.14 (top) and (3.20) are presented. It can be seen that the quality of group models' forecasts is much better than those of ATF model. At the same time figure (4.11) compares the forecasted flow hydrographs for one, four and nine

hours ahead produced by the GTF and ATF models. In all three cases the GTF outperforms the ATF.

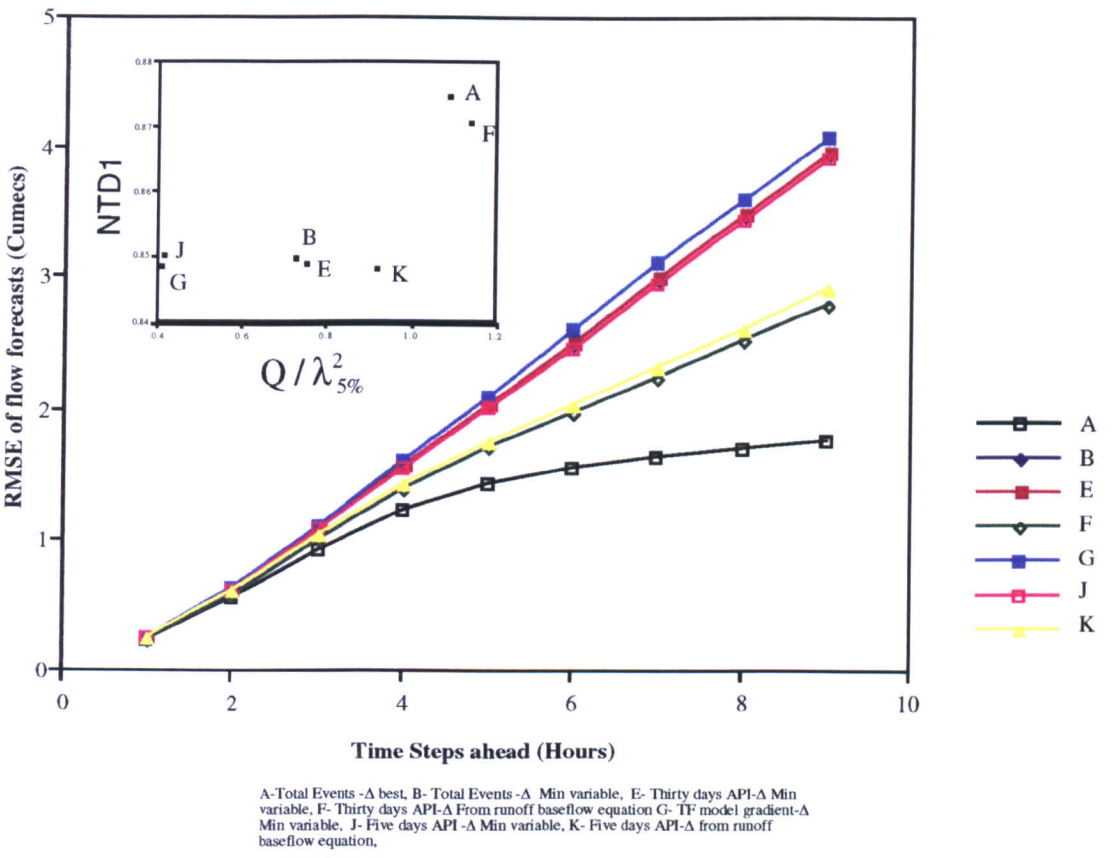

Fig. (4.9) Comparison of the RMSE, NTD1 and $Q/\lambda^2_{5\%}$ of flow forecasts in different cases, Orgeval catchment, event no. 1.

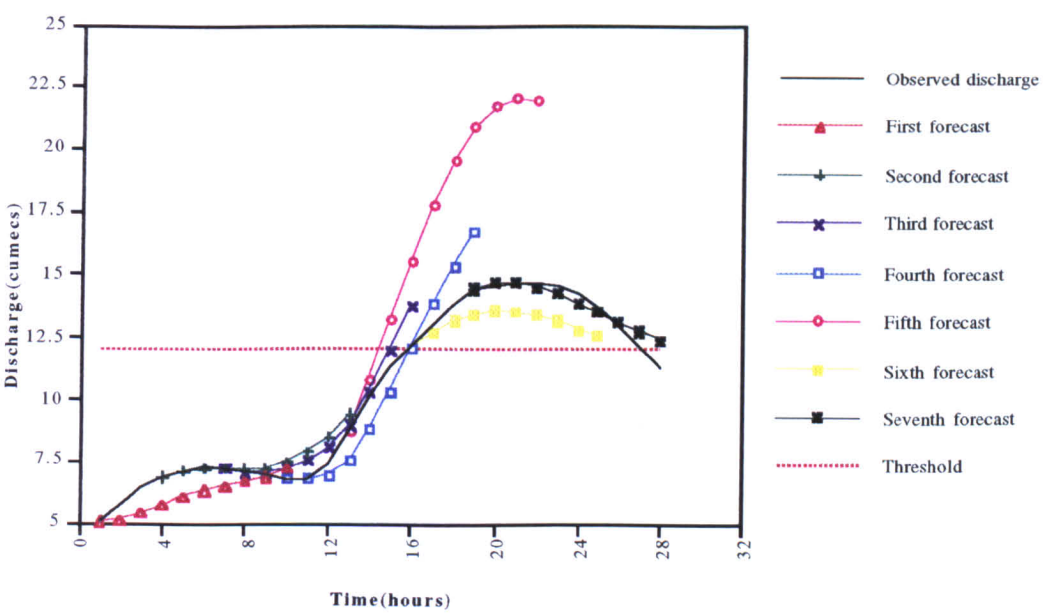

Figure (4.10) Seven multiple step ahead forecasts by GTF model, Orgeval, event no. 1.

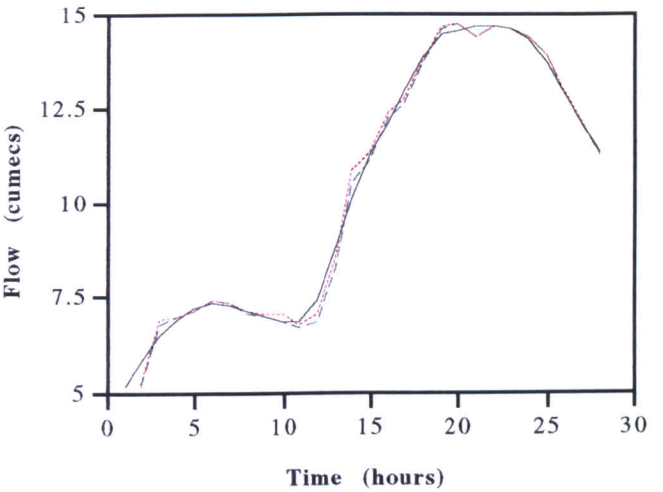

(i) One step ahead forecasts

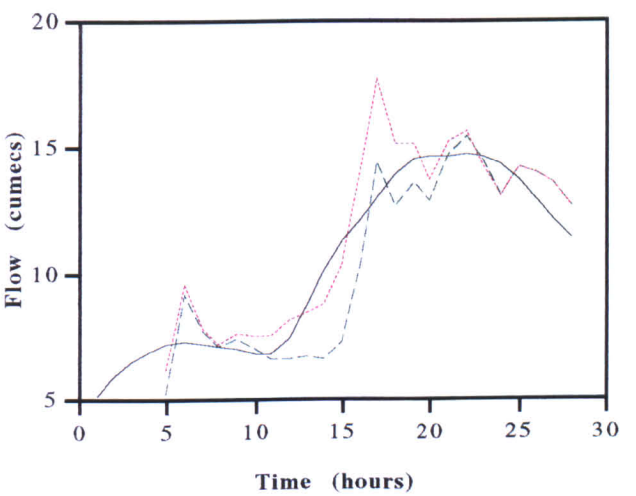

(ii) Four step ahead forecasts

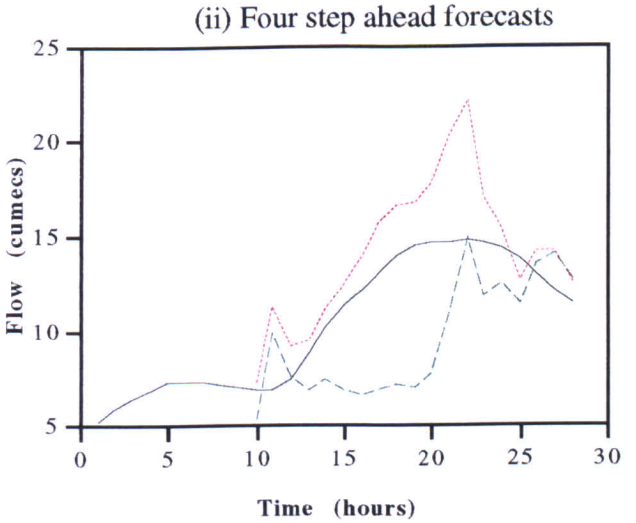

(iii) Nine step ahead forecasts

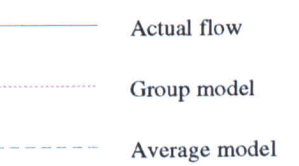

Figure (4.11) Forecast hydrographs, Orgeval catchment event no. 1

Event number two (2nd Feb. 1979)

In figure (4.12) the comparison of the RMSE of eleven cases are presented. As regards the comparison of the performance of $\Delta_{minvariable}$ in different cases, two group models provide better forecasts than the ATF model: the FDAP and PR gradient model and the PR gradient model. The figure shows that in each case as $\Delta_{minvariable}$ is replaced with Δ estimated from the runoff-base flow equation, the quality of result improves. On the whole it may be concluded that the group model obtained from the FDAP provides better results than the other models. It can be seen that the RMSE of this model is considerably lower than those of ATF model.

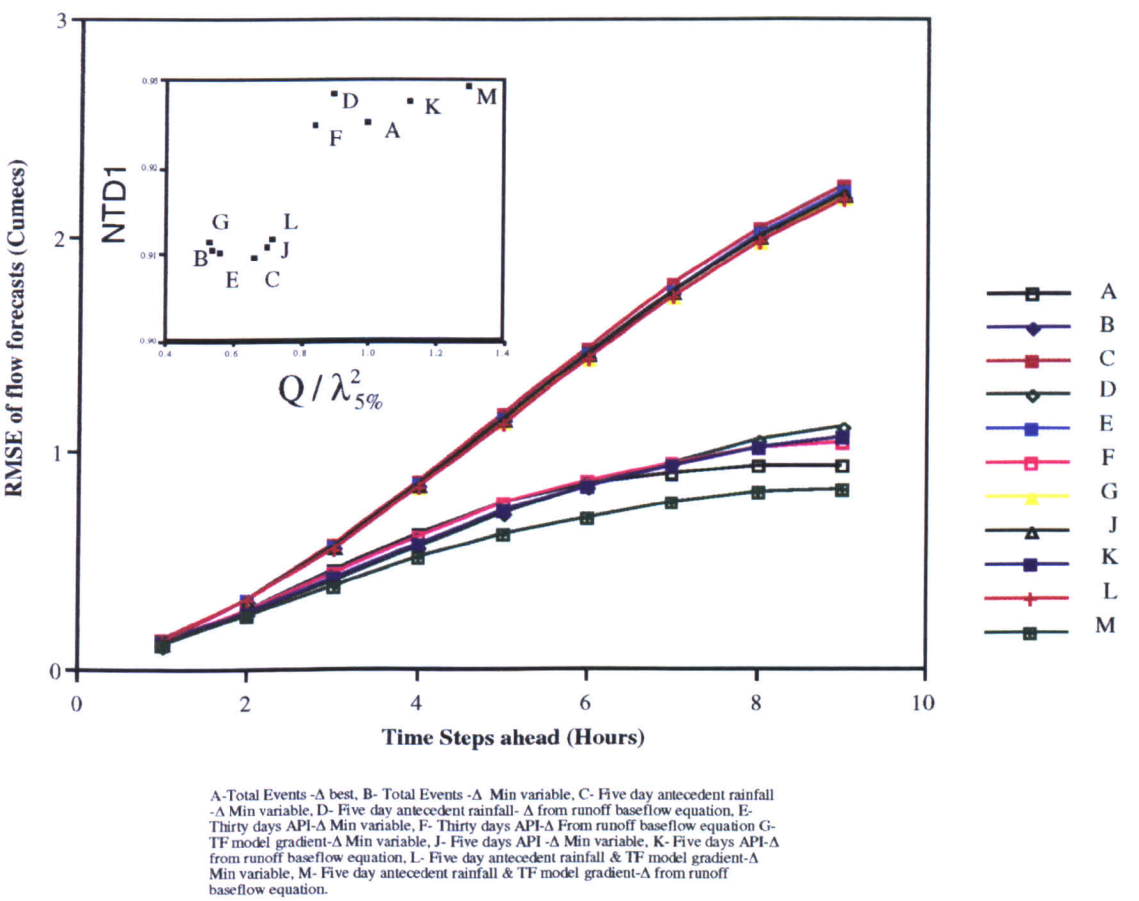

Fig. (4.12) Comparison of the RMSE, NTD1 and $Q/\lambda^2_{5\%}$ of flow forecasts in different cases, Orgeval catchment, event no. 2.

In figure (4.13) seven forecasts of this group model are presented whilst Figure (4.14) compares forecasted flow hydrographs for one, four and nine hours ahead compared with those forecasts of the average model. Results again show a great improvement in the quality of the forecasts as the group model is used.

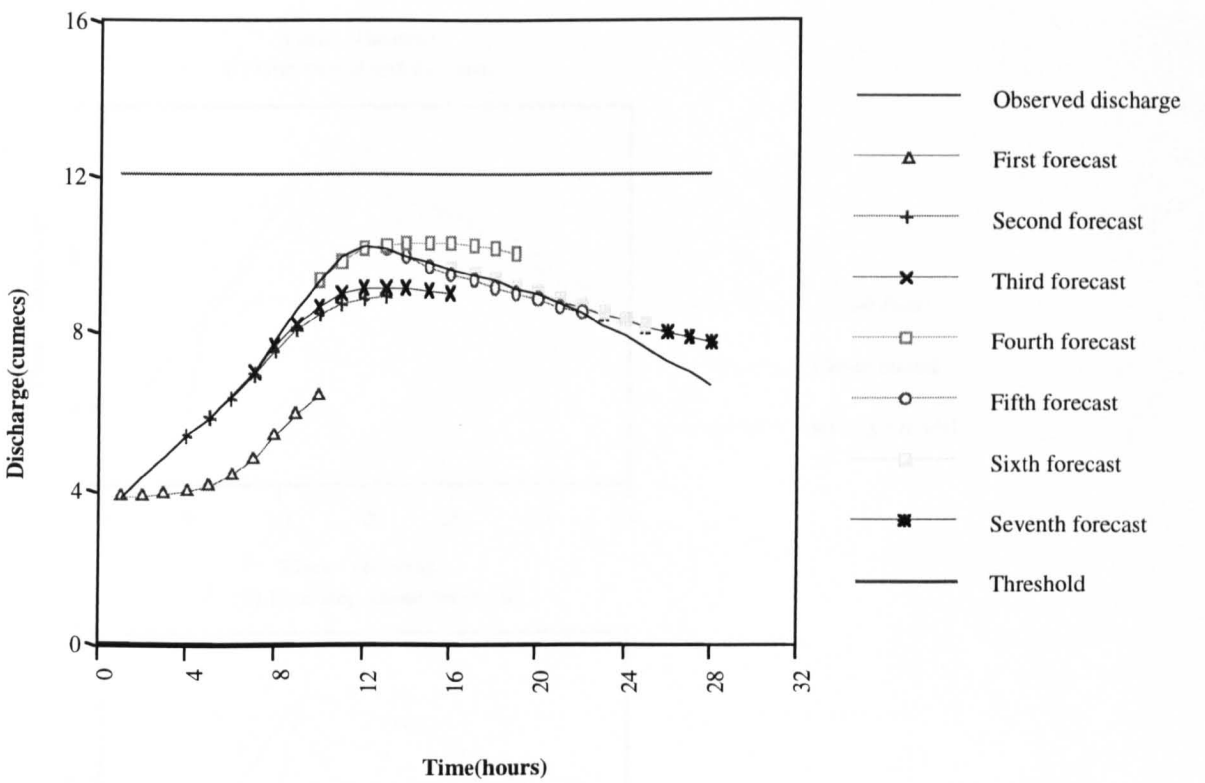

Figure (4.13) Seven multiple step ahead forecasts by GTF model, Orgeval, event no. 2.

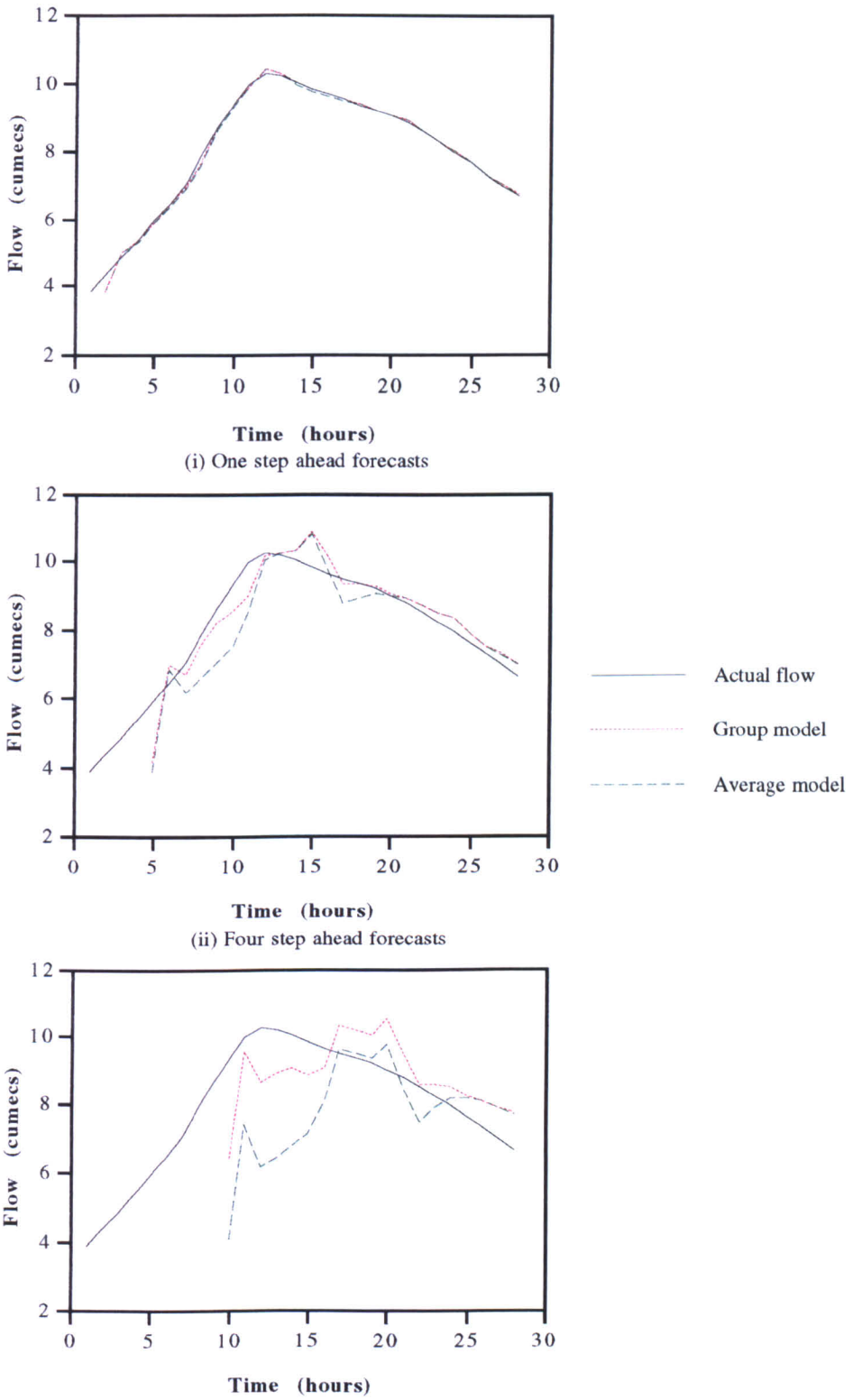

(i) One step ahead forecasts

(ii) Four step ahead forecasts

(iii) Nine step ahead forecasts

Figure (4.14) Forecast hydrographs, Orgeval catchment event no. 2

Event number three (10th March 1979)

As indicated in figure (4.15) eleven cases are evaluated. When comparing the performance of $\Delta_{minvariable}$ in the different model-cases almost all of the cases perform better than ATF. This itself confirms that the classification of the events will increase the quality of forecasts. Here again if the runoff-base flow equation is used for estimating the initial Δ, the performance of each model will be better. The figure also shows that the same problem related to NTD<0 still is remaining for all eleven models evaluated. The figure clearly indicates that the model which is constructed from the combination of the FDAP and PR gradient by far presents the best forecasting results.

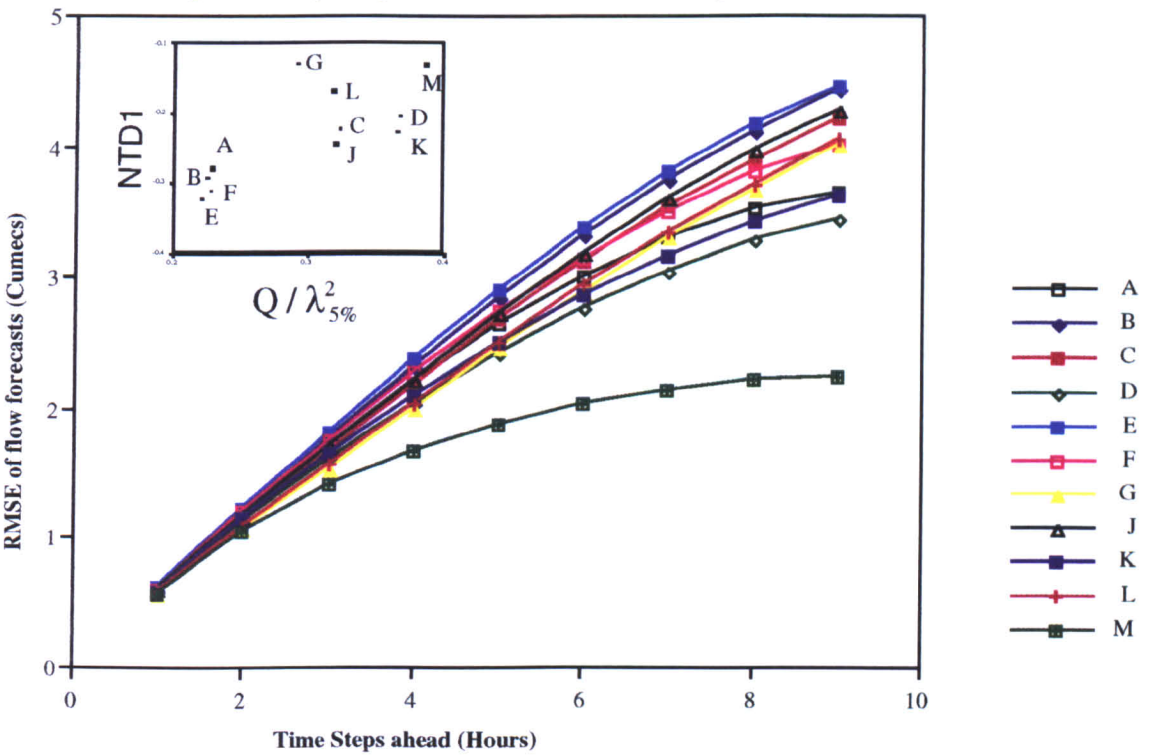

A-Total Events -Δ best, B- Total Events -Δ Min variable, C- Five day antecedent rainfall -Δ Min variable, D- Five day antecedent rainfall- Δ from runoff baseflow equation, E- Thirty days API-Δ Min variable, F- Thirty days API-Δ From runoff baseflow equation G- TF model gradient-Δ Min variable, J- Five days API -Δ Min variable, K- Five days API-Δ from runoff baseflow equation, L- Five day antecedent rainfall & TF model gradient-Δ Min variable, M- Five day antecedent rainfall & TF model gradient-Δ from runoff baseflow equation.

Fig. (4.15) Comparison of the RMSE, NTD1 and $Q/\lambda^2_{5\%}$ of flow forecasts in different cases, Orgeval catchment, event no. 3.

In order to compare the forecasting ability of the best GTF with those of the SPRTF and DPRTF (figures 3.15 top and 3.20) in figure (4.16) seven forecasts of the best GTF are presented. In addition, figure (4.17) shows forecasted flow hydrographs for one, four and nine hours ahead compared to same forecasts resulted by the average model. These figures demonstrate that the group model can provide more accurate forecasts than the ATF model.

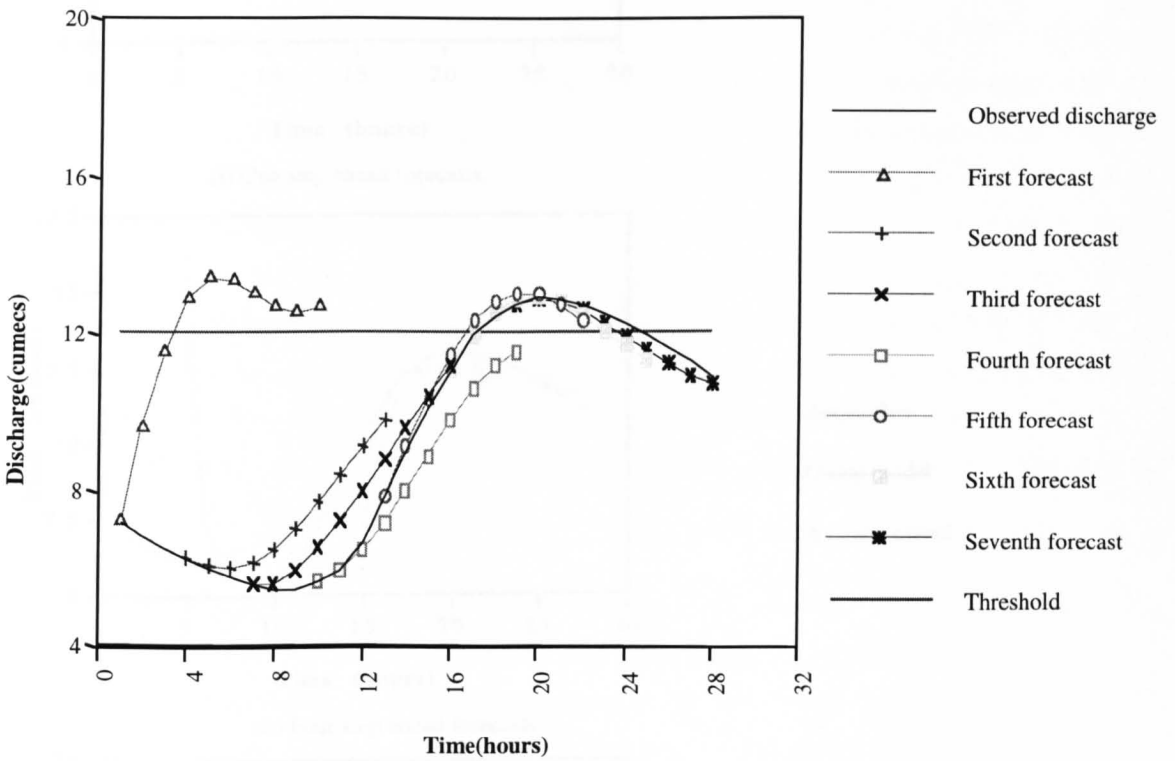

Figure (4.16) Seven multiple step ahead forecasts by GTF model, Orgeval, event no. 3.

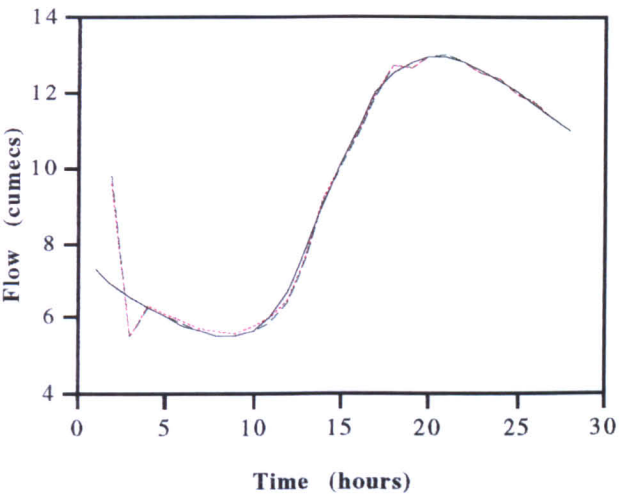

(i) One step ahead forecasts

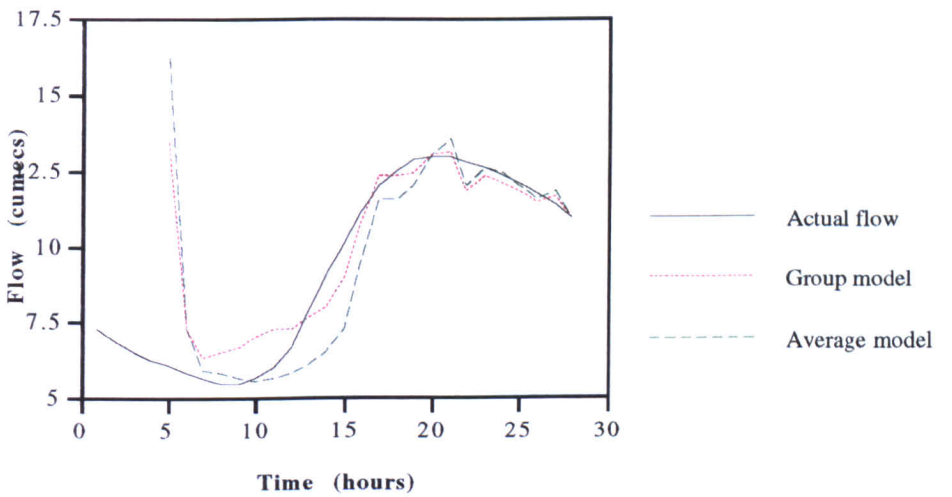

(ii) Four step ahead forecasts

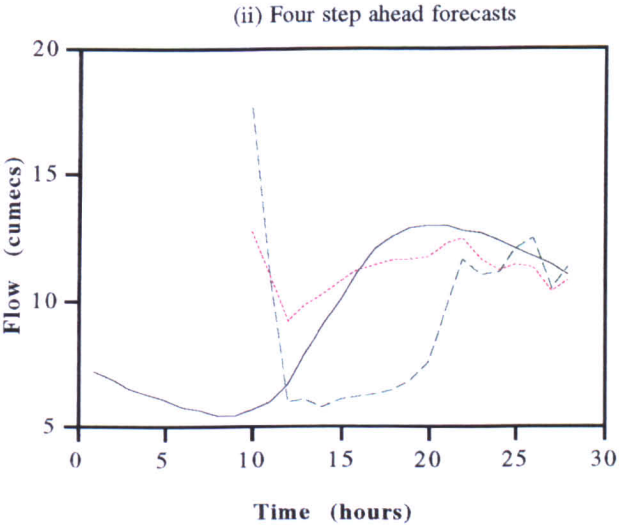

(iii) Nine step ahead forecasts

Figure (4.17) Forecast hydrographs, Orgeval catchment event no. 3

Event number four (13th March 1980)

Figure (4.18) details the objective comparison of the forecasting accuracy of eleven model-cases. When compared to the $\Delta_{minvariable}$ model almost all of the model-cases provide more accurate forecasts than the ATF model, indicating that the classification of events may lead to better forecasting results. Here the group model which consisted of the thirty day antecedent precipitation is an exception where the application of ATF resulted the better forecasts. As with other events investigated, when Δ is extracted from runoff-base flow equation the forecasting quality of each model improved. In contrast with other events here the ATF model with the best Δ used as initial Δ performs at least better for higher lead times. However, this conclusion cannot be used in reality when the best Δ of the coming event is not predictable in advance. Although when comparing the $\Delta_{minvariable}$ influence, the group model which is constructed from the events with same class of API30 is inferior to the ATF, it is superior to ATF model when Δ is extracted from runoff-base flow equation providing the second best results. The third best model is composed of the FDAP. Considering above expressions it was decided to select the last mentioned model as the best group model.

Figure (4.19) presents the seven forecasts of the best group model in the same format as the WMO workshop. Further, in figure (4.20) the forecasted flow hydrographs for one, four and nine hours ahead for the GTF model are compared to those forecasts produced by the average model. These two figures both indicate that the group model out performs the average TF model.

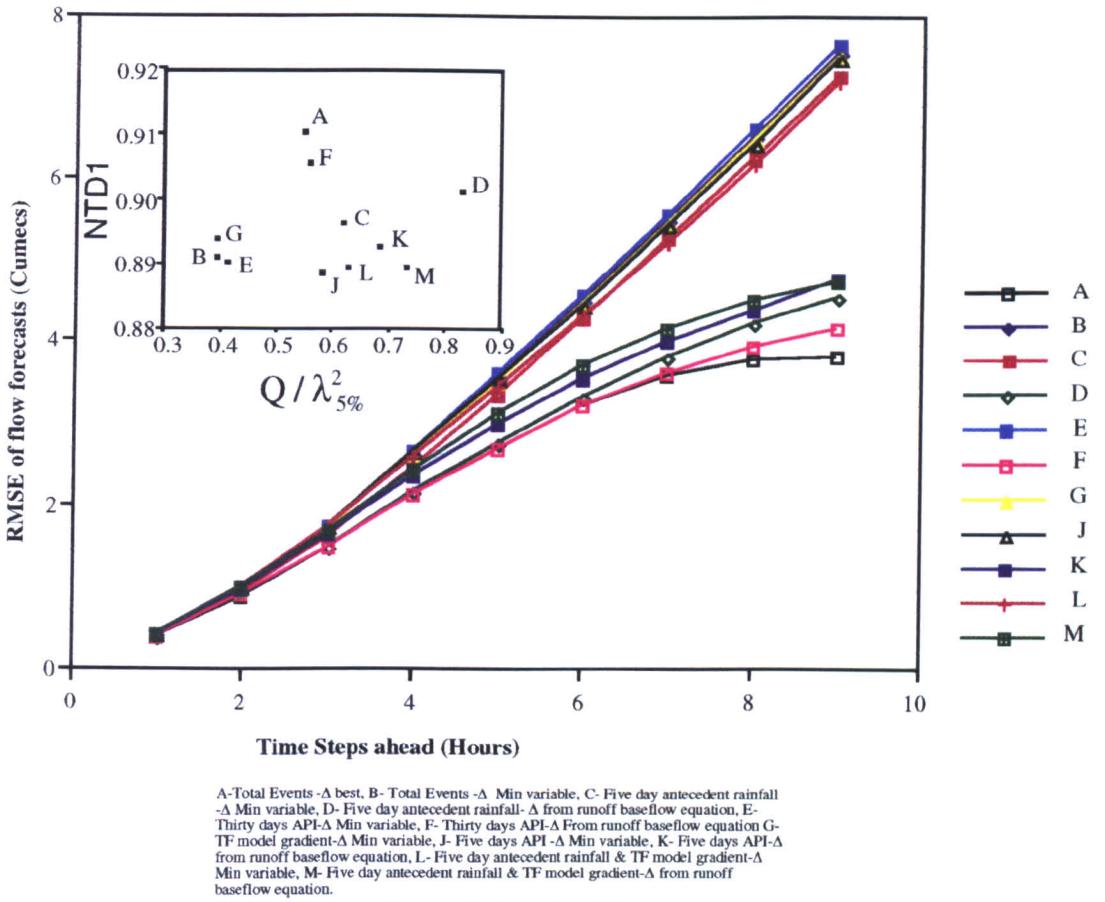

Fig. (4.18) Comparison of the RMSE, NTD1 and $Q/\lambda^2_{5\%}$ of flow forecasts in different cases, Orgeval catchment, event no. 4.

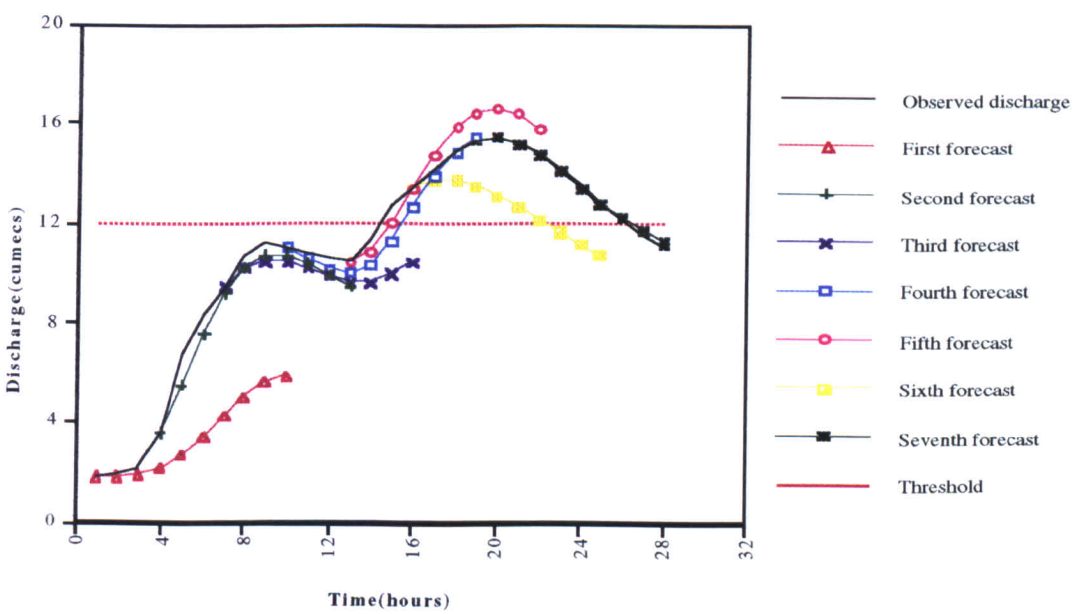

Figure (4.19) Seven multiple step ahead forecasts by GTF model, Orgeval, event no. 4.

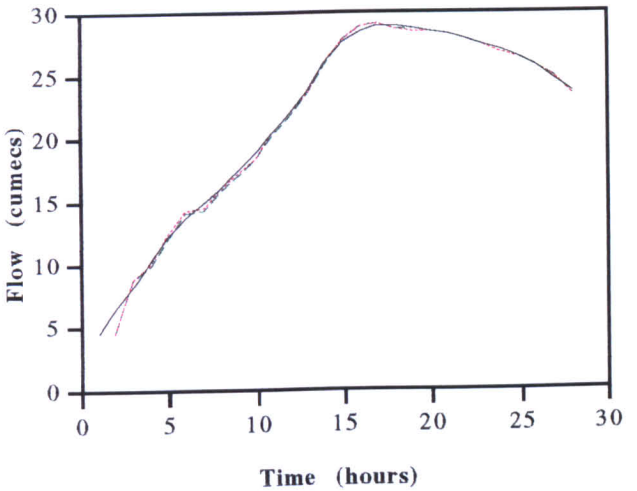

(i) One step ahead forecasts

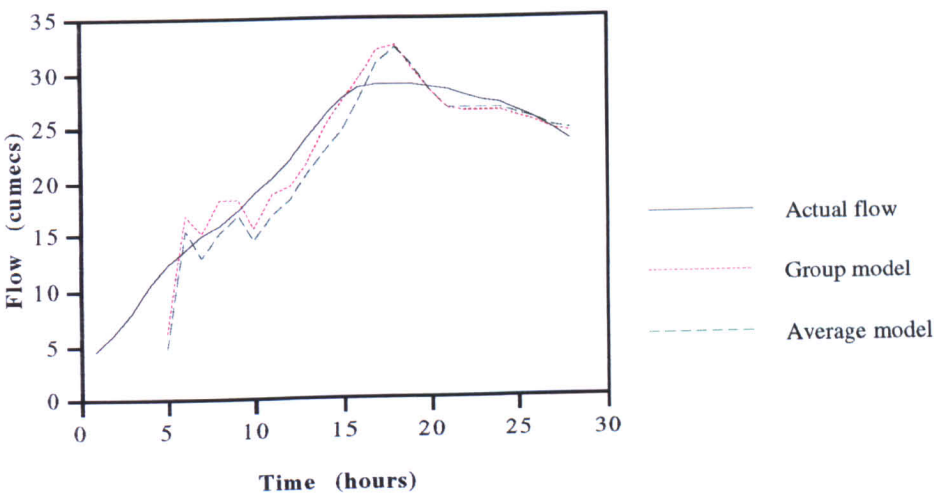

(ii) Four step ahead forecasts

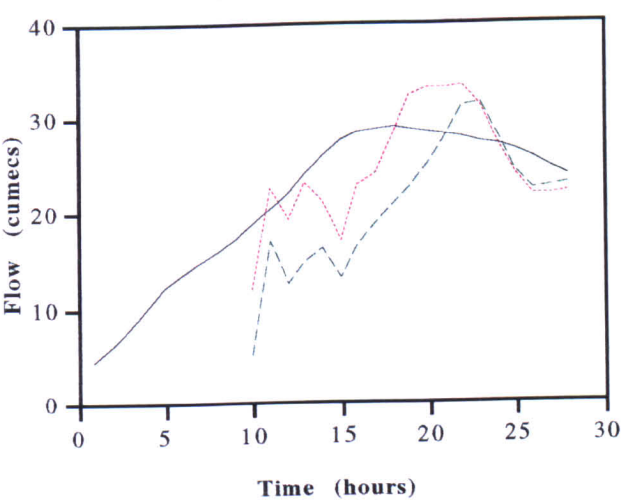

(iii) Nine step ahead forecasts

Figure (4.20) Forecast hydrographs, Orgeval catchment event no. 4

Event number five (13th July 1980)

Figure (4.21) compares all thirteen model-cases. The figure clearly shows that when $\Delta_{minvariable}$ is used almost all of the models out perform the ATF model. With respect to Δ derived from a runoff-base flow relationship, here again the quality of forecasts is considerably better than those model in which the $\Delta_{minvariable}$ is used. According to the figure the group model constructed from the combination of FDAP and PR gradient classes is by far the best.

Figure (4.22) presents seven forecasts of the best group model in the same format as the WMO workshop (cf. figures (3.16 top) and (3.20)). In addition, figure (4.23) compares forecasted flow hydrographs for one, four and nine hours ahead both for ATF and best GTF. From these figures it can be concluded that again the GTF out performs the ATF model.

Event number six (20th July 1980)

The graphs in figure (4.24) show the comparison of the RMSE of the flow forecasts obtained from all thirteen model-cases investigated along with the randomness-dispersion diagram. The portmanteau statistic in all cases exceeds unity, indicating significant auto correlation in the residuals. As regards the $\Delta_{minvariable}$ similar to other events, with almost all of the models outperforming the ATF model. Consistent with previous events is that when the initial Δ value is derived from the runoff-base flow equation, the quality of forecasts improves dramatically. The figure clearly indicates that the group model constructed from the combination of FDAP and PR gradient classes is the best model. Figure (4.25) shows the forecasting performance of the best group model in which only the same seven forecasts as figures (3.16 bottom) and (3.20) are presented. It can be seen that the quality of group model's forecasts is much better than those of the ATF. At the same time, figure (4.26) compares the forecasted flow hydrographs for one, four and nine hours ahead to those of the average model. In all three cases the group model provides more accurate forecasts than the average model.

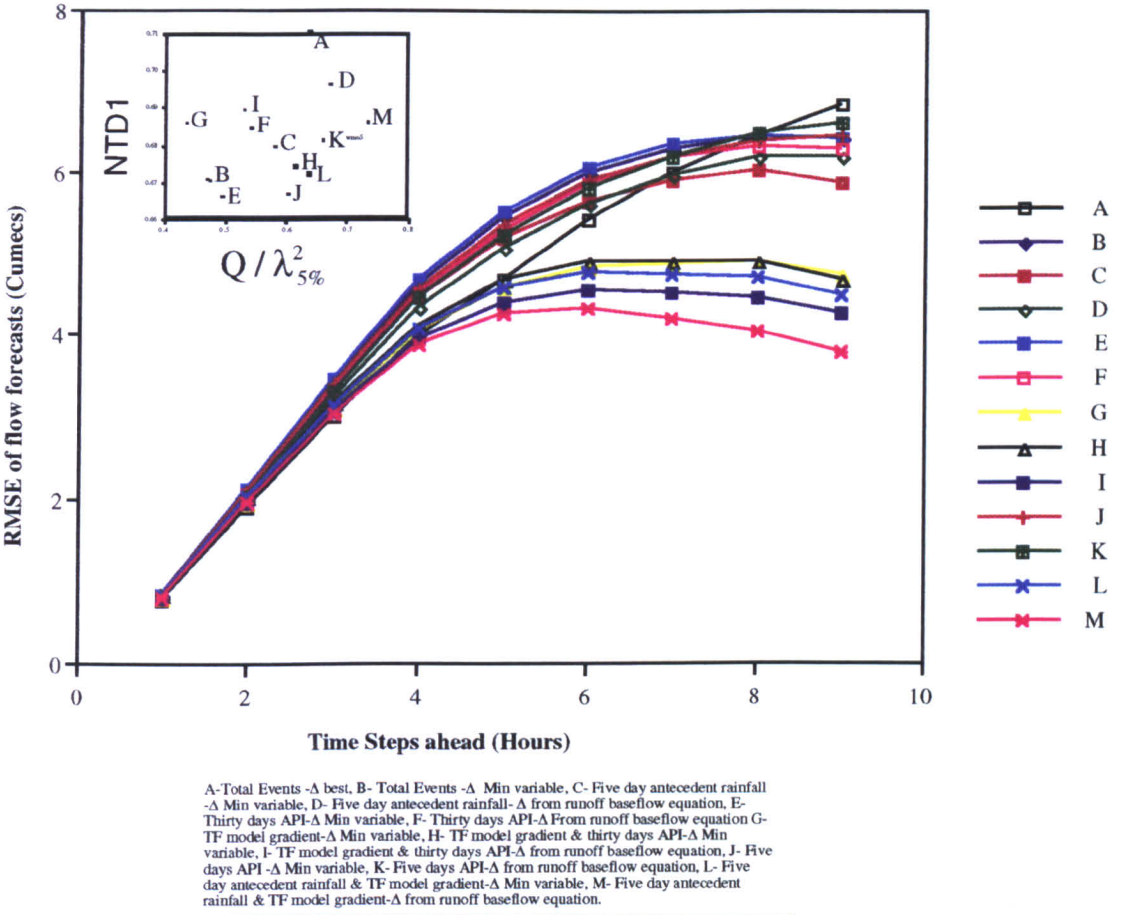

Fig. (4.21) Comparison of the RMSE, NTD1 and $Q/\lambda^2_{5\%}$ of flow forecasts in different cases, Orgeval catchment, event no. 5.

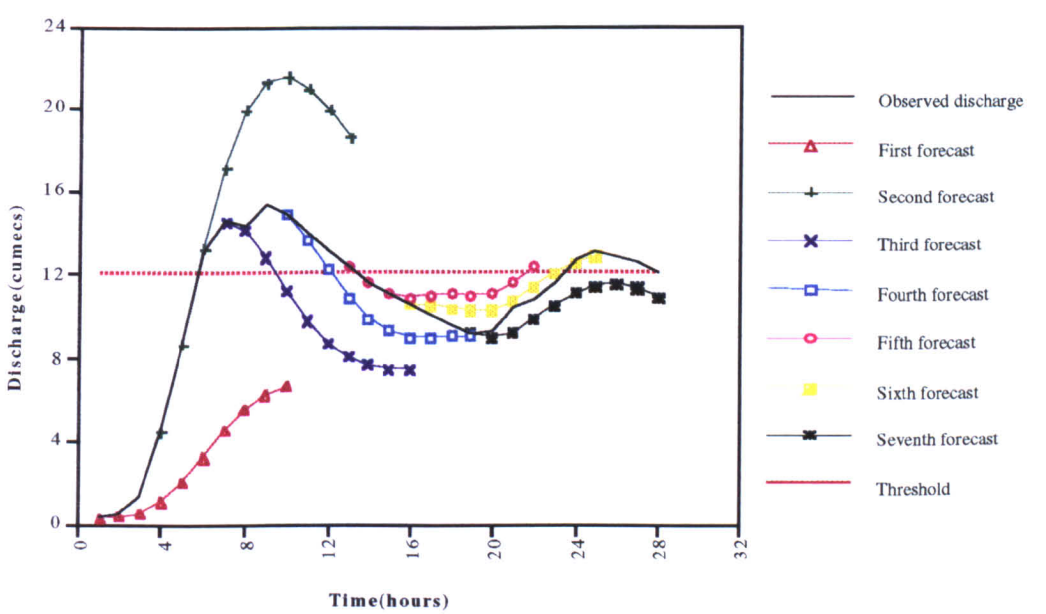

Figure (4.22) Seven multiple step ahead forecasts by GTF model, Orgeval, event no. 5.

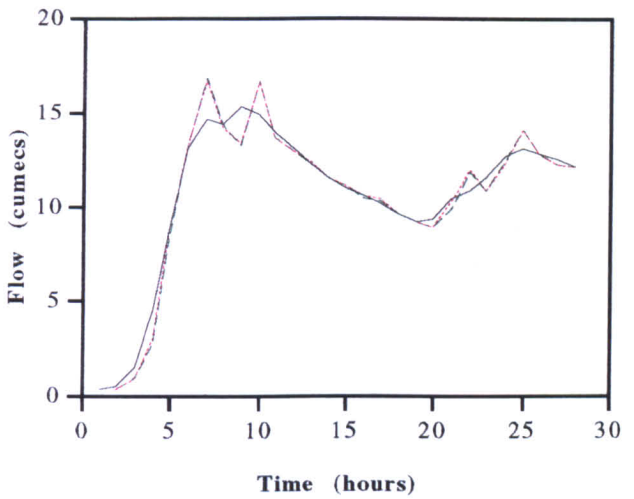

(i) One step ahead forecasts

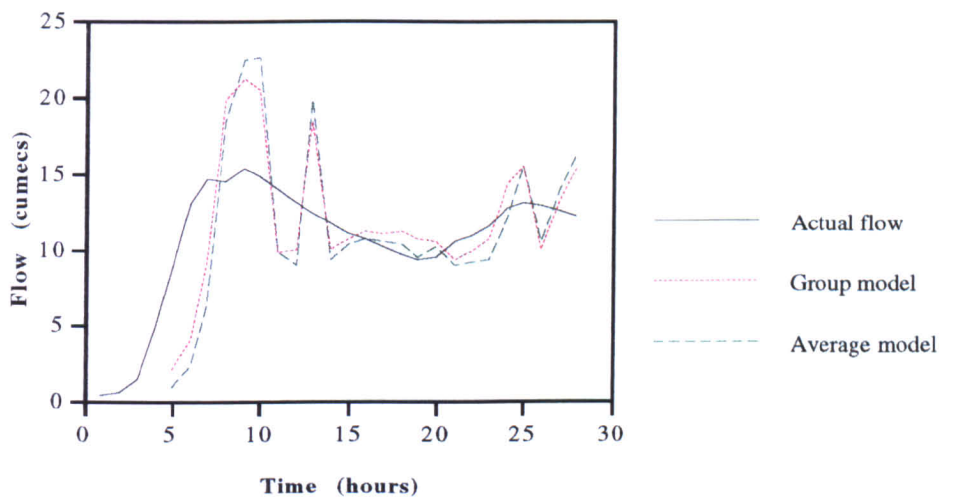

(ii) Four step ahead forecasts

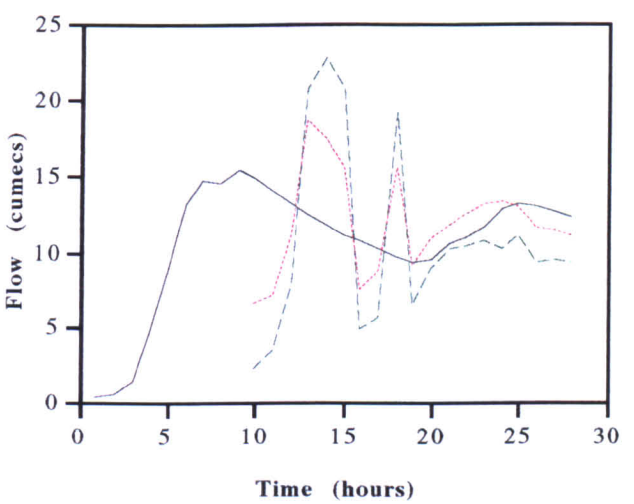

(iii) Nine step ahead forecasts

Figure (4.23) Forecast hydrographs, Orgeval catchment event no. 5

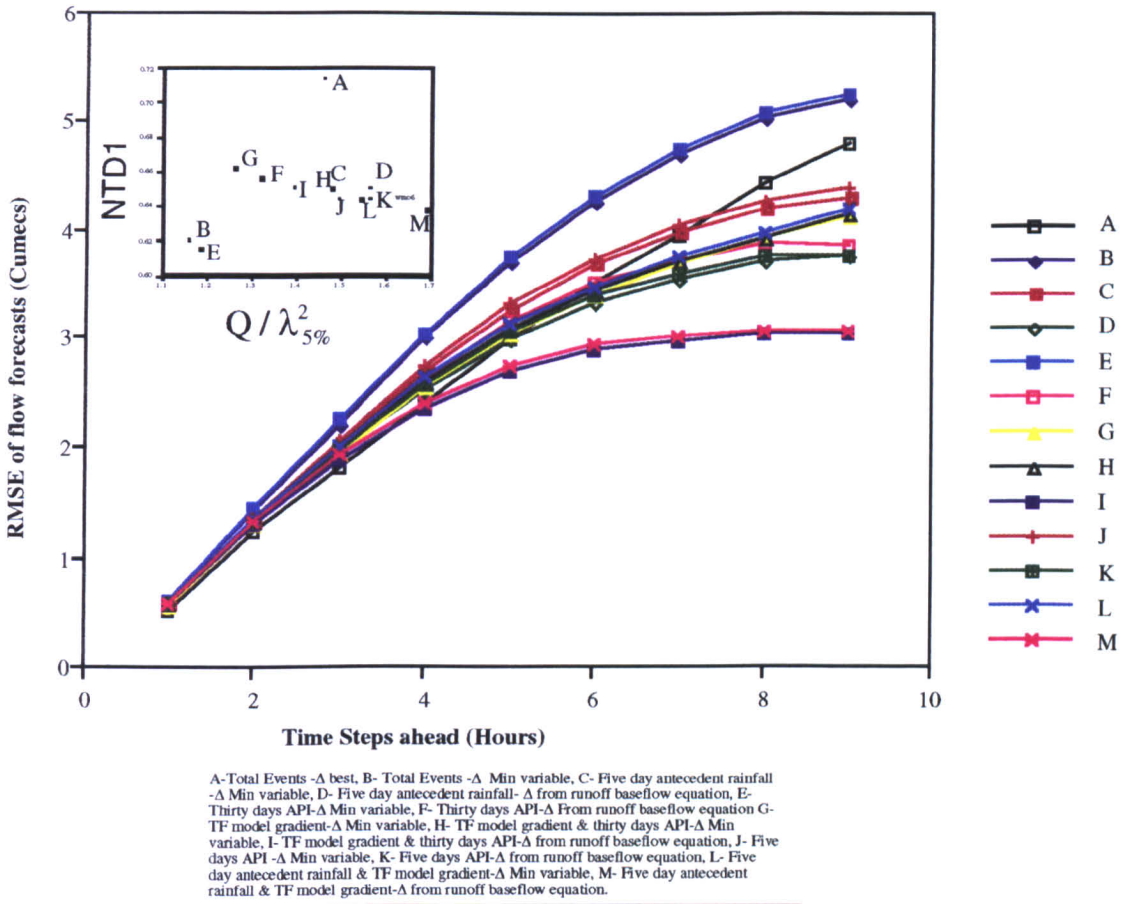

Fig. (4.24) Comparison of the RMSE, NTD1 and $Q/\lambda^2_{5\%}$ of flow forecasts in different cases, Orgeval catchment, event no. 6.

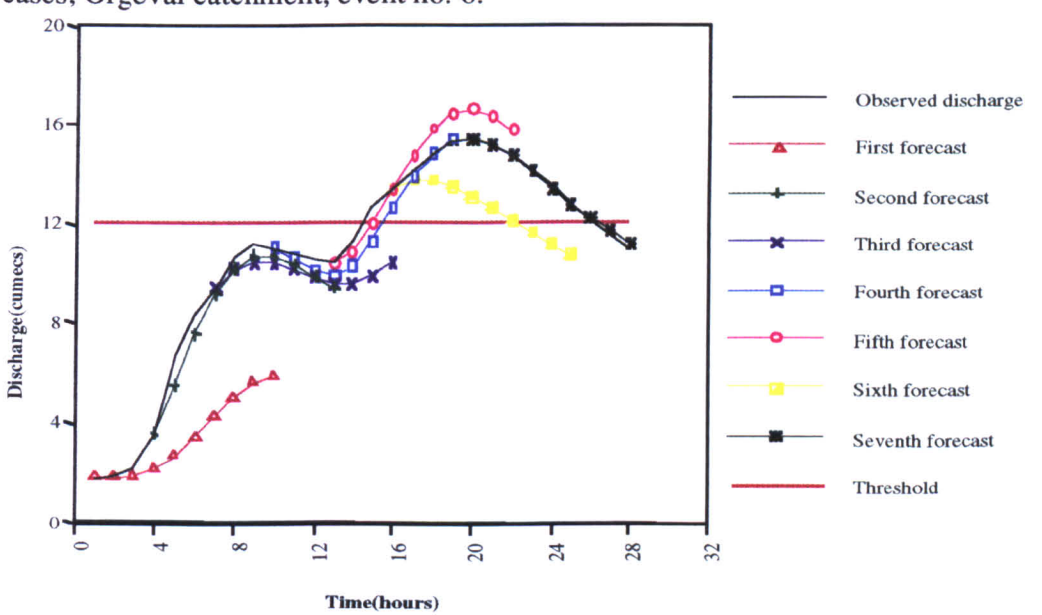

Figure (4.25) Seven multiple step ahead forecasts by GTF model, Orgeval, event no. 6.

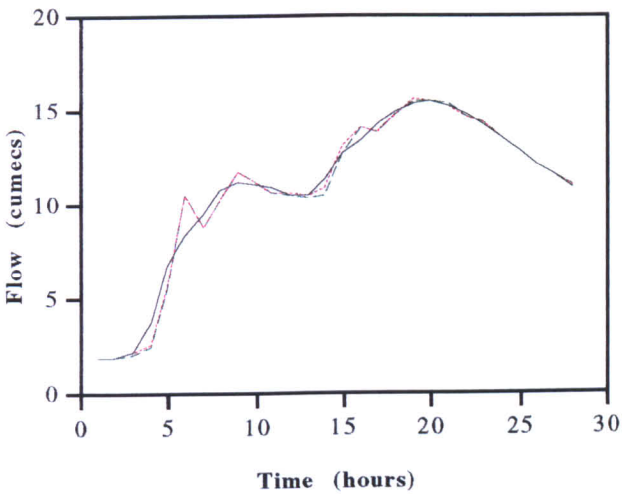

(i) One step ahead forecasts

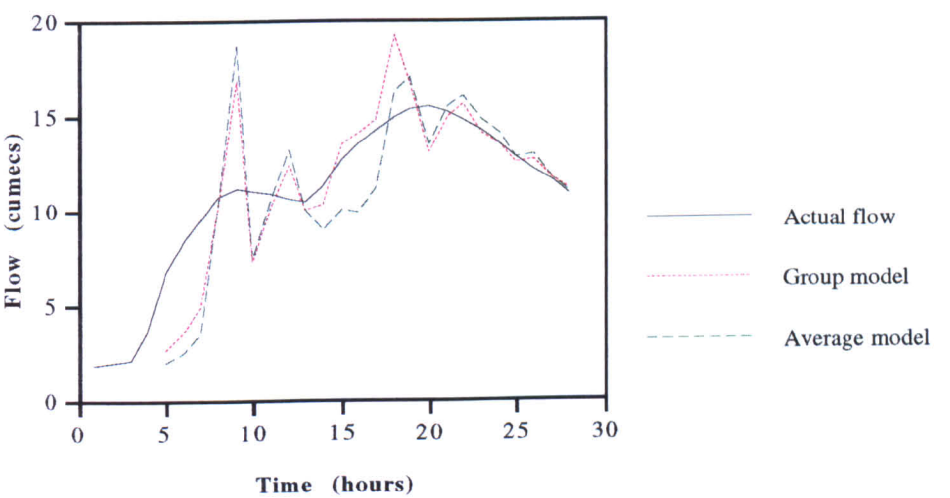

(ii) Four step ahead forecasts

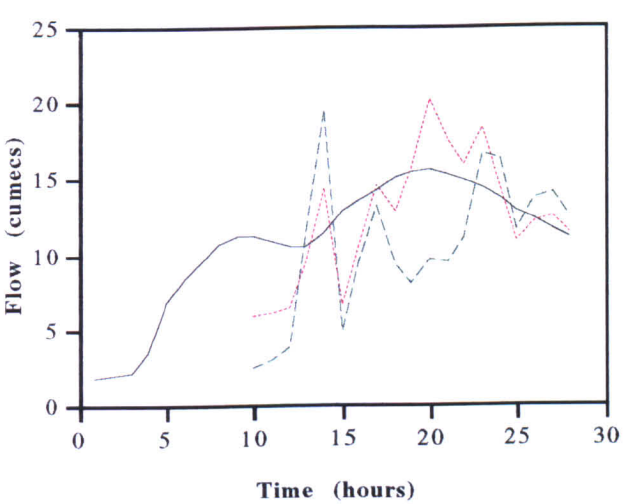

(iii) Nine step ahead forecasts

Figure (4.26) Forecast hydrographs, Orgeval catchment event no. 6

Event number seven (15th November 1973)

The event occurring during the 15th November 1973 was a small single peaked flood hydrograph with maximum flow of 2.41 m^3s^{-1} resulting from a four hours of relatively heavy rainfall totalling 11.8 mm. The event hyetograph and hydrograph are presented in appendix 2.

Figure (4.27) provides a comparison of the RMSE of all thirteen model-cases evaluated. All group models provide better forecasts than ATF model using $\Delta_{minvariable}$. The figure also shows that in each case as the $\Delta_{minvariable}$ is replaced with Δ estimated from the runoff-base flow equation, the quality of results is improved. According to the figure, it may be concluded that the model obtained from the FDAP provides better overall results than the other models.

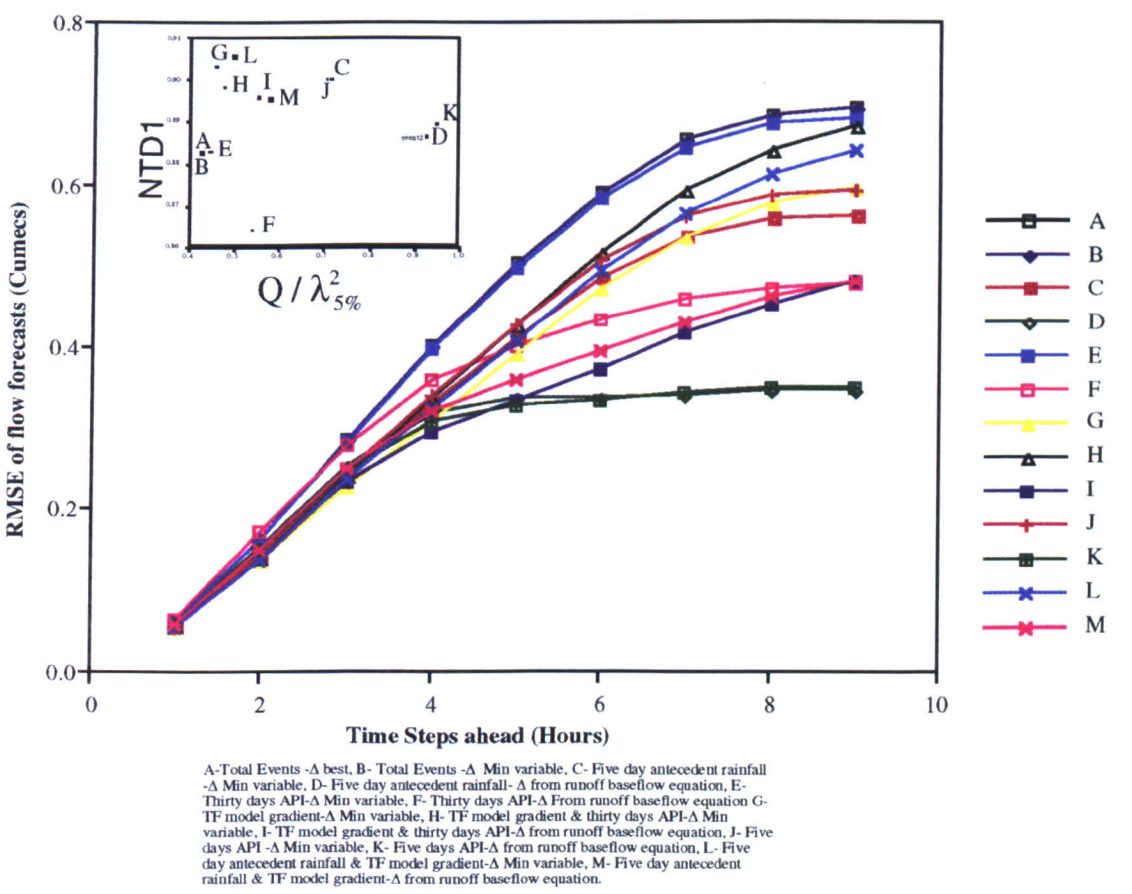

A-Total Events -Δ best, B- Total Events -Δ Min variable, C- Five day antecedent rainfall -Δ Min variable, D- Five day antecedent rainfall- Δ from runoff baseflow equation, E- Thirty days API-Δ Min variable, F- Thirty days API-Δ From runoff baseflow equation G- TF model gradient-Δ Min variable, H- TF model gradient & thirty days API-Δ Min variable, I- TF model gradient & thirty days API-Δ from runoff baseflow equation, J- Five days API -Δ Min variable, K- Five days API-Δ from runoff baseflow equation, L- Five day antecedent rainfall & TF model gradient-Δ Min variable, M- Five day antecedent rainfall & TF model gradient-Δ from runoff baseflow equation.

Fig. (4.27) Comparison of the RMSE, NTD1 and $Q/\lambda^2_{5\%}$ of flow forecasts in different cases, Orgeval catchment, event no. 7.

Event number eight (30th November 1974)

This event is also a small single peaked flood hydrograph with maximum flow of 2.99 m^3s^{-1}. The increase in flow was caused by long duration of light rainfall (18 hours) totalling 8.2 mm. As indicated in figure (4.28) eleven model-cases are evaluated. Most of the group model-cases outperform the ATF using $\Delta_{minvariable}$. Here again when the runoff-base flow equation is used for estimating the initial Δ, the performance of each individual model improves. As far as the selection of the best model is concerned, the figure shows that when the best Δ is used as initial Δ at least from RMSE point of view the ATF is the best amongst the models. However, firstly because the portmanteau of this model is bigger than unity and secondly as mentioned earlier the best Δ of coming event is not predictable in advance, it may be concluded that the FDAP model is the best one.

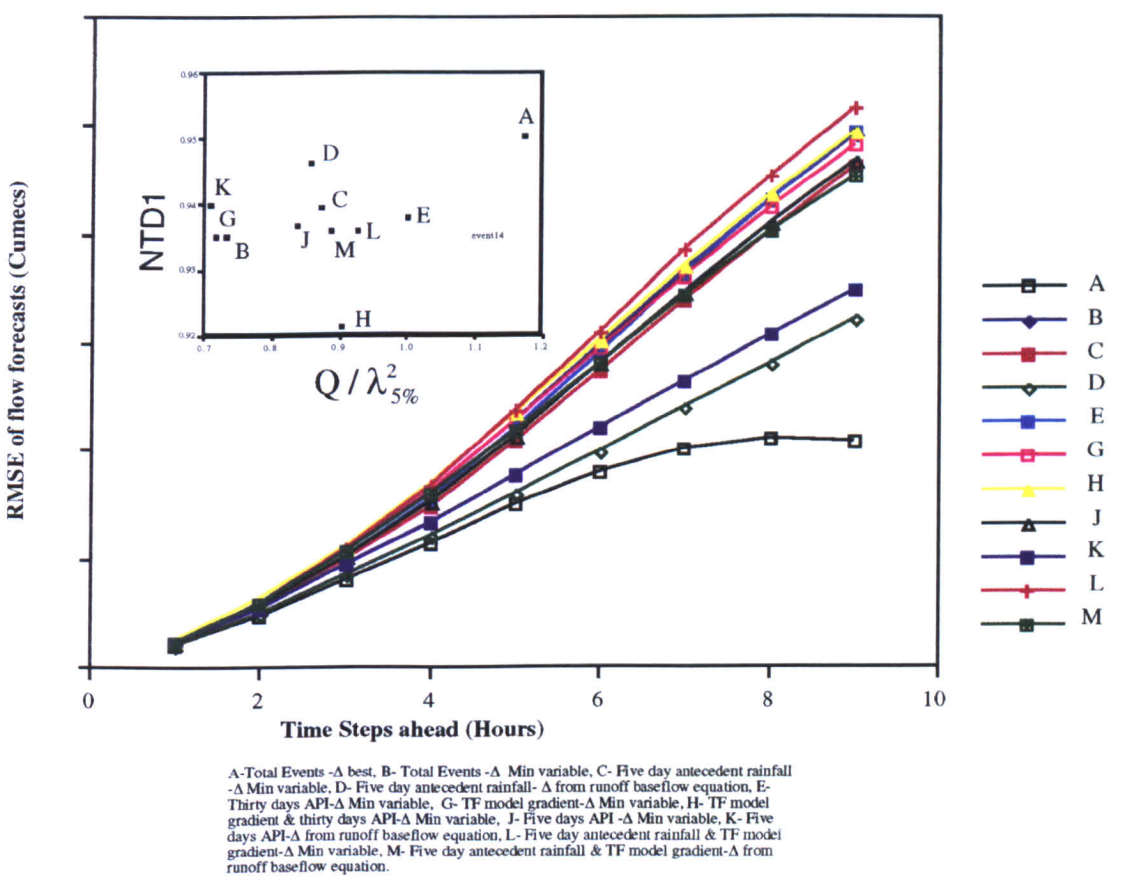

A-Total Events -Δ best, B- Total Events -Δ Min variable, C- Five day antecedent rainfall -Δ Min variable, D- Five day antecedent rainfall- Δ from runoff baseflow equation, E- Thirty days API-Δ Min variable, G- TF model gradient-Δ Min variable, H- TF model gradient & thirty days API-Δ Min variable, J- Five days API -Δ Min variable, K- Five days API-Δ from runoff baseflow equation, L- Five day antecedent rainfall & TF model gradient-Δ Min variable, M- Five day antecedent rainfall & TF model gradient-Δ from runoff baseflow equation.

Fig. (4.28) Comparison of the RMSE, NTD1 and $Q/\lambda^2_{5\%}$ of flow forecasts in different cases, Orgeval catchment, event no. 8.

4.3.2 PRTF model group results

In order to include group based PRTF models, the 32 events used to calibrate an average PRTF model were classified into two groups according to their FDAP . Each group was then used to calibrate two group PRTF (GPRTF) models. These two group models were then used for forecasting the same verification events analysed in previous sections. Both the static and dynamic GPRTF are evaluated.

For the purpose of assessment of the abilities of the GPRTF models an objective approach is used which compares the RMSE of the flow forecasts from both the average PRTF and GPRTF models. Table (4.4) shows the summary of this comparison at each time step ahead.

It should be noted that because the FDAP of verification event number one did not fall within either group no assessment has been performed for this event. Secondly in the majority of the cases the group models outperform the average model. It should be emphasised that there is still room for improvement in the performance of the GPRTF model, especially in dynamic form. The improvement could be obtained firstly through the detailed classification of the events in a similar manner to the OTF model and secondly through manual tuning of the PRTF model. As mentioned in section (2.5.2.2), for adjustment of the PRTF model parameters, the automatic mode was used. Although the automatic mode has some advantages, it attempts to optimise the accuracy of the whole forecast hydrograph and may therefore lead to poor representation of the peak of hydrograph in order to better model the recession limb.

4.3.3 Group model summary conclusions

As presented in previous sections eight verification events were used to evaluate the group model performance. It can be seen that in cases the use of a group model produced improved perform once over an ATF model. The study clearly demonstrated that it is much better to calibrate a TF model using a sequence of storms with similar characteristics. Note that the classification of events should be based on a series of characteristics which are known or predictable prior to occurrence of event. Therefore in such a manner it will be possible to tailor an appropriate ATF model to a coming event using an expert system approach.

Table (4.4) RMSE result of average and grouped PRTF models in different events (Orgeval catchment).

step ahead	Event number two Static APRTF	PRTF GPRTF	Dynamic APRTF	PRTF GPRTF	Event number three Static APRTF	PRTF GPRTF	Dynamic APRTF	PRTF GPRTF
1	0.145	0.144	0.332	0.350	0.396	0.390	0.382	0.331
2	0.356	0.352	0.654	0.691	0.801	0.787	0.753	0.650
3	0.607	0.603	0.959	1.016	1.225	1.200	1.109	0.952
4	0.883	0.877	1.244	1.322	1.677	1.641	1.445	1.231
5	1.64	1.158	1.506	1.604	2.159	2.110	1.754	1.486
6	1.441	1.436	1.749	1.866	2.647	2.583	2.028	1.707
7	1.708	1.704	1.972	2.105	3.133	3.053	2.265	1.892
8	1.938	1.936	2.160	2.307	3.592	3.498	2.456	2.032
9	2.117	2.117	2.305	2.462	4.025	3.920	2.605	2.128
NTD1	0.883	0.885	0.391	0.323	0.454	0.470	0.493	0.619
Q/λ^2	0.852	0.828	4.903	5.003	0.416	0.445	7.211	6.282

Table (4.4) Continued

step ahead	Event number four Static APRTF	PRTF GPRTF	Dynamic APRTF	PRTF GPRTF	Event number five Static APRTF	PRTF GPRTF	Dynamic APRTF	PRTF GPRTF
1	0.454	0.471	0.974	0.885	0.867	0.859	1.143	1.034
2	1.069	1.123	1.897	1.706	2.026	1.991	2.155	1.965
3	1.800	1.909	2.747	2.445	3.251	3.170	3.052	2.808
4	2.597	2.775	3.514	3.093	4.431	4.296	3.792	3.488
5	3.378	3.648	4.200	3.647	5.374	5.184	4.326	4.000
6	4.212	4.580	4.873	4.191	6.074	5.811	4.607	4.303
7	5.098	5.570	5.538	4.738	6.608	6.261	4.847	4.619
8	6.025	6.600	6.203	5.295	7.099	6.677	5.131	4.987
9	6.970	7.644	6.863	5.883	7.377	6.865	5.340	5.301
NTD1	0.873	0.863	0.416	0.518	0.651	0.658	0.393	0.504
Q/λ^2	0.783	0.797	3.554	2.844	0.400	0.394	2.721	2.681

Table (4.4) Continued

step ahead	Event number six Static APRTF	PRTF GPRTF	Dynamic APRTF	PRTF GPRTF
1	0.570	0.568	0.735	0.625
2	1.288	1.276	1.370	1.212
3	2.021	1.995	1.922	1.685
4	2.809	2.765	2.396	2.082
5	3.511	3.446	2.668	2.273
6	4.085	4.002	2.798	2.327
7	4.525	4.433	2.800	2.261
8	4.800	4.714	2.656	2.060
9	4.887	4.840	2.431	1.764
NTD1	0.651	0.653	0.419	0.580
Q/λ^2	0.693	0.682	1.837	2.417

In the current study events were classified according to the pulse response gradient of the event and antecedent precipitation characteristics. It has been shown that for all eight events the FDAP featured in the best group model. In verification events five and six, the best group model was one constructed from the events with a combination of FDAP and PR gradient. However, this study did not reveal a clear relationship between the PR gradient and the characteristics of the expected rainfall, and these findings are therefore of limited application in a real-time contest. It is possible that an extended event database might support the identification of a relationship between the PR gradient and the type as well as characteristics of coming rainfall

As far as the five day antecedent precipitation characteristics are concerned, an expert system can be used to match the antecedent catchment conditions as closely as possible to those of a group model previously calibrated and then use it for forecasting purpose. However, since the amount of the runoff from a storm is related to a number of physical characteristics including topography, type of soil, vegetation, and climatological conditions, any expert system knowledge base should involve all of these variables. As the appropriate data were not available for this analysis, a detailed investigation of these variables could not be conducted. Instead, in section (4.3.4) a relatively comprehensive methodology for future work is proposed.

In table (4.5) some statistics of observed flow and forecasted flow using the group models are presented.

4.3.4 Proposed format for grouped models

Earlier sections have demonstrated that group classification of events according to event/catchment characteristics improves the performance of TF models. In previous sections because of lack of data only a limited numbers of variables affecting the amount of runoff are considered. But there are other variables which also can affect the quantity of runoff. As discussed by Han (1991) and Suyanto *et al.* (1995) runoff response is determined by a large number of factors including: initial catchment wetness condition, the space-time distribution of rainfall; storm characteristics such as depth, duration, type, orientation and velocity, storm area; catchment geology and geomorphology; catchment characteristics such as size, physiography, and soil type. Furthermore, climatological conditions and vegetation cover should be considered.

Table (4.5) Performance of the grouped models in lead time of one hour in different events (Orgeval catchment).

Event no.	Name of model	Peak flow (cumecs)	Forecasted peak flow (cumecs)	Absolute error (cumecs)	Percent error
	OTF	14.61	14.66	-0.05	-0.3
1	SPRTF		-	-	-
	DPRTF		-	-	-
	OTF	10.25	10.40	-0.15	-1.5
2	SPRTF		10.46	-0.21	-2.1
	DPRTF		10.34	-0.09	-0.9
	OTF	12.94	12.91	0.03	0.2
3	SPRTF		12.99	-0.05	-0.4
	DPRTF		13.05	-0.11	-0.9
	OTF	28.79	28.95	-0.16	-0.6
4	SPRTF		29.00	-0.21	-0.7
	DPRTF		28.96	-0.17	-0.6
	OTF	15.32	16.71	-1.39	-9.1
5	SPRTF		16.51	-1.19	-7.8
	DPRTF		16.44	-1.12	-7.3
	OTF	15.45	15.54	-0.09	-0.6
6	SPRTF		15.58	-0.13	-0.8
	DPRTF		15.35	0.10	0.6

It is clear that the storm depth is the most important variable amongst the list, but there are some difficulties in direct investigation of depth. The position of rainfall within a catchment is a major factor affecting the runoff response. Rainfall in the lower area of catchment will produce a fast and peaked response. On the other hand, rainfall concentrated over the upper zone of catchment can generate a smooth response with longer time to peak. Finally, rainfall occurring in the middle part of catchment will produce a response which falls between two extreme limits. A storm moving upstream will generate a lower flow discharge than one moving down stream. Similarly, storms moving across the catchment can provide more flow discharge than storms moving upstream. A high intensity rainfall produces peakier and shorter response than one with lower intensity. The dry initial catchment wetness condition will generate lower flow discharge, because some part of rainfall will be absorbed and infiltrate into the deep soil. In a similar way vegetated covered catchment produces lower flow discharge than one which is bare.

Bishop and Watt (1989) presented an expert system knowledge based method to select appropriate forecasting method. The same classification procedure used to arrange factors affecting the runoff response. This is presented in figure (4.29). Upon examination it can be seen that some of the items are fixed factors for the particular catchment. For example, the size, physiography, soil type can be accounted for as fixed physical catchment

parameters. On the other hand, some other items are variable in the short term. Hence procedure suggested to classify the variables and to select an appropriate group model, requires a two-step approach. In the first step, fixed items are used to determine an essentially fixed hydrologically based category, and in the second step the other items which narrow down the choice of group model are used. For a given catchment the second step is most important.

From the above discussion it can be concluded that it is possible to classify historical data according to some pre-defined boundaries which will be determined for each catchment-variable. The classification of the historical events could then be implemented to construct an appropriate group model for similar events. It is clear that the number of groups will depend on the number of variables considered and the number of boundaries identified for each variable.

Once the appropriate classification of historical events has been implemented and proper models identified for each group, the choice of the best model for a future event could be made by an expert system approach using a series of IF/THEN rules in the form:

IF this condition is true, THEN this action is appropriate

Through such an approach it would be practicable to select a particular group model from a suite of forecasting models using a decision tree scheme.

The implementation of such an approach is not easy and needs an extensive historical data base (knowledge base) as well as detailed consideration of meteorological and hydrological factors. Detailed classification of the variables is possible which depends on the facilities available. The variables used for model selection must be known or predictable prior to the occurrence of the storm.

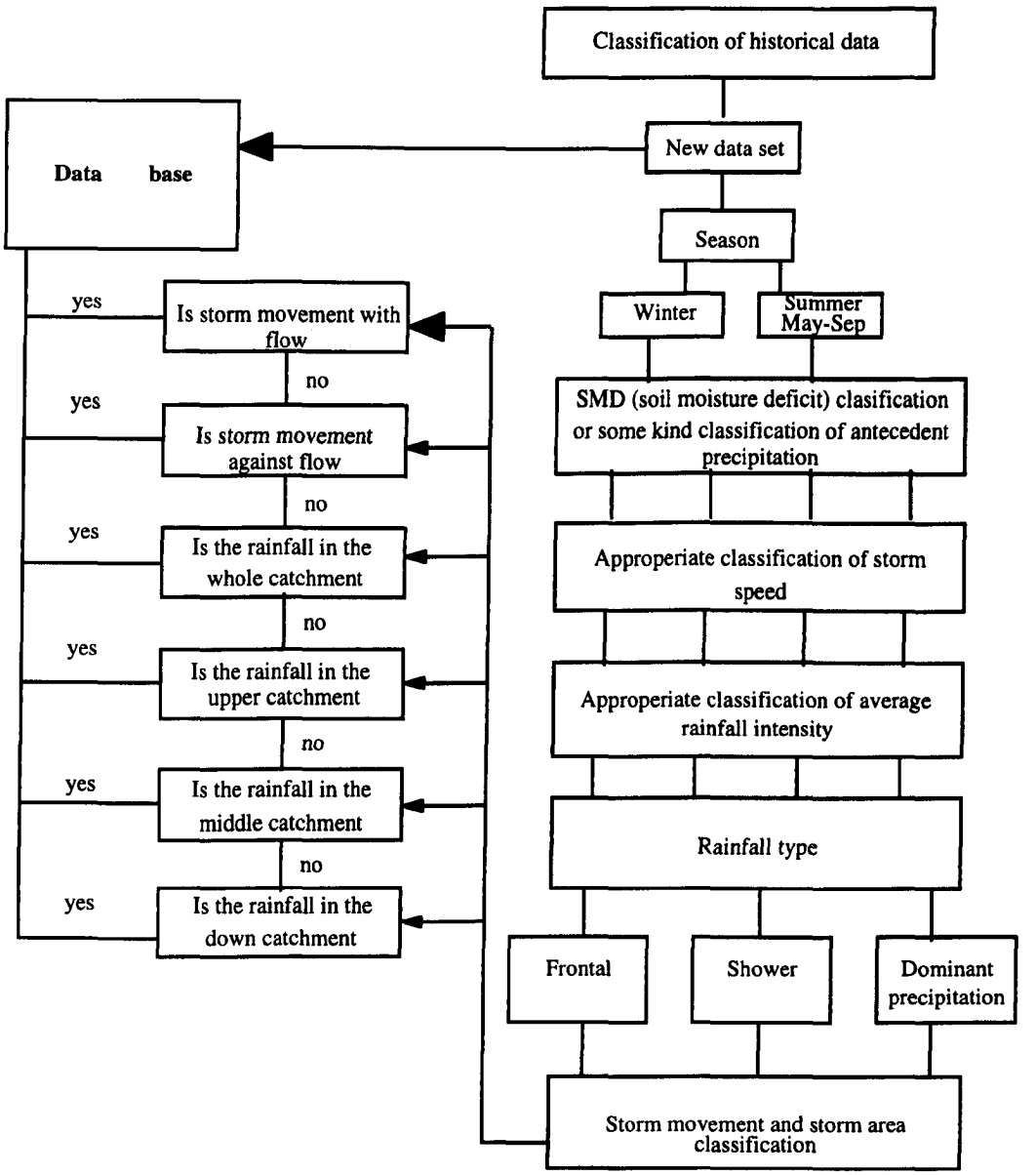

Figure (4.29) A semi detailed scheme to classify group events.

4.4 Single event model investigation

Occasionally modellers prefer model to operate without requiring a long memory of data prior to the flood event. In this case the model needs to be initialised with a short time data set before the main event. In order to investigate the forecasting accuracy of a model constructed from a single event, a study has been made using six verification events of the Orgeval catchment. In each case the data of the event immediately prior to main event was extracted and a model calibrated (the hyetographs and hydrographs of these pre-events are presented in appendix 2). The calibrated models were then used for forecasting

the six verification events. As usual the calibrated model was identified using the search and reduction technique described in section (2.5.1.4). This process has been applied to both ordinary TF model and PRTF model.

For the evaluation of the performance of the single-based event, an objective approach was used by comparing the RMSE of the flow forecasts at each time step ahead between the average transfer function and single-based event transfer function models. The results of this study are given in table (4.6).

From table (4.6) the following observation can be made. In verification event number one the average TF model outperforms the single-event based model in all of the OTF, SPRTF and DPRTF models. In event number two again the quality of the forecasts of both OTF and SPRTF in average mode is better than those of the single-based event mode. However, the DPRTF model provides better results for the single-based event. In contrast, in event number three all three models calibrated from the single-based event are superior to those of the average model. In event number four it was not possible to construct an appropriate calibrated model for the OTF case (because none of the resulted pulse response was valid from hydrological point of view), but an average model provided better forecasts than the PRTF model both in static and dynamic form. In event number five, static models constructed from the single-based event provided better results than an average model, whereas in dynamic form, the single-based event's result are inferior to the average model. Finally in event number six the PRTF models perform better in average mode than in the single-based event mode. At the same time OTF model resulted from the single-based event provide better forecasts.

On the whole it is not possible to draw a definite consistent conclusion concerning the performance of the average and the single-based event transfer function models from these six events. In order to extract a definite conclusion many more events would need to be investigated.

4.5 Overall comparison of the results of different models

First it should be stressed that for flood forecasting the RMSE criteria is the most useful, since it provides a measure of the absolute forecasting error. Although the portmanteau statistic is invaluable criteria of when a model is adequately modelling the data set, and it is not, but it is less useful to show the quantity of the forecasting error. As a general evaluation of comparison of the results of different models, the following conclusions can be stated:

Table (4.6) RMSE result of average and single-based event models for different events (Orgeval catchment).

	Event	number	one			
step	OTF		SPRTF		DPRTF	
ahead	average	single	average	single	average	single
1	0.254	0.288	0.279	0.307	0.433	0.803
2	0.638	0.697	0.674	0.715	0.811	1.251
3	1.096	1.156	1.127	1.165	1.118	1.600
4	1.573	1.632	1.603	1.630	1.356	2.037
5	2.034	2.111	2.076	2.103	1.537	2.547
6	2.498	2.599	2.556	2.592	1.683	2.909
7	2.988	3.090	3.042	3.080	1.805	3.085
8	3.473	3.565	3.510	3.550	1.895	3.417
9	3.961	4.017	3.951	3.995	1.959	3.639
NTD1	0.850	0.806	0.819	0.780	0.561	-0.510
Q/λ^2	0.726	1.313	0.884	0.947	1.683	4.315

Table (4.6) Continued

	Event	number	two			
step	OTF		SPRTF		DPRTF	
ahead	average	single	average	single	average	single
1	0.127	0.130	0.145	0.142	0.332	0.279
2	0.317	0.327	0.356	0.352	0.654	0.554
3	0.557	0.580	0.607	0.614	0.959	0.815
4	0.842	0.884	0.883	0.916	1.244	1.061
5	1.147	1.210	1.164	1.240	1.506	1.293
6	1.445	1.529	1.441	1.575	1.749	1.515
7	1.736	1.838	1.708	1.920	1.972	1.724
8	1.991	2.104	1.938	2.250	2.160	1.905
9	2.182	2.300	2.117	2.555	2.305	2.048
NTD1	0.911	0.907	0.883	0.889	0.391	0.571
Q/λ^2	0.541	1.038	0.852	0.760	4.903	3.443

Table (4.6) Continued

	Event	number	three			
step	OTF		SPRTF		DPRTF	
ahead	average	single	average	single	average	single
1	0.610	0.566	0.396	0.383	0.382	0.325
2	1.199	1.074	0.801	0.770	0.753	0.644
3	1.773	1.546	1.225	1.174	1.109	0.961
4	2.323	1.997	1.677	1.606	1.445	1.254
5	2.851	2.442	2.159	2.064	1.754	1.537
6	3.331	2.867	2.647	2.526	2.028	1.794
7	3.758	3.269	3.133	2.982	2.265	2.038
8	4.119	3.633	3.592	3.412	2.456	2.275
9	4.426	3.969	4.025	3.821	2.605	2.513
NTD1	-0.293	-0.114	0.454	0.490	0.493	0.632
Q/λ^2	0.225	0.278	0.416	0.499	7.211	3.916

Table (4.6 continued) RMSE result of average and single-based event models for different events (Orgeval catchment).

	Event	number	four			
step	OTF		SPRTF		DPRTF	
ahead	average	single	average	single	average	single
1	0.421	-	0.454	0.455	0.974	1.463
2	0.998	-	1.069	1.073	1.897	2.853
3	1.738	-	1.800	1.808	2.747	4.206
4	2.629	-	2.596	2.608	3.514	5.384
5	3.529	-	3.378	3.398	4.200	6.376
6	4.488	-	4.212	4.239	4.873	7.249
7	5.489	-	5.098	5.134	5.538	8.103
8	6.519	-	6.025	6.070	6.203	9.004
9	7.552	-	6.970	7.023	6.863	10.013
NTD1	0.891	-	0.873	0.873	0.416	-0.316
Q/λ^2	0.395	-	0.783	0.784	3.554	3.339

Table (4.6) Continued

	Event	number	five			
step	OTF		SPRTF		DPRTF	
ahead	average	single	average	single	average	single
1	0.842	1.330	0.867	0.842	1.143	2.325
2	2.096	2.342	2.026	1.909	2.155	4.118
3	3.405	3.305	3.251	2.988	3.052	5.325
4	4.620	4.064	4.431	4.006	3.792	6.295
5	5.443	4.545	5.374	4.805	4.326	6.994
6	5.999	4.672	6.074	5.317	4.607	7.266
7	6.300	4.607	6.608	5.645	4.847	7.291
8	6.443	4.606	7.099	5.969	5.131	7.239
9	6.418	4.517	7.377	6.053	5.340	6.843
NTD1	0.671	0.179	0.651	0.671	0.393	-1.509
Q/λ^2	0.472	4.749	0.399	0.383	2.721	2.245

Table (4.6) Continued

	Event	number	six			
step	OTF		SPRTF		DPRTF	
ahead	average	single	average	single	average	single
1	0.594	0.525	0.570	0.650	0.735	0.934
2	1.429	1.175	1.288	1.657	1.370	1.799
3	2.211	1.802	2.021	2.724	1.922	2.581
4	2.989	2.453	2.809	3.894	2.396	3.273
5	3.694	2.990	3.511	5.104	2.668	3.793
6	4.258	3.404	4.085	6.234	2.798	4.222
7	4.686	3.713	4.525	7.253	2.800	4.626
8	5.027	3.920	4.800	8.162	2.656	5.024
9	5.205	4.043	4.887	8.798	2.431	5.467
NTD1	0.621	0.703	0.651	0.545	0.419	0.062
Q/λ^2	1.161	0.558	0.693	1.199	1.837	1.147

1-PRTF model in static and dynamic form
From the RMSE the dynamic form out performs the static form in 60% of cases. However, from the portmanteau statistic the static form results are superior in almost all cases.

2-PRTF and OTF models
If only the RMSE results are considered, the ordinary transfer function model outperforms the PRTF model in 70% of cases. From the portmanteau statistic the performance of the models is the same.

3-Average and group PRTF models
Group PRTF models are superior to APRTF models with regards to both the RMSE and portmanteau statistic. In 80% of the cases evaluated, the group PRTF forecasts are more accurate than those of the APRTF models.

4-Group model and single-based event model
4-1 OTF model
From the RMSE and portmanteau statistics the group model performs better than the single event model in 90% and 80% of cases considered respectively.
4-2 PRTF model
The RMSE results of the group model are lower than the single event model for 60% of cases. However, for the portmanteau statistic the same figure is only 36%.

If both the OTF and PRTF models are considered together, then in almost 75% of cases investigated, the group models performed better than the single event models.

5-The group model performs considerably better than an average TF model.

Finally, the RMSEs of the Orgeval group model and ATF are compared with those of WMO workshop models. A summary of this comparison is presented in table (4.7).

The results of the group calibration approach are encouraging, with application of the group model increasing the quality of forecasts in all cases.

Table (4.7) Rank of models investigated, Orgeval catchment

One step ahead:

TF GAPI SMAR CEQUEAU NAMS11 SSARR SPRTF CLS HBV UBC HFS DPRTF

On average:

GAPI SMAR NAMS11 HBV CEQUEAU HFS TF CLS SSARR UBC DPRTF SPRTF

Nine step ahead:

HBV NAMS11 GAPI HFS CEQUEAU SSARR SMAR TF CLS UBC DPRTF SPRTF

Improvement in rank resulted from the group model

4.6 Conclusion

In the first section of the chapter a simple model to calculate the average pulse response is developed. The proposed model uses the average characteristics rather than average of the ordinates of pulse response. It has been shown that overall, the use of the proposed method is encouraging.

Although theoretically better models can be identified using a long sequence of gauge rainfall and flow series, it does not guarantee better forecasts than a model calibrated using a single isolated event. In order to compare the quality of forecasts obtained from average and isolated event TF models, an individual calibrated model was identified for each of six verification events, using the data of the event immediately prior to main event. Calibrated models were used for forecasting of the six verification events. Unfortunately, it has not been possible to draw a definite conclusion concerning the performance of the two different methods at least from these six verification events.

The chapter describes an extensive analysis of group calibrated TF models identified through the classification of similar events. Since the quantity of runoff from a storm depends on the storm and catchment characteristics, similarity should include both of these two variables. In such a manner, 33 calibrated events and eight verification events for the Orgeval catchment were classified into different groups on the basis of the gradient of the rising limb of an individual storm's pulse response (as an indicator of the rainfall type) and five and thirty day antecedent precipitation index as well as five day antecedent precipitation(all as an indicator of the antecedent moisture condition of the catchment).

This classification provided thirteen different groups which are used to construct thirteen individual models. Although the primary results of this classification revealed that there is not definite dependency between the type of rainfall and gradient of pulse response at least from the 41 events studied the benefits of calibrating a TF model using a sequence of storms whose characteristics are similar were demonstrated. Based on objective statistical results and subjective comparisons it is concluded that the use of group model resulted in a significant improvement on the quality of the forecasts. It is worth noting that for all eight events the five day antecedent precipitation was a feature in the best group model. Since the FDAP is known prior to event occurrence it would be possible to tailor an appropriate average transfer function model to forthcoming events using an expert based system approach. Finally since the amount of the runoff from a storm depends to the several other variables, an expert based system has been suggested, primarily as the basis for future work.

CHAPTER 5

SYSTEM IDENTIFICATION (PARAMETER ESTIMATION)

5.1 Introduction

This chapter deals with parameter estimation techniques in general and the one used in the previous chapters of the thesis in particular. The estimation of model parameters has been widely researched over many years. Numerous parameter estimation techniques exist: a comprehensive review of techniques was made by Ljung (1987), and a number of estimation techniques were evaluated by Harpin (1982). Parameter estimation in rainfall-runoff modelling is not an easy task and the difficulty increases as the number of model parameters increases. Three major reasons may be mentioned for these difficulties (Chiew *et al.*, 1993). First, because of discontinuities in the response of rainfall-runoff models due to use of constraints to prevent parameters from taking unrealistic values, an estimation run may be trapped in one of the discontinuities, consequently a local optimum set of parameter values will be selected. Second, usually various parameters of the models are interdependent. Third, the statistical assumptions of zero mean, constant variance, and normally distributed errors are rarely satisfied. Furthermore, in many cases misselection of the initial parameter values and criteria used to terminate the estimation run may be led to inappropriate parameters.

The main body of this chapter details the ordinary least squares and recursive parameter estimation procedures including the stochastic, sequential learning algorithm, recursive ordinary least squares, and Kalman filter estimators. Instrumental variable and neural network techniques are also addressed. The application of another estimation technique, genetic algorithm is discussed in chapter six.

5.2 Least squares batch estimation

As showed in section (2.5.1) the relationships presented in equation (2.39) cannot be expected to represent river flow behaviour exactly and an error term will be required. The error term represents the effects of model inadequacy and measurement noise in the flow and rainfall variables. The system represented in equation (2.39) can be written as:

$$\underline{y} = X\underline{\beta} + \underline{\zeta} \tag{5.1}$$

where

$$\underline{y} = \left(y_1 y_2 \ldots\ldots\ldots y_t y_{t+1}\right)^T = \text{output vector}$$

$$\underline{\beta} = \left(a_1 a_2 \ldots\ldots\ldots a_m b_1 b_2 \ldots\ldots\ldots b_n\right)^T = \text{parameter vector}$$

$$\underline{\zeta} = \left(\zeta_1 \zeta_2 \ldots\ldots\ldots \zeta_r\right)^T = \text{noise vector}$$

$$X_t = \begin{bmatrix} y_0 & 0 & . & 0 & u_0 & 0 & . & 0 \\ y_1 & y_0 & . & 0 & u_1 & u_0 & . & 0 \\ y_2 & y_1 & . & 0 & u_2 & u_1 & . & 0 \\ . & . & . & . & . & . & . & . \\ . & . & . & . & . & . & . & . \\ . & . & . & y_0 & . & . & . & u_0 \\ . & . & . & y_1 & . & . & . & u_1 \\ . & . & . & . & . & . & . & . \\ y_t & y_{t-1} & . & y_{t-m+1} & u_t & u_{t-1} & . & u_{t-n+1} \end{bmatrix} \tag{5.2}$$

The system is modelled by a set of parameter estimates $\hat{\underline{\beta}}$:

$$\hat{\underline{y}} = X\hat{\underline{\beta}} \tag{5.3}$$

An error vector $\underline{e}$ is defined such that:

$$\underline{e} = \underline{y} - \hat{\underline{y}} \tag{5.4}$$

As both positive and negative errors contribute in a positive sense to its value, usually a quadratic error criterion is defined as:

$$E = \underline{e}^T \underline{e} = \left(\underline{y} - \hat{\underline{y}}\right)^T \left(\underline{y} - \hat{\underline{y}}\right) \tag{5.5}$$

therefore

$$E = \left(\underline{y} - X\hat{\underline{\beta}}\right)^T \left(\underline{y} - X\hat{\underline{\beta}}\right) = \underline{y}^T \underline{y} + \left(X\hat{\underline{\beta}}\right)^T \left(X\hat{\underline{\beta}}\right) - \underline{y}^T \left(X\hat{\underline{\beta}}\right) - \left(X\hat{\underline{\beta}}\right)^T \underline{y} \tag{5.6}$$

Differentiating with respect to $\underline{\hat{\beta}}$ gives:

$$\frac{\partial E}{\partial \underline{\hat{\beta}}} = 2X^T X\underline{\hat{\beta}} - 2X^T \underline{y} \tag{5.7}$$

The least squares estimate of the parameter is now obtained by equating $\frac{\partial E}{\partial \underline{\hat{\beta}}}$ to zero, where E is a minimum. Therefore:

$$X^T X\underline{\hat{\beta}} = X^T \underline{y} \tag{5.8}$$

$$\underline{\hat{\beta}} = \left(X^T X\right)^{-1} X^T \underline{y} \tag{5.9}$$

This type of estimator is termed a batch estimator and can be seen that it requires a matrix inversion.

5.3 Recursive estimators

In many cases, and in particular in real-time, it is desirable that the model uses all observations up to the current time. Consequently, model parameters should be calculated repeatedly as and when new data became available. Identification techniques that comply with this requirement are called recursive identification methods. Other commonly used terms for such techniques are on-line or real-time identification, adaptive parameter estimation, or sequential parameter estimation (Ljung, 1987).

In batch estimation, all previously measured data are processed together. In recursive form, the previously estimated parameters and only newly available data are used, that is it considers the most recent observations, and disregards the old ones.

The principle of the recursive technique can be illustrated through the following simple example. If the mean of the series at time t, based on t previous measurement, is given by:

$$\mu_t = \frac{1}{t}\sum_{j=1}^{t} x_j \tag{5.10}$$

then the mean at time $t+1$ is given by:

$$\mu_{t+1} = \frac{1}{t+1}\sum_{j=1}^{t+1} x_j = \frac{1}{t+1}\sum_{j=1}^{t} x_j + \frac{1}{t+1}x_{t+1} \tag{5.11}$$

therefore

$$\mu_{t+1} = \mu_t + \frac{1}{t+1}(x_{t+1} - \mu_t) \tag{5.12}$$

Similarly, other statistical properties of the series can be calculated.

In all recursive estimation techniques, the form of the algorithm is:

$$\underline{\hat{\beta}}_{t+1} = \underline{\hat{\beta}}_t + G_t(y_t - \hat{y}_t) \tag{5.13}$$

(i.e. New parameter = old parameter + Gain x error)

where the term $\hat{y}_t$ is the forecast value of y_t. Differences between each type of recursive algorithm lies in the form of the gain term (G_t).

5.3.1 Stochastic technique

Perhaps the computationally simplest recursive algorithm is the stochastic approximation algorithm (Harpin, 1982):

$$\underline{\hat{\beta}}_{t+1} = \underline{\hat{\beta}}_t + \frac{1}{t}\underline{x}_t(y_t - \hat{y}_t) \tag{5.14}$$

where $\underline{x}_t$ is the input vector $\underline{x}_t = (y_{t-1}y_{t-2}.....y_{t-m}u_{t-1}u_{t-2}.....u_{t-n})$ and $\hat{y}_t$ is the previous prediction of the output:

$$\hat{y}_t = \underline{x}_t^T \underline{\hat{\beta}}_t \tag{5.15}$$

Note the autoregressive-moving average model of equation (2.39) can be defined by using:

$\underline{\hat{\beta}}_t = \left(\hat{a}_1\hat{a}_2.....\hat{a}_m\hat{b}_1\hat{b}_2.....\hat{b}_n\right)_t^T$ and $\underline{x}_t = (y_{t-1}y_{t-2}.....y_{t-m}u_{t-1}u_{t-2}.....u_{t-n})^T$.

However, instability makes this technique of little practical use.

5.3.2 Sequential learning algorithm

The sequential learning algorithm proposed by Nagumo and Noda (1967) is of the form:

$$\underline{\hat{\beta}}_{t+1} = \underline{\hat{\beta}}_t + \gamma \frac{\underline{x}_t}{\underline{x}_t^T \underline{x}_t}(y_t - \hat{y}_t) \tag{5.16}$$

where $0 < \gamma < 2$. In order to obtain a small state gain and rapid convergence, the coefficient γ must be less than unity. As the denominator of the gain, $\underline{x}_t^T \underline{x}_t$, is a scalar value, matrix inversion is not required. Harpin (1982) concluded that the gain can become infinitely large if there are no values in the input vector, x_t, as often occurs in rainfall-runoff sequences.

5.3.3 Recursive Ordinary Least Squares (ROLS)

It can be seen from equation (5.9) that if there are *(q)* parameters, application of the least squares batch estimator, requires the inversion of an *(q.q)* matrix. In real-time, when an additional piece of information is received at the $(t+1)^{th}$ time step, the recalculation and reinversion of the *(q.q)* matrix is necessary. Plackett (1950) derived a recursive technique to successively update the parameter estimates with the addition of new data, thus avoiding matrix inversion.

If an additional pair of observations are received at time *t+1*, equation (5.2) and (5.9) take the following form:

$$X_{t+1} = \begin{bmatrix} y_0 & . & . & u_0 & . & . \\ y_1 & . & . & u_1 & . & . \\ . & . & . & . & . & . \\ . & . & . & . & . & . \\ y_t & . & . & u_t & . & . \\ - & - & - & - & - & - \\ y_{t+1} & . & . & u_{t+1} & . & . \end{bmatrix} = \begin{bmatrix} X_t \\ - \\ \underline{x}_{t+1}^T \end{bmatrix} \tag{5.17}$$

$$\underline{\hat{\beta}}_{t+1} = \left(X_{t+1}^T X_{t+1}\right)^{-1} X_{t+1}^T \underline{y}_{t+1} \tag{5.18}$$

Defining

$$P_t^{-1} = X_t^T X_t \tag{5.19}$$

It can be shown that:

$$\underline{\hat{\beta}}_{t+1} = \underline{\hat{\beta}}_t + P_{t+1}\underline{x}_{t+1}\left(y_{t+1} - \underline{x}_{t+1}^T\underline{\hat{\beta}}_t\right) \tag{5.20}$$

where

$$P_{t+1} = P_t - \gamma_t P_t \underline{x}_{t+1}\underline{x}_{t+1}^T P_t$$

and

$$\gamma_t = \left(1 + \underline{x}_{t+1}^T P_t \underline{x}_{t+1}\right)^{-1}$$

As γ_t is a scalar there is no need for matrix inversion. The parameter estimate vector $\underline{\hat{\beta}}_t$ and P_t are initialised as:

$$\underline{\hat{\beta}}_0 = (00.....0)^T \tag{5.21}$$

$$P_0 = c \times I \qquad (I = \text{Identity matrix}) \tag{5.22}$$

where c is a large number (for example 1000).

Harpin (1982) concluded that the recursive least squares estimator is adequate for transfer function models in hydrological environments, despite the biased nature of the parameters away from the true values in the presence of coloured noise.

5.3.4 Kalman filter estimation

The following formulation are used in the Kalman filter approach:

$$\underline{\beta}_{t+1} = \underline{\beta}_t + \underline{w}_t \tag{5.23}$$

$$y_t = \underline{x}_t^T\underline{\beta}_t + V_t \tag{5.24}$$

where $\underline{w}_t$ and V_t are the system model and measurement noise respectively.

$$E\left[w_k w_j^T\right] = q^2\delta_{kj}$$

$$E\left[v_k v_j^T\right] = \gamma^2 \delta_{kj}$$

$$E\left[w_k v_j^T\right] = 0$$

$$E[w_k] = E[v_k] = 0$$

δ_{kj} is the Kronecker delta which is defined as zero if $j \neq k$ and unity if $j=k$.

The recursive algorithm of Kalman filter is:

$$\underline{\hat{\beta}}_{t+1} = \underline{\beta}_t + \underline{k}_{t+1}\left(y_{t+1} - \underline{x}_{t+1}\underline{\hat{\beta}}_t\right) \tag{5.25}$$

$$P_{t+1} = P_t - P_t \underline{x}_{t+1}\left(\underline{x}_{t+1}^T P_t \underline{x}_{t+1} + R\right)^{-1} \underline{x}_{t+1} P_t + Q \tag{5.26}$$

$$\underline{k}_{t+1} = P_t \underline{x}_{t+1}\left[\underline{x}_{t+1}^T P_t \underline{x}_{t+1} + R\right]^{-1} \tag{5.27}$$

where k_{t+1} is termed the Kalman gain. P_t is the covariance matrix of the estimation errors, e_t, where

$$e_t = y_{t+1} - \underline{x}_{t+1}^T \underline{\hat{\beta}}_t \tag{5.28}$$

Q is the covariance matrix of the system noise and R is the covariance of the measurement noise. Q and R must both be known *a priori* and this is the major problem of the Kalman filtering approach. Although the determination of Q and R in real-time application is dubious, off-line determination is possible, for example by considering them as design parameters, and calculating them through simulation experiments on historic data.

It can be seen if $Q=0$ and $R=1$ the algorithm is equivalent to the ROLS algorithm.

5.3.5 The instrumental variables technique

In the current approach an instrumental matrix, V, is defined such that $E\left[V^T \underline{\zeta}\right] = 0$. Where ζ as introduced in equation (5.1) is noise vector. Premultiplication of equation (5.1) by V^T leads to:

$$V^T \underline{y} - V^T X \underline{\beta} = V^T \underline{\zeta} \tag{5.29}$$

setting the left hand side to zero provides a simple derivation of the instrumental variable estimator:

$$\hat{\beta} = \left(V^T X\right)^{-1} V^T \underline{y} \tag{5.30}$$

The choice of a suitable instrumental matrix is the major problem of this method. Young used an auxiliary model algorithm (see for example Young, 1986) as:

$$\underline{\hat{\beta}}_{t+1} = \underline{\hat{\beta}}_t + P_{t+1}\underline{w}_{t+1}\left(y_{t+1} - \underline{x}_{t+1}^T \underline{\hat{\beta}}_t\right) \tag{5.31}$$

$$P_{t+1} = P_t - \gamma_t P_t \underline{x}_{t+1} \underline{w}_{t+1}^T P_t \tag{5.32}$$

$$\gamma_t = \left(1 + \underline{x}_{t+1} P_t \underline{w}_{t+1}^T\right)^{-1} \tag{5.33}$$

where

$$\underline{w}_t = \left(w_{t-1} w_{t-2} \ldots\ldots w_{t-m} u_{t-1} u_{t-2} \ldots\ldots u_{t-n}\right)^T \tag{5.34}$$

and w_{t-i} are the output from the auxiliary model:

$$w_t = \underline{w}_t^T \underline{\beta}_t^* \tag{5.35}$$

The parameter of the auxiliary model is obtained from:

$$\underline{\beta}_t^* = (1-\alpha)\underline{\beta}_{t-1}^* + \alpha \underline{\beta}_t \tag{5.36}$$

α is chosen so as to prevent instability in the estimation, for example, $\alpha = 0.03$ to 0.05.

Ede and Cluckie (1985) stated that the instrumental variables estimator, which produces unbiased estimates in the presence of coloured noise, does not necessarily produce better models for forecasting, and can on occasions produce worse.

5.4 Neural networks

The potential advantages of artificial neural networks have created considerable interest in the possibilities for engineering applications however, it can not be used for TF parameter estimation at current stage. Neural networks have been also used in water resources environments over the last ten years including by Karunanith *et al.*, (1994), Cox (1994),

and Norreys and Cluckie (1994). Many researchers are considering the use of hybrid systems which integrate artificial neural networks with, in particular, knowledge-based expert systems. This section gives an overview of artificial neural networks.

Based on biological models of the human brain's function, computation is modelled as a large network of interconnected simple processors and artificial neural networks (ANNs) can be trained to recognise input patterns and produce appropriate output responses.

An artificial neural network can be described in terms of the individual neurones, the network connectivity that defines the interconnections of the neurones, the weights associated with the connections, and the activation or threshold functions associated with each neurone. Figure (5.1) depicts the structure of a single node or neurone from an arbitrary artificial neural network. The neurone in the figure, designated the *k*th neurone, occupies a position in its network that is quite general; that is, this neurone both accepts inputs from other neurones and sends its output to other neurones. Any neurone in a totally interconnected network has this generality. In a layered network, however, some neurones are specialised for either input or output; in such a network, it is only the interior or hidden nodes that maintain generality. The generalised neurone gets its inputs from interconnections leading from the output of other neurones.

Following the biological terminology for the connections between nerve cells, these interconnections are also known as synapses. The synaptic connections are weighted. That is, when the *j*th neurone sends a signal to the *k*th neurone, that signal is multiplied by the weighting on the *k, j* synapse. This weighting can be symbolised as w_{jk}. If the output of the *j*th neurone is designated as x_j, then the input to the *k*th neurone from the *j*th neurone is $x_j w_{kj}$. Summing the weighted inputs to the *k*th neurone:

$$u_k = \sum_j x_j w_{kj} \tag{5.37}$$

This summing of the weighted inputs is carried out by a processor within the neurone. The sum that is obtained is called the activation of the neurone. This activation can be positive, zero, or negative. After summing its inputs to determine its activation, then the neurone's next job is to apply a signal transfer function to that activation, to determine an output.

A neural networks consists of interconnected nodes or neurones. Many topologies for a neural network are possible. Figure (5.2a) shows a totally connected network, in which every node output is connected to every other node. In figure (5.2b) there are three layers

of nodes, with total connection between layers. This case shows a feed forwards network, with no feedback from higher to lower layers. A network of mixed connectivity is shown in figure (5.2c).

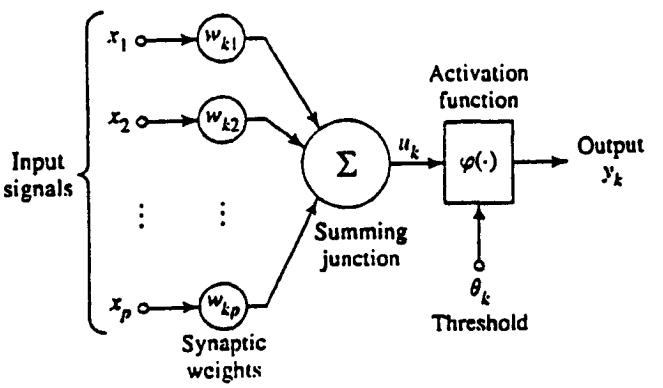

Figure (5.1) Structure of a single neurone from an arbitrary artificial neural network.

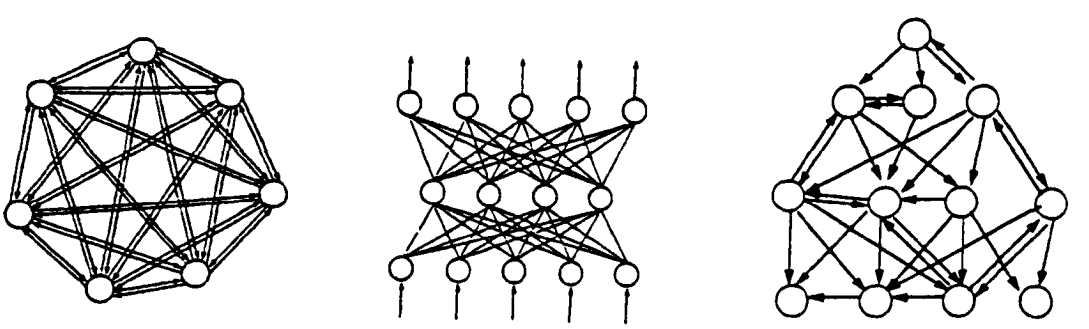

(a) totally connected network (b) feedforward network (c) mixed connectivity network

Figure (5.2) Some topologies for a neural network.

Among neural network models, the feed forward network is described here. If a network has one hidden layer, as in figure (5.3) the structure is termed as a two layer network. The actual operation of a feed forward network can be effectively described in terms of algebraic equations. Pattern μ, hidden unit j receives a net input:

$$h_j^\mu = \sum_k w_{jk}\zeta_k^\mu \tag{5.38}$$

and produces output:

$$V_j^\mu = g\left(h_j^\mu\right) = g\left[\sum_k w_{jk}\zeta_k^\mu\right] \tag{5.39}$$

output unit I thus receives:

$$h_i^\mu = \sum_j w_{ij}v_j^\mu = \sum_j w_{ij}g\left[\sum_k w_{ij}\zeta_k^\mu\right] \tag{5.40}$$

producing a final output:

$$O_i^\mu = g\left(h_i^\mu\right) = g\left[\sum_j w_{ij}v_j^\mu\right] = g\left[\sum_j w_{ij}g\left[\sum_k w_{jk}\zeta_k^\mu\right]\right] \tag{5.41}$$

where:

O_i = output units, V_j = hidden units, ζ_k = input terminals, w_{jk} = connections from inputs to the hidden units, w_{ij} = connections from hidden units to the output units, k = always refers to input, j = refers to a hidden unit, and I = refers to an output unit.

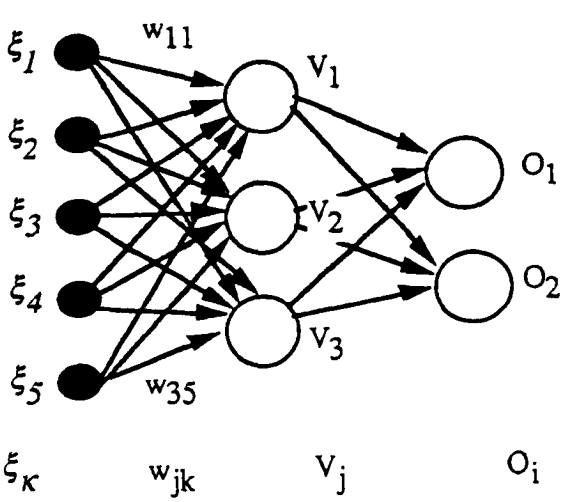

Figure (5.3) A two layer feed forward network detailing notation for units and weights.

5.5 Genetic Algorithms

Genetic algorithms (GA) can be used to search for a set of model parameters. GA are very powerful algorithm which search a function space for an optimal solution. GA based on natural evolution, in which the 'survival of the fittest' is the basis for the evolution of natural populations during many generations.

GA and their applications in hydrological environments are investigated in full in chapter 6.

5.6 Summary

There are several ways to fit models to a given set of observed data. Some procedures are only appropriate for off-line parameter estimation methods. In real-time applications it is necessary to use all observations up to the current time and repeat the procedure when new data become available, therefore some form of adaptive parameter estimation should be applied.

Recursive algorithms, which are dominant in real-time system identification have been described. A recursive algorithm can be derived from its off-line counterpart. Several recursive algorithms including stochastic, sequential learning, Kalman filter estimator and instrumental variable techniques are briefly reviewed. The recursive ordinary least squares method which is used in previous sections has been introduced in detail. The neural network technique, a relatively new approach is also reviewed.

CHAPTER 6

DEVELOPMENT OF A HYBRID GENETIC ALGORITHM PRTF MODEL

6.1 Introduction

The search for improved parameter estimation techniques has been an area of major activity during the last few decades. The research described in this chapter is based on the use of Genetic Algorithms (GA) as a methodology both for the identification and adjustment (updating) of PRTF model parameters. The effectiveness of a combined GA and conventional approach, named the Hybrid Genetic Algorithm (HGA) is demonstrated by simulation studies. Some new aspects of GA are included and the robustness of the HGA is investigated using several case studies.

This chapter consists of two sections. The first section presents the genetic algorithm's general characteristics whilst the second section concentrates on the application of the HGA and its new aspects. The application of the HGA technique is illustrated with several case studies.

6.2 Genetic Algorithm concepts

6.2.1 Optimisation

A genetic algorithm (GA) is a technique which can be used to search for a set of model parameters so that a defined performance index is maximised or minimised. There are many techniques related to optimisation including hill-climbing, random search, and iterated search.

Hill-climbing, searches directly for local optima by moving in a direction related to the local gradient. However, once it finds a local optima, no further progress can be made (Goldberg, 1989). In the random search, objective function values at every point in the search space are examined randomly. Therefore, this technique is a very 'unintelligent'

strategy (Goldberg, 1989). Iterated hill-climbing search is a combination of random search method and the hill-climbing method. In this method, hill-climbing is repeated with different randomly chosen starting points and provides better performance.

Genetic algorithms are search procedures based on natural evolution, in which the 'survival of the fittest' is the basis for the evolution of natural populations during many generations. GAs were proposed by John Holland in the 1970s' (Lawrence 1991) but only recently have been applied across a wide range of sciences. At present, genetic algorithms are being used for a range of applications including machine learning, artificial intelligence, neural networks, and operational research. Goldberg (1989) and Lawrence (1991) provide valuable information on genetic algorithms and this has been widely used here, especially to introduce GA concepts.

6.2.2 Genes, chromosomes, parents and children

GA are complicated and powerful algorithms which search a function space for an optimal solution of a non-linear system.

The genetic algorithm uses a number of genes that are responsible for transferring some properties from parents to children. A number of genes make a chromosome and a number of chromosomes produce a population. Each chromosome is called a member of population.

From an optimisation point of view, the number of genes is equal to number of parameters that should be computed. As an example suppose that the number of parameters (say α,β,γ) is three. Taking any of the three parameters in the three dimensional space as a gene, then any point $[\alpha_i,\beta_i,\gamma_i]$ i=1,2,3,.....N in the three dimensional space is a chromosome. The N chromosomes provide a population and is referred to as the population size. The objective of the genetic algorithm is to find the chromosome that is the best point in the three dimensional space.

A simple description of the genetic algorithm approach to model identification is:

1 Randomly initialise a population of chromosomes as initial parents.
2 Evaluate each chromosome in the population using a 'fitness factor'.
3 Choose a number of initialised chromosomes as a couple and produce 'children' chromosomes by mating them by 'mutation' and 'crossover'.
4 Evaluate the new chromosomes using the same fitness factor.
5 Delete the worst parents to make room for the best children.

6 If time is over, select the best chromosome as the best estimation, if not go to 3.

During the process, an initial population of unexceptional chromosomes will improve because the worst parents are sequentially replaced by better and better children. The best child in the final population, is the 'best' point in the dimensional space which thereby provides the optimal solution to the problem. It can be seen that GA provide an iterative procedure which works with a pre-defined population of individuals instead of with a single individual, therefore reduces the chance of getting stuck on a false optimum.

Some components of the simple description require further discussion.

6.2.3 Fitness and fitness scaling

For a genetic algorithm to work, a fitness factor which measures the goodness of fit is required. The fitness factor computed from simulated flow values using a PRTF forecasting model can be defined as:

$$Fitness = \frac{\sum_{t=1}^{n}[Q_0(t) - Q_s(t)]^2}{\sum_{t=1}^{n}[Q_o(t)]^2} \tag{6.1}$$

where Q_O is the observed flow
Q_s is the simulated flow (PRTF model output)
n is the number of available flow data.

It can be seen that the fitness factor is a dimensionless factor. The lower the value of fitness factor the better the match between measured and simulated flow.

The objective of parent selection in a genetic algorithm has been defined to give more reproductive chance, on the whole, to the best members of population. The technique that has been used here is roulette wheel parent selection as below:

1 Calculate the sum of the fitness factors of all the members; name the result total fitness.
2 Randomly generate a number between 0 and total fitness; call it M.
3 Select and return the first population member whose fitness factor, added to the fitness of preceding members, is greater or equal to M.

It can be seen that selection procedure is random, although, each parent's chance of being selected is directly proportional to its fitness. It is noted that fitness values of the chromosomes should be positive numbers. In the table (6.1), a classical example of roulette wheel parent selection is shown:

Table (6.1) Examples of roulette wheel parent selection

Chromosome	1	2	3	4	5	6	7	8	9	10	11	12	13	14	15
Fitness factor	9	15	22	7	17	25	13	19	6	5	27	11	3	27	4
Running total fitness	9	24	46	53	70	95	108	127	133	138	165	176	179	206	210

Random number	96	169	49	207	133
Chromosome chosen	6	11	3	14	9

It can be seen that the first random number (the fourth row of the table) is 96 which indicates that the sixth chromosome should be chosen because its running total fitness is 95. In similar manner because the second random number is 169 the 11th chromosome is chosen as the second chromosome.

Fitness scaling is a technique which can be used to prevent premature convergence. Premature convergence occurs when the differences between the best fitness factor and other fitness factors are too great so that the chances of the member with the best fitness factor being selected is too high. It means that there is no chance for other members, and consequently, the selected population is very similar and lacking in diversity. It is easy to understand, since in this case the members are similar crossover cannot work thus system works using only random mutation. To overcome this problem, the fitness factors should be scaled. To do this, following relationship between scaled (new) and unscaled (old) fitness factors are used:

$$\bar{\lambda}_N = \bar{\lambda}_O \tag{6.2}$$

$$\lambda_{NMax} = C\bar{\lambda}_O \tag{6.3}$$

$$\lambda_N = a\lambda_O + b \tag{6.4}$$

where $\bar{\lambda}_N$, $\bar{\lambda}_O$, λ_{NMax}, λ_N, and λ_O are new fitness average, old fitness average, new fitness max, new fitness and old fitness respectively.

Thus, the a and b coefficients will be computed as follows:

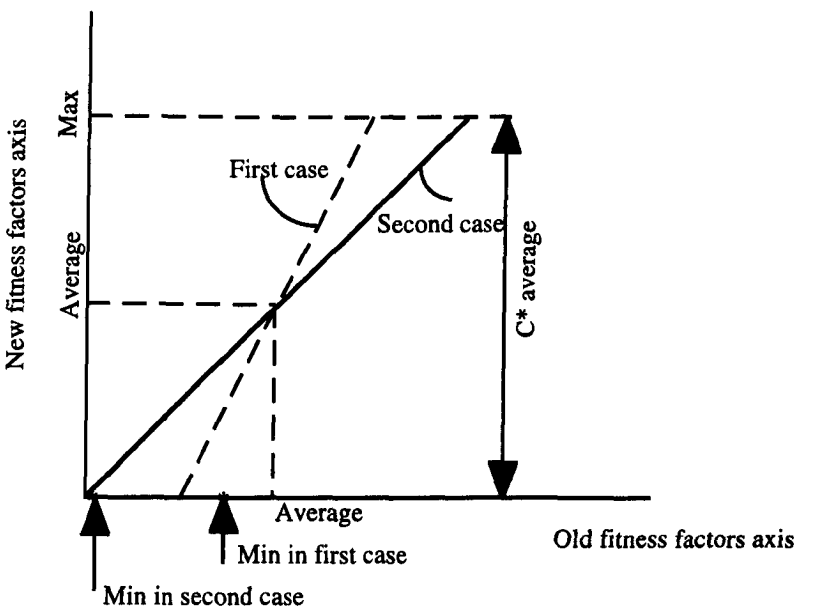

Figure (6.1) Relation between scaled and unscaled fitness factors (after Goldberg, 1989)

If:

$$\lambda_{OMin} > C \times \bar{\lambda}_O - \lambda_{OMax}/(C-1) \quad \text{[first case in figure 6.1]} \tag{6.5}$$

then:

$$\gamma = \lambda_{OMax} - \bar{\lambda}_O \tag{6.6}$$

$$a = (C-1) \times \bar{\lambda}_o / \gamma \tag{6.7}$$

$$b = (\lambda_{OMax} - C \times \bar{\lambda}_O) \times \bar{\lambda}_O / \gamma \tag{6.8}$$

otherwise [second case in figure 6.1]:

$$\delta = \bar{\lambda}_O - \lambda_{OMin} \tag{6.9}$$

$$a = \bar{\lambda}_O / \delta \tag{6.10}$$

$$b = -\lambda_{OMin} \times \overline{\lambda}_O / \delta \tag{6.11}$$

where the $\lambda_{OMax}, \lambda_{OMin}$ are old fitness max and old fitness min respectively. C is an arbitrary coefficient that could be varied among 1.2 -2.0.

It should be stressed that the average of fitness factors both in new fitness and old fitness is the same and the new fitness factors are used only in parent selection and throughout other components of main programme the old fitness factors are used.

6.2.4 Crossover and Mutation

Crossover is an extremely important component of a genetic algorithm and acts to combine the good figures already present. In nature, crossover can cause two parents to exchange parts of their corresponding chromosomes. In a genetic algorithm, crossover recombines the genetic material in two parent chromosomes to make two children. In one point crossover, a point is randomly selected and some parts of two parent chromosomes are swapped according to this selected point. Table (6.2) shows one example of the application of one point crossover in real number application. A feature of one point crossover is that no differences are introduced where both parents have the same value.

As indicated in table (6.2) in order to generate child1, the first part of parent1 (i.e. 25 32) is retained but its second part (i.e. 17 19 56) is swapped with second part of parent2 (i.e. 26 15 7) therefore, child1 determined as (25 32 26 15 7).

Table (6.2) Examples of one point crossover

Parent1	25	32	17	19	5€
Parent2	73	11	26	15	7
Child1	25	32	26	15	7
Child2	73	11	17	19	5€

Cross over point ↓

Mutation is applied to chromosomes and 'sweeps' down the genes, replacing each by a randomly selected gene. Mutation introduces diversity in to the population and is used to explore chromosomes that are similar. Mutation may cause the chromosomes of children

to be different from those of their parents. The mutation help to avoid the possibility of mistaking a local optimum for a global optimum.

Crossover and mutation complement each other. If mutation is deleted, some important figures may be missed. If crossover is deleted, the system lacks the capability of combining the best features already present.

6.2.5 Interview selection

Interview is same procedure as the main program, except it works until a predefined fitness factor is obtained. The generation number of interview is also less than that of main programme. For interview to work, a population of desired parameters are randomly generated. The fitness of each member in the population is evaluated and the fittest member of the population is found. This provides the first member of the first couple of the next generation. The fitness factors of the last generation are scaled (see section 6.2.3) and specified couples selected using a roulette wheel mechanism. Mutation and crossover are used to produce new children. The procedure is repeated until the desired generation are produced. If the fitness factor of the best children is less than defined fitness factor (Fitlmt in figure 6.5) this member is taken in to account as a member of the next phase otherwise the procedure will be repeated. The whole procedure is repeated until population size of suitable members are generated. The fitness factor of each of these new members is less than desired fitness factor. These members provide the first generation of the next phase (main programme).

6.3 Development of a hydrological Hybrid Genetic Algorithm (HGA)

6.3.1 Introduction

HGA is a combination of a GA and conventional technique. Yuan (1994) used some components of GA to identify a Conceptually Parametrised Transfer Function (CPTF) model. Furthermore, Liong *et al.* (1995) employed GA to a conceptual rainfall-runoff model. In the current study, some new aspects of genetic algorithms have been developed and incorporated into computer programs to increase the capability of HGA.

6.3.2 Identification of PRTF model

Whereas in section (2.5.2.1) a conventional identification procedure was used to determine the PRTF model parameters, this section describes the development and application of an iterative GA approach.

First, a sequence of B_i parameters plus time to peak will be generated randomly. The A_i parameters are then calculated according to the order of A_i and using formula (2.60) introduced in chapter 2. These provide a first generation individual. This procedure is repeated several times according to population size, say 20 times and these 20 individuals provide the total population of the first generation. Each individual in the population is evaluated by computing the fitness factor. The genetic algorithm then begins a series of cycles, replacing its current population of chromosome-B_i parameters and time to peak by a new population. Each cycle produces a new generation of chromosomes.

In reproduction, the parent selection technique (see section 6.2.3) will be used to pick two parents. In each reproduction event, the reproduction module gets two parents from the population module, applies crossover and mutation to the parents and sends the two children created to the population module until enough children have been generated to fill a new generation of chromosomes. These new chromosomes are evaluated, and they replace the current chromosomes to form the next generation. These generational cycles continue until the requirement individual chromosomes produce. It is noted that when chromosome- B_i parameters and time to peak are changed, A_i parameters will also be changed according to a new time to peak. It can be seen that if, for example, the order of B_i is 3 the objective of genetic algorithm searches five dimensional space.

6.3.2.1 Identification using real number representation

In order to examine the different components of a genetic algorithm an extensive study has been carried out on selected rainfall-runoff events. The main aspects of study are summarised below in order of increasing complexity;

a) Simple genetic algorithm without crossover: In this case, the initialisation and reproduction techniques are the same, the series of cycles of random generating of only one chromosome being repeated until the desired chromosome is obtained.

b) Full genetic algorithm with duplicates: In this case, all components of the genetic algorithm have been used. However, there is the possibility of duplicates, and all or part of parents or children in the generation may be the same. To study the influence of different couples in the parent selection technique and the parent deleted number the following three cases have been studied:

b-1 Number of selected parents is same as generation size : Here the population size is considered to be N=10. Since the population size and the

number of parents are the same, the total couple will be $N\times(N\text{-}1)/2=10\times9/2=45$. These couples produce 90 children in each generation.

b-2 Number of selected parents and generation size are different: Here again the population size is considered to be 10, but the number of parents is assumed to be 5. Therefore the number of total couples is $5\times4/2=10$ which will produce 20 children in each generation.

In both cases a population size of members randomly is generated, then using the roulette wheel mechanism, the desired couples are selected and their children produced using the mutation and crossover techniques. Finally, the 'worst' member of the last generation is replaced by the best child of the generation if the fitness of the best child is better than the fitness of the worst parent.

b-3 Full genetic algorithm with deletion of some of the less fit parents: In the current version of the genetic algorithm, deletion of some of the less fit parents was used instead of deletion one. The procedure is the same as the two last versions except that several worse members of the last generation are replaced by several better children in each cycle of running the programme.

The study demonstrated that the differences between three variant described above were not significant. This means that the number of parents deleted and the number of members selected in couple selection can be arbitrary.

c) Genetic algorithm without duplication: Children that are duplicates of current chromosomes in the population are discarded rather than inserting them into the population. When this reproduction technique is used, every member of the population will be different. This procedure allows much more efficient use of an allotted number of chromosomes by guaranteeing that reproduction never creates duplication in the population.

d) Unduplicated genetic algorithm with elitism: In the previous versions of genetic algorithm, the best member of the population may fail to produce offspring in the next generation. This version uses an elitist strategy to ensure that the best member of last generation is copied into the succeeding generation.

In order to determine suitable version of genetic algorithm for next phase of study, an extensive analysis has been carried out. Of these, only two of them are presented. In the first example, a number of events for the Orgeval catchment were selected and all the

genetic algorithms were run 50 times using different time steps. It should be mentioned that since genetic algorithms are stochastic, their performance usually varies from one run to another. Consequently, average performance is a more useful way to view the behaviour of a genetic algorithm than a representation of the behaviour of a genetic algorithm in a single run. The average performance of each GA variant is shown in figure (6.2) and some statistics summarising the behaviour of the different genetic algorithms are shown in table (6.3).

As another example, a simple GA and an unduplicated GA with elitism were run 20 times for a selected event from Orgeval catchment in different produced children. Average performance and some statistics of these two versions are shown in the figure (6.3) and table (6.4) respectively. It can be seen that the curves descend rapidly at the beginning of the run, and more slowly as the system nears a locally optimal solution, finally flattening at the end. Hence, most of the improvements come at the beginning of the run, with only small improvements in performance or no improvements at all tending to come at the end.

On the whole the performance of unduplicated version with elitism is better than other versions. Therefore this version of genetic algorithm was selected for next phase of the study.

A genetic algorithm using real number representation has been combined with a hill-climbing estimation method- and is called HGA. In order to guarantee that HGA always produces better estimation than hill-climbing method, the genetic algorithm is continued until better result is obtained. HGA for identification of PRTF model parameters using real numbers is illustrated in flowchart (6.4) and a numerical example illustrating the approach is given in appendix 3.

	Time Second	0.2	1	5	10	15	20	25	30
Simple GA (method a)	Mean	1.987	1.802	1.749	1.744	1.739	1.736	1.735	1.733
	Max	2.545	1.932	1.788	1.793	1.763	1.760	1.746	1.741
	Min	1.753	1.732	1.731	1.730	1.730	1.730	1.729	1.729
	St D	0.171	0.051	0.013	0.014	0.008	0.007	0.004	0.003
GA with duplicates Number of selected parents and generation size different (method b-2)	Mean	1.951	1.809	1.757	1.742	1.739	1.735	1.736	1.734
	Max	2.923	1.989	1.861	1.785	1.762	1.755	1.749	1.754
	Min	1.738	1.732	1.730	1.730	1.730	1.730	1.730	1.730
	St D	0.237	0.057	0.030	0.012	0.008	0.005	0.004	0.005
GA with duplicates Number of selected parents and generation size same (method b-1)	Mean	1.993	1.818	1.756	1.745	1.740	1.736	1.733	1.735
	Max	2.836	2.074	1.886	1.785	1.773	1.760	1.745	1.754
	Min	1.734	1.730	1.729	1.730	1.730	1.730	1.730	1.730
	St D	0.228	0.085	0.030	0.014	0.010	0.006	0.003	0.006
GA with deletion some parents (method b-3)	Mean	1.969	1.788	1.745	1.738	1.736	1.734	1.734	1.733
	Max	2.874	2.018	1.804	1.775	1.770	1.746	1.748	1.746
	Min	1.731	1.730	1.729	1.730	1.730	1.730	1.730	1.729
	St D	0.242	0.050	0.016	0.010	0.007	0.004	0.004	0.003
GA without duplicates (method c)	Mean	1.980	1.801	1.745	1.737	1.734	1.734	1.734	1.734
	Max	2.537	2.043	1.799	1.762	1.769	1.765	1.768	1.755
	Min	1.733	1.730	1.730	1.729	1.729	1.730	1.729	1.730
	St D	0.187	0.080	0.017	0.008	0.007	0.006	0.007	0.005
Unduplicated GA with elitism (method d)	Mean	2.012	1.801	1.745	1.734	1.734	1.733	1.733	1.732
	Max	2.404	2.119	1.784	1.766	1.760	1.729	1.762	1.751
	Min	1.747	1.730	1.730	1.730	1.730	1.754	1.729	1.729
	St D	0.180	0.080	0.016	0.008	0.005	0.006	0.005	0.004

Table (6.3) Some statistics of behaviour of different GA (RMSE, Orgeval catchment, average of 50 iterations)

	Time Second	0.2	1	5	10	15	20	25	30
Simple GA (method a)	Mean	0.1782	0.1457	0.1371	0.1364	0.1356	0.1352	0.1350	0.1347
	Max	0.2903	0.1674	0.1433	0.1441	0.1393	0.1388	0.1366	0.1359
	Min	0.1377	0.1344	0.1344	0.1342	0.1341	0.1341	0.1341	0.1341
	St D	0.0320	0.0083	0.0021	0.0022	0.0013	0.0010	0.0007	0.0005
GA with duplicates Number of selected parents and generation size different (method b-2)	Mean	0.1731	0.1468	0.1383	0.1361	0.1356	0.1350	0.1350	0.1349
	Max	0.3831	0.1773	0.1553	0.1428	0.1392	0.1380	0.1371	0.1379
	Min	0.1354	0.1345	0.1341	0.1341	0.1341	0.1341	0.1341	0.1341
	St D	0.0466	0.0093	0.0048	0.0019	0.0012	0.0008	0.0007	0.0009
GA with duplicates Number of selected parents and generation size same (method b-1)	Mean	0.1803	0.1484	0.1383	0.1365	0.1357	0.1351	0.1346	0.1349
	Max	0.3605	0.1928	0.1594	0.1427	0.1409	0.1389	0.1365	0.1380
	Min	0.1348	0.1342	0.1341	0.1341	0.1342	0.1341	0.1341	0.1341
	St D	0.0444	0.0143	0.0049	0.0022	0.0016	0.0010	0.0005	0.0010
GA with deletion some parents (method b-3)	Mean	0.1763	0.1434	0.1365	0.1354	0.1351	0.1348	0.1347	0.1346
	Max	0.3702	0.1825	0.1459	0.1413	0.1404	0.1366	0.1370	0.1366
	Min	0.1344	0.1341	0.1341	0.1341	0.1341	0.1341	0.1341	0.1341
	St D	0.0476	0.0083	0.0025	0.0016	0.0012	0.0006	0.0006	0.0005
GA without duplicates (method c)	Mean	0.1773	0.1457	0.1365	0.1352	0.1349	0.1348	0.1348	0.1347
	Max	0.2885	0.1872	0.1451	0.1392	0.1403	0.1397	0.1400	0.1381
	Min	0.1346	0.1342	0.1341	0.1341	0.1341	0.1341	0.1341	0.1341
	St D	0.0344	0.0135	0.0027	0.0013	0.0011	0.0009	0.0012	0.0007
Unduplicated GA with elitism (method d)	Mean	0.1828	0.1456	0.1365	0.1354	0.1348	0.1347	0.1346	0.1345
	Max	0.2590	0.2013	0.1427	0.1398	0.1388	0.1378	0.1391	0.1375
	Min	0.1367	0.1341	0.1341	0.1341	0.1341	0.1341	0.1341	0.1341
	St D	0.0330	0.0135	0.0025	0.0013	0.0009	0.0009	0.0008	0.0006

Table (6.3 Continued) Some statistics of behaviour of different GA (Fitness factors, Orgeval catchment, average of 50 iterations)

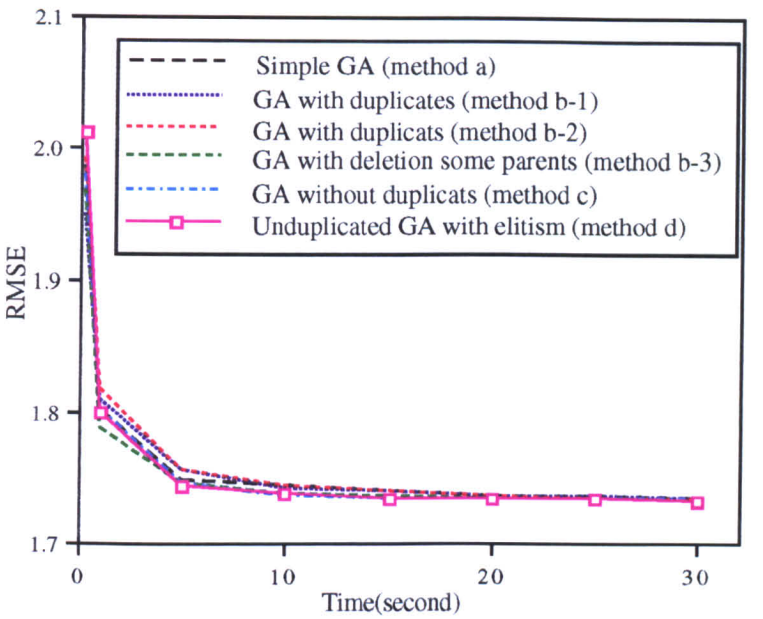

Figure (6.2) Performance graphs for several GA (average of 50 times running)

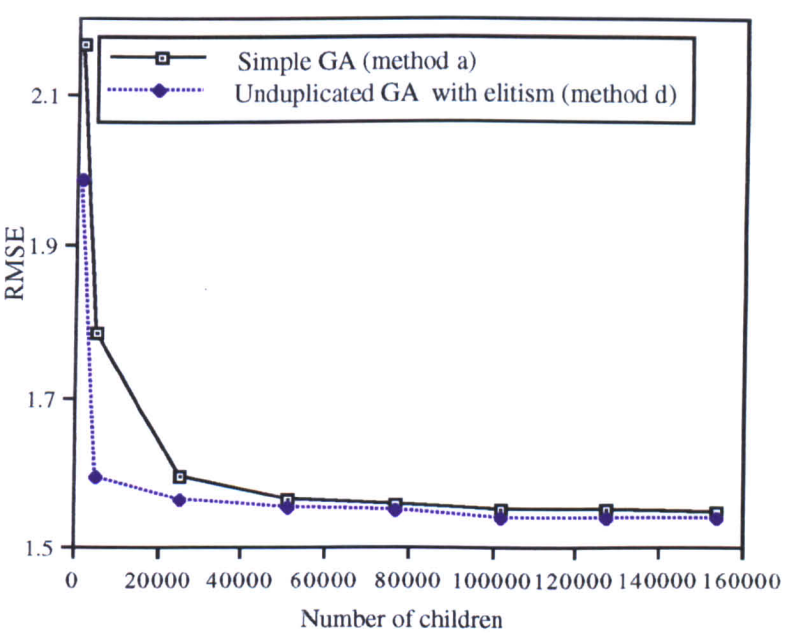

Figure (6.3) Performance graphs for simple GA and unduplicated GA with elitism in different produced children (average of 20 times running)

		Number of children	1000	5000	25000	51000	77000	102000	127000	154000
Root Mean Square Error (RMSE)	Simple GA	Mean	2.164	1.786	1.594	1.563	1.557	1.549	1.548	1.544
		Max	2.944	2.021	1.933	1.590	1.598	1.573	1.584	1.561
		Min	1.568	1.552	1.534	1.533	1.535	1.534	1.534	1.533
		St D	0.360	0.156	0.087	0.020	0.020	0.012	0.015	0.008
	Unduplicated GA with elitism	Mean	1.989	1.595	1.562	1.551	1.550	1.539	1.539	1.538
		Max	2.579	1.755	1.750	1.599	1.656	1.560	1.557	1.548
		Min	1.542	1.534	1.533	1.533	1.533	1.533	1.533	1.533
		St D	0.244	0.056	0.048	0.021	0.027	0.007	0.007	0.004
Fitness Factor	Simple GA	Mean	0.0365	0.0244	0.0193	0.0186	0.0184	0.0182	0.0182	0.0181
		Max	0.0658	0.0310	0.0284	0.0192	0.0194	0.0188	0.0191	0.0185
		Min	0.0187	0.0183	0.0179	0.0179	0.0179	0.0179	0.0179	0.0179
		St D	0.0125	0.0042	0.0023	0.0005	0.0005	0.0003	0.0003	0.0002
	Unduplicated GA with elitism	Mean	0.0305	0.0193	0.0186	0.0183	0.0183	0.0180	0.0180	0.0180
		Max	0.0505	0.0234	0.0232	0.0194	0.0208	0.0185	0.0184	0.0182
		Min	0.0181	0.0179	0.0179	0.0179	0.0179	0.0179	0.0179	0.0179
		St D	0.0074	0.0014	0.0012	0.0005	0.0007	0.0002	0.0002	0.0001

Table (6.4) Some statistics of behaviour of simple GA and unduplicated GA with elitism (Orgeval catchment, average of 20 times running)

Figure (6.4) Flowchart for HGA in identification of PRTF model using real numbers

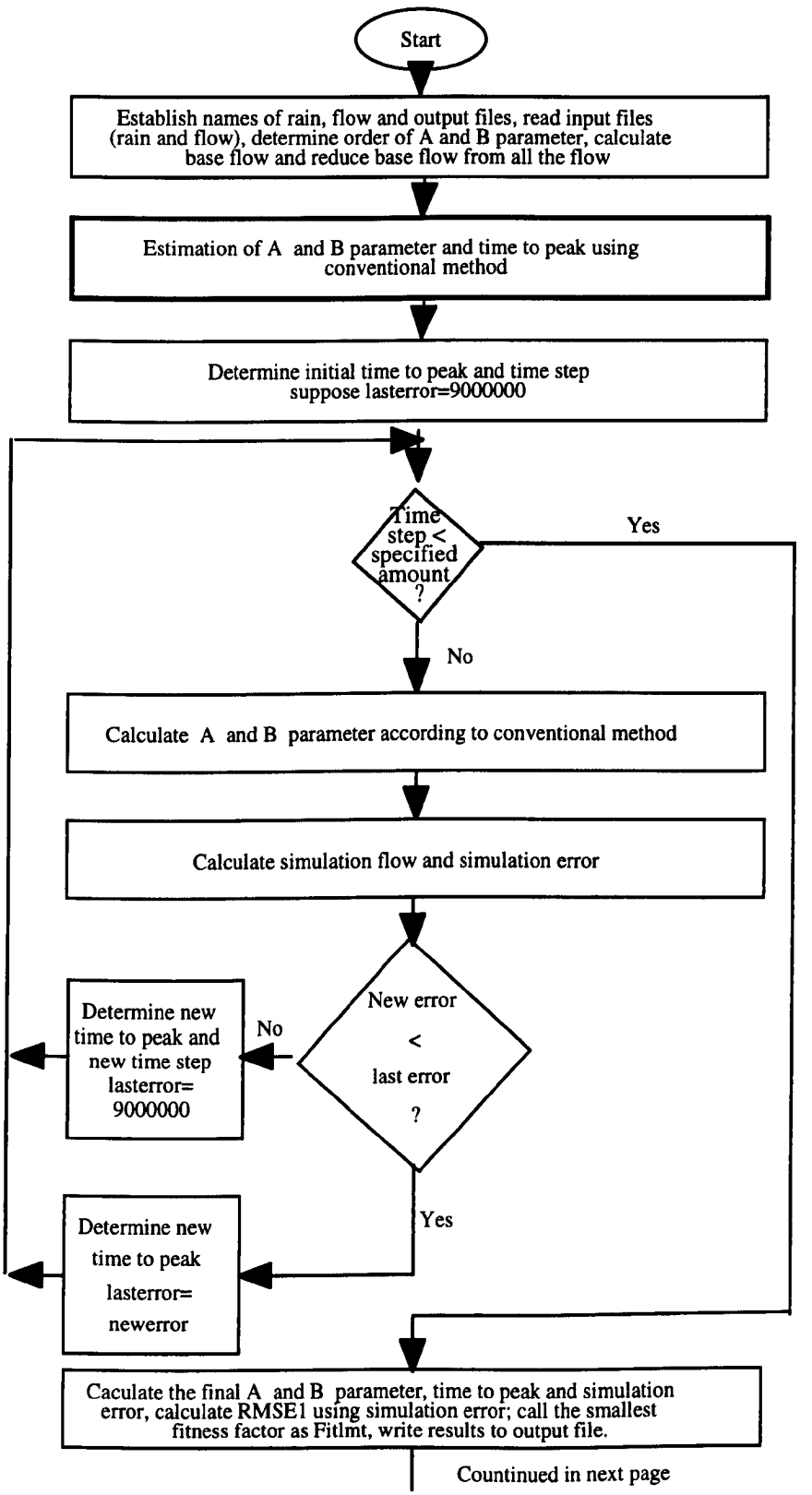

Figure (6.4) Continued

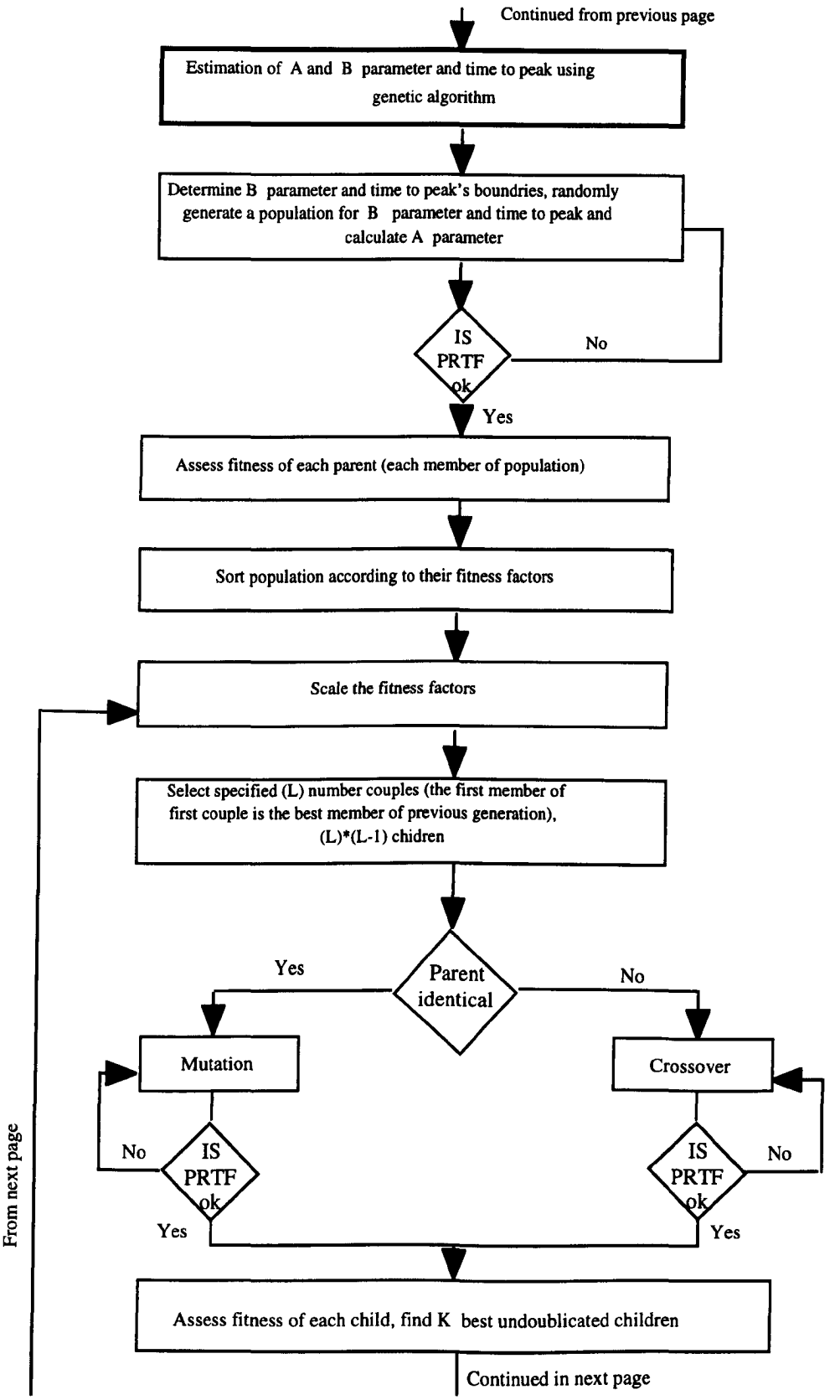

Figure (6.4) Continued

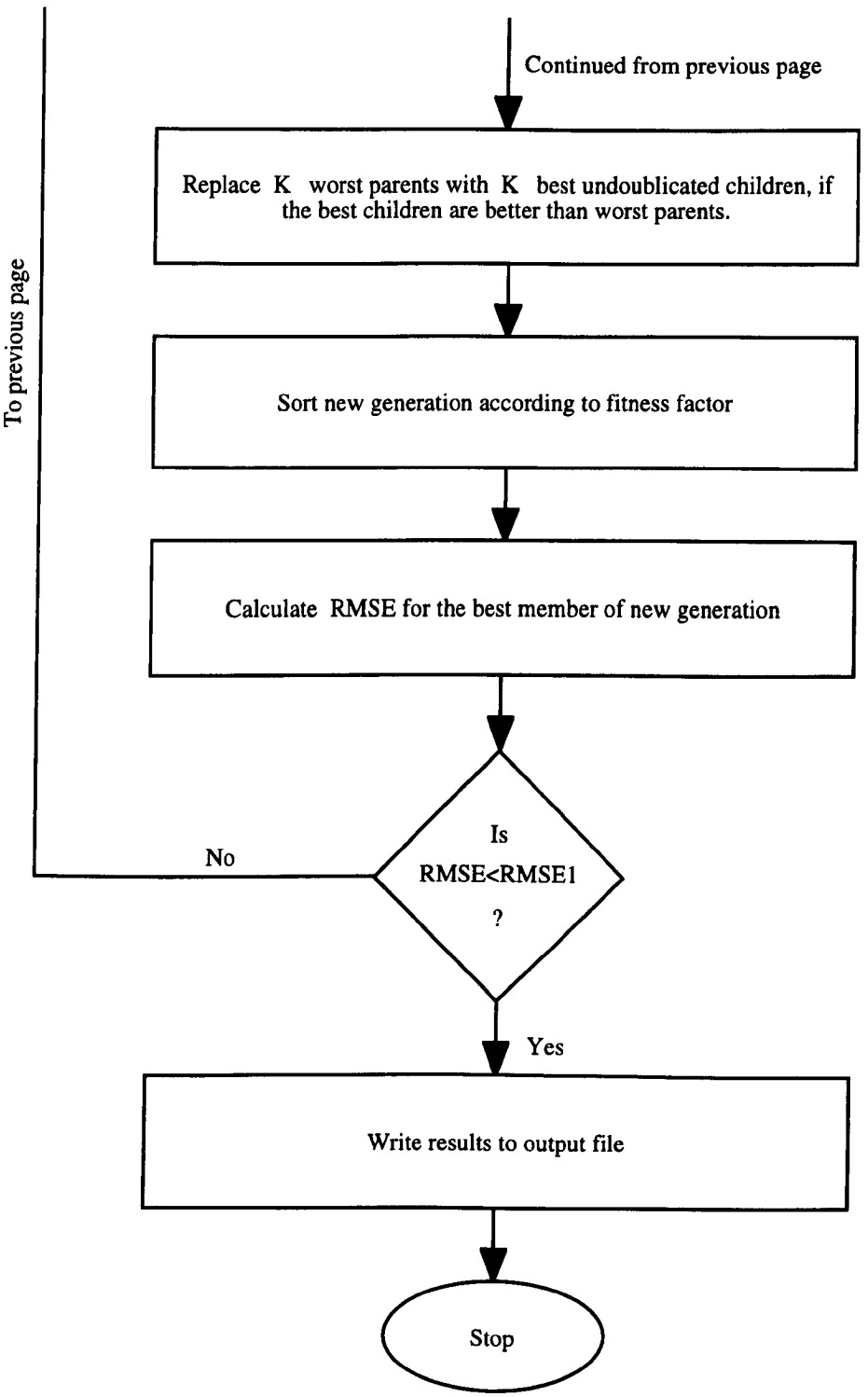

6.3.2.2 Identification using binary representation

Many genetic algorithm practitioners use a binary representation approach even though most applications involve numerical problems. Therefore in addition to numerical representation studied in the previous section, the current section considers the use of binary representation.

Binary representation produces chromosomes composed of a list of binary digits, i.e. each position can be either 1 or 0. To produce one digit, a number is generated randomly, if this generated number is less than or equal to 0.5 (probability) the digit is considered to be 1 otherwise it will be 0.

Decoding and multiple crossover as well as random mutation are other components of binary genetic algorithm which will be considered as following:

Decoding: If the number of digits of each gene (variable) is N, its equivalent real number could range between (2^N -1) and 0. Conversely if accumulated number (computed integer value associated with coded parameter) and the boundaries of real number are assumed to be *accum, Max,* and *Min* respectively, the decoded number is computed as:

$$(Max - Min)accum/(2^N - 1) + Min \tag{6.12}$$

and the accuracy of encoding will be:

$$(Max - Min)/(2^N - 1) \tag{6.13}$$

Multiple crossover: Multiple crossover is the same as one point crossover, except multiple cut points rather than one are selected as random. Here one point crossover is applied to each gene and the chromosomal material swapped between the one cut point. This crossover works on the parents with a certain probability rate, the higher the probability, the more quickly new children are introduced into the population. Table (6.5) shows three point crossovers applied to an example chromosome.

Random bit mutation: Bit mutation sweeps down the list of bits, replacing each by a randomly selected bit if a probability test is passed. Here, as in nature, probability is quite low and the probability of implementation of random bit mutation is very low. An example of the operation of bit mutation is shown in the table (6.6). For random bit

mutation to operate, randomly, a number is generated for each bit. If the generated number is equal to or less than the mutation probability, the bit is replaced by a contrary bit (i.e. a 0 bit is replaced by 1 and vice versa). If bit is not passed, the probability test it will be unchanged.

Table (6.5) Examples of multiple crossover

	Gene1	Gene2	Gene3
Parent1	1101|100	1|011011	10001|10
Parent2	0001|011	0|111100	01100|11
Child1	1101011	1111100	1000111
Child2	0001100	0011011	011001C

Cross over point ↓

In the following example it is supposed that the mutation probability is 0.05. It can be seen that for the first chromosome, as will be the case for most of the time, the probability test is never passed, and so in this case the output of bit mutation is the same as the input. For the second chromosome, the probability test is passed for the third bit, and so, the chromosome is changed by the random bit mutation.

Table (6.6) Examples of random bit mutation

Old chromosome	Random number	New chromosome
10011	0.981 0.520 0.250 0.332 0.258	10011
10001	0.725 0.912 **0.046** 0.523 0.790	10101

As mentioned earlier random bit mutation and crossover work together to produce new children.

A combined genetic algorithm using binary representation is developed which is described in flowchart (6.5) and a numerical example is given in appendix 3.

Figure (6.5) Flowchart for HGA in identification of PRTF model using binary numbers

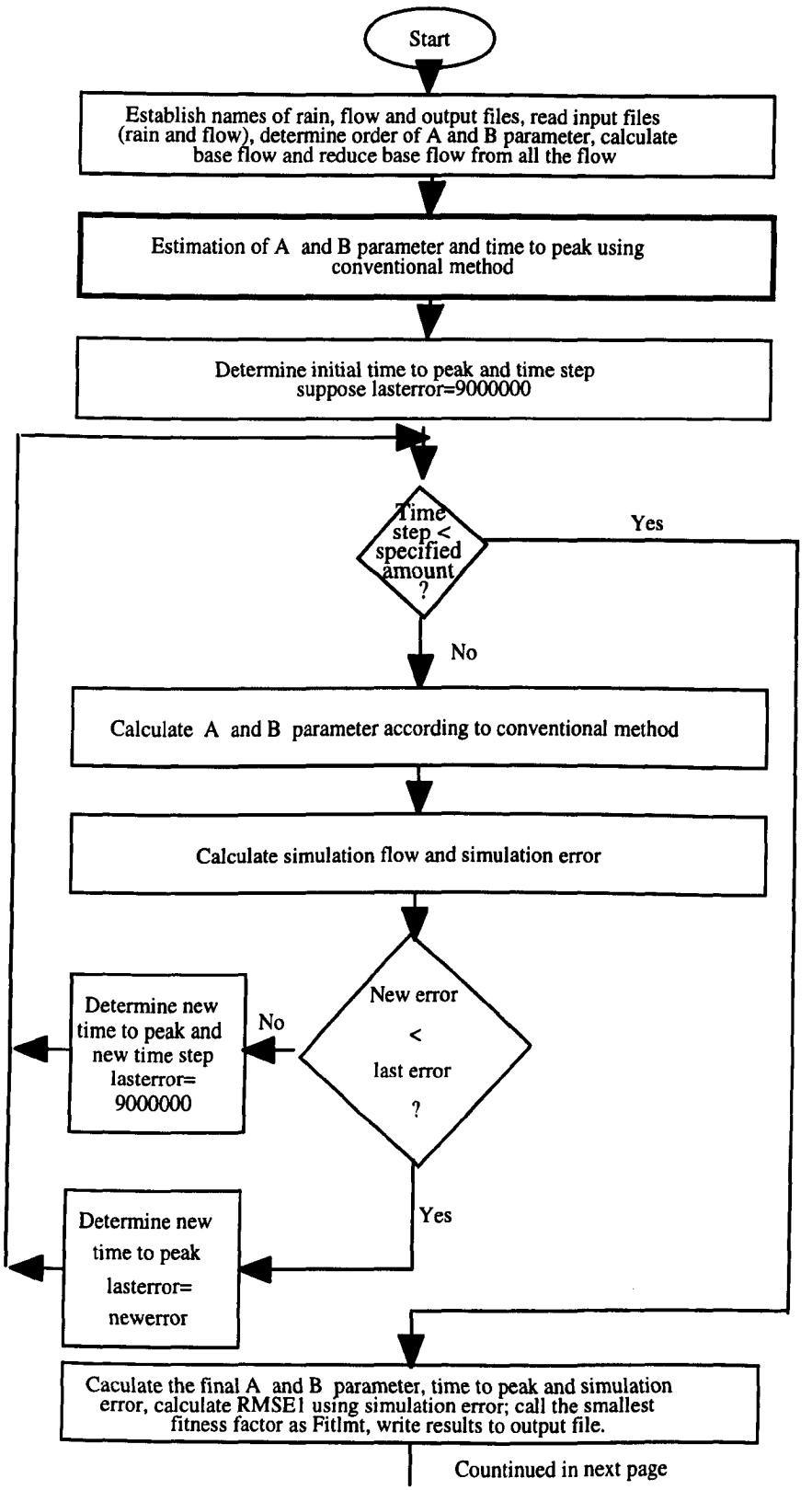

Figure (6.5) Continued

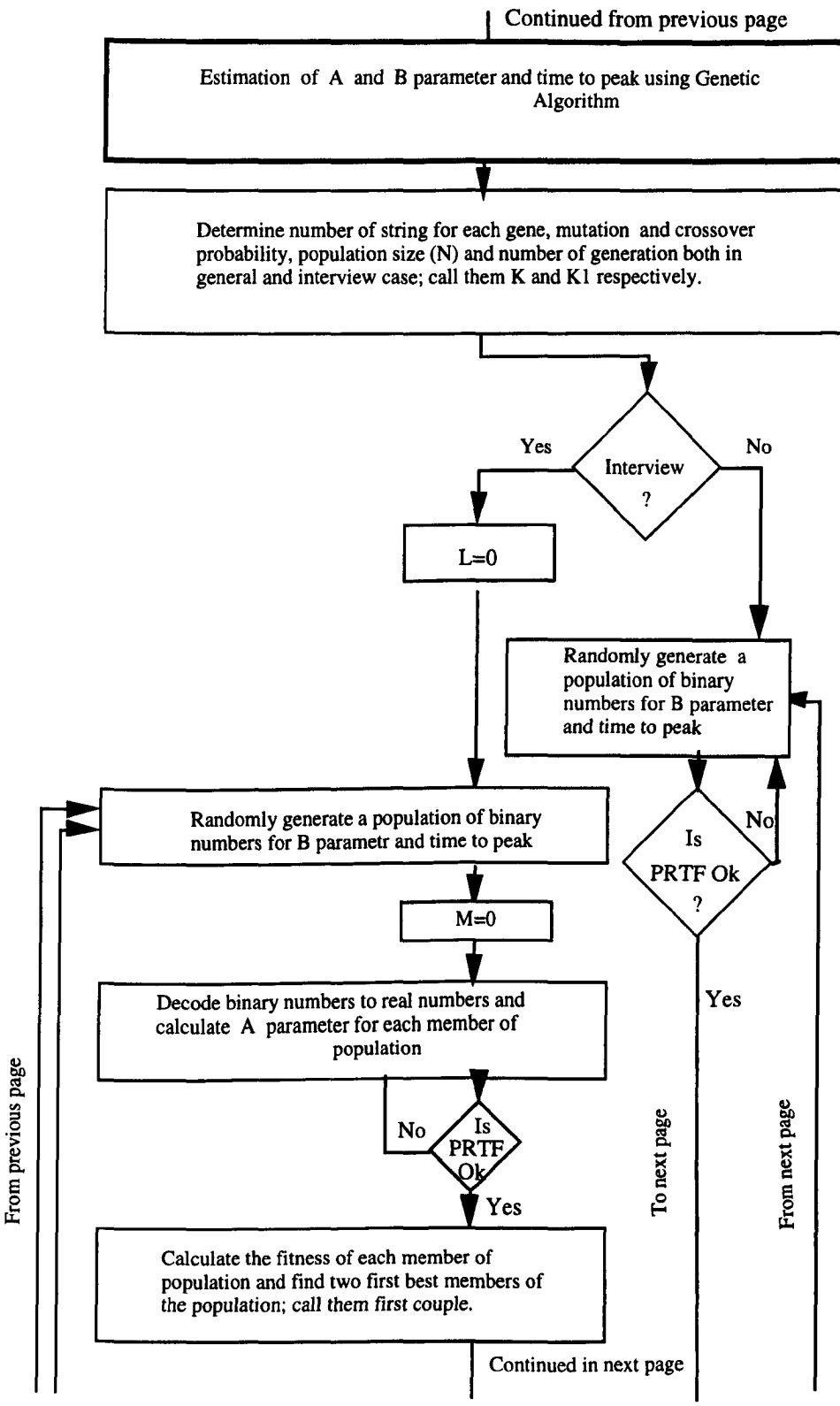

Figure (6.5) Continued

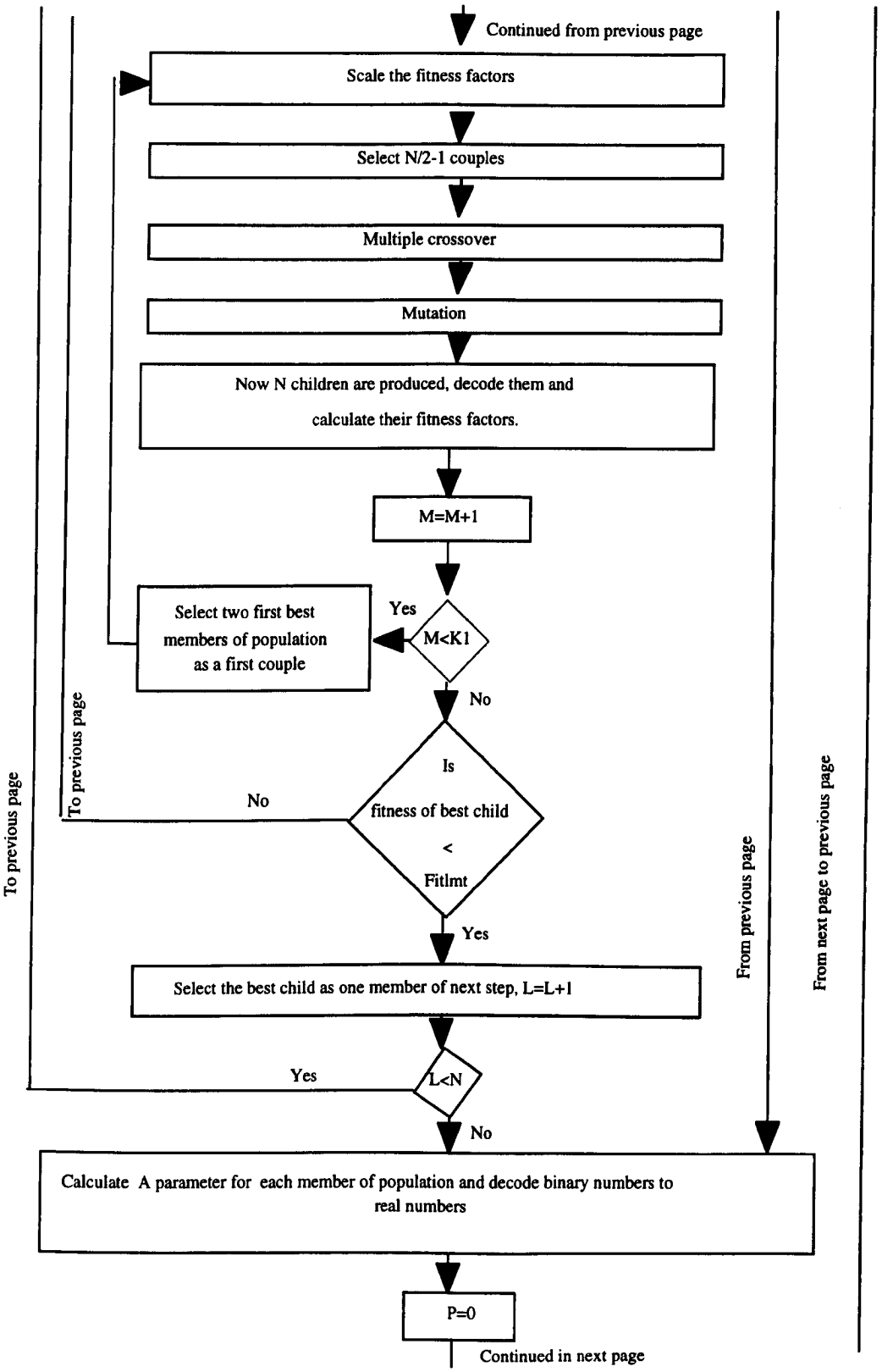

Figure (6.5) Continued

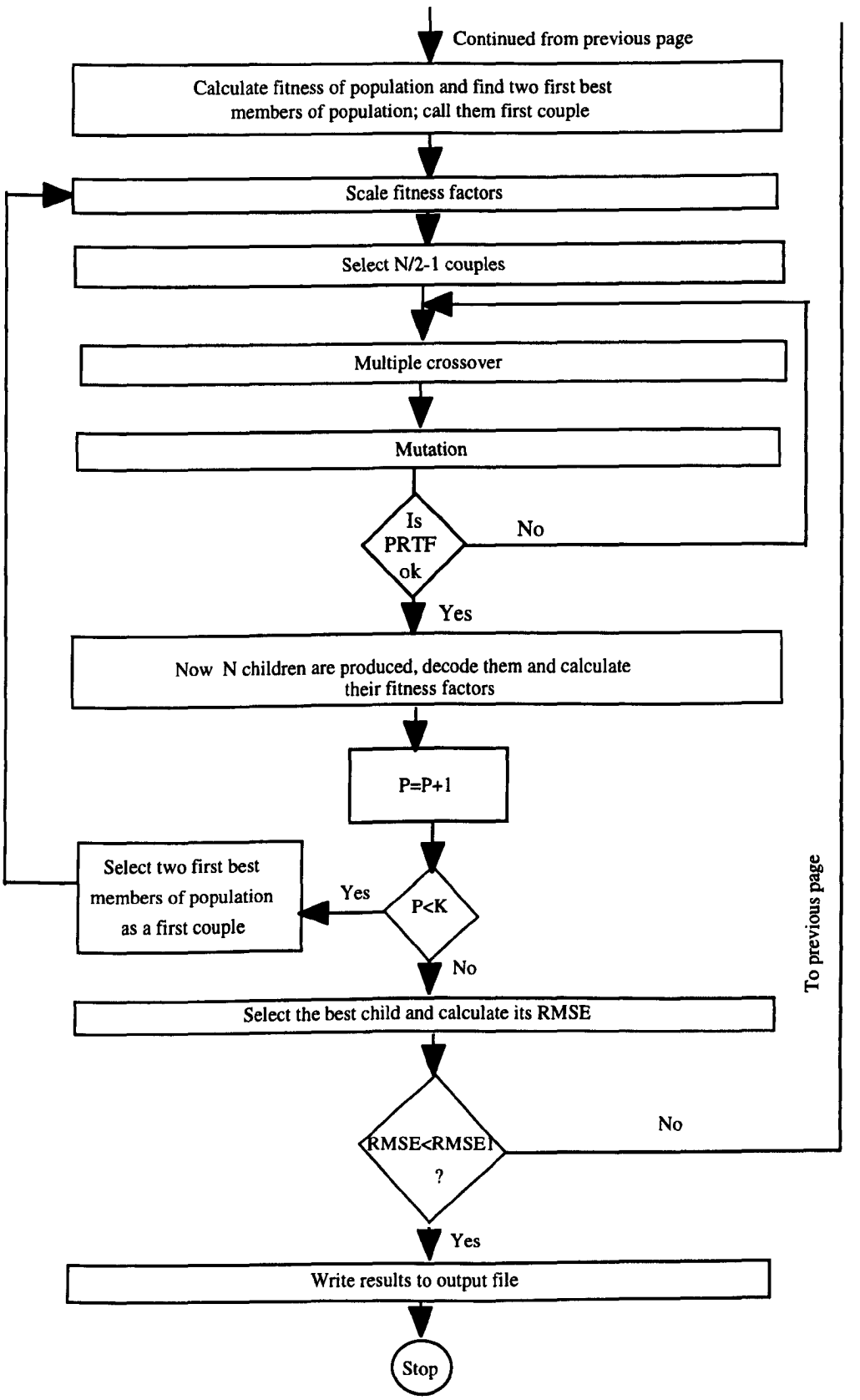

6.3.3 Simulation (updating) of PRTF model using HGA

Updating of the PRTF model involves determining the new values of the model parameters, via the α-volume, γ-shape, and τ-time adjustment factors. Here, the procedures are same as the identification phase except, since some shape adjustment factors produced by the genetic algorithm are not suitable (illegal number which makes pulse response being unstable) for the PRTF model, each shape adjustment factor generated must first be checked. If it is legal the procedure continues, otherwise another shape adjustment factor will be generated. This process is repeated until the best factor is obtained.

After producing the parent members in a population of the desired size, the genes of the produced chromosomes are partially crossed over and mutated if a probability test is passed, to produce children's generation. The children are then checked from a generated shape factor point of view, with illegal members being rejected. By comparing the fitness of the parents and the children's generations the less-fit parent members can be replaced by fitter children members thus producing a second generation. This reproduction-evaluation process is repeated until the specified time limit is up or the desired member is produced.

Further details of the hybrid genetic algorithm developed for updating the PRTF model both in real number and binary representation are included in the flowcharts figure (A3.1) and figure (A3.2) presented in appendix 3.

6.4 Summary of results

For HGA to work it is necessary to restrict the evolving space, using the parameters obtained from a hill-climbing method. The following constraints are defined to estimate the desired parameters. These can be changed according to the computer capacity and desired accuracy of computation:

Identification phase

Time to peak: from (time to peak of current method -5) to (time to peak of current method+5)

B parameters: from (B parameters of current method -5) to (B parameters of current method +5)

Updating phase

Shape factor from -10 to 10

Volume factor	from	-0.95 to 3.0
Time delay	from	0 to 10

In addition to the above specifications, some further assumptions are required before the genetic algorithm in binary representation can be applied. These are summarised below:

- number of generation, 500
- number of generation in each sub run of interview selection, 10
- length of each variable (number of digit in each gene), 12
- random mutation probability, 0.05
- crossover probability, 0.80
- population size, 20
- *C* Coefficient in fitness scaling, 2.0.

The estimation accuracy for time to peak and B parameters is 2.442×10^{-3} and for shape factor and volume factors are 4.884×10^{-3} and 9.646×10^{-4} respectively (see equation 6.13).

From all of the HGA variants considered, four have been used to investigate the capability of combined genetic algorithms for flood forecasting. In order to carry out this investigation an event from Orgeval catchment was chosen and a (3,2,0) PRTF model identified using both the conventional (MATH) procedure as described in section (2.5.2) and the newly developed HGA software. The RMSE of the actual and convoluted flow in HGA is smaller than that of MATH software, and also that the pulse response produced by the HGA model is more reasonable than that of the MATH PRTF model because it increases monotonically from 0 to the peak (figure 6.6).

Next the parameters of both PRTF models were adjusted using the conventional approach. The simulated flow hydrograph of the HGA and MATH models along with observed flow are shown in figure (6.7). It can be seen there are no obvious differences between two different calibrated models except for a marginal improvement in the peak time estimation of the HGA model.

As a final step, the parameters of the calibrated PRTF model were updated (adjusted) using the HGA approach. The simulated flows provided by the model are also shown in figure (6.7). The RMSE statistic of the HGA approach is smaller than that of the conventional method, and the simulated flow obtained from the HGA better fits actual flows.

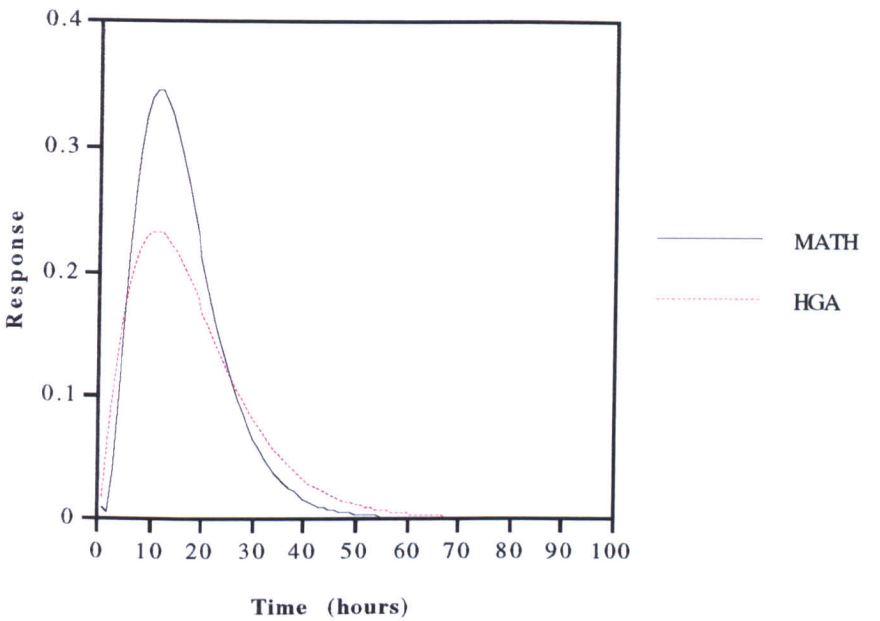

Figure (6.6) Comparison of pulse response obtained from MATH and HGA, Orgeval.

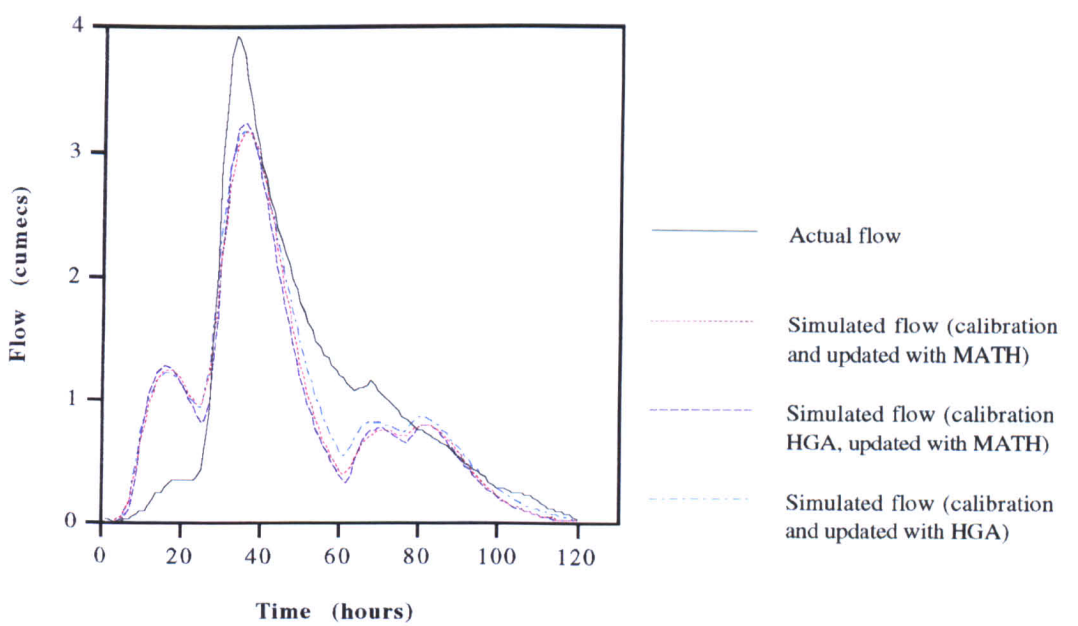

Figure (6.7) Comparison of actual and simulated flow obtained from different method

For further performance evaluation objective approach was used comparing the RMSE of the current method and HGA. To do this one event from the Bird Creek catchment and two events from the Orgeval catchment (a single event referred to as event number 6, and a composite event composed of a combination of six other individual events) were selected and HGA run 20 times both for identification and updating for real number and binary representations in each of selected event.

The results of this objective comparison between the application of HGA and current method for the three catchment-events are presented in table (6.7). Although the software developed can use interview selection for real numbers representation HGA has been applied without this.

The errors for each case are represented by the RMSE of simulated and actual flows averaged over 20 HGA runs. In addition, in order to compare the accuracy of RMSE, the maximum, minimum and standard deviation of RMSE for the 20 runs are also presented.

The results show that for each event, a significant reduction in the RMSE's is achieved by the HGA compared to the current PRTF approach. Within the HGA further reduction in error arise from the use of a binary representation compared to a real number representation, and were conducted, binary representation with interview selection provided the best model calibration. The reason for this improvement is thought to be because binary representation uses the multiple crossover and random bit mutation.

Furthermore, HGA has shown the ability to adapt to the variety of the catchments and events. This means that HGA is robust enough to be applied to various conditions. It should be emphasised there is scope for further improvements in HGA. This is because HGA is limited to cut off immediately after its fitness factor is lower than current method, it means if HGA continue to work better results will be obtained.

These results led to conclusion that HGA is a powerful tool for application in PRTF model both in identification and updating.

6.5 Conclusion

In this chapter an extensive investigation the application of genetic algorithms to the Physically Realisable Transfer Function (PRTF) model developed by Han (1991) has been presented. A new parameter estimation technique (Hybrid Genetic Algorithm) has been developed by combining conventional procedures with a genetic algorithm. The Hybrid Genetic Algorithm (HGA) has been successfully used both in identification

(calibration) and simulation (updating) of the PRTF model. The new genetic algorithm techniques of interview and scaled procedures as well as random bit mutation and multiple crossover are included in HGA. Furthermore, both binary and real numbers encoding techniques have been used. Finally four software packages including two packages for the model identification phase both in binary and real number encoding and two packages for model updating phase have been developed. Extensive development and testing has shown that the performance of HGA is more accurate and powerful than conventional procedures and HGA guarantees that model estimation error will be less than current method because it is programmed that the RMSE of HGA to be less than RMSE of current method.

Table (6.7)Comparison of the application of hybrid genetic algorithm and current method in PRTF model (average of 20 times running)

Catchment-event			Bird creek				Orgeval-event no 6				Orgeval-composite events			
Method			Current method	HGA			Current method	HGA			Current method	HGA		
				Real numbers without interview	Binary numbers			Real numbers without interview	Binary numbers			Real numbers without interview	Binary numbers	
					Without interview	With interview			Without interview	With interview			Without interview	With interview
Identification (calibration)	Root Mean Square Error (RMSE)	Mean	471.63	102.10	84.57	83.72	5.036	3.826	2.644	1.833	2.059	1.931	1.812	-
		Max	471.63	138.74	87.32	87.31	5.036	5.025	4.655	2.362	2.059	2.056	2.029	-
		Min	471.63	76.93	83.11	83.11	5.036	2.180	1.660	1.071	2.059	1.751	1.729	-
		St D	0	15.98	1.64	1.31	0	0.856	0.763	0.505	0	0.092	0.093	-
Updating(simulation)	Root Mean Square Error (RMSE)	Mean	166.01	155.53	116.36	-	1.576	1.551	1.539	-	1.730	1.729	1.729	-
		Max	166.01	165.77	116.46	-	1.576	1.575	1.565	-	1.730	1.729	1.729	-
		Min	166.01	134.73	116.35	-	1.576	1.534	1.533	-	1.730	1.729	1.729	-
		St D	0	9.31	0.02	-	0	0.010	0.010	-	0	0	0	-

CHAPTER 7

REAL-TIME UPDATING

7.1 Introduction

Due to the incapability of models to perfectly portray complex natural systems and due to faulty model input data, every forecast is subject to an error. Consequently, it is necessary to correct the forecast in the light of recent model performance to minimise the forecasting error. Updating is the technique of incorporating recent measurements of flow to improve flow forecasts (Nemec, 1986).

Although a large number of models have been considered in the literature, updating techniques are not so widely discussed (Serban and Askew, 1991). However, some references investigated updating procedures including Bramley (1981), Serban and Askew (1991), Nemec(1986), Harpin (1982), Reed (1984) and WMO (1992). Indeed as referred to in WMO (1987) the final report of the Simulated Real-time Inter-comparison of Hydrological Models (WMO, 1992) was one of the first, if not the first, publication in which the updating procedures used by operational models were described in any detail.

This chapter presents a general review of updating techniques and some newly developed procedures to improve updating procedures in transfer function models.

7.2 What is updating ?

Neither the models nor data used in flood forecasting are perfect. Consequently, estimated flows, will rarely, if ever, be exactly equal to observed flows, there always being some kinds of error between the estimated and observed flow. The error in estimated flow may be related to either inaccuracy in the measurement of input data or forecast procedure (model), whilst the error in observed flow can be due to inaccurate measurement of data only. One type of classification of errors is as follows:

- random errors which are independent and difficult to clarify. These kind of errors can result from either failure of an measurement instrument, or erroneous of data processing.

- Correlated errors, occurring at least in a few sequential forecasting time steps. These errors can be obtained from systematic instrument error and unsuitability of the rating curve used amongst others (Nemec, 1986).

As mentioned in section (2.5.2.2) and figure (2.15) errors between estimated and measured flow are generally of three types:

- incorrect volume or amplitude, generally resulting from miscalculation of infiltration or errors in the model input data.
- incorrect shape due to misrepresentation of model components.
- time or phase errors, mainly introduced by time delay between rainfall input and flow.

In practice different combinations of these three types of error can occur.

Real-time hydrological forecasting models are composed of a simulation model and a technique for forecast updating. The simulation (process) model is a mathematical operation containing state variables and parameters which transforms a set of inputs to a set of outputs without reference to the measured outputs. Note that the state variables vary in time while parameters remain constant.

As long as the differences between estimated and observed flow remain within acceptable bounds, there is no need to adjust estimated flow. However, once the differences become unacceptable one or more of the state variables should be adjusted, in order to minimise the magnitude of any further errors. To do this the observed flow should be taken into consideration. The use of current or recent measurements of river flow obtained via telemetry to improve model forecasting performance is called updating (Serban and Askew, 1991). It should be emphasised that updating procedures differ from the periodic, historic recalibration of model parameters which is necessary when the characteristics of a basin or of a river bed change in time (WMO, 1992). Figure (7.1) presents the principle of updating.

7.3 Methods of real-time updating

According to Bramley (1981), three main steps should be considered in each updating procedure. They are:

- recognition of the feature to be updated.
- collection of information on the performance of the system to date.
- utilisation of information to forecast the future behaviour of the update feature.

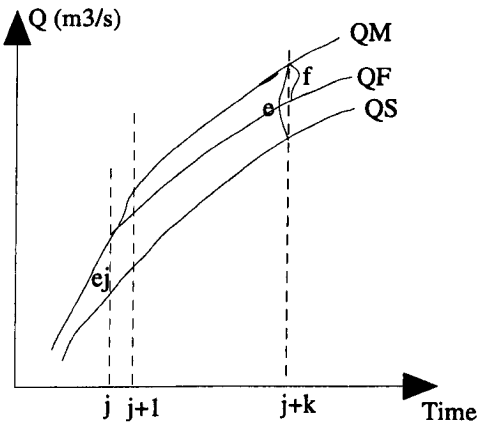

QS simulated hydrograph, QM measured hydrograph, J time of preparation of forecast, QF forecasted hydrograph, e simulation error, f forecasting error

Figure (7.1) The principle effect of updating (after Serban and Askew, 1991)

There are four distinct forms of updating procedure in common use (Serban and Askew, 1991 and Reed, 1984):

- procedures which involve the model input variables;
- procedures which involve the variables of state in the model of the system;
- procedures which involve the parameters in the model of the system;
- procedures which involve the model output variables. These procedures are often referred to as error prediction.

Various combinations of these four types of updating procedures can be applied in real-time operational practice.

Since parameter variability is often a reflection of an inadequate model structure, the use of parameter updating is often unattractive (Moore, 1993). Furthermore, the modification of one parameter would require the modification of other parameters because the parameters are not independent.

Updating for real-time operation can be automatic or manual (interactive). In manual adjustment, the forecaster views some sort of machine-produced display and makes a subjective decision to adjust the estimated flow. In automatic adjustment there is no human intervention and adjustment can be applied through the programming the computer to make the decisions. Forecast updating procedures are presented in figure (7.2). Some

components of the figure, including Kalman filtering, trial-error procedure and autoregressive models and different updating procedures are described in next section.

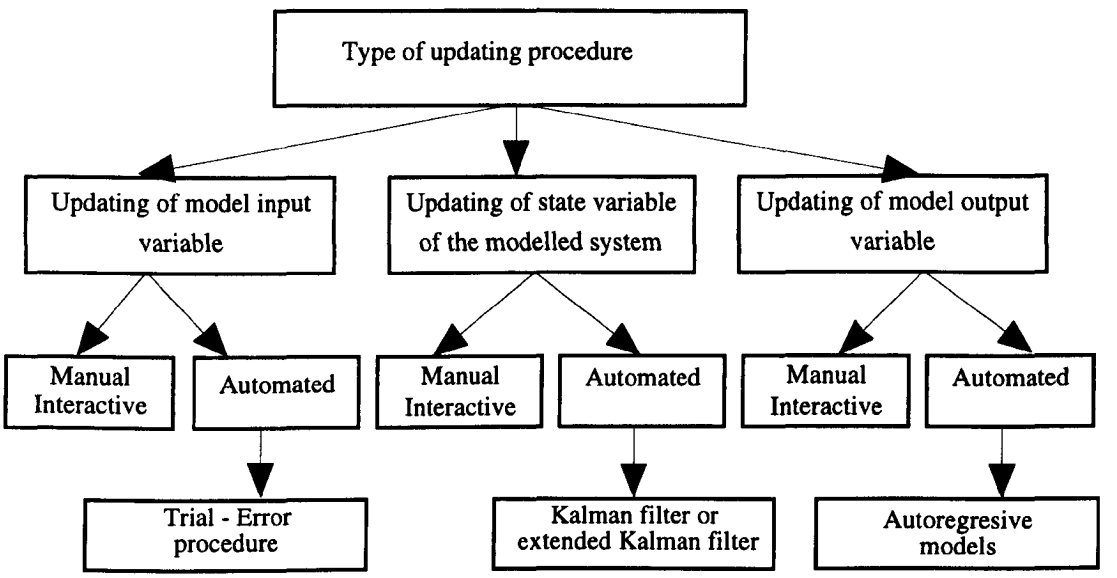

Figure (7.2) Types of updating procedures (adapted from Serban and Askew, 1991)

7.3.1 Input variables updating (trial and error)

This updating procedure was a manual, subjective adjustment of input variables. Input variable updating procedures are interactive and use a trial and error approach to inversely determine the model input when the model output and parameters are given. A block diagram for a trial and error updating procedure is presented in figure (7.3).

First the input variables to be adjusted, adjustment increment for each variable and maximum change allowed in any computation period should be selected. Then, at each forecasting moment j, the following stages are followed:

- calculation of the error 'e_j' between the measured and simulated hydrograph.
- comparison of the error with a pre-defined acceptable level of error TE_j. If the error is less than the threshold value, the procedure terminates.
- rerunning of the model using the adjusted input variables.

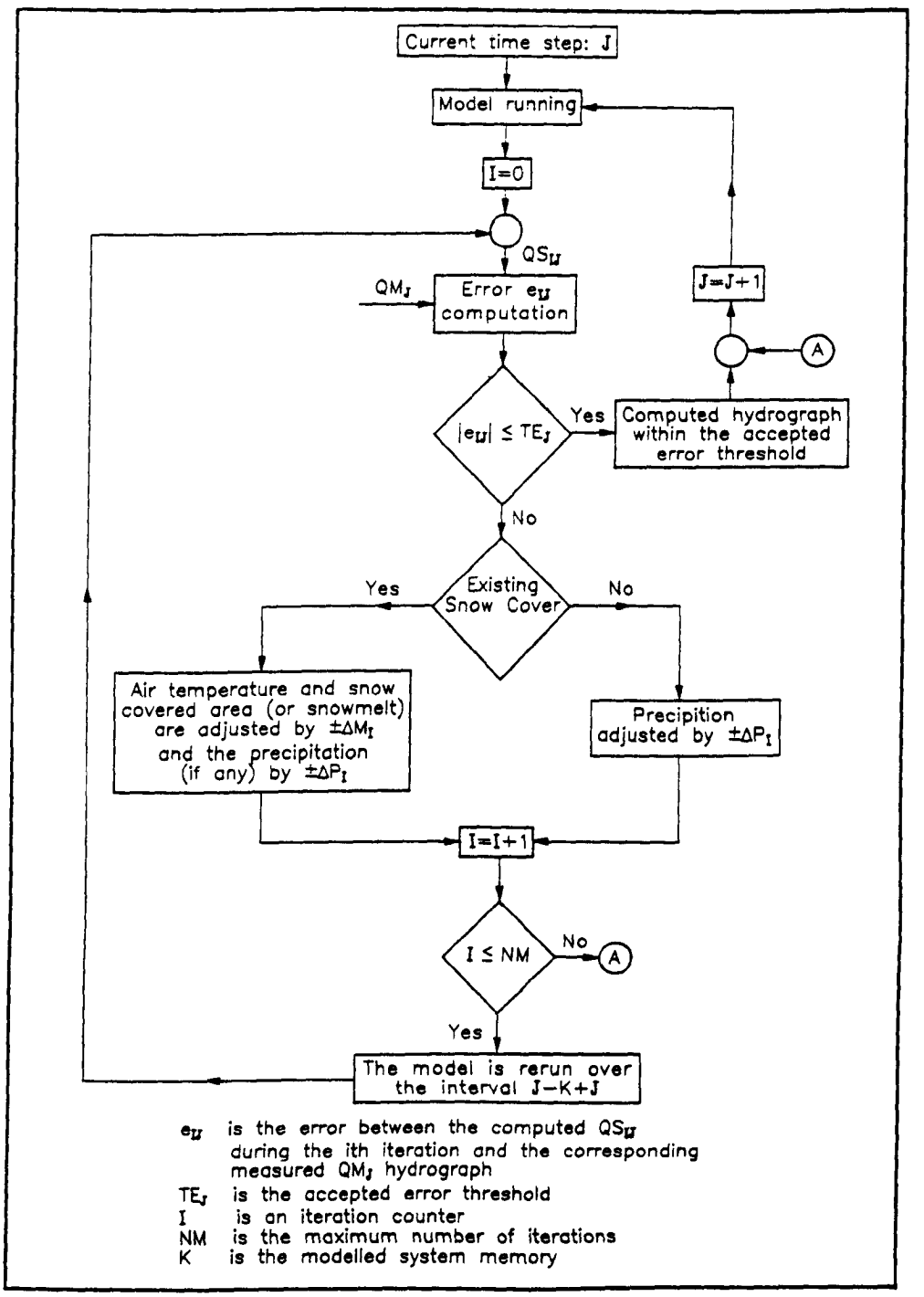

Figure (7.3) Block diagram of updating procedure of the trial-and-error type for input variables (adapted from WMO, 1992)

It can be seen that working on input data is complicated. Although in some cases a proportion of the forecast error may be due to poor data rather than any limitations in the model, in other cases there may be no direct link between input and output, meaning that inaccuracy in the output may not necessarily result from a corresponding error in input data (Bramley, 1981). Furthermore, the updating of input variables may affect the state variables of the model (WMO, 1992).

7.3.2. State and parameter updating

This technique systematically adjusts one or more of the state variables or model parameters until the best agreement between estimated and observed flow is obtained. Typical state variables that may be adjusted include the water contents of the soil, surface and ground water stores, and snow water equivalent. Coefficients describing the hydrograph shape may be updated as a model parameter. Parameters can be updated using a least squares optimisation technique.

In order to update the state variables a set of linear operations can be applied through the Kalman filter (KF) algorithm. An extended KF may be used for non linear dynamics models. During last two decades the application of the KF within hydrology has increased considerably. The KF may be combined with a transfer function model (Harpin, 1982), or with conceptual hydrological models, such as the HFS model (Georgakakoas *et al.*, 1988), the NAMKAL model (Refsgaard *et al.*, 1983, and Assaf and Quick, 1991). KF algorithms are also described by Serban and Askew (1991) for the application of a linear KF to the study of a physical system - the prime requirements being:

- a description of the system dynamics as a system of linear equations of the form:

$$X_j = \phi X_{j-1} + \Gamma U_{j-1} + W_{j-1} \tag{7.1}$$

- a definition of the measurement equation relating the measurements generally carried out on the system output with the variable of state:

$$Z_j = HX_j + V_j \tag{7.2}$$

where:
X is the vector of the state variables;
U a control vector containing the input variables;
ϕ the transition matrix;

Γ the input adjustment matrix;
W the modelling error vector;
Z the measurement vector;
H the measurement selection matrix ;
V the measurement error vector.

The matrixes ϕ, Γ and H defining the characteristics of the modelled system can be time-constant or variable in time. The V and W errors are considered independent and normally distributed.

$$V \approx N(0,R); W \approx N(0,Q); E(V^T, W^T) = 0$$

Q is system noise covariance matrix, R is the measurement error covariance matrix.

As the $\hat{X}$ state quantities at any time step are only estimates of the 'true' X values, the covariance matrix for the estimation errors is defined as:

$$P_{j/j-1} = E\{(X_j - \hat{X}_{j/j-1})(X_j - \hat{X}_{j/j-1})^T\} \tag{7.3}$$

Once the initial values for X_0 and P_0 are pre-established, the equations of the linear Kalman filter for the forecasting and the updating stages are the following:

Forecast at moment j

- the vector of state:

$$\hat{X}_{j+1/j} = \phi \hat{X}_{j/j} + \Gamma Uj \tag{7.4}$$

- the matrix of estimation errors:

$$P_{j+1/j} = \phi P_{j/j} \phi^T + Q_j \tag{7.5}$$

Forecast updating using the measurement at moment j+1

- the correction matrix k_{j+1}

$$K_{j+1} = P_{j+1/j} H^T [H P_{j+1/j} H^T + R_{j+1}]^{-1} \tag{7.6}$$

- the vector of state

$$\hat{X}_{j+1/j+1} = \hat{X}_{j+1/j} + K_{j+1}[Z_{j+1} - H\hat{X}_{j+1/j}] \tag{7.7}$$

- the matrix of estimation errors

$$P_{j+1/j+1} = P_{j+1/j} - K_{j+1}HP_{j+1/j} \tag{7.8}$$

The algorithm is repeated by substituting the estimated values of the state vector $\hat{X}_{j+1/j+1}$ and of the matrix of errors $P_{j+1/j+1}$ obtained through equation (7.7) and (7.8) into equations (7.4) and (7.5).

The term $H\hat{X}_{j+1/j}$ of relation (7.7) represents the estimation $\hat{Z}_{j+1/j}$ of the observed value, Z_{j+1} using the equation:

$$\hat{Z}_{j+1/j} = H\hat{X}_{j+1/j} \tag{7.9}$$

A schematic representation of Kalman filter updating is represented in figure (7.4)

According to Rungo *et al.*, (1989) KF techniques are more efficient in correcting amplitude errors than phase errors.

KF algorithms have been successfully applied in parameter estimation (see for example Ramos *et al.*,1995). However, its application to the forecasting and updating of hydrological models as stated, for example, by Ahsan and O'Connor (1994), Reed (1984), Plate *et al.*, (1988), Schultz (1988), Bramley (1981) and Wilke and Barth (1991) is dubious. From the above discussion it can be seen that KF needs *a priori* knowledge of the variation of the system noise and the measurement noise covariance matrix, as well as an estimate of initial state and the state error covariance matrix. However, these are never known for hydrologic system. Ahsan and O'Conner (1994) quoted that KF can be used in flow forecasting if the measurements errors in flow data are either ignored or are absent. However, even if this special condition is met, the KF algorithm simplifies to a representation that is identical with the time series approach.

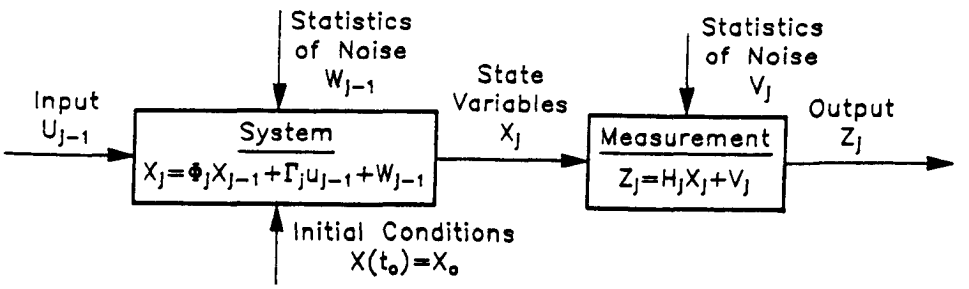

Figure (7.4) Schematic representation of Kalman filter updating (adapted from WMO, 1992)

7.3.3 Error prediction (blending method)

The structure of forecasting errors can be analysed, predictors of future errors based on this developed and then predictions of the error added to the deterministic model prediction to obtain the updated model flow forecast (Moore, 1993). The purpose of the technique is blending the two pieces of information, that is, model prediction and telemetered flow observations, together (Reed, 1984). This procedure is a simple, yet very efficient technique and is used more than any other updating technique. The technique works very well if there is a tendency for errors to persist, otherwise it can make an already poor forecast even worse. This technique is not very effective in the case of phasing errors.

Of the models that participated at the WMO workshop, the output variables of UBC, CEQUEAU, SMAR and NAMS11 were updated using autoregressive models that were fitted to the errors 'e' between the computed and measured hydrographs as follows (WMO, 1992):

$$e_j = \phi_1 e_{j-1} + \phi_2 e_{j-2} + ... + \phi_p e_{j-p} + a_j \qquad (7.10)$$

where
ϕ_1, ϕ_2, ..., ϕ_p are coefficients of the auto-regressive model, aj are residual (uncorrelated) errors.

The order and coefficients of the autoregressive model are determined by means of the 'e' errors series over a relatively short period of time before the forecast time. The forecast error ($e_{j+k/j}$) at time $j+k$ using the AR model is given by:

$$e_{j+k/j} = \phi_1 e_{j+k-1/j} + \phi_2 e_{j+k-2/j} + \phi_3 e_{j+k-3/j} + \ldots\ldots \quad (7.11)$$

The forecasted discharge at time j+k, QFj+k/j, will be

$$QF_{j+k/j} = QS_{j+k} + e_{j+k/j} \quad (7.12)$$

where QS_{j+k} is simulated discharge at time $j+k$ in terms of the model.

7.3.4. Simultaneous adjustment of amplitude and phase error

As mentioned earlier, error prediction and KF procedure both assume that the deviations are amplification error only. Consequently, there will be a problem if there is a phase deviation between measured and simulated values.

One solution for this problem, presented by Han (1991) was illustrated in section (2.5.2.2). Rungo *et al.*, (1989) described another approach as follows:

In current procedure the simulated curve is moved both along the time axis and along the discharge axis, until the best agreement between the simulated and measured curve is achieved. The best agreement is measured by the minimum of the sum of square deviation between simulated and measured values.

According to figure (7.5) and on the assumption that the phase error is less than Δ_t, the best agreement is found as:

$$MIN\left(\sum_{i=1}^{n}\left\{F_i\left[M_i - \left(S_i - \left(S_i + A_e - \frac{S_i - S_{i+1}}{\Delta_t} P_e\right)\right)\right]\right\}^2\right) \quad (7.13)$$

Where A_e (m^3/s) is the amplitude error, p_e (s) is the phase error, M (m^3/s) is the measured discharge, S (m^3/s) is the simulated discharge, F is the weighting factor, n is the number of values taken into account and Δ_t is the time-step (s).

By differentiating the equation with respect to A_e and P_e and then solving these two equations the values of A_e and P_e can be calculated. Similar calculation can be made for:

$\Delta_t < p_e < 2\Delta_t, 2\Delta_t < p_e < 3\Delta_t, etc.$

Therefore it is possible to have an estimate of the phase and amplitude errors at the time of forecast.

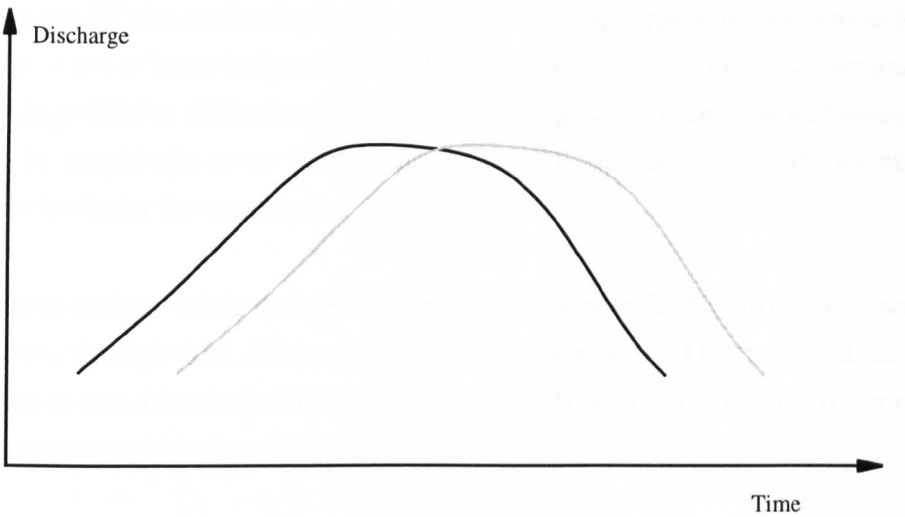

Figure (7.5) The need for real-time correction ____ measured and ------- simulated discharge.

7.3.5 Which updating method?

The choice and correct application of an updating procedure can be as important as the choice of model. Although in general, updating procedure can increase the accuracy of the forecast over that of simulation, misselection and misapplication of updating procedure may lead to less accurate forecasts.

The likely cause of errors can help to select an appropriate updating procedure. If it is known that a particular part of model is responsible for the errors, then a parameter-updating procedure may be useful. Where as if it is suspected that the cause of the error is related to either input data or misinitialization of the model, the state-updating technique could be the best choice. Finally if there is no evidence about the likely cause of the error, an error prediction method is probably the safest choice (Reed, 1984). Furthermore, the amount and quality of available past data and the reliability of the real-time data collection, transmission and processing may be affect the choice of updating procedure, because without sufficient data even the most advanced simulation model is of no use (Nemec, 1986). According to Reed (1984) if good quality telemetered flows are available, a simple model plus sophisticated updating procedure is preferable to sophisticated model plus simple updating procedure.

Serban and Askew (1991) summarised advantages and disadvantages of different updating procedures as follows:

In order to use KF the model should be linearized and re-written in state space form and in addition, *a priori* knowledge of the system and measurement errors is necessary. The programming of KF is difficult and needs quite a long time to run. The technique is more effective in amplitude error than phase error. KF makes it possible to determine confidence limits for forecast discharge.

Standard time series models such as AR models are suitable for following the variation of forecast error through time. AR models are easy to program and to apply and take a quite a short time to run. However, their efficiency depends on the degree of error persistence between the measured and computed hydrograph.

In terms of an overall updating strategy most researchers including Clausen and Refsgaard (1984), Bramley (1981), Serban and Askew (1991) stated that output updating procedures using time series models such as AR model are much more suitable than other procedures. Indeed among 14 models taking part in the WMO workshop, eight update process model outputs. Of these, one updates both input and output, two update state parameters and output, and one updates both parameter and output in combination. Both automated and manual interactive updating procedure are used. Among the same 14 models submitted to the WMO inter-comparison project, seven models used automated updating procedures, six used manual-interactive ones and one employed automated procedures for discharge and manual-interactive procedures for snow cover extent.

7.4 Current updating procedures in TF models

As mentioned in section (2.5.1) the main shortcoming of TF models and the relationship expressed by equation (2.39) is that they use a linear equation to explain the non-linear relationship between runoff and rainfall.

One technique to overcome this weakness is to incorporate the antecedent condition of the catchment (Δ_t) as an additional input in equation (2.39), following O'Connell and Clarke, (1981):

$$y_t = a_1 y_{t-1} + a_2 y_{t-2} + \ldots\ldots + a_m y_{t-m} + b_1 u_{t-1-l} + b_2 u_{t-2-l} + \ldots\ldots + b_n u_{t-n-l} + c\Delta_t \qquad (7.14)$$

C is an additional parameter. There are a number of ways to determine the variable Δ_t. If only antecedent rainfall data are available, at each time point an antecedent precipitation index (API) could be computed as:

$$API_t = KAPI_{t-1} + P_{t-1} \tag{7.15}$$

Where K is a decay factor in the range of 0.85-0.98 (Linsley *et al.*, 1983). If soil moisture deficit (SMD) data are available, then a catchment wetness index (CWI) could be computed using equation (2.14). Variables such as API_t or CWI_t can then be used directly in equation (7.14) as the variable Δ_t. Although the resulting model is linear in the parameters it is non-linear in the system theory (O'Connell and Clarke, 1981).

Todini (1988) used another approach to cope with the non linearity in basin response through a system split into two linear systems depending on the value of the antecedent precipitation index. For dry soil, that is value of *API* is equal to or less than a threshold value *T*, rainfall is transformed into runoff by the first linear model, but if the API is larger than threshold value, the second linear model is used. Therefore, rainfall input u_t divided into two separate input series $u1_t$ and $u2_t$ according to the value of *API*.

$$API > T : u_{1_t} = u_t; u_{2_t} = 0$$
$$API \leq T : u_{1_t} = 0; u_{2_t} = u_t$$

The resulting model is then a multiple input type of the form:

$$y_t = \sum_{j=1}^{m} a_j y_{t-j} + \sum_{i=1}^{2} \sum_{k=0}^{n} b_{ik} u_{i,t-l-k} \tag{7.16}$$

It can be seen that the response of a basin to rainfall under "wet" and "dry" conditions can be represented by separate pulse responses (see figure 2.4)

Instead of directly using Δ_t such as in equation (7.14), Δ_t can be used to scale the rainfall component of the model. Owens (1986) used Δ_t as a scaling factor of rainfall parameters to match the steady-state gain (section 2.5.1.1) of the model to the event percentage runoff. This method is analogous to the variable proportional loss method of defining effective rainfall.

Since *a posteriori* knowledge is necessary to determine the average percentage runoff of an event, which is not available in real-time, one step ahead forecast error is used to update Δ_t. The final form of transfer function model including the on-line updating and a time delay is presented in equation (2.53). The block diagram representation of the transfer function model in figure (7.6) highlights the structure of the model. Lees *et al.*, (1994) suggested similar factor as Δ_t in their work on an adaptive flood warning scheme.

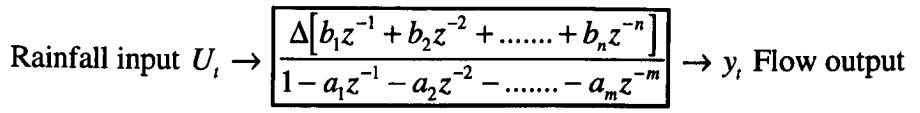

Figure (7.6) Block diagram representation of the final form of TF model

Owens (1986) used following equation to update Δ:

$$\Delta_t = \mu\Delta_{t-1} + (1-\mu)\frac{y_t - [a_1 y_{t-1} + a_2 y_{t-2} + \ldots\ldots + a_m y_{t-m}]}{[b_1 u_{t-1} + b_2 u_{t-2} + \ldots\ldots + b_n u_n]} \tag{7.17}$$

where μ is a smoothing factor ($0 \le \mu \le 1$ usually μ=0.5) which helps limit erratic behaviour in the value of Δ through time. Updating of Δ does not take place if runoff is below a present threshold (1.2 times the river base flow), and if the total amount of rainfall in the memory of the model is below a pre-defined threshold. In addition, Δ can be at most 1.5 times greater or less than previous Δ.

Since Δ is concerned with the proportion of rainfall contributing to runoff, the initial value of Δ may be related to antecedent catchment conditions. Due to difficulties of estimating the initial value of the antecedent conditions, an initial value of Δ=1 is normally used which corresponds to the average percentage runoff of the model calibration data.

The updating procedure used by the PRTF model is described in section (2.5.2.2) and figures (3.17) to (3.19).

7.5 Further improvement of updating procedures in TF models

7.5.1 PRTF model

7.5.1.1 An investigation to find the most important adjustment factor

As a first step to improving the updating performance of the PRTF model an investigation was conducted to find the most important of the three adjustment factors α (volume adjustment factor), γ (shape adjustment factor), and τ (time adjustment factor) (see section 2.5.2.2). In order to carry out this investigation, several independent storm events were selected for the Orgeval catchment and were examined. Here only the results of the

same five events which used in previous chapters are presented. For each event the appropriate calibration model was identified. In each event, the rainfall and runoff data were divided into different data sets commencing at 3 then 4 and so on until n = available number of calibration data set. Different parameters including α, γ, τ, simulated discharge, average rainfall intensity, cumulative rainfall and actual discharge were determined sequentially using the calibrated model and adjustment (updating) procedure (see section 2.5.2.1 and 2.5.2.2).

The main relationships between the different parameters of the PRTF model summarised from section (2.5.2.2) can be described by the following equations:

$$t_{peaknew} = t_{peak} + \gamma \tag{7.18}$$

$$N = 2, \beta_{new} = e^{\frac{1}{t_{peaknew}+1}}$$
$$N = 3, \beta_{new} = e^{\frac{2t_{peaknew}+3}{(t^2_{peaknew}+3t_{peaknew}+2)}} \tag{7.19}$$

$$C = \frac{\beta^N(\beta_{new}-1)^N}{\beta^N_{new}(\beta-1)^N} \tag{7.20}$$

$$C(i) = C \times b(i) \tag{7.21}$$

$$B(i) = C(i)(1+\alpha) \tag{7.22}$$

$$N = 2, A(1) = \frac{2}{\beta_{new}}, A(2) = -\frac{1}{\beta^2_{new}} \tag{7.23}$$

$$N = 3, A(1) = \frac{3}{\beta_{new}}, A(2) = -\frac{3}{\beta^2_{new}}, A(3) = \frac{1}{\beta^3_{new}} \tag{7.24}$$

The investigation was conducted for the following cases:

1- α, γ and τ can be different in different data sets. Referring to equations (7.18) to (7.23) it can be seen that in this case the A and B parameters can be different according to the values of α, γ, and τ.

2- γ = constant = 0 but α and τ can be different in separate data sets. In this case the A parameters are always constant but the B parameters can be different for separate data sets.

3- α = constant = 0 but γ and τ can be different for separate data sets. In this case both the A and B parameters can be different for separate data sets.

4- $\gamma = \tau = 0$ = constant but α can be different for separate data sets. The A parameters remain constant but the B parameters can be different for separate data sets.

5- τ = constant = 0 but α and γ can be different for separate data sets. In this case both the A and B parameters can be different for separate data sets.

It is expected that the best simulated discharge (simul best) would obtained if the $\alpha, \gamma,$ and τ all differ in the separate data sets. Therefore, the accuracy of the simulated discharges resulting in each case, can be judged by comparison with simul best. To do this the simulated discharge hydrograph arising in the different cases are compared with simul best for each event under evaluation (see figure 7.7). The RMSE of differences are presented in table (7.1).

The graphs in figure (7.7) and RMSE in table (7.1) show that the most dominant factor is the volume adjustment factor α. This is because when it is assumed to be constant the quality of the simulated discharge decreases significantly. Overall the second most important factor is the shape adjustment factor γ. Therefore in order to gain better forecasting performance an updating procedure necessarily should include a volume adjustment factor.

It is interesting to note that for all events investigated the simulated discharge when three adjustment factors are variable, do not differ greatly from the simulated discharge when the shape and time adjustment factors are constant.

Table (7.1) Comparison of RMSE result of simulated discharge in different cases.

Event number	$\tau=\gamma=0$ α variable	$\alpha=0$, τ and γ variable	$\tau=0$, α and γ variable	$\gamma=0$, α and τ variable
1	0.451	1.646	0.456	0.574
2	0.770	0.443	0.195	0.770
3	0.264	0.404	0.191	0.253
4	0.547	3.818	1.068	0.993
5	1.076	1.503	0.839	1.219

7.5.1.2 Observations on relating adjustment factors to time and average rainfall intensity

A further attempt was made to relate the adjustment factors to time and average rainfall intensity. Figure (7.8) shows the temporal variation of α for the same five events. The

graphs indicate that when γ is constant the values of α differ significantly from the value of α when α, γ, and τ vary in time. (Variation of α with time in two cases is similar). Consequently, once again it can be concluded that the second important adjustment factor is the γ parameter.

In order to investigate the probable relationship of α, γ, and τ, the simultaneous temporal variation of all three has been examined. The graphs in figure (7.9) summarising this investigation for four selected storm events indicate that almost all various combinations of different variation of these parameters (27 combinations) can occur. However, the occurrence frequency of each varies. In more than 90% of cases the τ parameter remains constant during two successive times. In almost 30% of cases all three parameters remain constant together during two successive time. In 18% of cases α and γ parameter increase together. In 16% of cases both α and γ increase whilst τ parameter remains constant. In 13% of cases both α and γ decrease but τ parameter remains constant. Only in 2% of cases both α and τ parameter increase together during two successive time. Finally only in 0.4% of cases do all three parameters increase together.

The adjustment parameters vary rapidly with time and it is impossible to extract a persistent general relationship concerning the combined variations of α, γ, and τ parameters.

Further research attempted to construct a relationship between the adjustment factors and average rainfall intensity. To do this a scatter graph of each parameter against average rainfall intensity was prepared for each event under investigation. The results of this investigation are summarised in figure (7.10). As can be seen from the figure there is no reasonable and persistent relationship between the adjustment factors and average rainfall intensity. Furthermore, the same results were obtained in attempts to relate the adjustment factors to rainfall depth, accumulated rainfall and previous discharge. Variation of γ and τ with α and γ with τ also did not show a comprehensive relationship.

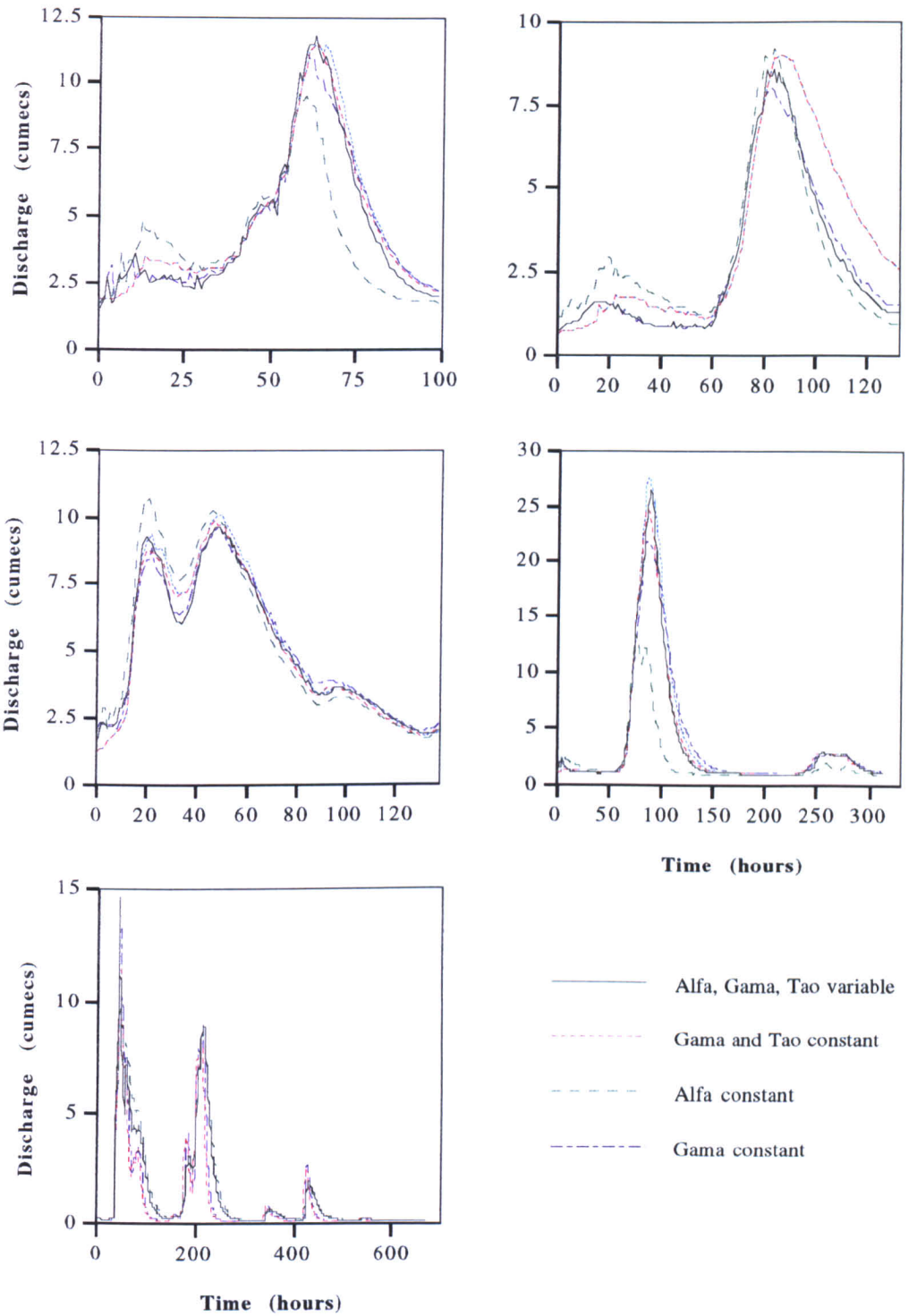

Figure(7.7) Comparison of simulated discharge in different cases, Orgeval catchment (Top left event 1, Top right event 2, Middle left event 3, Middle right event 4, Bottom left event 5)

7.5.1.3 New procedure for updating the (B) parameters in simulation of PRTF model

As shown in section (7.5.1.1) the volume factor (α) is the most important parameter of the three adjustment factors. In order to develop α updating the simultaneous temporal variation of runoff and α (both when three adjustment factors are variable and when shape and time adjustment factors are constant) were examined. The graphs in figure (7.11) show that although there is not a consistent pattern related the volume adjustment factor, some dominant patterns are observed.

During a significant event, α gradually increases and approaches a constant value. The turning points of α can be at the beginning or end of rainfall. After the peak a significant change in the volume factor is usually observed. The α-time curve exhibits a flattered top at time of flow peaks. Between peaks α invariably increases when flow is rising and often remains constant as flow decreases. In most of cases it is possible to divide the α-time curve into several straight lines, with each segment being expressed by a simple algebraic function. Consequently, prediction of α is feasible and relatively satisfactory forecasts of runoff can be made using the predicted rainfall and predicted volume factor using an adaptive PRTF model identified using 'up-to-now' information.

As can be seen in figures (3.17) to (3.19), the existing PRTF forecasting procedure determines α, γ, and τ using 'up-to-now' information. Following this, the A and B parameters will be calculated using equations (7.18) to (7.24) and the adjustment factors determined. The simulated hydrograph is then calculated using past and forecasted rainfall up to the forecasting lead time and finally the simulated hydrograph is shifted proportional to the differences between the actual and simulated flow at the time of forecasting. The A and B parameters will be constant over the forecast lead time.

In the proposed procedure, α, γ and τ are determined sequentially by dividing the available historical information as described in the previous two sections. A relationship between α (volume factor) in the different data sets is constructed and used to predict future α over the forecast lead time. The predicted α is then used to calculate the future B parameters. Although the A and B parameters at the forecasting time are the same as in the existing procedure, the B parameters over the forecasting lead time differ. The final step of the new procedure is to calculate the simulated hydrograph over the forecast lead time and shifting the simulated hydrograph proportional to the differences between actual and simulated flow at the time of forecasting.

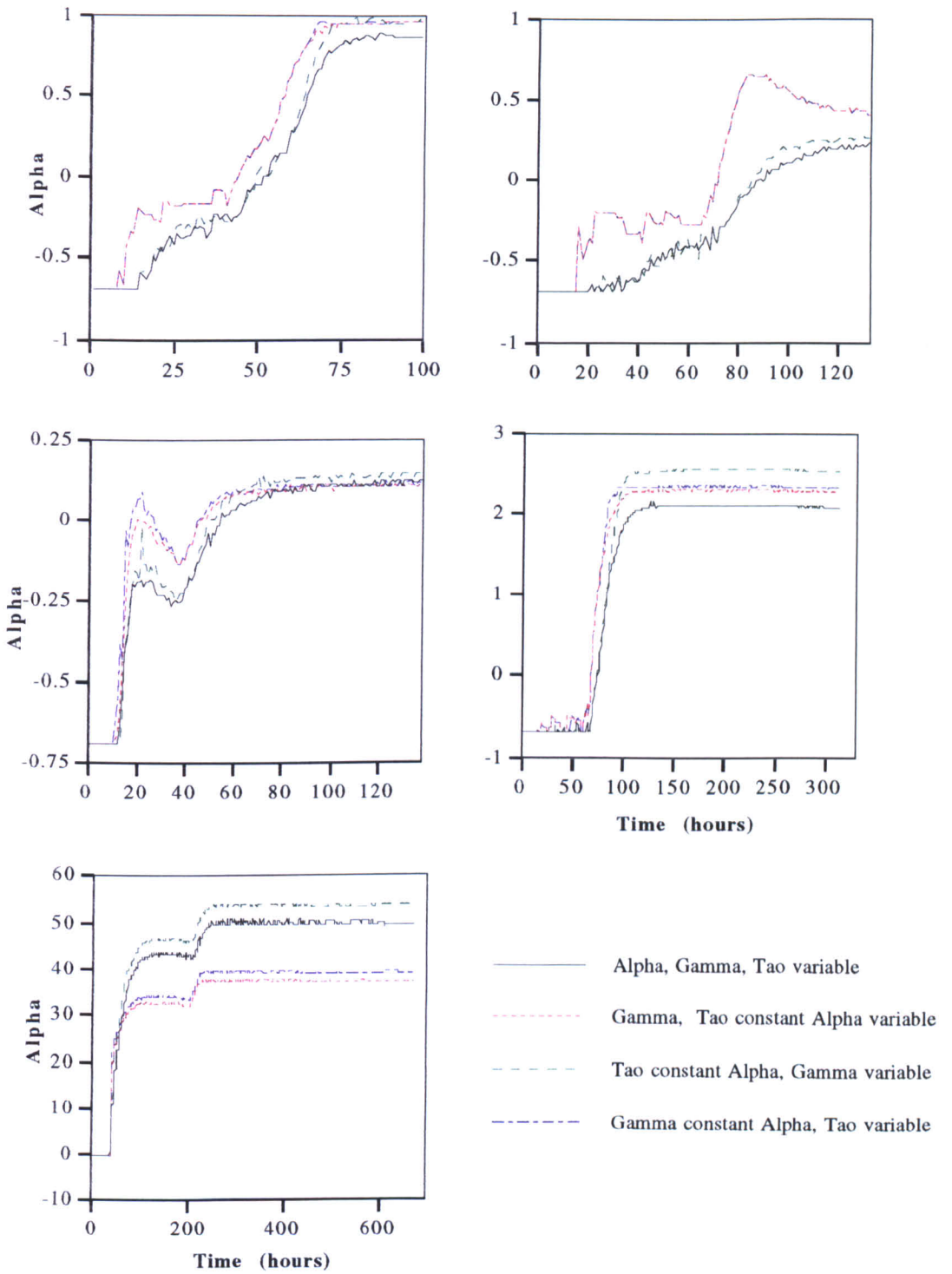

Figure (7.8) Variation of Alpha (volume adjustment factor) due to time in different cases, Orgeval catchment (Top left event 1, Top right event 2, Middle left event 3, Middle right event 4, Bottom event 5)

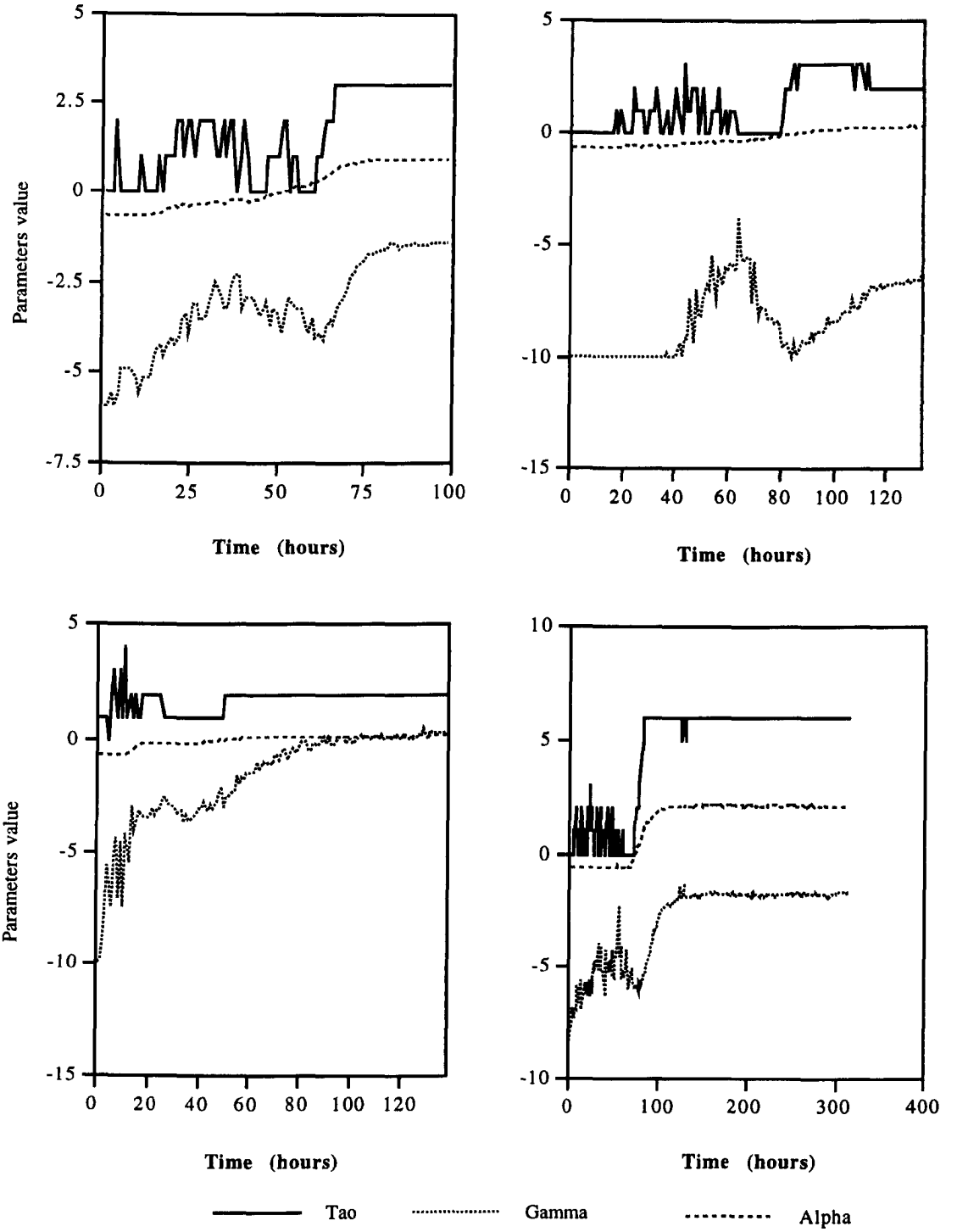

Figure (7.9) Variation of Alpha, Gamma, and Tao due to time, Orgeval catchment (Top left event 1, Top right event 2, Bottom left event 3, Bottom right event 4)

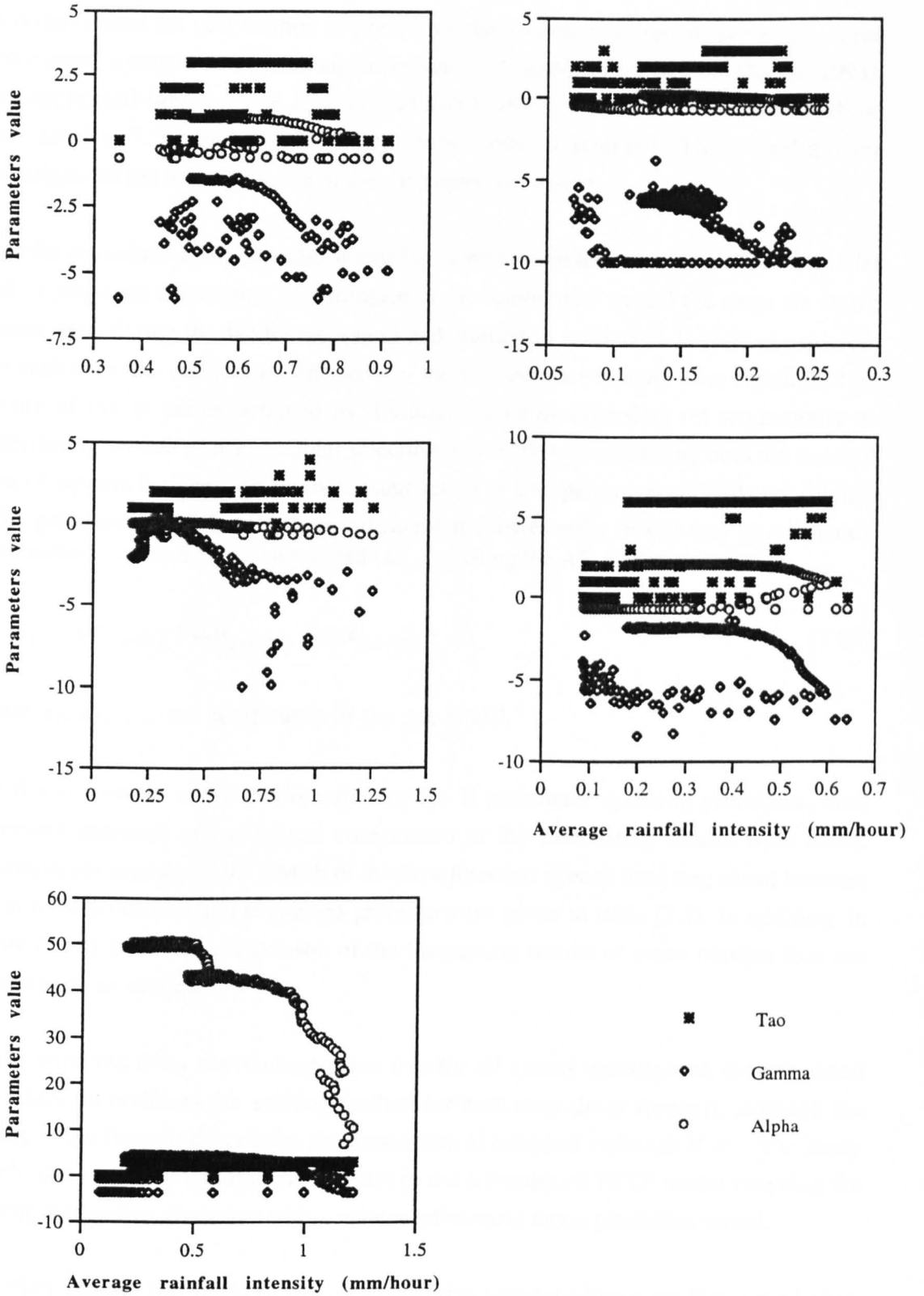

Figure (7.10) Variation of Alpha, Gamma, Tao due to average rainfall intensity, Orgeval catchment (Top left event 1, Top right event 2, Middle left event 3, Middle right event 4, Bottom event 5)

In order to find the best method of predicting the volume adjustment factor (α), three procedures: a simple correlation equation (see for example Arthanari and Dodge, 1993), an exponential function (see Janacek and Swift, 1993), and an autoregressive method (see section 7.3.3 and NAG library) have been considered. These preliminary investigations led to the adoption of the autoregressive model.

In order to include a volume adjustment factor prediction technique in the PRTF model and to judge the forecasting performance of the 'combined' model the same six storm events used during the WMO workshop and studied in section (4.4) were considered. For each event the order and coefficients of the autoregressive model were determined by means of the α series obtained by dividing the calibration data set sequentially as described in section (7.5.1.1). Order selection was made by considering both the residual sum of squares between the estimated and actual α and parameter redundancy (higher order parameters with small values indicate that a lower order model may be adequate). Forecasted α in time j for k step ahead ($\alpha_{j+k/j}$) using the AR model is given by:

$$\alpha_{j+k/j} = a_1\alpha_{j+k-1/j} + a_2\alpha_{j+k-2/j} + a_3\alpha_{j+k-3/j} + \ldots\ldots \tag{7.25}$$

where a_1, a_2, ...are coefficients of the AR model.

For the evaluation of the performance of the B parameter updating procedure, both objective approach and graphical comparison of the forecasting results were made. Objective comparison of the RMSE of the flow forecasts at each time step ahead between the current procedure and suggested procedure are given in table (7.2). In addition, in figure (7.12) graphical comparison of the forecasting results of event number four are presented as an example.

It was observed from above comparison that for all events investigated, the suggested procedure outperforms the existing method for each step-ahead forecast, although the quality of the forecast depends on the persistence of temporal variation of α . The study clearly demonstrated that it is much better to use a combined PRTF model coupling the existing forecasting procedure with a volume adjustment factor prediction model.

A further attempt was made by use of an adaptive volume adjustment factor prediction model. In the proposed method at each forecasting time, the coefficients of the α prediction AR model are calculated separately using the newly available data. However, a comparison of the RMSE results, indicates that the simple AR model with constant coefficients is adequate, and that the adaptive AR model does not providing any additional advantages.

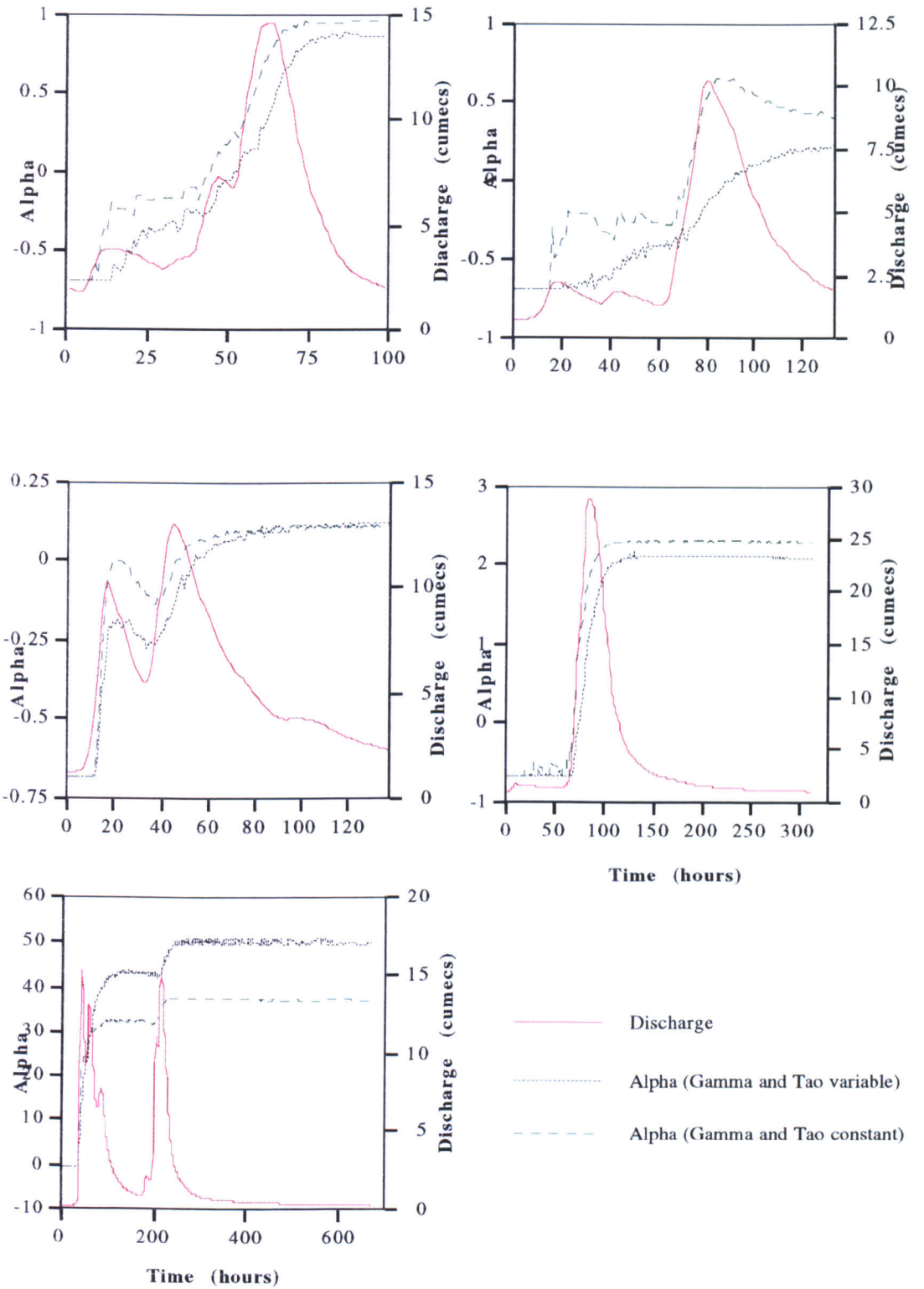

Figure (7.11) Comparison of discharge and volume factor, Orgeval catchment (Top left event 1, Top right event 2, Middle left event 3, Middle right event 4, Bottom left event 5)

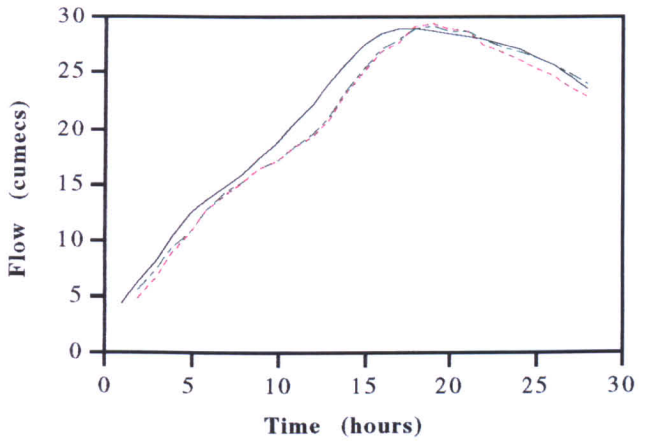

(i) One step ahead forecasts

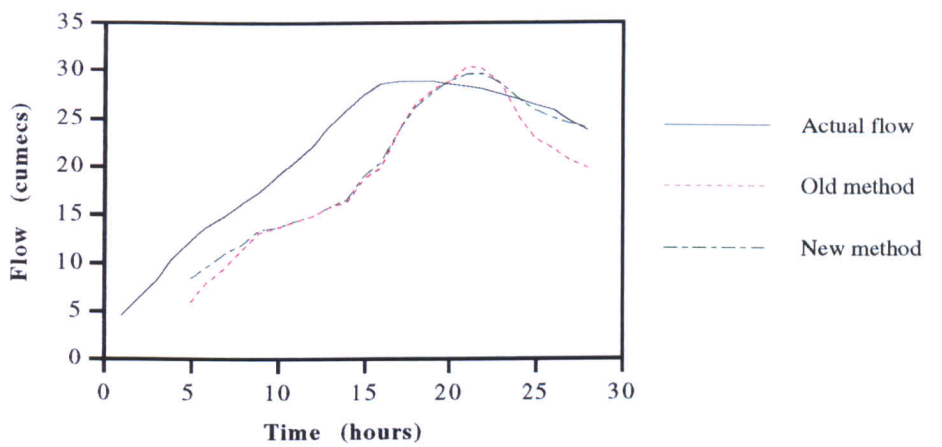

(ii) Four step ahead forecasts

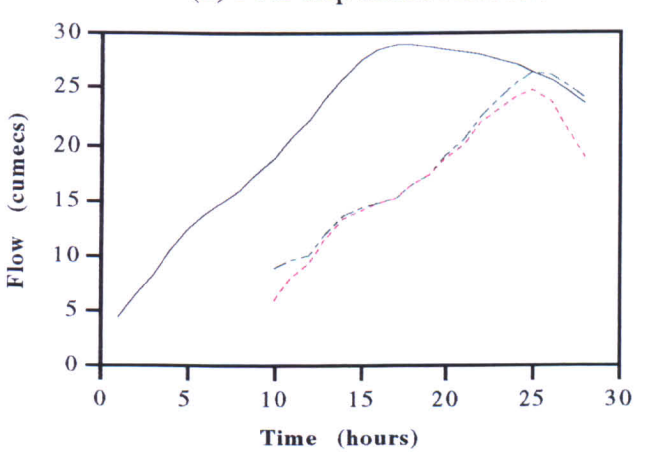

(iii) Nine step ahead forecasts

Figure (7.12) Comparison of the forecast hydrographs, Orgeval catchment event No. 4, PRTF model

Table (7.2) RMSE result of current and modified updating procedure of PRTF model for different events (Orgeval catchment)

	Event	No. 1	Event	No. 2	Event	No. 3	Event	No. 4
Step ahead	Current model	Modified model	Current model	Modified model	Current model	Modified model	Current model	Modified model
1	0.803	0.792	0.279	0.276	0.325	0.325	1.463	1.236
2	1.251	1.235	0.554	0.546	0.644	0.644	2.853	2.460
3	1.600	1.582	0.815	0.803	0.961	0.961	4.206	3.677
4	2.037	2.018	1.061	1.042	1.259	1.259	5.384	4.772
5	2.547	2.524	1.293	1.268	1.537	1.537	6.376	5.746
6	2.909	2.893	1.515	1.481	1.794	1.794	7.249	6.629
7	3.085	3.081	1.724	1.682	2.038	2.038	8.103	7.516
8	3.417	3.423	1.905	1.856	2.275	2.275	9.004	8.452
9	3.639	3.660	2.048	1.992	2.513	2.513	10.013	9.418
AR order	-	4	-	1	-	1	-	1

Table (7.2) Continued

	Event	No. 5	Event	No. 6
Step ahead	Current model	Modified model	Current model	Modified model
1	2.325	2.207	0.934	0.891
2	4.118	3.856	1.799	1.730
3	5.325	4.999	2.581	2.469
4	6.295	5.922	3.273	3.101
5	6.994	6.580	3.793	3.539
6	7.266	6.829	4.222	3.846
7	7.291	6.872	4.626	4.113
8	7.239	6.832	5.024	4.406
9	6.843	6.442	5.467	4.801
AR order	-	4	-	1

7.5.2 Static TF model

7.5.2.1 Searching for best smoothing factor

Equation (7.17) shows how the value of μ (smoothing factor) affects the amount of adjustment of Δ.

In theory, the smoothing factor can range from 0.01 to 1.00. However, large values cause the updated value of Δ to include a large percentage of the previous value resulting in a Δ that responds quickly to change in the previous values. This is undesirable if the changes in the Δ are irregular and affected by erratic noise. Conversely, when μ is close to zero, the new Δ will be similar to the $\frac{y_t - [a_1 y_{t-1} + a_2 y_{t-2} + ... + a_m y_{t-m}]}{[b_1 u_{t-1} + b_2 u_{t-2} + ... + b_n u_{t-n}]}$. The speed at which past values of the Δ lose their importance depends on the value of μ. For stability a small smoothing factor is appropriate whereas a rapid response to recent change

requires a large smoothing factor. Consequently the optimum choice of μ which has a major impact on forecasting performance is a compromise.

In order to examine the performance of different values of smoothing factor a study using the five verification events described in section (4.4) has been made using data immediately prior to the main event. In each case a model is calibrated using its pre-event data and the same data is then used for forecasting. To find the best μ, an interative trial and error technique is applied, whereby for a range of μ values. The value of μ is selected when the best agreement between observed and forecasted flow hydrographs in the pre-event data is obtained. This value is then used to forecast the main event.

Surprisingly, in four out of five events investigated, the best calculated μ is 0.5, the value used in equation (7.17). Only in pre-verification event number one was a different value found (0.9). At the same time when applied to the event, no improvement in forecast quality was observed.

Although overall, 0.5 constitutes the best value for the smoothing factor analysis of more events is required to provide a firmer conclusion.

7.5.2.2 Adapting an AR model using forecasting error

No hydrological model provides a perfect forecast, there will always be some discrepancies (errors) between forecasted and observed river flows. TF models are no exception. Model errors may result from inaccuracy in the model structure, model parameters, and in the model inputs. If the cause of errors can be determined *a priori* the selection of an updating procedure is straightforward. However, usually this is not the case and the reason for the error is unknown. In such circumstances error prediction methods based on time series analysis can be used to model the forecast errors.

Although in TF models inaccuracy in the rainfall input can to some extent be corrected by the Δ updating procedure, there are still some errors, mainly due to either inappropriate model structure or model parameters which Δ updating procedure cannot correct. In this section a statistical (autoregressive model) error model is utilised in conjunction with the original ordinary TF model.

In order to implement this research, the same five storm-events of the Orgeval catchment studied in section (4.4) are considered and the performance of the combined model (original TF model + error prediction model) is compared with that of the original TF model.

Once again, in each case a calibrated model was identified using the data of the event immediately prior to main event. The calibrated model was then used for forecasting the same pre-event, and forecasting errors calculated for each step-ahead forecast. An autoregressive model was identified for each step ahead forecast, and these models then used in combination with the original TF models to forecast the main event river flows. As the variation of forecast errors through time may be different in separate step ahead forecasts, the parameters of the error prediction model in each step ahead forecast were determined independently. As in section (7.5.1.3) to determine the order and parameters of AR model both the residual sum square between estimated and actual error as well as parameter redundancy are considered.

The results of an objective comparison of the performance of original TF model and the combined TF model are presented in table (7.3). It can be seen that in four out of five events, the combined model outperforms the original TF model and only in verification event number five does the original TF model provides better forecasts (although the forecast quality of original model also is poor). The reason of the poor performance of the combined model for event number five may be explained as follows. Table (4.6) showed that the ratio of portmanteau statistic to critical chi-squared of the original TF model in event number five was 4.749. This indicates that the original TF calibrated model which is obtained from pre-event data was inadequate for the original event. Consequently it may be said that the error prediction model obtained from the pre-event data is also inadequate for forecast residuals of main event. In figure (7.13) graphical comparison of the forecasting results of event number two are presented as an example.

Overall it may be concluded that the combined model improves the forecasting quality, although more events need to be investigated in an extended study.

7.6 Conclusion

This chapter began with a comprehensive review of updating procedures of flood forecasting models. The sources of forecasting errors have been addressed and the basic structure and operational characteristics of the different updating procedures assessed. The parameters affect the choice of updating procedures outlined. The chapter continued by introducing the current updating procedures of TF models.

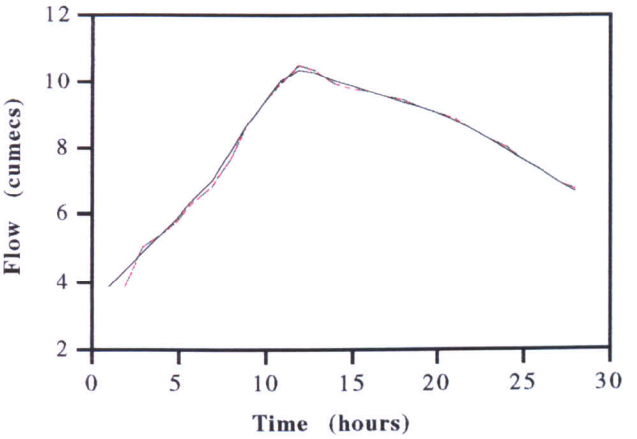

(i) One step ahead forecasts

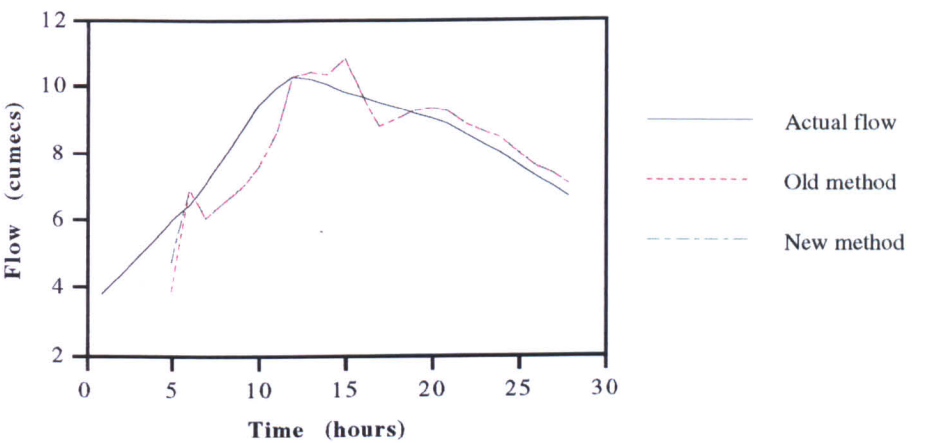

(ii) Four step ahead forecasts

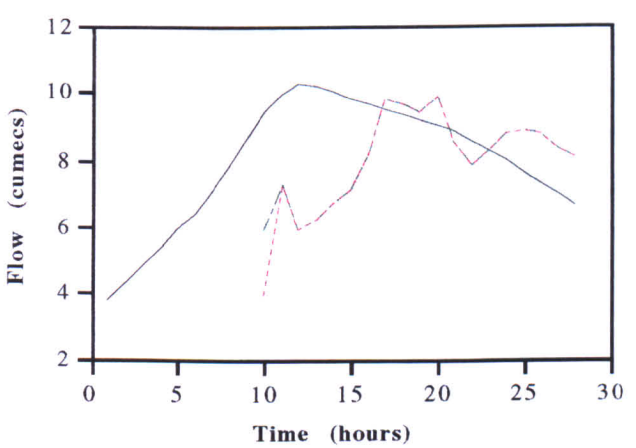

(iii) Nine step ahead forecasts

Figure (7.13) Comparison of the forecast hydrographs, Orgeval catchment event No. 2, TF model

Table (7.3) RMSE result of current and modified updating procedure of TF model for different events (Orgeval catchment)

	Event	No. 1	Event	No. 2	Event	No. 3	Event	No.5
Step ahead	Current Model	Modified Model	Current Model	Modified Model	Current Model	Modified Model	Current Model	Modified Model
1	0.288	0.288	0.130	0.130	0.566	0.565	1.330	1.330
2	0.697	0.681	0.327	0.318	1.074	1.070	2.342	2.344
3	1.156	1.149	0.580	0.570	1.546	1.545	3.305	3.315
4	1.632	1.627	0.884	0.813	1.997	1.976	4.064	4.085
5	2.111	2.111	1.210	1.100	2.442	2.373	4.545	4.579
6	2.599	2.601	1.529	1.393	2.867	2.787	4.672	4.713
7	3.090	3.095	1.838	1.658	3.269	3.342	4.607	4.651
8	3.565	3.569	2.104	1.890	3.633	3.679	4.606	4.656
9	4.917	4.021	2.300	2.091	3.969	4.049	4.517	4.571
AR order	-	1	-	1	-	3	-	1

Table (7.3) Continued

	Event	No. 6
Step ahead	Current Model	Modified Model
1	0.525	0.525
2	1.175	1.174
3	1.802	1.801
4	2.453	2.452
5	2.990	2.984
6	3.404	3.398
7	3.713	3.706
8	3.920	3.907
9	4.043	4.026
AR order	-	4

The remainder of the chapter was allocated to describing further improvements in TF model updating procedures. Extensive research has been conducted to find the most important adjustment factor of the PRTF model. The research evaluated the impacts of the volume, shape, and time adjustment factors on forecast quality and concluded that the volume adjustment factor is the most important factor of the three. Several attempts have been made to relate the adjustment factors to different elements including time, average rainfall intensity, accumulated rainfall, and discharge. Different interaction of adjustment factors are also investigated.

A new updating procedure has been developed using an autoregressive model to determine the B parameters of the PRTF model through the prediction of future volume adjustment factor over the forecast lead-time. An autoregressive model has also been combined with an ordinary TF model to include error prediction model in the original TF model structure. Relatively extensive testing has shown that the performance of both new transfer function models are superior to conventional procedures.

CHAPTER 8

REAL-TIME UPDATING OF TF MODELS USING WEATHER RADAR DATA

8.1 Introduction

Advances in technology over the last fifty years has made it possible to develop active microwave radars specifically to observe rainfall patterns such as: areally distributed rainfall, rainfall intensity, accumulated rainfall, system movement, storm structure, severe weather probability and vertically integrated liquid water (Gutierrez, 1995). This chapter is not intended to provide a comprehensive review of radar technology which have been detailed elsewhere (see for example Collier, 1989, Tilford, 1992, and Atlas, 1990). Instead a summary of the background and information necessary to gain an understanding of radar principles, basic theory, radar classification and problems associated with radar is given. The chapter continues by an application of real-time updating procedure of the TF models using weather radar data.

8.2 Background

Radar by definition is an electromagnetic system which performs the tasks of Radio Detection And Ranging on distant target objects. The more formal definition of radar as expressed by Battan (1973) is: 'the art of detecting by means of radio echoes the presence of objects, determining their direction and range, recognising their character and employing the data thus obtained'.

Radar was invented by Watson-Watt in 1936 (Atlas, 1990). During the Second World war when radars were first used for military purposes it was seen that rainfall was a significant source of noise and techniques were developed for its removal. Since then, the use of radars for meteorological application has expanded rapidly (Collier, 1989). Ligda (1951) as reffered to by Atlas (1990), stated that the first time rain was observed by radar occurred on the 20th of February 1941, somewhere on the south coast of England.

The Marshall-Palmer relationship between reflectivity and rainfall rate (equation 8.12) is still one of the most important equations in radar meteorology. This equation is the research product of a group established in 1943 and led by Stuart Marshall (the Stormy Weather Radar Group) in Canada. David Atlas in 1945 in the United States and R. F. Jones in 1946 in England set up research and operational centres for radar meteorology in their countries which quickly became the basic centres of radar meteorology. During the last two decades several countries extended their national meteorological radar network including USA, UK, Germany, Canada, Italy, New Zealand, China, India, Japan and Brazil amongst others. For a review of historic development of weather radar in different countries see Atlas (1990).

In the UK at a practical level, several X-band (3cm wavelength) radar were placed at various locations on major air routes and one on the roof of the Air Ministry in London in 50's (Collinge, 1987). In the mid 1960's the major movement is made from rainfall detection to rainfall measurement through the Dee Weather Radar Project (DWRP). DWRP resulted in the installation a S-band (10cm wavelength) on the Llandegla. In 1973 the radar was converted to a C-band (5cm wavelength).

Although research using weather radar in the UK continued since its discovery in 40's, it was not until the mid-70's that hardware advances enabled data to be processed in real-time, transmitted from the site and displayed remotely.

A network of twelve, C-band radars were suggested as a national weather radar network by a group of experts to cover the British Isles (Bulman and Browning, 1971). Following the DWRP recommendations, a Plessey C-band radar was established at Hameldon Hill in May 1980 by a consortium including the Meteorological Office and the North West Water Authority.

There are currently some 14 C-band weather radars (plus an S-band device at Shannon Airport) networked and in operation in the UK. Their distribution and coverage is shown in figure (8.1). An example of rainfall information of meteorological C-band radar is shown in figure (8.2).

The development of weather radar and the advent of satellite sensor provide the appropriate sources of data for short period mesoscale rainfall forecasting. In the UK these two data sources were combined through the Short Period Weather Forecasting Pilot Project (SPWFPP) and its successor, Forecasting Rainfall Optimised using New Techniques of Interactively Enhanced Rainfall and Satellite (FRONTIERS) (Viner, 1992).

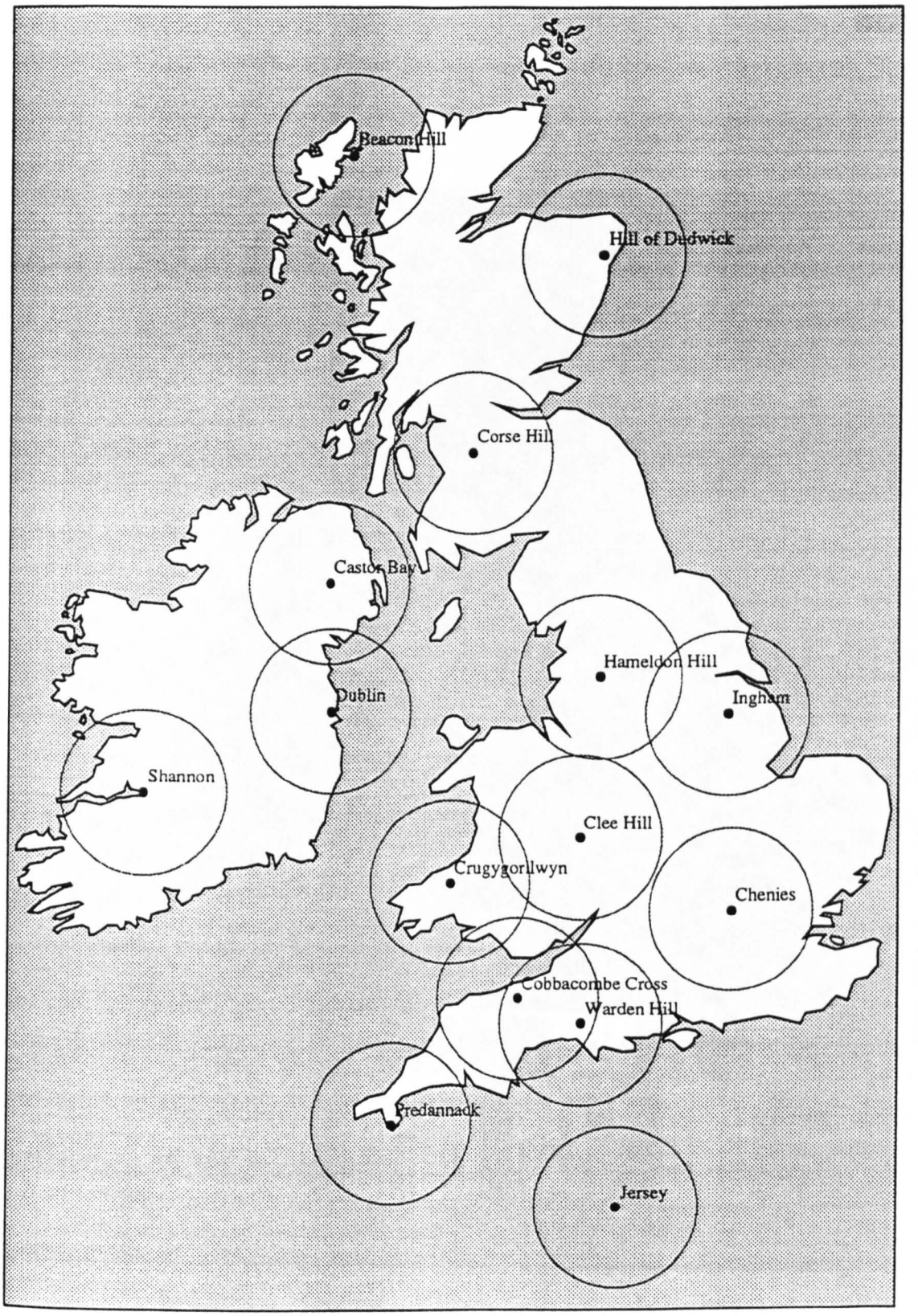

Figure (8.1) The UK Weather Radar Network as at December, 1992. (Circles Correspond to a Range of 75km)

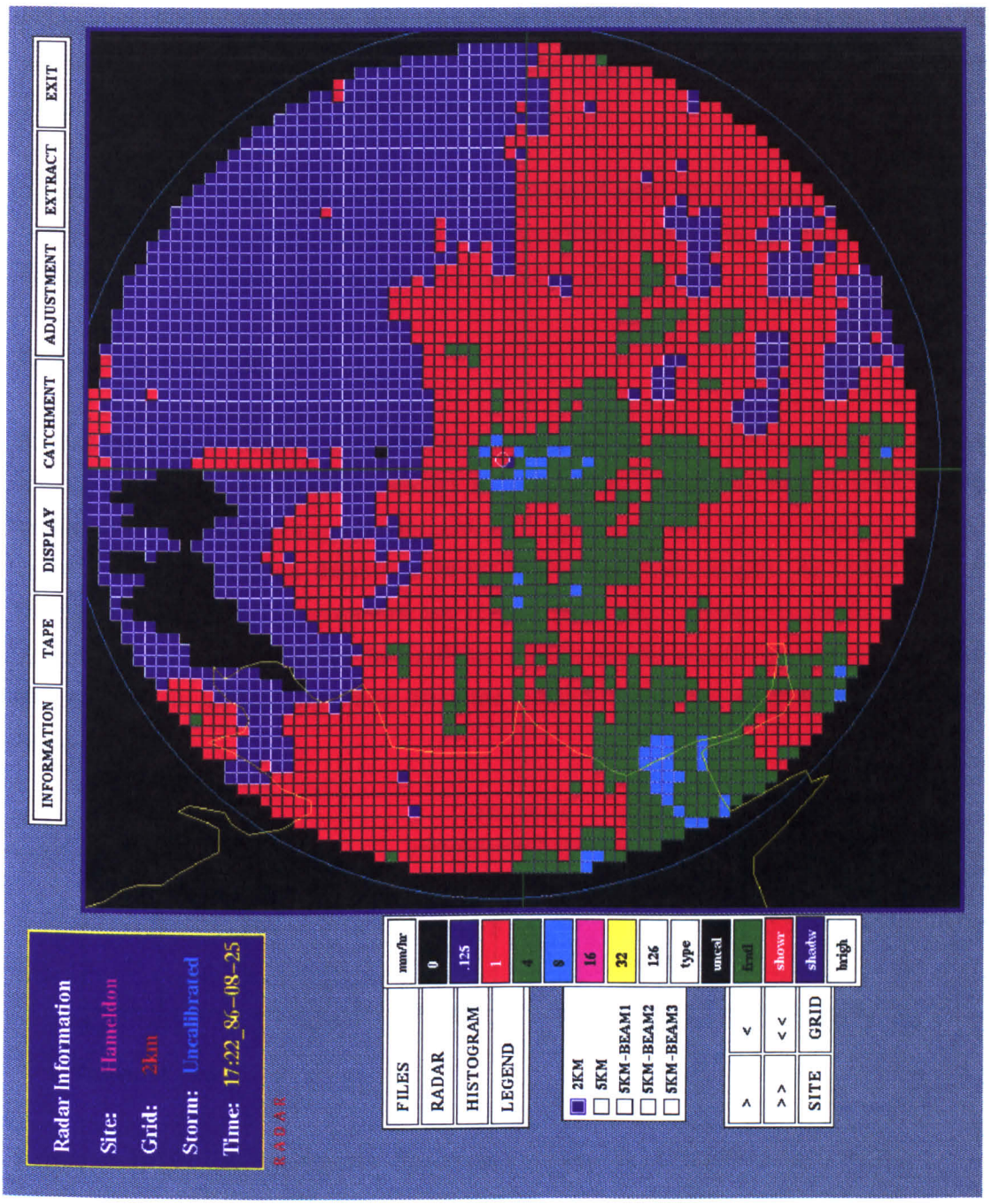

Figure 8.2 An Example of Radar Rainfall Information Using Meteorological C-band Radar

Radar data are first collected in polar co-ordinates and are then converted to Cartesian co-ordinates at site of the original radar. Network data are, only available from Meteorological Office headquarters at Bracknell. In order to create the national network images at Bracknell radar data are composited with data from other UK radars. These data are also composited with European radar data to produce COST73 images and with Meteosat data to form FRONTIERS information.

Salford University in a co-operation with Auckland University in New Zealand currently operate three vertically pointing X-band radars (VPR) (two mobile) and a low-power C-band device. This work is being beyond the scope of this thesis.

8.3 Basic theory

Radars provide an indirect measurement of rainfall by emitting electromagnetic energy and observing the nature of the energy reflected back. As shown in figure (8.3) radars utilise the microwave range of frequency (f) spectrum. For meteorological purposes usually radars are often described in terms of their wavelength (λ) rather than the frequency. These two parameters are related by $c=\lambda.f$, where c is speed of light. In general the smaller the size of the particles, the shorter the wavelength required to detect the particles. In meteorology most often the C-band (5cm) or S-band (10cm) wavelength are used.

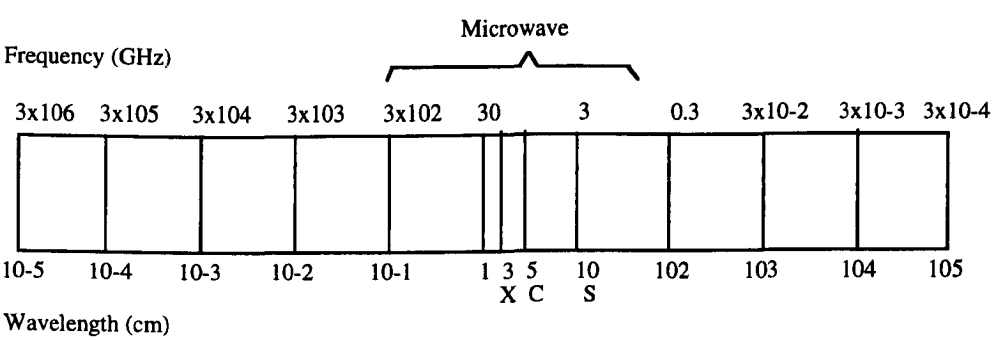

Figure (8.3) The Electromagnetic Spectrum Frequencies of $3x10^6$ to $3x10^{-4}$ GHz

A schematic of the hardware of weather radar operation is shown in figure (8.4). A transmitter emits an electromagnetic pulse at a known and given frequency. This energy is propogated through an antenna. When it intercepts an object (target), the pulse is partially reflected and returns to the same antenna. The antenna then directs any returned echoes to a receiver by means of a transmit-receive switch. The radar receiver directs the received echo to a so-called digital video processor and computer processor. Through these, the

signal is converted into meaningful information which can be displayed on a computer screen. The distance from the object also is determined by measuring the time interval between the transmission of the radio energy and the reception of the reflected signal.

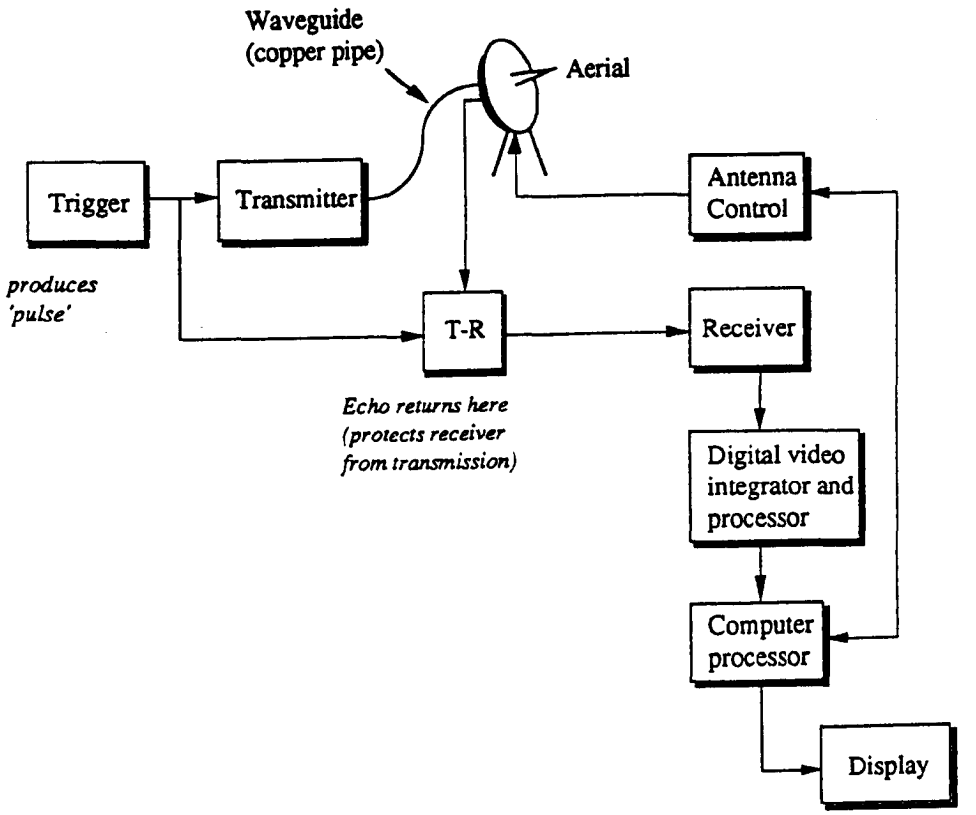

Figure (8.4) Main components of a weather radar system

As indicated by Ruck *et al.*, (1970) the power received, p_r is a function of the transmitter system, the propagation path from the transmitter system to the target, the propagation path from the target to the receiving system, and the receiving system. The radar equation may be summarised as follows:

$$\bar{p}_r = A.B.C.D.E.\Sigma\sigma \tag{8.1}$$

where the terms represent:

A = transmitting system = $p_t.G_t / L_t$

B = propagating medium = $1/\left(4.\pi r_t^2.L_{mt}\right)$

C = propagating medium = $1/\left(4.\pi r^2.L_{mr}\right)$

D = receiving system = $G_r.\lambda^2 /\left(4\pi L_r\right)$

E = polarisation effects = $1/L_p$

σ = radar cross section (also called back scattering cross section)

and the parameters are defined as:

p_t = transmitter power in watts;

G_t = gain of the transmitting antenna in the direction of the target (the amount that antenna focusing increases power);

L_t = numerical factor to account for losses in the transmitting system;

L_r = a similar factor for the receiving system;

L_{mt}, L_{mr} = numerical factors which allow the propagating medium to have loss;

r_t = range between the transmitting antenna and the target;

r = range between the target and receiving antenna;

G_r = gain of the receiving antenna in the direction of the target;

λ = radar wavelength; and

L_p = numerical factor to account for polarisation losses.

Usually it can be assumed that:

$G_t = G_r = G$ and $r_t = r$ therefore, the equation (8.1) can be written as:

$$\bar{p}_r = \frac{p_t G^2 \lambda^2}{(4\pi)^3 r^4} \times \sum \sigma \tag{8.2}$$

The radar cross-section, σ, was defined by Ruck *et al.*, (1970) as: 'given the target echo at the receiving system, σ is the area which would intercept sufficient power from the transmitted field to produce the gain echo by isotropic radiation.' The amount of energy back-scattered from the hydrometers depends upon the number of particles within the pulse volume of the radar beam, their size, composition, relative position, shape and orientation.

Mie (1908) expressed the back-scattering cross-section σ as:

$$\sigma = \frac{\pi D^2}{4\alpha^2}\left(\sum_{n=1}^{\infty}(-1)^n(2n+1)(a_n - b_n)^2\right) \tag{8.3}$$

where D is the drop diameter, $\alpha = \pi D/\lambda$ and is called the electrical size, a_n *and* b_n are coefficients of the scattering field. If the drop diameter is small compared to the

wavelength (i.e. $\alpha < 0.13$) then a simplification of equation (8.3) may be used in accordance with the theory of Rayleigh scattering as:

$$\sigma = \frac{\lambda^2 \alpha^6}{\pi} \left| \frac{m^2 - 1}{m^2 + 2} \right|^2 \tag{8.4}$$

where $m = n\text{-}ik$ (the complex index of refraction), n = the ordinary refractive index, k= a coefficient of absorption. If $K = \left| \frac{m^2 - 1}{m^2 + 2} \right|$ then the equation (8.4) can be written as:

$$\sigma = \frac{\pi^5}{\lambda^4} |K^2| D^6 \tag{8.5}$$

this shows that scattering cross-section is proportional to the sixth power of the drop-size diameter.

Probert-Jones (1962) expanded the equation (8.2) to allow for the beam shape and other factors as:

$$\bar{p}_r = \frac{p_t G^2 \lambda^2 \theta \phi h L}{512(2L_n 2)\pi^2 r^2} \times \frac{1}{\Delta v} \sum_{vol} \sigma \tag{8.6}$$

where L is the sum of all the losses which includes the attenuation by atmospheric gases, precipitation and the radome; θ and ϕ are the vertical and horizontal beam widths and h is the pulse length, and Δv is the pulse volume. An idealised radar beam, of width θ and inclined at angle α under conditions of normal atmospheric propagation is shown in figure (8.5).

Substitution of equation (8.5) into (8.6) gives:

$$\bar{p}_r = \frac{p_t G^2 \theta \phi h L \pi^3}{512(2L_n 2) r^2 \lambda^2} |K|^2 \frac{1}{\Delta v} \sum_{vol} D^6 \tag{8.7}$$

If the radar constant (C) and radar reflectivity (Z) are assumed to be:

$$C = \frac{p_t G^2 \theta \phi h L \pi^3}{512(2L_n 2)\lambda^2} \tag{8.8}$$

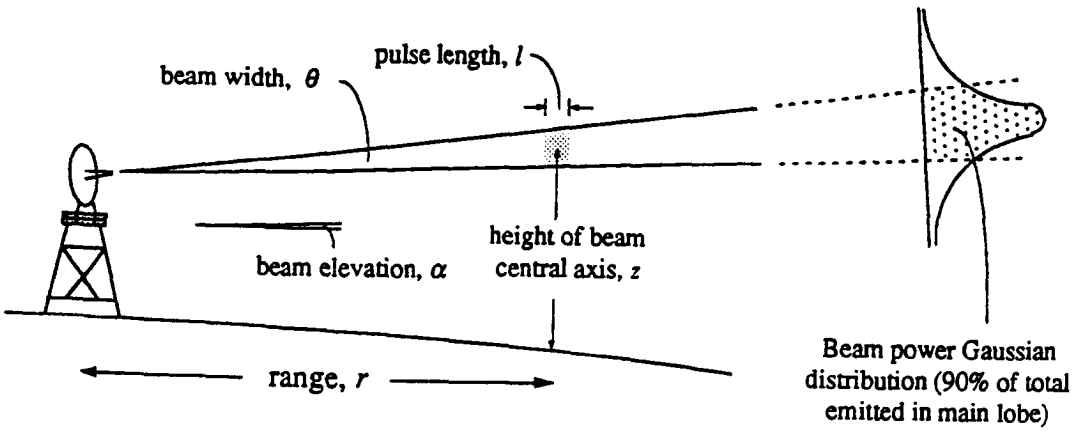

Figure (8.5) Geometry of an idealised pulse volume

$$Z = \frac{1}{\Delta v} \sum_{vol} D^6 \tag{8.9}$$

then the equation (8.7) can be written as:

$$\bar{p}_r = \frac{C|K|^2 Z}{r^2} \tag{8.10}$$

Equation (8.10) is subject to numerous assumptions which are listed by Collier (1989), the principal ones being that:

- Rayleigh scattering theory is applicable;
- the pulse volume is completely filled by randomly distributed precipitation particles;
- Z is uniform throughout the sampled pulse volume and is constant during the sampling interval;
- $|K|^2$ is the same for all of the hydrometers within the sample, i.e. they are either water drops or ice particles;
- absorption of the transmitted signal by ground clutter in the beam is negligible.

It should be emphasised that it is not practical to measure operationally $\sum D^6$, therefore Z (radar reflectivity) may be calculated according to equation (8.10) if the range r and the average received power, $\bar{p}_r$ are known. In order to calculate rainfall intensity Z then is related empirically to the rainfall intensity by the Z-R relationship as follows:

$$Z = aR^b \tag{8.11}$$

where R is the rainfall intensity and a and b are empirically derived constants. The appropriate units for Z and R are mm^6m^{-3} and $mmhr^{-1}$ respectively. The values of a and b parameters are a function of rainfall type, radar properties, and a range of values have been estimated for use in varying conditions. A wide range of values of a and b parameters have been identified by different researchers for different precipitation. Most widely used for homogeneous events is that of Marshall-Palmer as:

$$Z = 200R^{1.6} \tag{8.12}$$

There are a number of problems to use weather radar which are described in section (8.4.2).

8.4 Operational utilisation of weather radar

8.4.1 Radar information display types

In order to interpret the returned signals the radar data which has been received should be displayed. The basic principles of radar information display can be expressed through the following example. Suppose that the radar is observing a storm that extends from range r_1 to r_2 in a particular direction from the radar (figure 8.6). A pulse is emitted from the radar at time $t=0$ and encounters the storm, at time t_1, the raindrops reflect some energy back toward the antenna so that at time $2t_1$ the antenna starts to receive meaningful signals. If it is assumed that at time t_2, the pulse reaches the outer extent of the storm, antenna will not receive meaningful signal after $time=2t_2$. Therefore the signals would appear on an A-scope similar to second part of figure (8.6). If the antenna rotates in a circle at a fixed beam elevation the horizontal extent of a rainfall field within the operational range of the radar may be displayed on a polar co-ordinate system. This kind of display is called the Plan-Position Indicator (PPI). In the UK, data are converted to a Cartesian representation before being displayed.

If a number of beam elevation are used a vertical profile of the storm can be examined. This kind of representation is called Range-Height Indicator (RHI). PPI and RHI indicators are shown in figure (8.7).

Another radar display is the Constant-Altitude-Plan-Position Indicator or (CAPPI) in which data from various beam elevations is used to form a plan of the precipitation. In this procedure the altitude does not increase with range (figure 8.8).

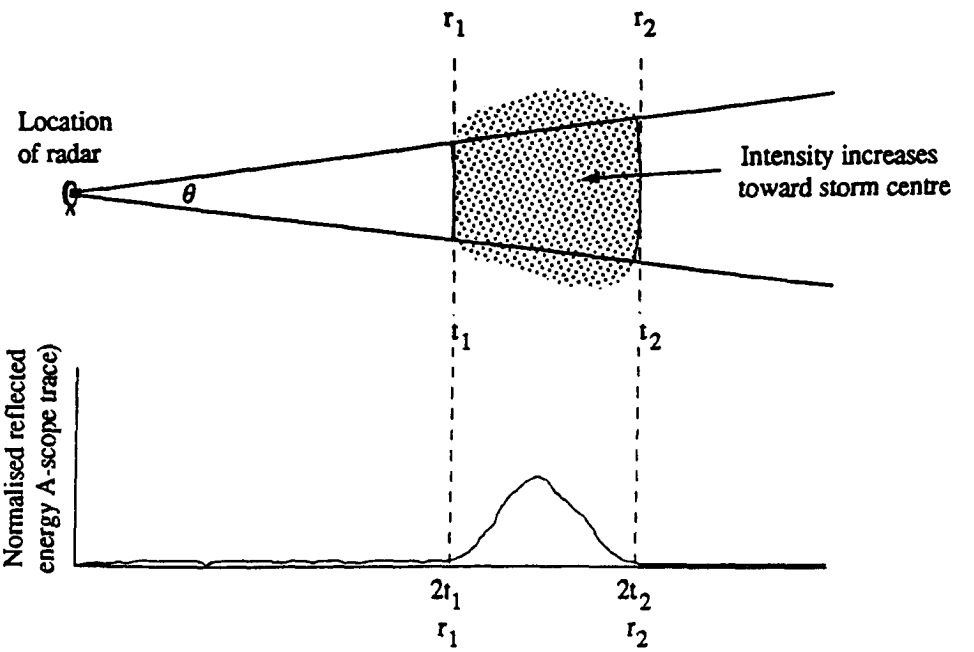

Figure (8.6) Essentials of radar detection and measurement of precipitation (adapted from Grayman and Eagleso, 1970)

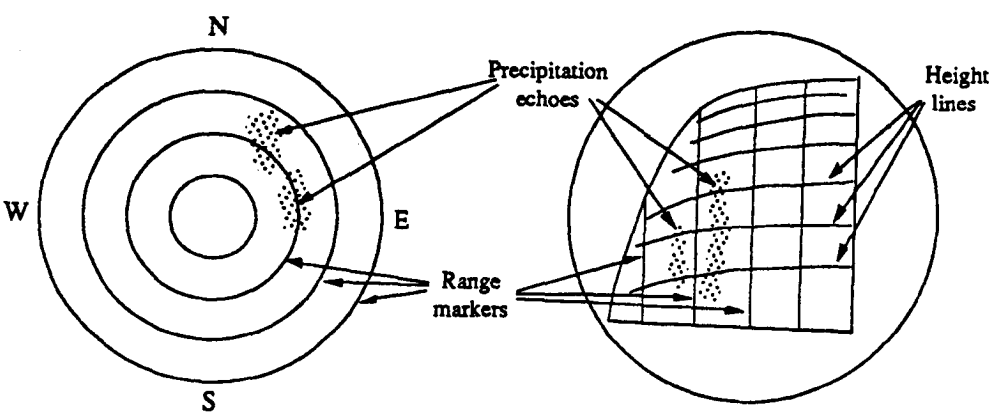

Figure (8.7) Common radar display modes (Battan, 1973)

Radars in the current network in the UK operate on a five minute cycle producing successive 360° scans at (usually) four different elevations (e.g. 0.5°, 1.5°, 2.5°, and 4°). Each rotation takes approximately one minute, the fifth minute is allocated for at-site

data processing (including conversion of polar to Cartesian co-ordinates, and correction and calibration of the data). An estimate of surface rainfall is usually made from the lowest beam, data from higher elevations being used when the lowest beam is obstructed.

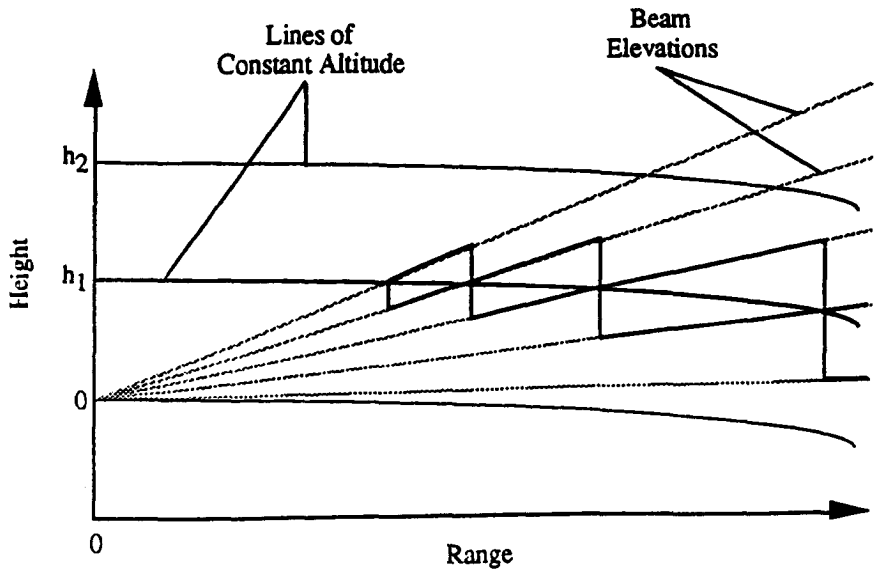

Figure (8.8) Compilation of a Constant-Altitude Plan-Position Indicator Domain.

8.4.2 Problems associated with radar

There are a number of difficulties in measuring precipitation by radar. Usually they can classified into two major groups: those originating from meteorological, atmospheric or topographical features, and those errors due to the radar installation itself, such as software or hardware reliability. The first group of errors includes: beam attenuation, clutter (permanent echo), anomalous propagation (anaprop), bright band, earth curvature effects, and Z-R relationship. The main problems associated with radar itself can be listed as: dynamic range, radar wavelength, beam width, and beam infilling.

• beam attenuation: some portion of the radar beam is completely absorbed by atmospheric gases, liquids and solids, clouds and heavy precipitation causing attenuation of the radar beam. Attenuation is as the reduction of intensity of the electromagnetic wave along its path. Some attenuation is related to radome wetting. (A radome is used to protect the radar from pollutants and precipitation and eliminate wind stress on the mechanical equipment). Attenuation due to precipitation is inversely related to the wavelength of the microwaves. Although S-band radar does not attenuate appreciably even in high intensity rainfall, due to a relatively smaller and cheaper aerial, C-band radars are installed in the

UK network. Attenuation of C-band radar is negligible for all but the most intensive rainfall.

• clutter (permanent echo): Permanent echo is caused from blocking of the radar beam by ground clutter or from ground-based objects such as towers, trees and radio masts; especially when they are close to the radar. One solution to this problem is to increase the beam elevation, however this may result in low-level rain being 'overshot'. A widely utilised technique is clutter map constructed from returned signals on clear day scans when no rain is present. These maps have certain drawbacks because they assume a constant reflectance from the echoes which is not necessarily true when surfaces become wet. The ground clutter echo strength is almost independent of wavelength.

• anomalous propagation (anaprop): In the normal conditions due to refraction of the radar beam by the atmosphere the beam follows a calculable curve path. Refractive index changes with altitude and can be determined considering the pressure, temperature and water vapour. However, if a strong temperature inversion or high hydrolapse (i.e. rapid increases in humidity) condition occurs, reflective profile follows an anomalous curve resulting radar beam to be deflected onto a circular path around the Earth and ground clutter appearing when not expected. To a certain extent this can be corrected, or at least recognised if the vertical profile of the density of the atmosphere is known. Anaprop is most common in anticyclonic or warm sector conditions especially during the night when the inversion is developed. Anaprop may also be observed, though less frequently, in cyclonic condition when very dry air is present above moist air at low levels. Anaprop may be occurred when the height of the inversion/hydrolapse is about 100m above the radar. Anarprop rarely occurs when the inversion is more than about 1200m above the radar. Anaprop will not occur when the radar beam is above the hydrolapse/inversion.

• bright band (melting layer) is one of the most common (and severe) problems in measuring rainfall from radar in the UK. At cloud top level because of low temperature small ice particles are formed which produce low radar reflectivities. However, when these particles fall, they aggregate and begin to melt because of the temperature increase. As ice particles and snowflakes with a thin coating of water produce much higher reflected signal (approximately five times) then either the ice particles above or the rain droplets below, there is a large increase in the radar return followed by a decline as their size decreases and fall speed increases. A bright band is observed when the radar beam intersects the melting layer. The bright band is normally found some 200-300m below the 0 °C isotherm. If the bright band formed at a low altitude and therefore able to fill the entire beam volume at short range, its effect on the radar signal became greatest and can

cause overestimation in the precipitation by a factor of 5 or 6. The thickness of melting layer is usually only a few hundred meters and can be located anywhere between ground level and some 4 or 5 km above sea level in the UK. Identification and correction of bright band is difficult, and in the UK adjustment is usually limited to implicit rain gauge adjustment procedures (section 8.4.3).

• Earth curvature effects: As mentioned earlier the path followed by a radar beam depends on refractive index of the atmosphere and is a curve rather than a straight path. If the Earth curvature is also considered the combination causes the path of the beam to diverge from the earth's surface resulting with an area between the bottom of the beam and the earth's surface in which neither detection nor measurement is possible. In a standard atmospheric composition, the impact of refraction and of the earth's curvature can be calculated using the four-thirds earth approximation equation (8.12):

$$h(r,\theta) = r\left[\frac{3r}{8E}\cos\theta + \sin\theta\right] \tag{8.12}$$

where h is the height of the beam above site level in km, r is the range in km, E is the radius of the earth in km and θ is the elevation of the radar beam axis in radians. It can be seen when the range and beam elevation are increased, the area which radar is unable to detect is also increased. It is clear that the divergence between the beam and the earth's surface is one of the most significant limiting factors of radar because the characteristics of low level precipitation may be missed.

• Z-R relationship: A most common used relationship between the reflectivity and rainfall intensity is shown in equation (8.12). However, because the size and distribution of particles within a given volume of the radar pulse varies considerably, either temporally or spatially both within storms and from one kind of precipitation to another the a and b parameters can vary considerably. Therefore misselection of a and b parameters could lead incorrect assessment by a factor of 10 or more. Although some researchers have reported that generally with increasing convective intensity a increases and b decreases, it cannot provide a practical solution. Instead in the UK the Z-R relationship is updated in real-time with reference to a small number of ground-based telemetering rain gauges (see section 8.4.3).

• dynamic range: The dynamic range of a radar system is the range of signals which can be detected. The range will be changed when the system's gain control is adjusted. If the dynamic range is too small, either heavy precipitation will be reduced in apparent intensity or light rainfall will not be detected. As the dynamic range is related to the physical

rainfall process of the region the dynamic range required in a temperate climate differs from that required in a tropical region.

• radar wavelength: As mentioned earlier, radars can be classified according to wavelength. Usually five wave bands are considered: L-band (29cm), S-band (10cm), C-band (5.6cm), X-band (3cm), and K-band (1cm). L band radars have no hydrometeorological application because of their cost. S-band radars are much suitable for regions with heavy rainfall and attenuation. However, they need a large reflector to produce a small beam width and are consequently very expensive. C-band radars are often adopted as the best compromise between hardware costs and performance in estimating precipitation rates for most meteorological conditions in temperate regions. Although X-band radar can cost approximately one-tenth of a conventional C-band system it suffers from potentially severe attenuation problems which restricts its range in temperate latitudes to approximately 35km, or less. K-band radar is rarely used for hydrometeorological applications because of its excessive attenuation.

• beam width: The received signal is directly proportional to the effective antenna aperture of the radar. Therefore the largest antenna will give the best results. However, for meteorological purposes operational and economic considerations dictate that the antenna diameter is limited to about 7m. In a circular parabolic reflector the beam width θ (in radians), antenna diameter d, and wavelength λ are related by $\theta = 1.2\lambda / d$. If beam propagation arguments and practical and economical problems are considered for hydrometeorological applications a beam width of 1° is regarded as near optimal. Although it looks that the shorter wavelengths is preferable it should be considered that the shorter the wavelength, the more attenuation is a problem. The most important problems related to beam width is that two targets separated by less than the beam width in angle cannot be distinguished. As an example for a 1° beam width and a range of 100 km, individual cells must be approximately 1.75 km apart before they can be distinguished.

• beam infilling: As mentioned in section (8.3) the Z-R relationship assumes that the radar beam is completely filled by precipitation. If the radar beam is not filled completely the reflected energy will be less than the rate of precipitation. The narrower the beam width the more accurate that the scattering particles uniformly distributed in size and number throughout the volume. The greater the range, the chance that the beam will be incompletely filled.

8.4.3 Local adjustment of radar

As mentioned in previous section there are many errors inherent within raw radar data. Although rain gauges provide a ground-truth value of rain, they only measure rainfall at a point (a small fraction of one km^2). On the other hand radar provides much better estimate of areal rainfall. A number of researchers have attempted to develop techniques which combine the point accuracy of rain gauges with the spatial information of radar, to provide a composite rainfall field more accurate than either used in isolation (Collier *et al.*, 1983).

In this section two techniques for adjusting radar rainfall estimates using rain gauge derived rainfall are described. These two techniques are the method employed by the UK Meteorological Office (domain-adjustment), and a technique developed by Tilford, 1992 (local adjustment).

In the domain-adjustment technique an assessment factor (AF) that is the ratio of hourly radar and rain gauge values is applied on radar values at the given domain (Collier, 1989). At present between four and seven telemetering rain gauges are used for each radar site. The Meteorological Office procedure involves the calculation of the harmonic analysis of the continuous series of hourly mean assessment factors which provides an indication of the temporal uniformity of the event. A significant problem is the variability of the assessment factor both temporally and spatially. Rainfall type was recognised as a major factor in causing this variability. Therefore four synoptic types of precipitation are incorporated into two geographical domain sets: one set for bright band and shower conditions, and another for frontal and rain-shadow. If radar value is zero, a default assessment factor of unity is applied.

A shortcoming in the domain procedure is that spatial discontinuities can exist at the domain boundaries. Also areas of temporal instability exist, particularly when bright band conditions are present. If the storm type is wrongly identified the adjustment factors may vary by a ratio of 50:1 (Shepherd, 1987) causing large errors to be introduced. It is noted that assessment factor is much greater than unity in showers and bright band situation and variations in showers are rapid and slower in frontal rainfall and bright band situations.

The local adjustment procedure which developed by Tilford (1992) utilises a locally operated (dense) rain gauge network and sophisticated two-dimensional surface fitting and consists of three phase process as:

- computation of assessment factors at each rain gauge location.
- two-dimensional surface fitting of the scattered assessment factors to produce a regularly distributed assessment factor field on a grid coincident with the Cartesian grid used by the radar (5km grid).
- node by node multiplication of the radar data by the 'mapped' assessment factors to produce an adjusted rainfall field.

Unlike the Meteorological Office domain procedure, no attempt is made to relate or modify the assessment factors by physically related factors.

8.4.4 Radar data output

On the completion of calibration and correction procedure, several formats of output can be obtained from the UK weather radar network including those described below:

- digital radar data are available for two intensity resolutions. The highest resolution data are held in eight binary bits, the binary values therefore range from $(00000000)_2$ to $(11111111)_2$. Only 208 of the possible 256 (2^8) discrete values are used in practice. Low intensity resolution data are held in three binary bits providing binary values ranging from $(000)_2$ to $(111)_2$. In the high resolution data, the two high order bits of the byte are called the exponent and the other six bits are the mantissa. Since the units of 1/32 mm/hr are used the following equation is used for decoding (convert to decimal) purposes:

$$R = \left[\frac{\left(2^{2\times X}\right) \times Y}{32} \right] \tag{8.13}$$

where R is rainfall intensity in mm/hr X and Y are exponent and mantissa (in real number) respectively. The biggest number which can be identified is equal to $(11111111)_2$, consequently the biggest intensity can be calculated as:

$$R = \left[\frac{\left(2^{2\times 3}\right) \times 63}{32} \right] = \frac{4032}{32} = 126 mm/hr$$

Whilst 208 intensity levels can be obtained through the high resolution data, only eight slice colour ranges are used to display the data. The low resolution data provides only 8 intensity levels. In order to derive the numerical corresponding three-bit values from two bounds of eight-bit representation, different assignment schemes can be applied including

arithmetic mean, geometric mean and harmonic mean. The numerical three-bit values resulting from each of these assignment schemes are shown in table (8.1).

• There are two alternatives spatially resolution, a 2km Cartesian grid (256*256) which is obtainable for a range of 75km from a radar and a 5km Cartesian grid (128*128) which is produced to a range of 210km.

• The temporal resolution is limited by the time involved in completing a full set of scans in four beam elevation (one minute each) when processing time is also included (one minute) the maximum temporal resolution available from the existing radar system is 5 minutes. Some data sets such as the subcatchment average are only produced every 15 minutes.

The areal rainfall estimates are calculated from averaging the most appropriate grid data.

Table (8.1) Data slice ranges and three-bit assigned values

Intensity level	Eight-bit slice range (mm/hr)	Three-bit assigned values (mm/hr) Aritmetic	Geometric	Harmonic
0	<0.125	0.00	0.00	0.00
1	0.125-1	0.56	0.35	0.22
2	1-4	2.50	2.00	1.60
3	4-8	6.00	5.66	5.33
4	8-16	12	11.31	10.67
5	16-32	24.00	22.63	21.33
6	32-126	79.00	63.50	51.04
7	>126	319.00	180.00	150.00

8.5 Application of weather radar data

8.5.1 Catchment and data description

In order to study the application of real-time updating of TF models using weather radar data, Blackford Bridge, a subcatchment of the Irwell, in North West England was chosen. This subcatchment, lying on the river Roch, is well within the coverage of the weather radar at Hameldon Hill. The drainage area of the subcatchment is approximately 186 km^2 and is predominantly elevated moorland with 8% urban coverage (Owens,

1986). The Hameldon radar coverage and the Blackford Bridge subcatcment is shown in figure (8.9).

The Hameldon radar produces quantitative subcatchment rainfall totals at 15 minute intervals processed and calibrated at-site. Flow data for the catchment comes from the slightly insensitive weir at Blackford Bridge and is available also at 15 minute intervals.

In figure (8.10) the location of the Blackford Bridge area in relation to the National Grid and the position of the flow measuring weir and rain gauge are shown.

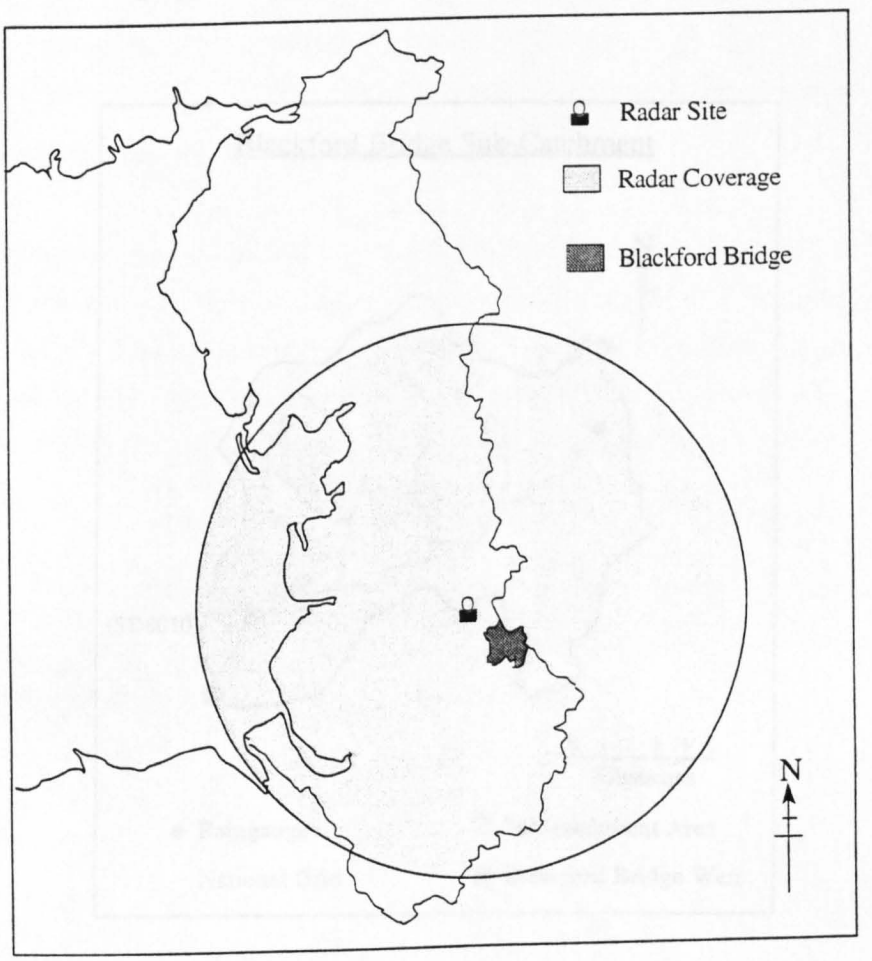

Figure (8.9) The North West region, showing Hameldon Hill radar with 75 km quantitative range at the Blackford Bridge catchment.

Six storm events, in which there are flow and rainfall records, were chosen for investigation. In order to initialise the model for each event a short time data set before the main event is also chosen as pre-event data. Initial processing of radar data was carried

out to identify and remove any errors in the event record, such as missing frames, anomalous propagation and bright-band. Figure (8.2) shows one frame from a typical rainfall radar sequence.

Runoff data was obtained in the form of river stage or height. In order to convert river data from stage to flow, the National Rivers Authority stage-discharge parameters in a rating equation is used as below:

$$Q = 44.558(H + 0.173)^{2.408}$$

where Q is discharge (cumecs) and H is stage height (metres).

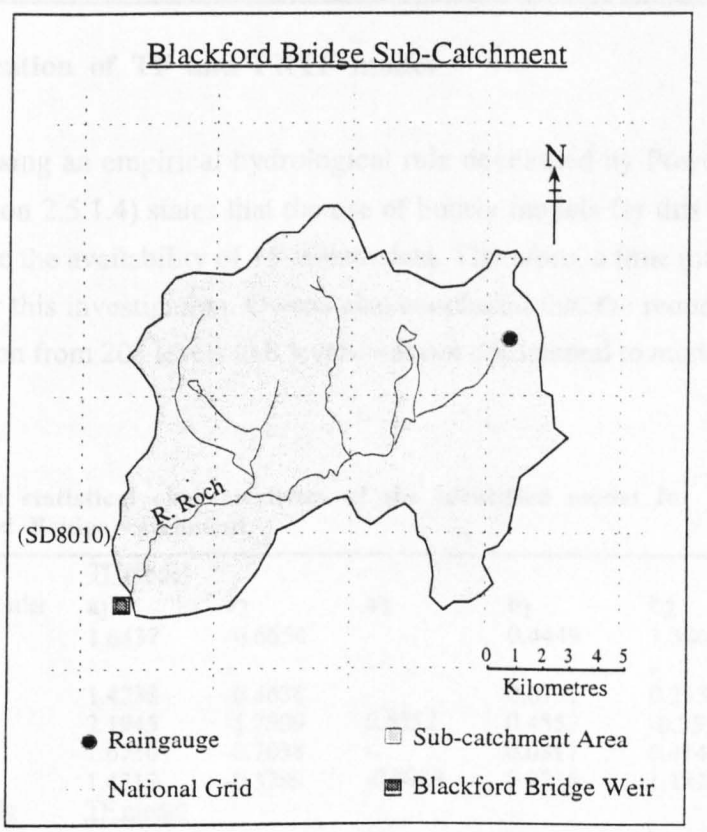

Figure (8.10) The Blackford Bridge subcatchment

The main characteristics of each event and pre-event are summarised in the table (8.2). Rainfall hyetographs and discharge hydrographs used in the catchment rainfall-flow analysis are shown in Appendix 2.

Table (8.2) Main specification of the events studied, Blackford Bridge catchment

Event no.	Start time	End time	Duration (hours)	Maximum rainfall (mm/hour)	Peak flow (cumecs)	Average percentage runoff
	Main event					
1	16:00/03/01/82	04:00/05/01/82	36	4.4	68.4	56.1
2	05:00/10/03/82	10:00/11/03/82	29	2.9	30.2	31.2
3	24:00/08/11/83	11:00/10/11/83	35	8.7	84.7	36.5
4	20:00/06/02/84	24:00/07/02/84	28	2.2	31.6	78.4
5	01:00/30/10/86	01:00/31/10/86	24	1.7	15.4	23.4
6	02:00/01/01/87	06:00/02/01/87	28	4.4	57.7	43.5
	Pre-event					
1	06:00/02/01/82	15:00/03/01/82	33	2.0	36.7	97.8
2	15:00/09/03/82	04:00/10/03/82	13	3.7	27.0	12.8
3	00:00/08/11/83	23:00/08/11/83	23	2.7	10.3	12.8
4	21:00/05/02/84	19:00/06/02/84	22	8.3	80.7	27.8
5	00:00/27/10/86	00:00/30/10/86	72	12.1	18.9	19.8
6	15:00/29/12/86	01:00/01/01/87	58	8.2	130.8	56.6

8.5.2 Identification of TF and PRTF model

Owens (1986) using an empirical hydrological rule developed by Powell and Cluckie (1985) (see section 2.5.1.4) states that the use of hourly models for this catchment was sufficient, despite the availability of 15 minute data. Therefore, a time interval of 1 hour was accepted for this investigation. Owens also concluded that the reduction of rainfall intensity resolution from 208 levels to 8 levels was not detrimental to model estimation or forecasting.

Table (8.3) Some statistical characteristics of the identified model for the pre-events studied, Blackford Bridge catchment

	Static	TF model					
Event no	Model order	a_1	a_2	a_3	b_1	b_2	b_3
1	(2,2)	1.6437	-0.6654	-	0.4449	1.3066	-
2	-	-	-	-	-	-	-
3	(2,2)	1.4238	-0.4638	-	0.0732	0.2139	-
4	(3,3)	2.1945	-1.7509	0.5252	0.4552	-0.3511	0.5355
5	(2,2)	1.6716	-0.7038	-	0.0817	0.4148	-
6	(3,3)	1.4312	-0.3789	-0.0983	0.2736	1.1823	-0.0295
	Dynamic	TF model					
Event no	Model order	a_1	a_2	a_3	b_0	b_1	b_2
1	(2,2)	1.7597	-0.7741	-	0.1209	1.0803	-
2	(2,3)	1.7349	-0.7524	-	0.6495	-0.9075	0.8783
3	(2,3)	1.7349	-0.7524	-	0.1886	-0.1814	0.1862
4	(2,2)	1.7349	-0.7524	-	0.6363	-0.0975	-
5	(3,3)	2.3911	-1.9057	0.5063	-0.0955	-0.1443	0.1715
6	(3,3)	2.2976	-1.7597	0.4492	0.3398	-0.1574	0.3205

In order to identify the optimal model for each pre-event, the search procedure was used. The model parameters, model percentage runoff, root mean square error, and pulse response characteristics of each structure in each selected pre-event, were considered.

Some statistical characteristics of the identified model both for static and dynamic TF model for each pre-event are presented in table (8.3). It is noted in pre-event number two that it was not possible to construct an appropriate calibrated model for the static TF case, because none of the resultant pulse responses were valid from a hydrological point of view.

8.5.3 Comparison of current and modified updating procedures of PRTF model

In this section the performance of the updating procedure introduced in (7.5.1.3) using weather radar data is evaluated. Six storm events together with six pre-events described in table (8.2) were considered. Once again α series are determined sequentially by dividing the pre-event data sets. An autoregressive model is then fitted to α series and used to predict future α over the forecast lead time. Future B parameters of the PRTF model are then calculated using the predicted α. Simulated hydrograph over the forecast lead time are determined and shifted proportional to the differences between actual and simulated flow at the time of forecasting.

Both RMSE statistic results and forecast hydrographs of existing and modified methods are compared. The RMSE results for all events studied are given in table (8.4) and an example of the forecast hydrographs are presented in figure (8.11). Table (8.4) shows that in five out of six events, the suggested procedure slightly outperformed the existing method for most forecast lead times and only in event number six does the original PRTF model provides better forecasts. The reason for this is the temporal variation of α series of the event. Overall this study revealed that combined PRTF model can improve the forecasting quality.

8.5.4 Comparison of current and modified updating procedures of TF model

The performance of the original TF model and the combined error prediction model introduced in (7.5.2.2) using weather radar data are compared in this section. The same five events and pre-events of the Blackford Bridge catchment described in table (8.2) were considered. As mentioned in section (7.5.2.2) for each event, an autoregressive model was identified for each step of forecasting lead time using the forecasting errors obtained from the application of the calibrated model on the same pre-event data. These models were then used in combination with the original TF models to forecast the main event hydrographs.

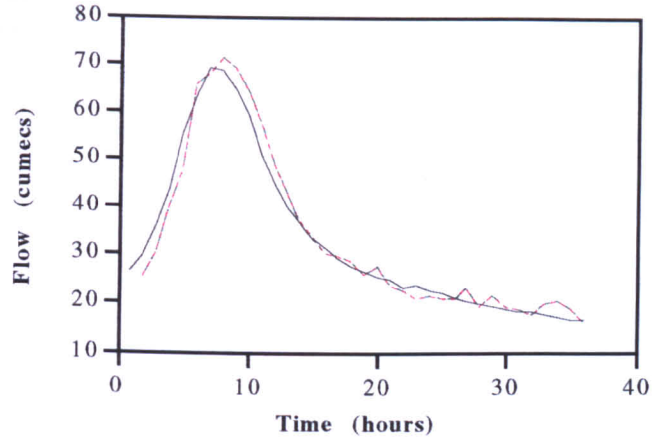

(i) One step ahead forecasts

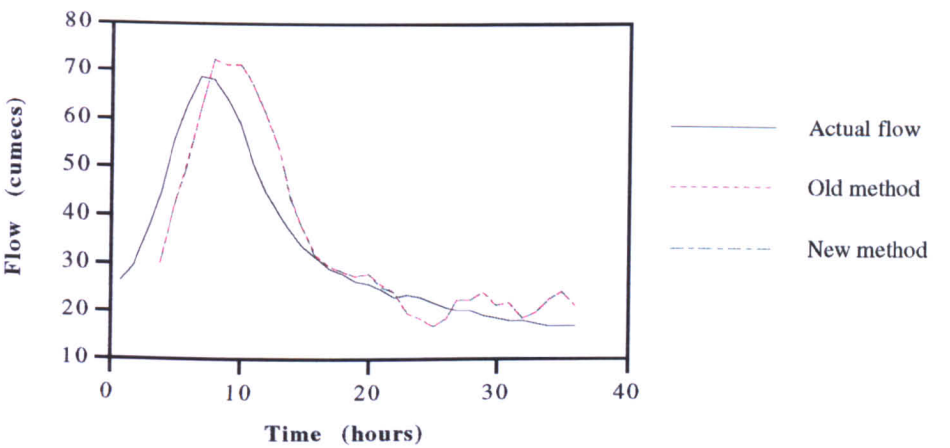

(ii) Three step ahead forecasts

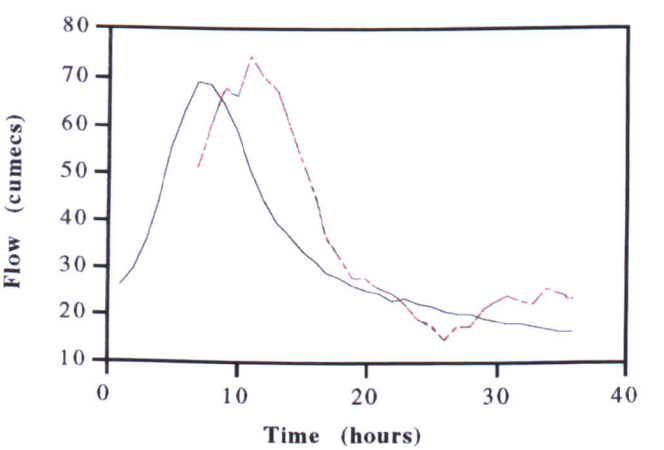

(iii) Six step ahead forecasts

Figure (8.11) Comparison of the forecast hydrographs, Blackford Bridge catchment, event No. 1, PRTF model.

Table (8.4) RMSE result of current and modified updating procedure of PRTF model for different events (Blackford Bridge catchment)

	Event	No. 1	Event	No. 2	Event	No. 3	Event	No. 4
Step ahead	Current model	Modified model	Current model	Modified model	Current model	Modified model	Current model	Modified model
1	2.945	2.952	1.234	1.235	5.448	5.364	0.608	0.607
2	5.136	5.155	2.078	2.076	9.281	9.216	1.053	1.052
3	7.540	7.567	2.918	2.914	12.407	12.373	1.395	1.393
4	9.384	9.407	3.612	3.608	14.988	15.006	1.750	1.745
5	10.846	10.856	4.469	4.461	17.293	17.337	2.058	2.053
6	11.964	11.948	5.126	5.114	19.257	19.373	2.275	2.268
7	12.713	12.665	5.642	5.628	20.803	20.910	2.372	2.361
8	13.683	13.606	5.987	5.970	22.305	22.455	2.377	2.361
9	14.695	14.594	6.107	6.089	23.663	23.834	2.368	2.345
AR order	-	3	-	3	-	3	-	3

Table (8.4) Continued

	Event	No. 5	Event	No. 6
Step ahead	Current model	Modified model	Current model	Modified model
1	2.007	1.909	3.804	3.804
2	2.793	2.654	6.503	6.502
3	4.086	3.864	9.059	9.060
4	5.496	5.179	11.114	11.116
5	6.569	6.197	12.677	12.680
6	6.898	6.519	13.752	13.757
7	6.574	6.222	14.357	14.364
8	5.904	5.596	14.529	14.537
9	4.973	4.719	14.221	14.229
AR order	-	3	-	3

The performance of the combined TF model was evaluated using a combination of an objective approach, in which the RMSE of the flow forecasts at each time step ahead between the current and modified procedure are compared, and a graphical comparison of the forecasting results. The results of the objective comparison are given in table (8.5). In figure (8.12) graphical comparison of the forecasting results of event number three are also presented as an example. Table (8.5) shows that in four out of five events, in most steps of forecasting lead time the combined model slightly outperforms the original TF model and only in event number five in most steps of forecasting lead time the original TF model provides better forecasts. It is noted that the forecast quality of the original model also is poor. The reason for the poor performance of the combined model is the same as that for event number six in section (8.5.3) namely, the temporal variation of error series of event.

8.6 Summary and conclusion

This chapter consists of two sections. The first section provides a brief review and discussion about weather radar and its applications. The second section presents the results of extending the updating procedures of TF models developed in chapter 7 to an English catchment with weather radar data.

Table (8.5) RMSE result of current and modified updating procedure of TF model for different events (Blackford Bridge catchment)

	Event No. 1		Event No. 3		Event No. 4		Event No. 5	
Step ahead	Current model	Modified model	Current model	Modified model	Current model	Modified model	Current model	Modified model
1	1.618	1.580	3.735	3.734	4.088	4.075	1.123	0.980
2	3.555	3.412	6.605	6.597	7.347	7.277	2.017	1.922
3	5.964	5.765	9.713	9.707	8.828	8.854	2.401	2.335
4	8.211	8.078	13.560	13.549	8.664	8.774	2.700	2.760
5	10.063	10.026	16.823	16.813	7.529	7.620	2.966	3.503
6	11.347	11.275	20.070	20.076	6.447	6.463	3.095	3.669
7	12.090	12.086	23.116	23.109	5.667	5.508	3.143	3.178
8	12.547	12.825	25.411	25.401	5.347	5.147	3.116	3.646
9	12.769	13.201	27.773	27.750	5.171	4.969	3.083	3.133
AR order	-	3	-	3	-	2	-	3

Table (8.5) Continued

	Event No. 6	
Step ahead	Current model	Modified model
1	1.886	1.889
2	3.173	3.173
3	5.037	5.037
4	6.585	6.576
5	7.671	7.665
6	8.296	8.290
7	8.463	8.497
8	8.474	8.554
9	8.295	8.357
AR order	-	3

It is well known, that two rain gauges, even if located a couple of kilometres apart, frequently show different records for the same precipitation event. Weather radar, however, can provide a more realistic spatial variability of the rainfall amounts at acceptable levels of accuracy, although there are some aspects of weather radar that deserve further investigation and improvement. Basic concepts of radar, including fundamental theory, radar classification, radar data products and its operational utilisation, problems associated to radar and areas affecting the calibration weather radar have been addressed.

In order to examine the practical problems related to utilisation of weather radar data a catchment which is well within the cover of the weather radar was selected and all aspects of radar data processing including visual display, identification and elimination of errors in the event record, such as missing frames, anomalous propagation and bright-band and finally digital encoding of radar images have been applied. Twelve storm events were selected through this approach and were then used to investigate the updating procedures developed in chapter 7.

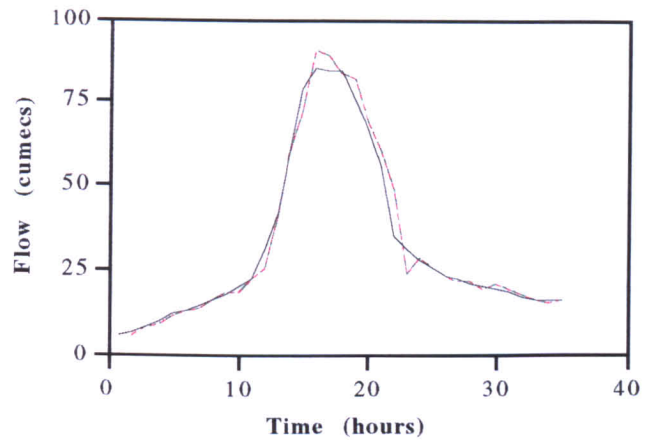

(i) One step ahead forecasts

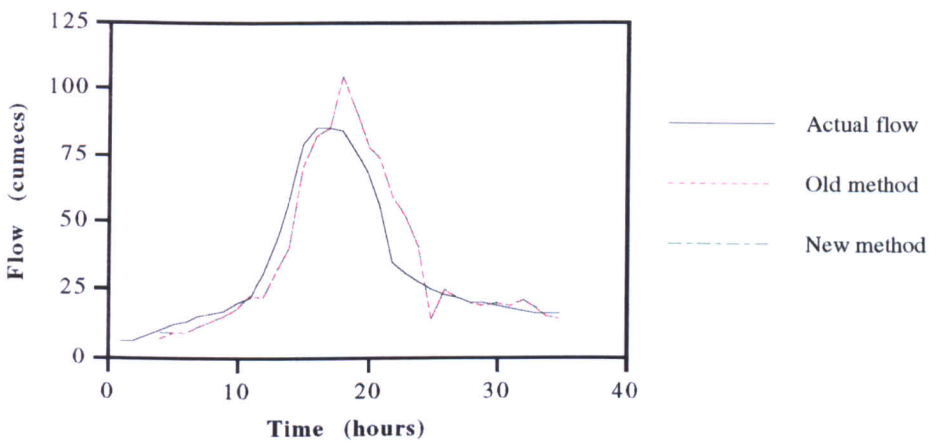

(ii) Three step ahead forecasts

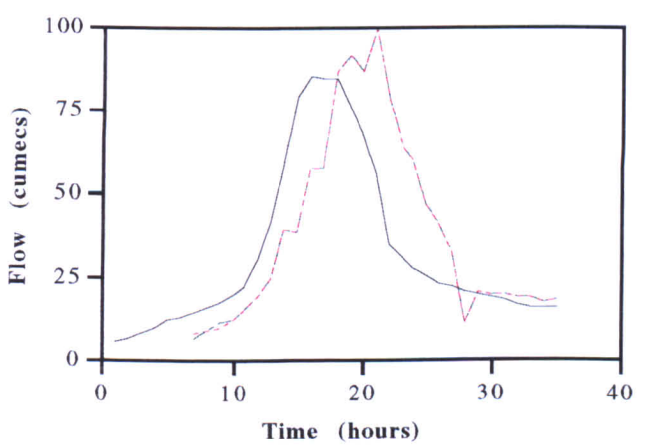

(iii) Six step ahead forecasts

Figure (8.12) Comparison of the forecast hydrographs, Blackford Bridge catchment, event No. 3, TF model.

It has been shown that updating procedures of both static and dynamic TF model works just as well for radar derived rainfall as for rain gauge data. So that for the PRTF model, in 11 out of 12 events (rain gauge and radar derived rainfall) the suggested procedure outperforms the existing method. On the other hand, in static TF model the combined updating model provides better results in 8 of 10 events. However, it is noted that in a small number of events (14%) possibly because of inconsistency in temporal variation of the error, the original procedures outperform the suggested methods.

CHAPTER 9

CONCLUSIONS AND RECOMMENDATIONS

This chapter outlines the main conclusions of the research and makes recommendations for future work.

An extensive review into flood forecasting models with particular emphasis on the WMO simulated real-time inter-comparison of hydrological models has been conducted and is presented at the start of the thesis. The review introduces the basic structure and operational characteristics of the models and provides a foundation for their further improvement.

A description of criteria which may be used to classify flow forecasting models and factors affecting the choice of a suitable model have been outlined. Different methods of effective rainfall determination have been reviewed; in particular the review identified the problems associated with trying to accurately define effective rainfall in real-time (one of the major reasons total rainfall is frequently used for real-time applications).

An outline has been presented of the utilisation of transfer function (TF) models in representing the rainfall-runoff process, and the main problems associated with this class of model. It has been shown that TF models can be calibrated for a range of catchments and for any scale without the need for large amounts of data describing the catchment, because they are based solely upon the relationship between total rainfall (input) and a flow (output). TF models are relatively simple to identify and calibrate, easy to apply, are parametrically efficient and computationally fast. The implicit feedback mechanism of the TF model enables the model to self-correct, and the natural lag between the occurrence of rainfall and the response of streamflow is also included in the models.

In order to carry out an extended inter-comparison of real-time flood forecasting models, the theoretical structure of TF models (both static and physically realisable) are combined and their forecasting results are compared with those of fourteen models used in the

WMO workshop for twelve case studies on two river catchments from climatologically and geographically varied conditions.

Some statistical criteria that can be used to measure model performance are reviewed and a cross-validation scheme consisting of root mean square errors and the relatively new randomness-dispersion diagram have been used to evaluate the TF model performance. Objective statistical results used along with graphical displays of forecasted and observed flow facilitate the best assessment of a model's performance. The TF models use a factor (Δ) to compensate for variation in the proportion of total rainfall contributing to runoff. The influence and importance of the choice of initial Δ is demonstrated through an investigation for the one of the test catchments.

The results of the comparison of the performance of different models indicate that there is no strict rule in the performance of models on an event basis. However, an attempt has been made to rank the flood forecasting models, both on an event basis and overall. It has been observed that a model may have the first rank for one event and the last rank in other, so that no particular model consistently provides the best result. The comparison revealed that an increase in model complexity does not necessarily lead to an increase in forecast accuracy. Absolute forecast error increases with lead time: however, the relative increase of the RMSE for different models with increasing forecast lead-time is not consistent. TF models generally perform better for short time steps probably because the one step-ahead forecast error is considered to select the best calibration model. It is concluded that there is not a significant difference between the quality of the forecasts derived from the static and dynamic TF models.

A simple novel model to calculate the average response has been developed. The proposed model uses average characteristics rather than average of the ordinates of pulse response. The proposed method is encouraging, although more data are required to confirm this preliminary conclusion.

Further research has compared the quality of forecasts obtained from average and isolated TF models. Since this was applied on a limited numbers of storm events it has not been possible to draw a definite conclusion concerning the performance of the two different methods.

It is clear that the pulse response function derived from a sequence of storms reflects the average catchment response to those storms. However, every event has its own distinguishing features according to antecedent conditions of the catchment and storm characteristics. This implies that if a sequence of storms with similar characteristics are

selected for calibration, the resultant average TF may provide better forecasting performance for future events with similar characteristics. This would enable a suite of several average TF models to be constructed, and used to forecast flows for events whose characteristics closely matched. An extensive analysis of group calibrated TF models was carried out after classifying events on the basis of storm and catchment characteristics. In total 41 storm events have been chosen and were classified into different groups on the basis of the gradient of the rising limb of an individual storm's pulse response (as an indicator of the rainfall type) and five and thirty day antecedent precipitation index as well as five day antecedent precipitation (all as indicators of the antecedent moisture conditions of the catchment). This classification provided thirteen different groups.

Suites of models are calibrated individually, representing the rainfall-runoff responses associated with different storm-catchment characteristics type. An attempt to relate the type of rainfall and gradient of pulse response did not reveal a definite dependency between them although it is possible that an extended event database might better support the identification of a relationship between the PR gradient and the type as well as characteristics of coming rainfall.

The benefits of calibrating TF models using a sequence of storms whose characteristics are similar have been demonstrated. Objective statistical results and subjective comparison clearly revealed that the use of group model resulted in a significant improvement in the quality of the forecasts. Therefore it is much better to calibrate a TF model using a sequence of storms with similar characteristics. For all events investigated, the five day antecedent precipitation was a feature in the best group model.

Since the amount of runoff from a storm depends on the several other variables, further work on group models requiring an extended database of flow and rainfall measurements as well as other corresponding information. An expert system approach has been suggested to automate the selection of the most appropriate pulse response during the course of an event. The classification of events should be based on a series of characteristics which are known or predictable prior to occurrence of event.

Several methods of system identification both off-line and on-line have been assessed. Recursive algorithms for adaptive parameter estimation have been described. Recently new techniques like genetic algorithms and neural networks are being investigated. On the basis of this review, the recursive ordinary least squares method is used in most parts of thesis.

An extensive investigation into the application of genetic algorithm to the physically realisable transfer function model has been presented. A new parameter estimation technique known as the hybrid genetic algorithm (HGA) has been developed by combining conventional procedures with a genetic algorithm. The techniques of interview selection and fitness scaling as well as random bit mutation and multiple crossover have been included in HGA and both binary and real number encoding technique have been assessed. The HGA has been successfully applied in identification (calibration) and simulation (updating) of the dynamic TF model. Four software packages have been developed and extensive development and testing has proved the viability of this approach and has shown that the performance of HGA is more accurate and powerful than conventional procedures.

Due to the incapability of models to perfectly portray complex natural systems, and due to faulty model input data, every forecast is subject to an error. Consequently, it is necessary to correct (update) the forecast in the light of recent model performance to minimise the forecast error. The sources of forecasting errors have been reviewed, and the basic structure and operational characteristics of the different updating procedures critically assessed. A description of the parameters affecting the choice of a suitable updating procedure have been outlined. In particular, the review indicated that a simple model plus sophisticated updating procedure is preferable to sophisticated model plus simple updating procedure. Furthermore, it is concluded that if there is no evidence about the likely cause of the error, an error prediction method is probably the best choice.

In order to improve the current updating procedure of TF model, extensive research has been conducted to find the most important adjustment factor of the dynamic TF model. The impact of the volume, shape and time adjustment factors on forecast quality has been evaluated through a sequential determination of the different parameters which may affect the model.

It has been concluded that the volume adjustment factor is the most important factor of the three. Furthermore, several attempts have been made to relate the adjustment factors to different elements including time, average rainfall intensity, accumulated rainfall, and discharge. The interaction of adjustment factors has also been investigated.

An autoregressive model has been used to develop a new updating procedure for the dynamic TF model by the determination of the B parameters through the prediction of future volume adjustment factor over the forecast lead-time.

An autoregressive error prediction model has also been combined with a static TF model. Relatively extensive testing has shown that the performance of both new transfer function models are superior to conventional procedures.

An inter-comparison of the dynamic TF updating procedures for an English catchment using radar rainfall data is also included. Weather radar is an alternative method of rainfall measurement to the use of rain gauges. Rain gauge records are only point measurement of rainfall whereas radar measures (in this case) rainfall in 2km x 2km pixels (up to about 75 km range), and, hence, the spatial variation can be better assessed.

The basic concepts of weather radar and the problems associated with it are reviewed. Although the qualitative information of the radar data is readily apparent the quantitative quality remains an open question. Nevertheless, some aspects of radar deserve further investigation, mainly those related to radar calibration. It is certain that even if radar could not improve on the absolute magnitude of the rainfall amount, it would still provide valuable information on the spatial variation and time evolution of the precipitation events.

Recommendations for further work

Following this study, a number of aspects requiring further investigation are identified. Listed below are topics where future research could be usefully directed.

To extend the lead-time of forecasts especially in quickly responding catchments the most important information is the anticipated future rainfall, therefore, rainfall forecasting algorithms should be developed. As the spatial distribution, dynamics and type of the rainfall also influence the runoff generation process, these areas should also be investigated.

One possible solution to decrease the relative increase of RMSE of TF models over larger forecast lead-times is through the calibration of the model using longer step ahead errors as the objective function.

Certain areas of the study, for example development of a simple model to calculate the average response and comparison of average and isolated TF models, have been demonstrated with a limited number of events. A further extension of these works to a larger number of events is required.

Genetic algorithms are implemented as an efficient tool for the minimisation of the modelling errors. However, the genetic algorithm field is changing rapidly, and an

extension of this work to incorporate the latest techniques to hydrological environments could be useful. In particular using genetic algorithm in a parallel-processing environment (connected computers) with the aid of powerful and fast computer facilities is recommended.

In order to fully realise the benefits of group calibrated TF models, establishment of an extensive database of flow, rainfall and antecedent catchment conditions is necessary.

The proposed updating techniques only use magnitude error to update the model forecast. Techniques which also consider the phase error and corresponding criteria should also be investigated.

With regard to the forecasting algorithm of the dynamic TF model, it may be necessary to establish a relationship between simulated and observed flow instead of shifting the simulated flow.

REFERENCES

(A)

Ahsan, M., and O'Conner, K. M. (1994) 'A reappraisal of the Kalman filtering technique, as applied in river flow forecasting.' Journal of hydrology, 161, pp:197-226.

Akaike, H. (1970) 'Statistical predictor identification.' Ann. Inst. Stat. Math., vol. 22, pp 203-217.

Anderson, M. G. and Burt, T. P. (1985) 'Modelling strategies.' Hydrological forecasting. John Wiley & Sons.

Anglian radar information project (1988) 'An evaluation of the influence of radar rainfall intensity resolution for real-time operational flood forecasting.' ARIP report NO. 2, Department of Civil Engineering, Salford University.

Arthanari, T. S. and Dodge, Y. (1993) 'Mathematical programming in statistics.' John Wiley & sons, Inc. 413 p.

Askew, A. J. (1989) 'Real-time inter-comparison of Hydrological models.' IAHS publ. 181.

Assaf, H. and Quick, M. C. (1991) 'Updating Hydrological model forecasts.' Can. J. Civ. Eng. Vol. 18. pp: 663-674.

Atlas, D. (1990) 'Radar in meteorology.' American Meteorological Society.

(B)

Battan, L. J. (1973) 'Radar observation of the atmosphere.' The Univ. of Chicago press 324 p.

Bergstrom, S. (1975) 'The development of a snow routine for the HBV-2 model' Nordic Hydrology 6. pp: 73-92.

Bergstrom, S. (1978) 'Spring flood forecasting by conceptual models in Sweden.' Proceedings modelling of snow cover runoff.

Bergstron, S. and Forsman, A. (1973) 'Development of a conceptual deterministic rainfall-runoff model.' Nordic Hydrology 4, pp: 147-170.

Bertoni, J. C., Tucci, C. E. and Clarke, R. T. (1992) 'Rainfall-based real-time flood forecasting.' Journal of Hydrology, 131, pp: 313-339.

Bishop, R. and Watt, W. E. (1989) 'Development of an expert system for selection of flood forecasting methods.' Can. Water Resources Journal Vol. 14, No. 3, pp: 5-17

Box, G. E. P. and Jenkins, G. M. (1976) 'Time series analysis forecasting and control.' Revised Edition, Holden day.

Bramley, E. A. (1981) 'Updating of forecasts in real time.' Severn Trent water, Trent area unit.

Bulman, P. J. and Browning, K. A. (1971) 'National Weather Radar Network.' Royal radar establishment report, Malvern, July, 17p.

Burnash, R. J. C., Ferral, R. L., and McGuire, R. A. (1973) 'A generalised streamflow simulation system-conceptual modelling for digital computers.' National weather service, NOAA, and state of California department of water resources technical report.

(C)

Cavadis, C. S. and Morin, G. 'A note on the Randomness-Dispersion diagram.' Dept. of Civil Eng. & applied Mechanics, McGill university, (personal communication).

Chatfield, C. (1989a) 'Statistics for technology: A course in applied statistics.' Third edition, Chapman and Hall.

Chatfield, C. (1989b) 'The analysis of time series, An introduction.' Fourth edition Chapman.

Chiew, F. H. S., Stewardson, M. J. and McMahon, T. A. (1993) 'Comparison of six rainfall-runoff modelling approaches.' Journal of Hydrology, 147 pp: 1-36.

Chow, V.T., Maidment, D.R. and Mays, L.W. (1988) 'Applied Hydrology.' McGraw-Hill.

Clausen, T. j. and Refsgaard, J. C. (1984) 'A Mathematical Modelling System for flood forecasting.' Nordic Hydrology 15. pp: 307-318.

Cluckie, I. D. and Han, D. (1996a) 'Development of a Physically Realisable Transfer Function (PRTF) model for real time flood forecasting.' I) Model characteristics. To be published.

Cluckie, I. D. and Han, D. (1996b) 'Development of a Physically Realisable Transfer Function (PRTF) model for real time flood forecasting.' II) Model identification. To be published.

Cluckie, I. D. and Han, D. (1996c) 'Development of a Physically Realisable Transfer Function (PRTF) model for real time flood forecasting.' III) Model updating. To be published.

Cluckie, I. D., Yu, P. S. and Tilford, K. A. (1989) 'Real-time flood forecasting, model structure and data resolution.' Proc. Seminar on weather radar networking, Brussels, Belgium.

Collier, C. G. (1989) 'Application of weather radar systems. A guide to uses for radar data in Meteorology and Hydrology.' Ellis Horwood series in Space and Space technology.

Collier, C. G. (1994) 'Precipitation estimation and forecasting.' World Meteorological Organisation commission for Hydrology, Incomplete draft.

Collier, C. G., Larke, P. R. and May, B. R. (1983) 'A weather radar correction procedure for real-time estimation of surface rainfall.' Quart. J. Royal Meteorol. Soc., 109, pp 589-608.

Colling, V. K. (1987) 'The development of weather radar in the United Kingdom in Collinge, V. K. and Kirby, C. (Eds.) 'weather radar and flood forecasting.' Wiley, Chichester, pp. 3-18.

Corradini, C., Melone, F. and Ubertini, L. (1986) 'A semi-distributed adaptive model for real-time flood forecasting.' Water Resources bulletin, American Water Resources Association Vol. 22 No. 6. pp: 1031-1038.

Correia, F. N. and Seytoux, M. (1985) 'OMEGA: A physically-based rainfall-runoff model for simulation and real-time forecast of river flows. IFAC. System Analysis Applied to Water and Related Land Resources, Lisbon; Portugal.

Cox, J. P. (1994) 'Hydrometeorological aspects of drought management.' PhD thesis, University of Salford.

Cundy, T. W. and Brooks, K. N. (1981) 'Calibrating and verifying the SSARR model-Missouri river Watersheds study.' Water Resources bulletin, American Water Resources Association Vol. 17 No. 5. pp: 775-782.

(D)

Delderfield, E. R. (1953) 'The Lynmounth flood disaster.' David and Charles Ltd, Newton Abbott.

Dobson, C. (1993) 'Forecasting flows in the Severn and Trent catchments.' BHS National meeting 23 June 1993.

Dooge, J. C. I. (1986) 'Theory of flood routing. River flow modelling and forecasting. Edited by A. D. Kraijenhoff and J. R. Moll, D. Reidel publishing Co.

(E)

Ede, P. F. and Cluckie, I. D. (1985) 'End-point use a criterion for model assessment.' IFAC Identification and System Parameter Estimation, York, UK.

(F)

Fernando, D. A. and Fernando K. S. (1989) 'Computer modelling of a Hydrological forecasting system for catchment areas.' 4th Conference on Civil and structural engineering pp: 185-196.

Fleming, G. (1975) 'Computer simulation techniques in hydrology.' Elsevier, Environmental Science series pp: 333.

(G)

Georgakakos, K. P., Rajaram, H. and Li, S. G. (1988) 'On improved operational hydrologic forecasting of stream flows.' IIHR report No. 325.

Georgakakos, K. P. and Smith, G. F. (1990) 'On improved Hydrologic forecasting-results from a WMO real-time forecasting experiment.' Journal of Hydrology, 114 pp: 17-45.

Goldberg, D. E. (1989) 'Genetic Algorithms in search, optimisation, and machine learning.' Addison-Wesley, New York, 412pp.

Grayman, W. M., and Eagleson, P. S. (1970) 'A review of the accuracy of radar and rain gauges for precipitation measurement.' Hydrodynamics Laboratory Rep. No 119, Massachusetts Institute of Technology.

Gutierrez, E. O. P. (1995) 'Real-time flood forecasting system based on precipitation forecasts.' Proceeding of the III International Symposium on Hydrological applications of weather radars. August 20-23, 1995 Sao Paulo Brazil.

(H)

Hagget, C. M., and May, B. C., and Crees, M. A. (1993) 'Advance in operational flood forecasting in London.' in: H. Verwoorm (ed.), Hydrological application of Weather Radar, Proc. Second Int. Symp. paper n2, 11.

Han, D. (1991) 'Weather radar information processing and real-time flood forecasting.' PhD thesis, University of Salford.

Han, D. (1992) 'MATH, A program for the application of PRTF model.' Software profile a user manual for MATH. Water Resources Research Group. Department of civil engineering, University of Salford.

Harpin, R. (1982) 'Real time flood routing with particular emphasis on linear methods and recursive estimation techniques.' PhD thesis, University of Birmingham.

Havno, K., Brorsen, M. and Refsgaard, J. C. (1985) 'Generalised mathematical modelling system for flood analysis and flood control design.' 2nd International Conference on the Hydraulics of floods & flood control. Cambridge, England: 24-26 Sep., 1985.

Hendrickson, J. and Sorooshian, S. (1990) 'Rainfall-runoff forecasting of desert flash floods.' Hydraulic Engineering. pp: 986-991.

Hino, M. and Kin, C. H. (1986) 'Non-linear flood forecasting by the filter separation AR method.' Journal of Hydrology, 88 pp: 165-184.

Horton, R. E., (1935) 'Surface runoff phenomena: part I, Analysis of the hydrograph.' Horton Hydrol. Lab. pub. 101. (Ann Arbor, Mich.: Edwards Bros. Inc.

(J)

Jakeman, A. J., Littlewood, I. G. and Whitehead, P. G. (1990) 'Computation of the instantaneous unit hydrograph and identifiable component flows with application to two small upland catchments.' Journal of Hydrology, 117, 275-300.

Jakeman, A. J. and Hornberger, G. M. (1993) 'How much complexity is warranted in a rainfall-runoff model?' Water Resources Research, Vol. 29 No. 8 pp: 2637-2649.

Janacek, G. and Swift, L. (1993) 'Time series, forecasting, simulation, applications.' Ellis Horwood. p: 28.

(I)

Ibbitt, R., Woods, P., Leong, D. C. and Gorling, D. G. (1990) 'Real-time flood forecasting in New Zealand.' Hydraulic Engineering. pp: 998-1003.

(K)

Kamen, E. (1987) 'Introduction to signals and systems.' Chapter 13, State representation. MacMillan publishing company.

Karunanith, N., Grenney, W. J. Whtley, D. and Bovee, K. (1994) 'Neural Networks for river flow prediction.' Journal of Computing in Civil Engineering, Vol. No. 2 pp: 201-220.

Krzysztofowicz, R. (1995) 'Recent advances associated with flood forecasting and warning systems.' Reviews of Geophysics, Supplement, pp: 1139-1147.

Kuhnke, B. and Nguyen, T. (1977) 'Modification of the SSARR watershed model for flow forecasting in Alberta.' Presented at Canadian Hydrology Symposium '77 Floods' Edmonton, Alberta, Aug. 29-31, 1977.

(L)

Lawrence, D. (1991) 'Hand book of Genetic Algorithm.' Van Nastrand Reinhold New York.

Lees, M., Young, P., Ferguson, S., Beven, K. and Burns, J. (1994) 'An adaptive flood warning scheme for the river Nith at Dumfries.' 2nd International Conference on River Flood Hydraulics, White, W. R. and Watts, J. (Eds.), HR Wallingford, John Wiley & Sons Ltd.

Ljung, L. (1987) 'System identification theory for the user.' Prentice-Hall information and system Sciences series.

Linsley, Jr. R. K., Kohler, M. A. and Paulhus, J. L. H. (1983) 'Hydrology for Engineers.' Third edition McGraw-Hill & MeiYa publication, Inc. Taipei.

Liong, S. Y., Chan, W. T. and Shreeram, J. (1995) ' Peak-flow forecasting with Genetic Algorithm and SWMM.' Journal of Hydraulic engineering Vol. 121 No. 8 pp: 613-617.

Lundberg, A. (1982) 'Combination of a Conceptual Model and an Auto regressive Error Model for Improving Short Time Forecasting.' Nordic Hydrology, 1982, pp: 233-246.

(M)

Manley, R. E., Douglas, J. R. and Pirt, J. (1980) 'Conceptual models in a flow forecasting system.' IAHS- Proceeding of the Oxford Symposium. AISH publ. No. 129.

Marino, L. and Crawford, N. H. (1990) 'Stream flow forecasting, experiences in development of customised system for hydropower operations.', Hydraulic Engineering pp: 992-997.

Martinec, J. and Rango, A. (1989) 'Effects of climate change on snow melt runoff patterns.' Remote sensing and large scale global processes. IAHS publication No. 186, Edited by A. Rango.

McCarthy, G. T. (1938) 'The unit hydrograph and flood routing.' unpublished paper presented at the conference of the North Atlantic Division, Corps of Engineers, printed by U. S. Army, New London, Connecticut, 24 June 1938. printed by U. S. Engr. Office, Providence, Rhode Island.

Mie, G. (1908) 'Beitrage Zur Optik truber Medien, Speziell Kolloidaler Metallosungen.' (Contributions to the Optics of suspended Media, specifically Colloidal Metal suspensions.) Ann. Phys., (Leipzig), 25, pp: 377-445.

Moore, R. J. (1980) 'Real-time forecasting of flood events using transfer function noise models.' Part 2, A report on work carried out under contract to the Water Research Centre, Medmenham, UK. Institute of Hydrology, Wallingford.

Moore, R. J. (1993) 'Real-time flood forecasting systems: perspectives and prospects.' British-Hungarian workshop on flood defence, Budapest, 6-10 Sept. 1993, 51 pp.

Moore, R. J. and O'Connell, P. E. (1978) 'Real-time forecasting of flood events using transfer function noise model.' Part 1. A report on work carried out under contract to the Water Research Centre, Medmenham, UK. Institute of Hydrology, Wallingford.

Murthy, K. V. R., Gupta, P. K., Kshirsagar, M. M. and Tongaonkar, S. A. (1989) 'Electronic analogue computer for flood forecasting for Tapi basin.' Journal Institute Engineering (India) C. Eng. Div. V. 70, Pt. 1 pp: 5-15.

(N)

NAG (1990) Numerical Algorithm Group limited

Nagumo, J. I. and Noda, A. (1967) 'A learning Method for System Identification.' IEEE Transactions on Automatic control, Vol. Ac-12, No. 3. pp: 282-287.

Nalbantis, I. (1995) 'Use of multiple time-step information in rainfall-runoff modelling.' Journal of Hydrology 165, pp: 135-159.

Nash, J. E., and Sutcliffe, J. V. (1970) 'River flow forecasting through conceptual models, part I- a discussion of principles.' Journal of Hydrology, No. 10 pt. 3 pp 282-290.

Nemec, J. (1986) 'Hydrological forecasting.' D. Reidel publishing company.

NERC (National Environment Research Council) (1975) 'UK flood studies report.' Whitefriars press, London.

Norreys, R. J. and Cluckie, I. D. (1994) 'Neural network modelling of urban drainage systems.' report for North West Water ltd, Dept. Civil Eng. University of Salford.

Norton, J. P. (1986) 'An introduction to identification.' Academic press.

Novotny, V. and Zheng, S. (1989) 'Rainfall-runoff transfer function by ARMA modelling.' Journal of Hydraulic Engineering, Vol. 115, No. 10. American Society Civil Engineering.

(O)

O'Connell, P. E. and Clarke, R. T. (1981) 'Adaptive hydrological forecasting- A review.' Hydrological Sciences-Bulletin-des science Hydrologiques. 26, 2, 6 pp: 179-205.

Olason, T. and Watt, W. E. (1986) 'Multivariate transfer function-noise model of river flow for hydropower operation.' Nordic Hydrology, 17, pp: 185-202.

Owens, M. D. (1986) 'Real-time flood forecasting using weather radar data.' PhD thesis. University of Birmingham.

(P)

Pade, H. (1982) 'Sur la Representation Aprochee d' une fonction par des fractions rationelles, Anales scientifique du lecole Normal spuperieure, 3rd series (suppl), vol. 9, pp 519-593.

Pearse, I. (1993) 'Flood warning in the North West.' A paper presented in IWEM Warrington 9th Sept. 1993.

Plackett, R. L. (1950) 'Some theorems in least squares.' Biometrika, Vol 37, pp: 149-157.

Plate, E. J., Ihringer, J. and Lutz, W. (1988) 'Operational models for flood calculations.' Journal of Hydrology, 100 pp: 489-506.

Poularikas, A. D. and Seely, S. (1991) 'Signals and systems.' PWS-KENT publishing Company.

Powell, S. M. (1985) 'River basin models for operational forecasting of flow in real-time.' PhD thesis. University of Birmingham.

Powell, S. M. and Cluckie, I. D. (1985) 'Mathematical Hydraulic models for the real-time analysis of floods.' 2nd International Conference on the Hydraulics of floods and Flood Control.' Cambridge, England: 24-26 Sep. 1985.

Probert-Jones, J. R. (1962) 'The radar equation in meteorology.' Q. J. R. M. S., 88, pp: 485-495.

(Q)

Quick, M. C. and Pipes, A. (1976) 'A combined snow melt and rainfall-runoff model.' Can. J. Civ. Eng. 3. pp: 449-460.

Quick, M. C. and Pipes, A. (1977a) 'U. B. C. Watershed model.' Hydrological Sciences-bulletin XXII, 1, 3. pp: 153-161.

Quick, M. C. and Pipes, A. (1977b) 'Snow melt floods in mountain catchments.' Presented at the Canadian Hydrology Symposium 'Floods 77' Sponsored by the Assoc. committee on Hydrology National Research Council, Edmonton, Alberta, Aug. 29-31.

(R)

Ramos, J., Mallants, D. and Feyan, J. (1995) 'State-space identification of linear deterministic rainfall-runoff models.' Water Resources research, Vol. 31, No. 6 pp: 1519-1531.

Rango, A. (1980) 'Remote sensing of snow covered area for runoff modelling.' IAHS-AISH publ. No. 129. Proceeding of Oxford Symposium. pp: 291-297.

Reed, D. W. (1984) 'A review of British flood forecasting practice.' Institute of Hydrology. Report No. 90.

Reed, D. W. and O'Connell, P. E. (1980) 'Models for real-time flow forecasting.' Institute of Hydrology, Colloquium on real-time River Flow Forecasting held at WRC Medmenham Laboratory.

Refsgaard, J. C., Rosbjerg, D. and Markussen, L. M. (1983) 'Application of the Kalman filter to real-time operation and to uncertainty analyses in hydrological modelling.' IAHS publ. No. 147 pt:147 pp: 273-282, Scientific procedures applied to the

planning, design and management of water Resources Systems (Proceeding of the Hamburg Symposium.)

Ruck, G. T. and others (1970) 'Radar cross section hand-book.' Plenum press New York 472 p.

Rungo, M., Refsgaard, J. C. and Havno, K. (1989a) 'Improvement of the updating routine in the MIKE11 modelling system for real-time flood forecasting.'

Rungo, M., Refsgaard, J. C. and Havno, K. (1989b) 'The updating procedure in the MIKE11 modelling system for real-time forecasting.' Proceeding of the International Symposium on Hydrological application on weather radar. pp: 497-508.

(S)

Schultz, G. A. (1988) 'Remote sensing in Hydrology.' Journal of Hydrology 100, pp: 239-265.

Serban, P. and Askew, A. J. (1991) 'Hydrological forecasting and updating procedures.' Hydrology for the Water Management of Large River Basins, Proceeding of the Vienna Symposium, Agu. 1991. IAHS publ. No. 201. pp: 357-369.

Shepherd, G. W. (1987) 'On the utilisation of weather radar in the simulation of urban drainage networks.' PhD thesis, Dept. of Civil Engineering, University of Birmingham, 240 p.

Shaw, E. M. (1994) 'Hydrology in practice.' third edition, Chapman and Hall 569 pp.

Sherman, L. K. (1932) 'Stream flow from rainfall by the unit graph method.' Engineering News Record, Vol. 108, pp: 501-505.

Simpson, R. J., Wood, T. R. and Hamlin, M. J. (1980) 'Simple self-correcting models for forecasting flows on small basins in real-time.' IAHS-AISH publ. No. 129. Hydrological forecasting proceedings of the Oxford Symposium.

Sugawara, M. (1961) 'On the analysis of runoff structure about several Japanese rivers.' Japan journal Geophysics, V. 2 pt. 4.

Sugawara, M. et al (1986) 'Tank model programs for personal computer.'

Suyanto, A. and O'Connell, P. E. (1995) 'The influence of storm characteristics and catchment conditions on extreme flood response: A case study based on the Brue river basin, UK.' Surveys in Geophysics 16 pp: 201-225.

(T)

Tilford, K. A. (1987) 'Real-time flood forecasting using low intensity resolution radar rainfall data.' MSc thesis Dept. of Civil Engineering, University of Birmingham.

Tilford, K. A. (1990a) 'TFCAL (Transfer Function CALibration), Software profile, A user manual for TFCAL, A program for the identification and calibration of a simple linear transfer function model using a recursive least square algorithm.' Dept. of civil engineering, Salford University.

Tilford, K. A. (1990b) 'TFFOR (Transfer Function FORecasting), Software profile, A user manual for TFFOR, A program for the validation and testing of real-time transfer function models using detailed error analysis and incorporating the delta updating technique.' Dept. of civil engineering, Salford University.

Tilford, K. A. (1992) 'Weather radar data for operational Hydrology.' PhD thesis, Dept. of Civil Engineering, Salford University.

Todini, E. (1978) 'Using a desk-top computer for an on-line flood warning system.' IBM J. Develop. Vol. 22 No. 5. pp: 464-471.

Todini, E. (1988) 'Rainfall-runoff modelling-past, present and future.' Journal of Hydrology, 100 pp: 341-352.

Tsang, F. C., Young, P. C. and Beven, K. J. (1995) 'A comparison of the use of radar and rain gauge data in flow forecasting of the River Ribble, Lancashire.' Proceeding of the Hydrological uses of weather radar, B. H. S. occasional paper No. 5.

(U)

Unbehauen, H. and Gohring, B. (1974) 'Tests for determining model order in parameter estimation.' Automatica, Vol. 10, pp: 233-244.

(V)

Vadaele, W. (1983) 'Applied time series and Box Jenkins models.' Academic press, Inc.

Viner, D. (1992) 'The Hydrological utilisation of the Frontiers system.' PhD thesis. Civil engineering dept. University of Salford.

(W)

Wanielista, M. (1990) 'Hydrology and water quantity control.' John Wiley and Sons.

Wilke, K. and Barth, F. (1991) 'Operational river-flood forecasting by Wiener and Kalman filtering.' IAHS publ. No. 201. Hydrology for the water management of large river basin, Vienna symposium.

WMO (1975) 'Inter-comparison of conceptual models used in operational hydrological forecasting.' WMO No. 429. Operational Hydrology report No. 7

WMO (1986) 'Inter-comparison of models of snow melt runoff.' WMO No. 646. Operational Hydrology report No. 23.

WMO (1987) 'Real-time inter-comparison of Hydrological models.' Technical report to the commission for Hydrology No. 23. WMO/TD No. 255.

WMO (1991) 'Simulation real-time inter-comparison of hydrological models.' 'first draft'.

WMO (1992) 'Simulation real-time inter-comparison of hydrological models.' WMO No. 779. Operational hydrology report No. 38.

WRIP (Weather Radar Information Processor) (1994) ' A program for the real-time radar information processing and flood forecasting.' Software profile, WRIP user's guide, Water Resources Research Group Dept. of Civil Engineering, University of Salford.

Wyman, B. F., Sain, M. K., Conte, G. and Perdon, A. M. (1989) 'On the zeros and poles of a transfer function.' Linear algebra and its applications 122/123/124 pp: 123-144. Elsevier Science publishing Co.

(Y)

Yapo, P. and Sorooshian, S. (1993) 'A Markov chain flow model for flood forecasting.' Water Resources Research, Vol. 29. No. 7 pp: 2427-2436.

Young, P. C. (1986) 'Time-series methods and recursive estimation in Hydrological systems analysis.' River flow modelling and forecasting, edited by D. A. Kraijenhoff and J. R. Moll. pp: 129-180. D. Reidel publishing Company.

Young, P. C. (1992) 'Parallel processes in Hydrology and water quality: A unified time-series approach.' J. IWEM.

Young, P. C. and Beven, K. J. (1994) 'Data-based mechanistic modelling and the rainfall-flow non-linearity.' Environmetrics, Vol. 5, pp: 335-363.

Yu, P. S. (1989) 'Real-time Grid based distributed rainfall-runoff model for flood forecasting with weather radar.' PhD thesis. University of Birmingham.

Yuan, J. (1994) 'Hydrological modelling with weather radar in urban drainage systems.' PhD thesis, Dept. of Civil Engineering, University of Salford.

APPENDIX 1
ERROR ANALYSIS

A.1.1 Introduction

Randomness-dispersion diagram (a valuable tool to comparison the model performance) is introduced in this appendix. In order to understand the principle of technique first some basic statistical concepts should be considered.

A.1.2 Auto correlation functions

The correlation is an indicator of the degree of dependency of a variable to another variable. Sample auto correlation coefficient provides an important guide to the properties of a time series. Given N observations $X_1, X_2, \ldots\ldots, X_N$ on a discrete time series, (N-1) pairs of observations exist (i.e. X_1, X_2, and $X_2, X_3, \ldots\ldots X_{N-1}$, X_N).

The degree of dependency between each variable in a pair is obtained by: (see for example Chatfield, 1989)

$$r_1 = \frac{\sum_{t=1}^{N-1}(x_t - \bar{x}_1)(x_{t+1} - \bar{x}_2)}{\sqrt{\left[\sum_{t=1}^{N-1}(x_t - \bar{x}_1)^2 \sum_{t=1}^{N-1}(x_{t+1} - \bar{x}_2)^2\right]}} \qquad \text{(A.1.1)}$$

where:

$\bar{x}_1 = \dfrac{\sum_{t=1}^{N-1} x_t}{N-1}$ is the mean of the first (N-1) observations.

$\bar{x}_2 = \dfrac{\sum_{t=2}^{N-1} x_t}{N-1}$ is the mean of the last (N-1) observations

The coefficient r_1 measures correlation between successive values and is called an auto correlation coefficient or serial correlation coefficient.

It is supposed that $\tilde{x}_1 \approx \tilde{x}_2$ and N/N-1 ≈ 1 for large N, therefore equation A.1.1 may be simplified to:

$$r_1 = \frac{\sum_{t=1}^{N-1}(x_t - \bar{x})(x_{t+1} - \bar{x})}{\sum_{t=1}^{N-1}(x_t - \bar{x})^2} \tag{A.1.2}$$

In same manner, the correlation between observation a distance K apart is given by:

$$r_k = \frac{\sum_{t=1}^{N-k}(x_t - \bar{x})(x_{t+1} - \bar{x})}{\sum_{t=1}^{N-1}(x_t - \bar{x})^2} \tag{A.1.3}$$

which is the auto correlation at lag K.

In practice, the auto correlation coefficients is calculated by computing the series of autocovarince coefficient C_K. Covariance itself is same as variance except first the mean value is subtracted from the original variables. Therefore C_K can be calculated as:

$$c_k = \frac{1}{N}\sum_{t=1}^{N-k}(x_t - \bar{x})(x_{t+k} - \bar{x}) \tag{A.1.4}$$

then:

$$r_k = \frac{c_k}{c_0} \tag{A.1.5}$$

A.1.3 The portmanteau statistic

Besides the auto correlation coefficients individually, usually a series of autocorrelations of the variables taken as a whole is investigated. It is proved (Box and Jenkins 1976) that the model is appropriate if:

$$Q = N.\sum_{k=1}^{k} r_k^2 \tag{A.1.6}$$

is distributed approximately as chi-squared (λ^2) with (k-p-q) degrees of freedom. where p and q are the number of flow and rainfall parameters in the TF model and (Q) is the portmanteau static. An observed value of Q is compared with a table of the percentage

points of λ^2 (see table A.1.1) to judge whether the model is appropriate. Ljung and Box (1978) introduced a modified version of formula (A.1.6) as:

$$Q = N(N+2)\sum_{k=1}^{k}\frac{r_k^2}{N-k} \tag{A.1.7}$$

A.1.4 NTD criterion

A standardised measure of the magnitude of the model errors can be provided by computing the NTD as:

$$NTD_1 = 1-\left[\frac{\sum\left(y_{o,1}-y_{f,1}\right)^2}{\sum\left(y_{o,1}-y_{Nf,1}\right)^2}\right] \tag{A.1.8}$$

where

$y_{o,1}$ = observed flow at time t+1.

$y_{f,1}$ = one step-ahead forecast for time t+1.

$y_{Nf,1}$ = one step-ahead for time t+1 as computed by a 'naive' model.

In a naive model flow forecasted for time t+1 equals flow observed at time t.

A.1.5 Example

The randomness-dispersion diagram can be interpreted through the following example. Consider a data set comprising of 25 value which is modelled by say, a (3,4) (p=3, q=4) transfer function model. The number of degrees of freedom for the λ^2 distribution is therefore [25-(3+4)]=18. This corresponds to a critical λ^2 value of 28.9 at the 5% confidence level.

Point a on figure A.1.1 represents perfect model performance. An NTD_1=1 indicates zero forecast error, whilst a $\frac{Q}{\lambda^2}$ value of zero denotes a complete absence of auto correlation in the residuals.

Consider the following two scenario for the data series:

I. Q=23.1. Then $\frac{Q}{\lambda^2}$ =0.80

Assume NTD_1=0.71

This point is marked b on figure A.1.1.

ii. Q= 5.8. Then $\frac{Q}{\lambda^2}$ =0.2

Assume NTD_1 =0.30

This point is marked c on figure A.1.1.

Point b represents smaller forecast errors (as indicated by the NTD criterion) and higher auto correlation of the model residuals-though still random (as measured by the $\frac{Q}{\lambda^2}$ statistic).

It is noted that from hydrological point of view the NTD criterion is more crucial since the magnitude of the forecast errors in flood forecasting is the most important single factor.

Point d indicates significant auto correlation of the forecast residuals. A non-random structure suggests inadequate model performance: it is likely that the model is inappropriate for the data. A negative NTD denotes superiority of forecasts derived by a simple naive model.

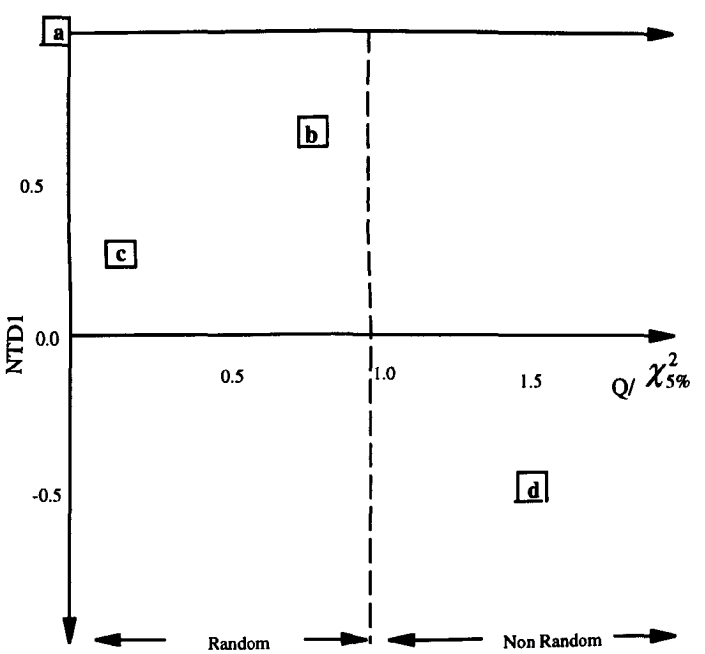

Figure A.1.1 : Example randomness-dispersion diagram

Table (A.1.1.) Distribution table

TABLE F TAIL AREAS OF THE CHI-SQUARE DISTRIBUTION

p	ε														p
	0.995	0.99	0.975	0.95	0.9	0.75	0.5	0.25	0.1	0.05	0.025	0.01	0.005	0.001	
1	—	—	—	—	0.016	0.102	0.455	1.32	2.71	3.84	5.02	6.63	7.88	10.8	1
2	0.010	0.020	0.051	0.103	0.211	0.575	1.39	2.77	4.61	5.99	7.38	9.21	10.6	13.8	2
3	0.072	0.115	0.216	0.352	0.584	1.21	2.37	4.11	6.25	7.81	9.35	11.3	12.8	16.3	3
4	0.207	0.297	0.484	0.711	1.06	1.92	3.36	5.39	7.78	9.49	11.1	13.3	14.9	18.5	4
5	0.412	0.554	0.831	1.15	1.61	2.67	4.35	6.63	9.24	11.1	12.8	15.1	16.7	20.5	5
6	0.676	0.872	1.24	1.64	2.20	3.45	5.35	7.84	10.6	12.6	14.4	16.8	18.5	22.5	6
7	0.989	1.24	1.69	2.17	2.83	4.25	6.35	9.04	12.0	14.1	16.0	18.5	20.3	24.3	7
8	1.34	1.65	2.18	2.73	3.49	5.07	7.34	10.2	13.4	15.5	17.5	20.1	22.0	26.1	8
9	1.73	2.09	2.70	3.33	4.17	5.90	8.34	11.4	14.7	16.9	19.0	21.7	23.6	27.9	9
10	2.16	2.56	3.25	3.94	4.87	6.74	9.34	12.5	16.0	18.3	20.5	23.2	25.2	29.6	10
11	2.60	3.05	3.82	4.57	5.58	7.58	10.3	13.7	17.3	19.7	21.9	24.7	26.8	31.3	11
12	3.07	3.57	4.40	5.23	6.30	8.44	11.3	14.8	18.5	21.0	23.3	26.2	28.3	32.9	12
13	3.57	4.11	5.01	5.89	7.04	9.30	12.3	16.0	19.8	22.4	24.7	27.7	29.8	34.5	13
14	4.07	4.66	5.63	6.57	7.79	10.2	13.3	17.1	21.1	23.7	26.1	29.1	31.3	36.1	14
15	4.60	5.23	6.26	7.26	8.55	11.0	14.3	18.2	22.3	25.0	27.5	30.6	32.8	37.7	15
16	5.14	5.81	6.91	7.96	9.31	11.9	15.3	19.4	23.5	26.3	28.8	32.0	34.3	39.3	16
17	5.70	6.41	7.56	8.67	10.1	12.8	16.3	20.5	24.8	27.6	30.2	33.4	35.7	40.8	17
18	6.26	7.01	8.23	9.39	10.9	13.7	17.3	21.6	26.0	28.9	31.5	34.8	37.2	42.3	18
19	6.84	7.63	8.91	10.1	11.7	14.6	18.3	22.7	27.2	30.1	32.9	36.2	38.6	43.8	19
20	7.43	8.26	9.59	10.9	12.4	15.5	19.3	23.8	28.4	31.4	34.2	37.6	40.0	45.3	20
21	8.03	8.90	10.3	11.6	13.2	16.3	20.3	24.9	29.6	32.7	35.5	38.9	41.4	46.8	21
22	8.64	9.54	11.0	12.3	14.0	17.2	21.3	26.0	30.8	33.9	36.8	40.3	42.8	48.3	22
23	9.26	10.2	11.7	13.1	14.8	18.1	22.3	27.1	32.0	35.2	38.1	41.6	44.2	49.7	23
24	9.89	10.9	12.4	13.8	15.7	19.0	23.3	28.2	33.2	36.4	39.4	43.0	45.6	51.2	24
25	10.5	11.5	13.1	14.6	16.5	19.9	24.3	29.3	34.4	37.7	40.6	44.3	46.9	52.6	25
26	11.2	12.2	13.8	15.4	17.3	20.8	25.3	30.4	35.6	38.9	41.9	45.6	48.3	54.1	26
27	11.8	12.9	14.6	16.2	18.1	21.7	26.3	31.5	36.7	40.1	43.2	47.0	49.6	55.5	27
28	12.5	13.6	15.3	16.9	18.9	22.7	27.3	32.6	37.9	41.3	44.5	48.3	51.0	56.9	28
29	13.1	14.3	16.0	17.7	19.8	23.6	28.3	33.7	39.1	42.6	45.7	49.6	52.3	58.3	29
30	13.8	15.0	16.8	18.5	20.6	24.5	29.3	34.8	40.3	43.8	47.0	50.9	53.7	59.7	30

Table of $\chi^2_\varepsilon(p)$ such that $P_r\{\chi^2(p) > \chi^2_\varepsilon(p)\}$

where:
p is the number of degrees of freedom.

APPENDIX 2

Rainfall hyetographs and runoff hydrographs

used in the thesis

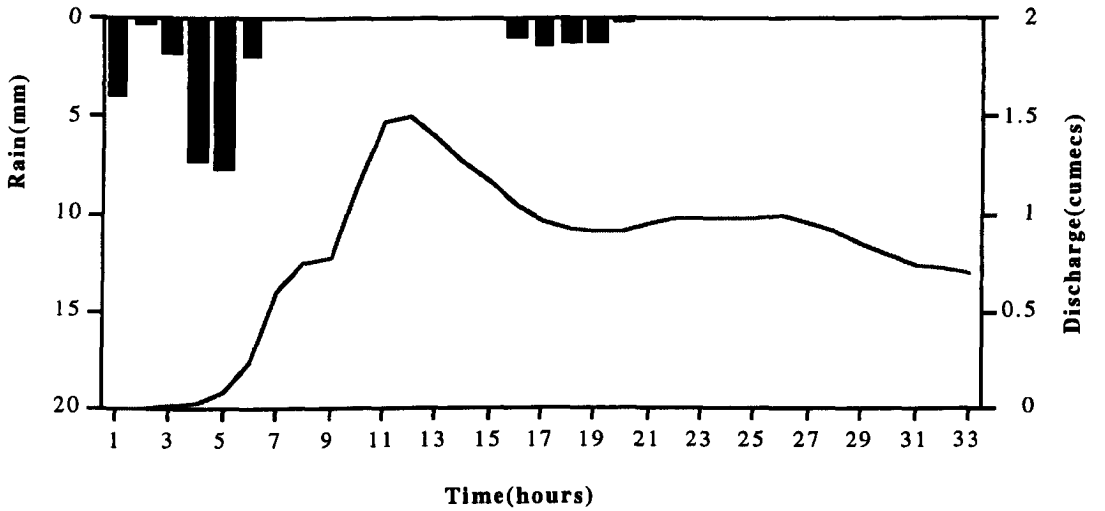

Calibration event no. 1 (5.11.73) Orgeval catchment

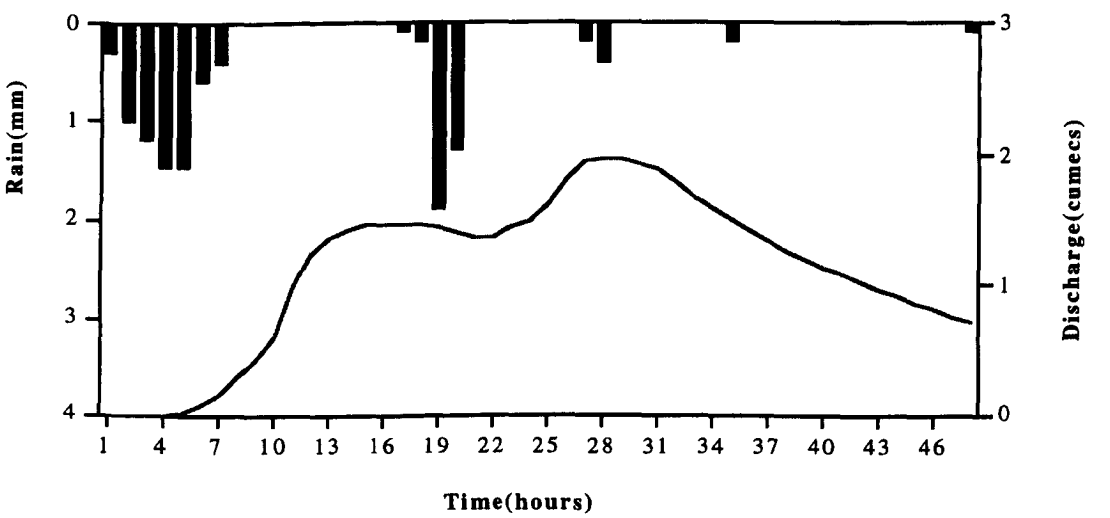

Calibration event no. 2 (7.12.73) Orgeval catchment

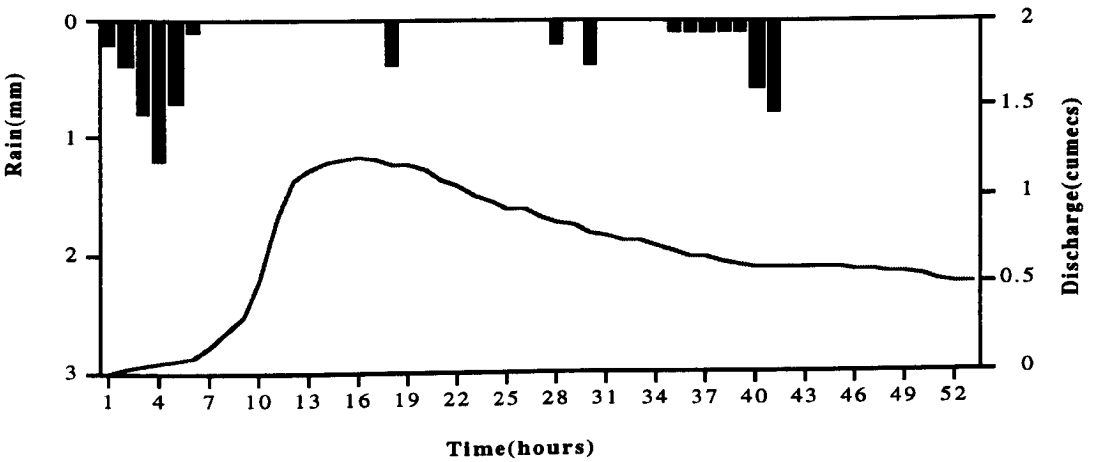

Calibration event no. 3 (13.12.73) Orgeval catchment

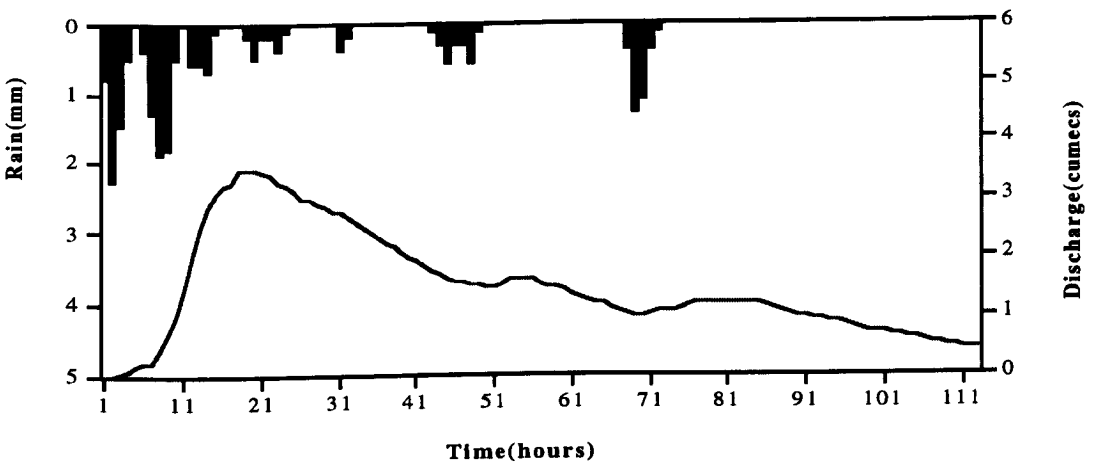

Calibration event no. 4 (21.12.73) Orgeval catchment

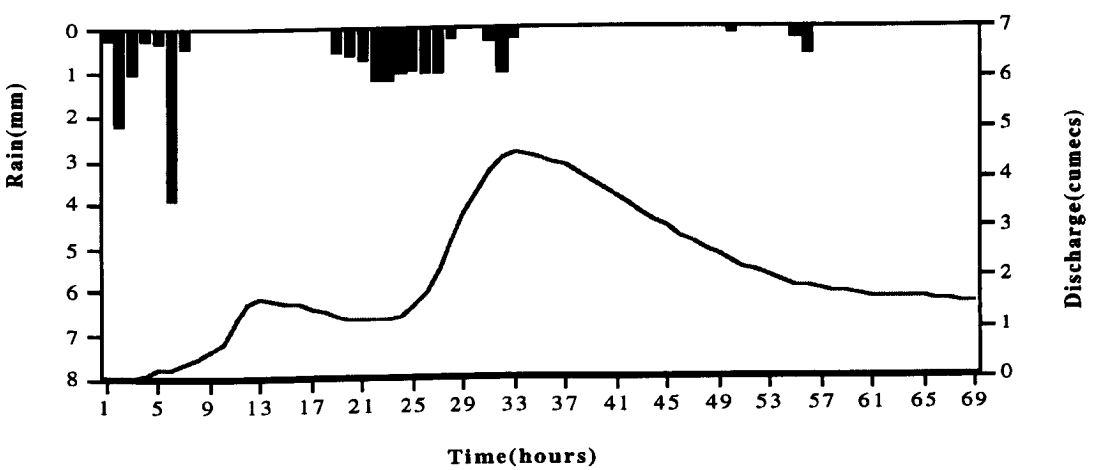

Calibration event no. 5 (8.01.74) Orgeval catchment

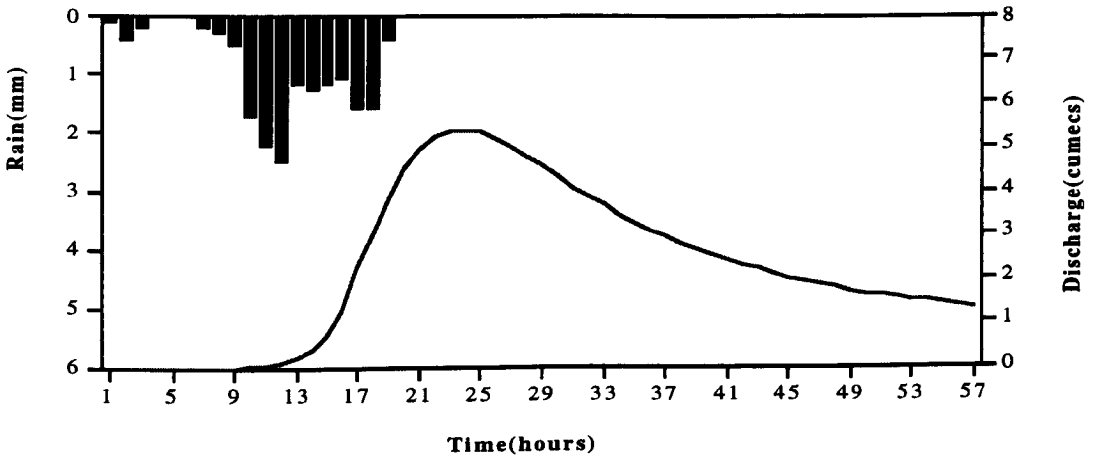

Calibration event no. 6 (28.01.74) Orgeval catchment

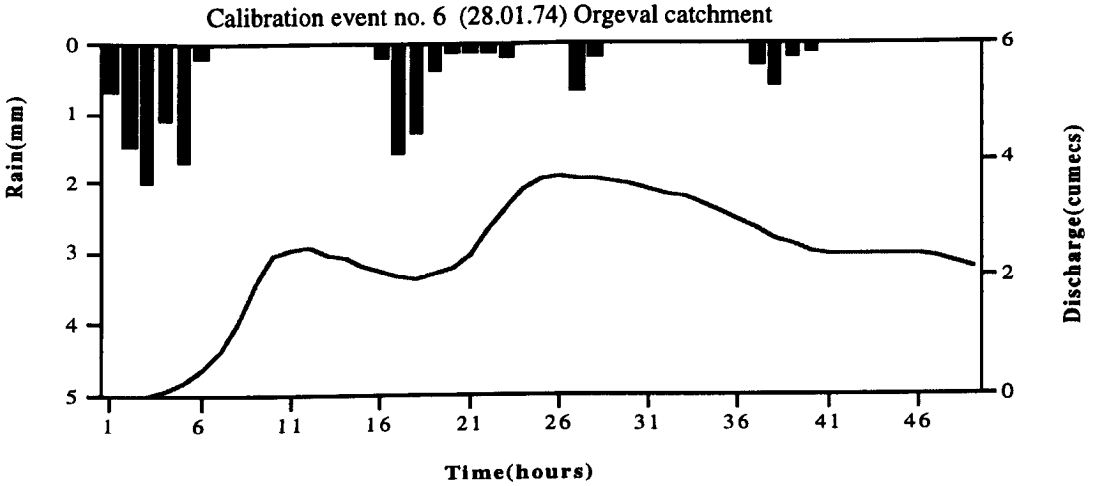

Calibration event no.7 (5.02.74) Orgeval catchment

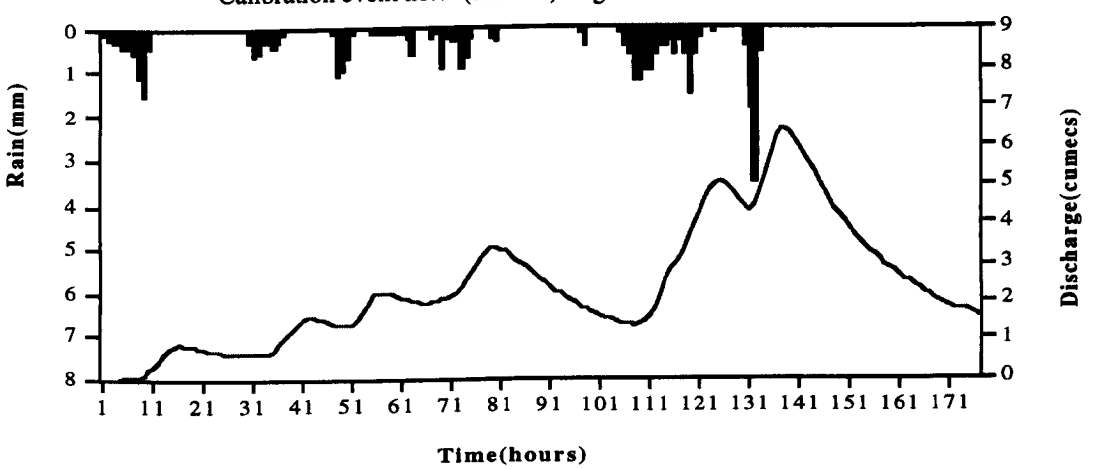

Calibration event no. 8 (15.03.74) Orgeval catchment

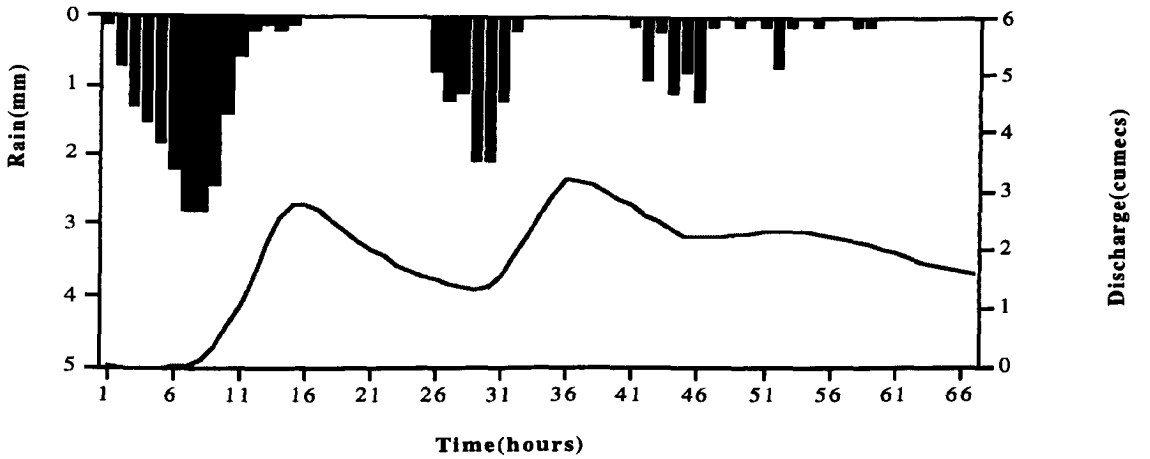

Calibration event no. 9 (18.10.74) Orgeval catchment

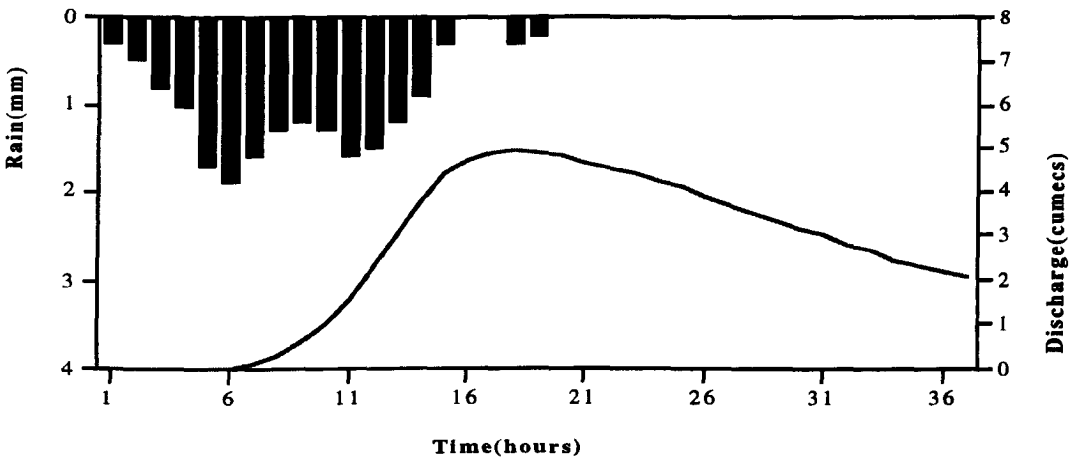

Calibration event no. 10 (23.10.74) Orgeval catchment

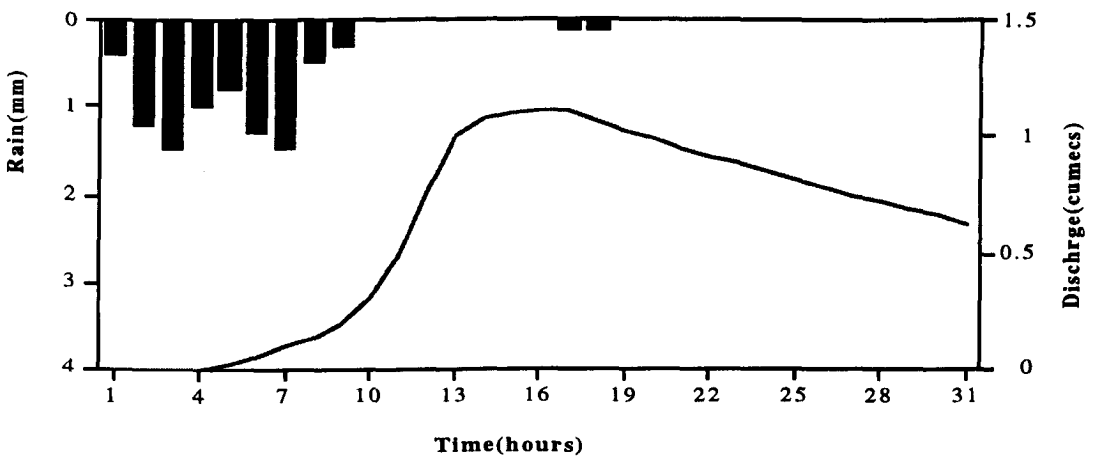

Calibration event no. 11 (3.11.74) Orgeval catchment

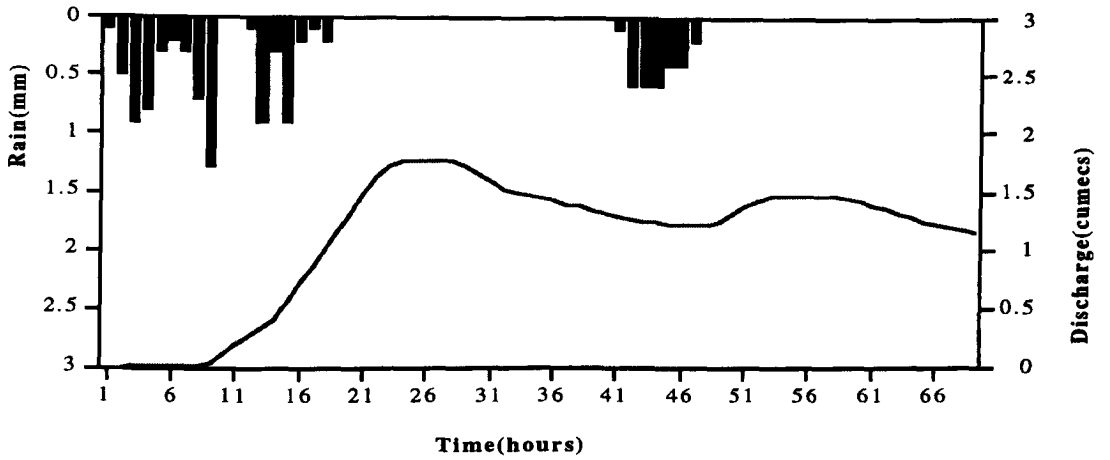

Calibration event no. 12 (21.11.74) Orgeval catchment

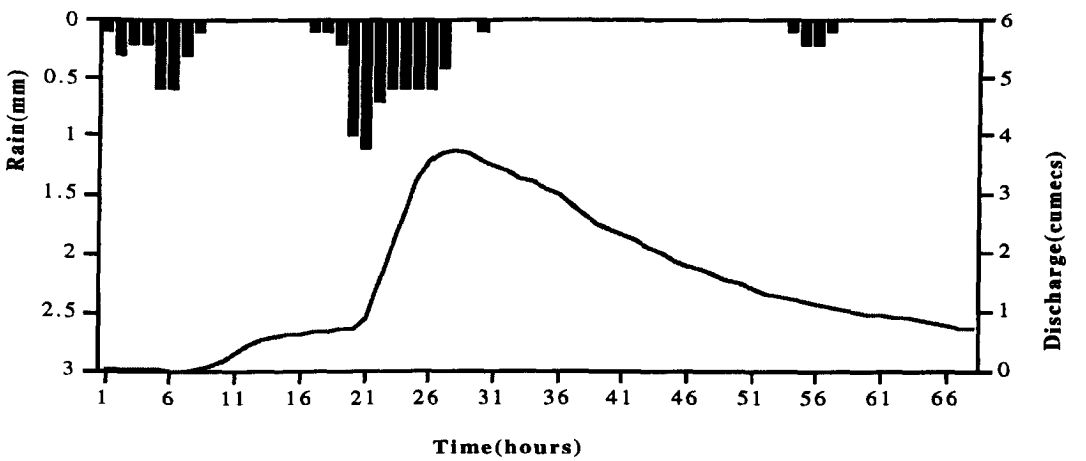

Calibration event no. 13 (16.12.74) Orgeval catchment

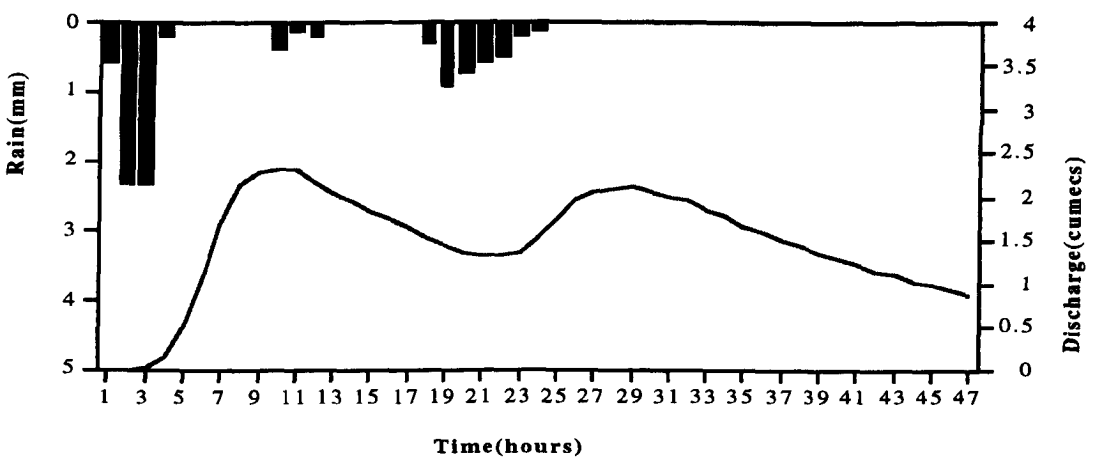

Calibration event no. 14 (27.12.74) Orgeval catchment

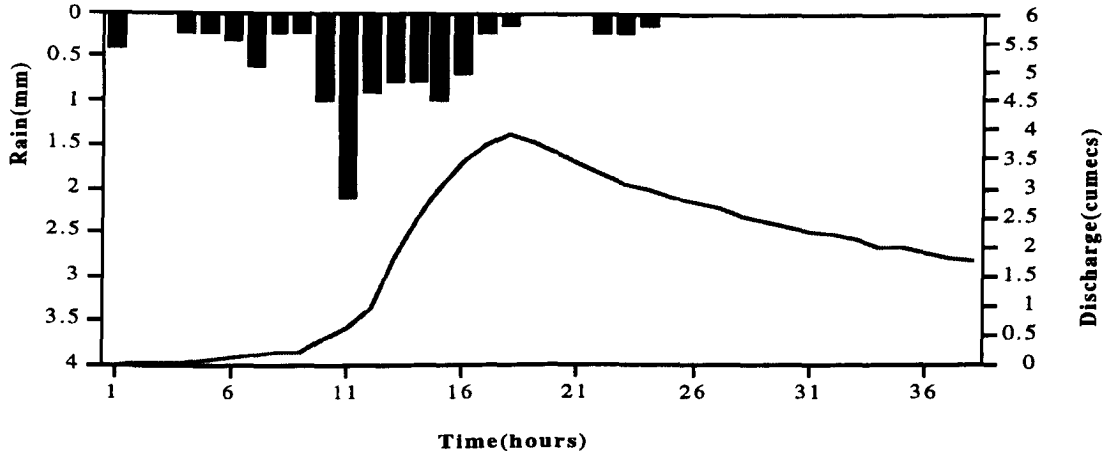

Calibration event no. 15 (7.01.75) Orgeval catchment

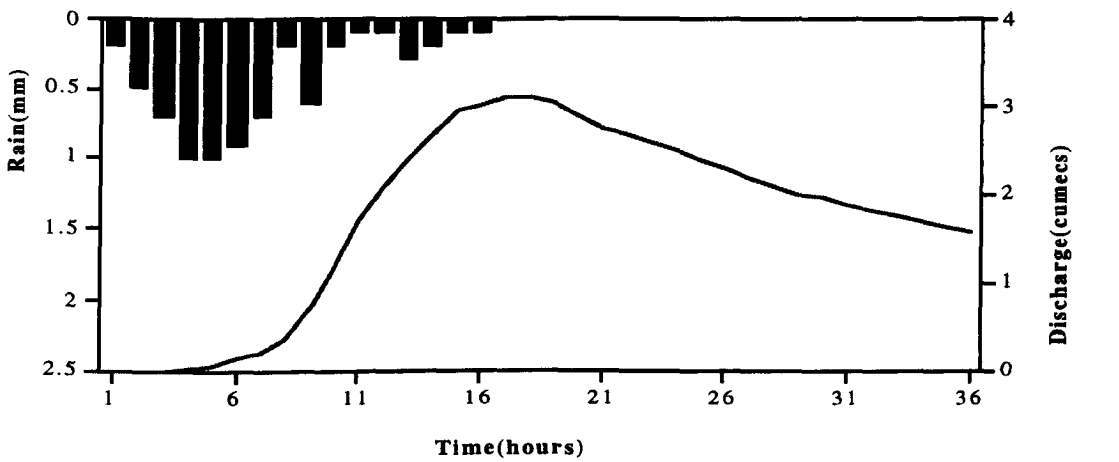

Calibration event no. 16 (22.01.75) Orgeval catchment

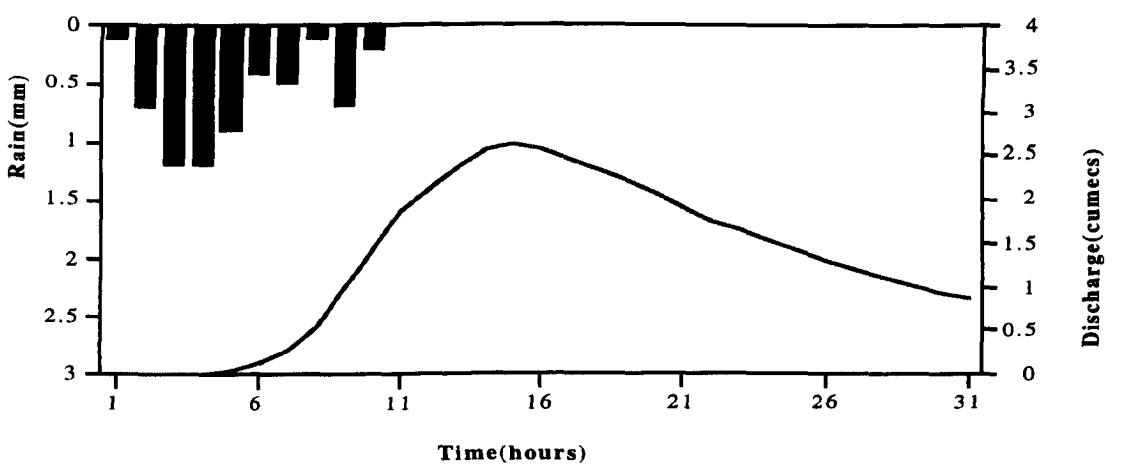

Calibration event no. 17 (25.01.75) Orgeval catchment

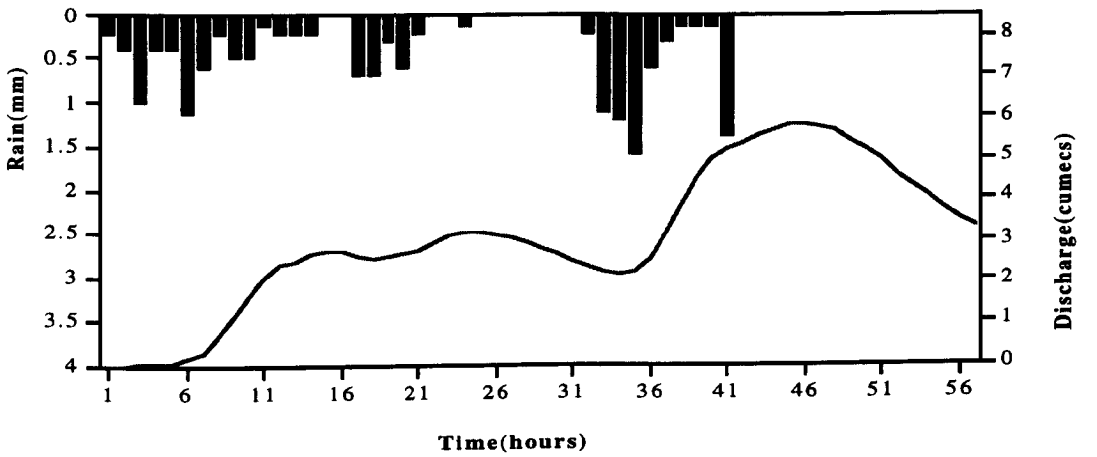

Calibration event no. 18 (27.01.75) Orgeval catchment

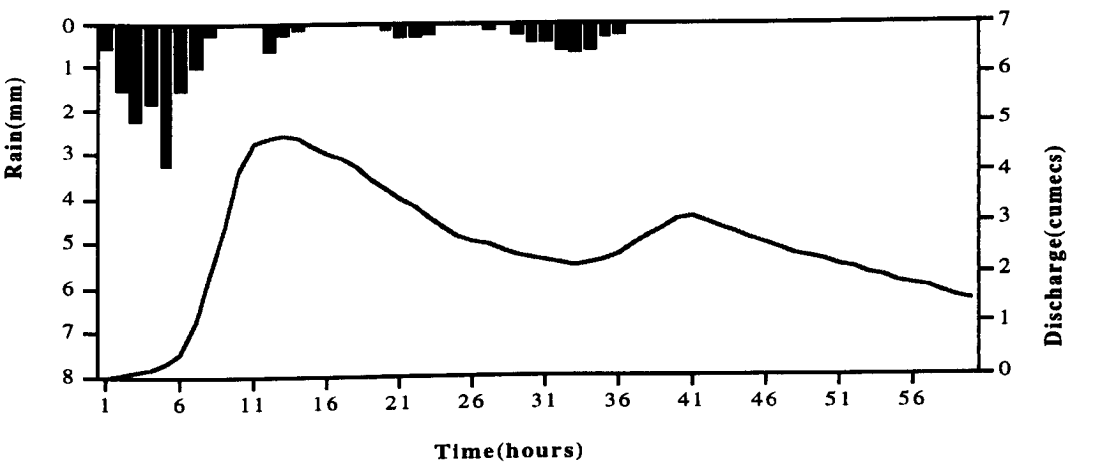

Calibration event no. 19 (11.01.78) Orgeval catchment

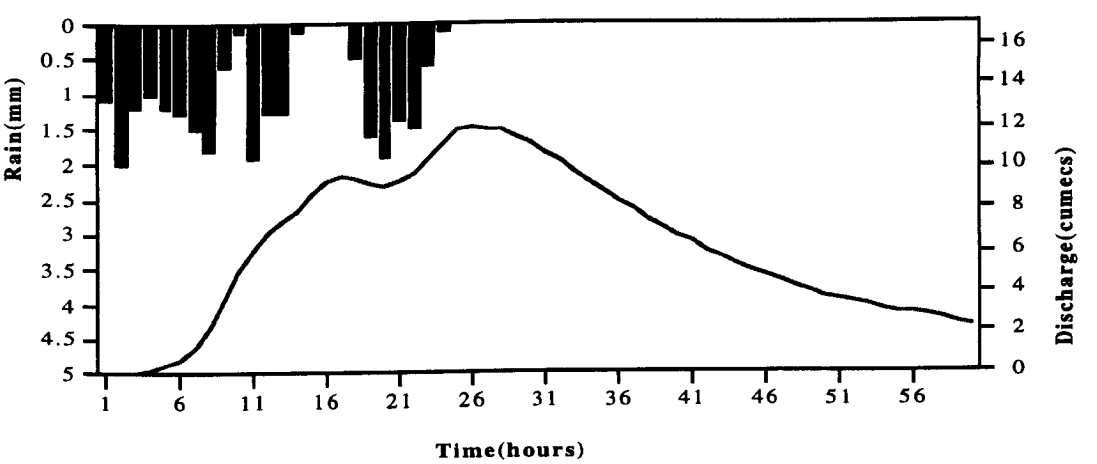

Calibration event no. 20 (23.01.78) Orgeval catchment

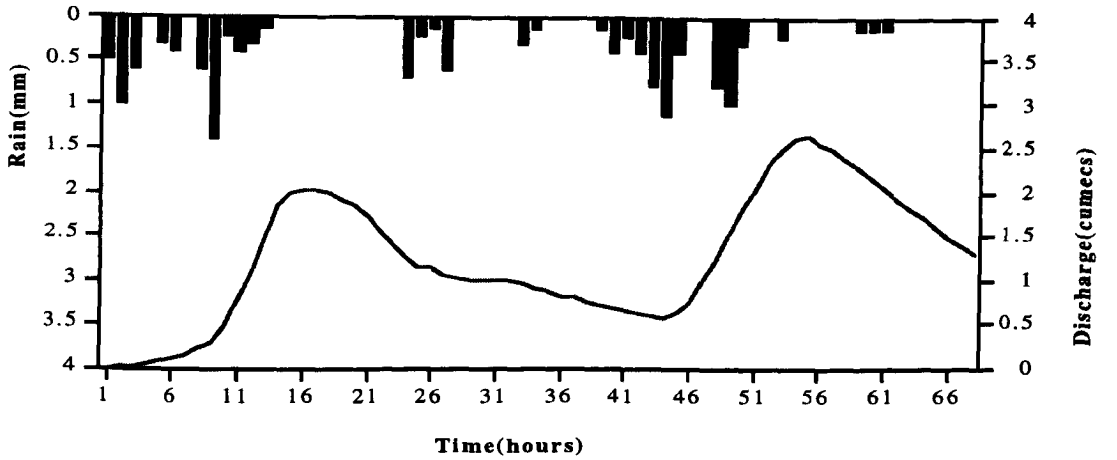

Calibration event no. 21 (28.01.78) Orgeval catchment

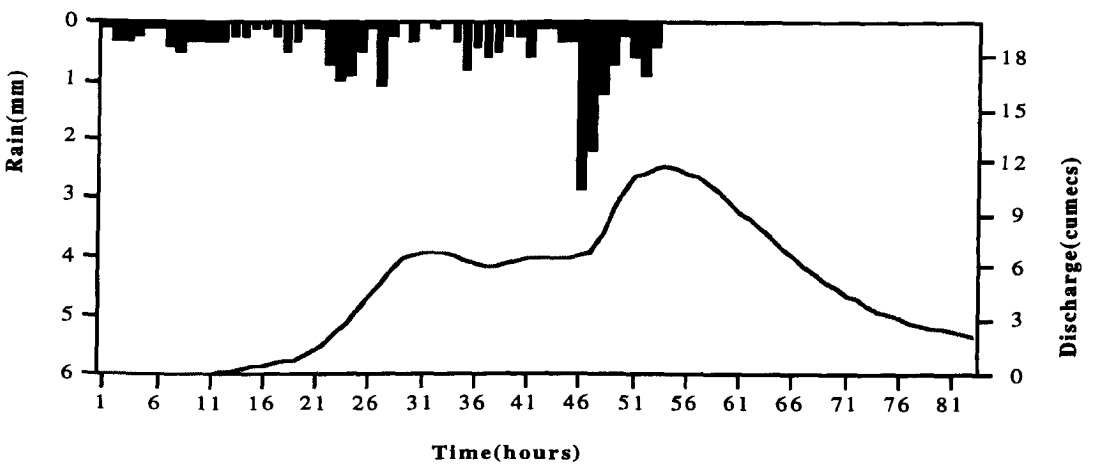

Calibration event no. 22 (31.01.78) Orgeval catchment

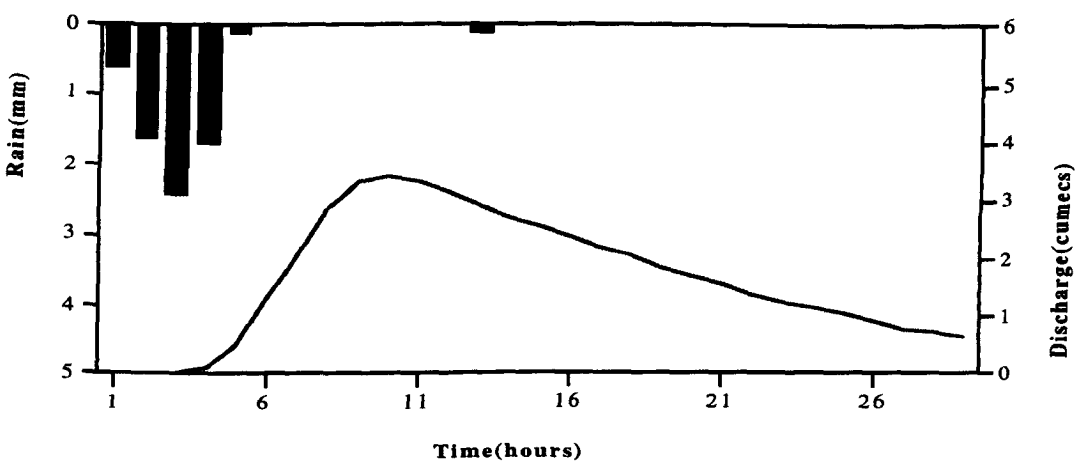

Calibration event no. 23 (7.02.78) Orgeval catchment

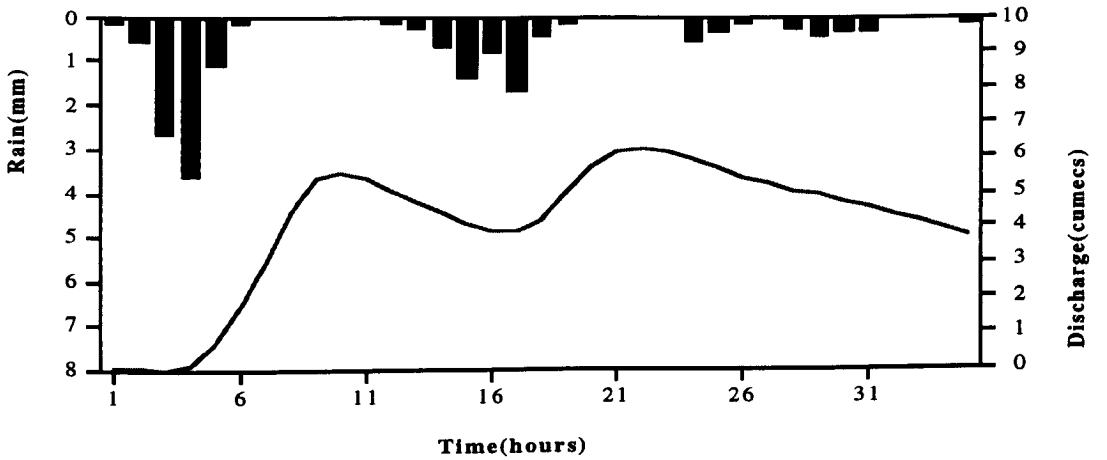

Calibration event no. 24 (16.03.78) Orgeval catchment

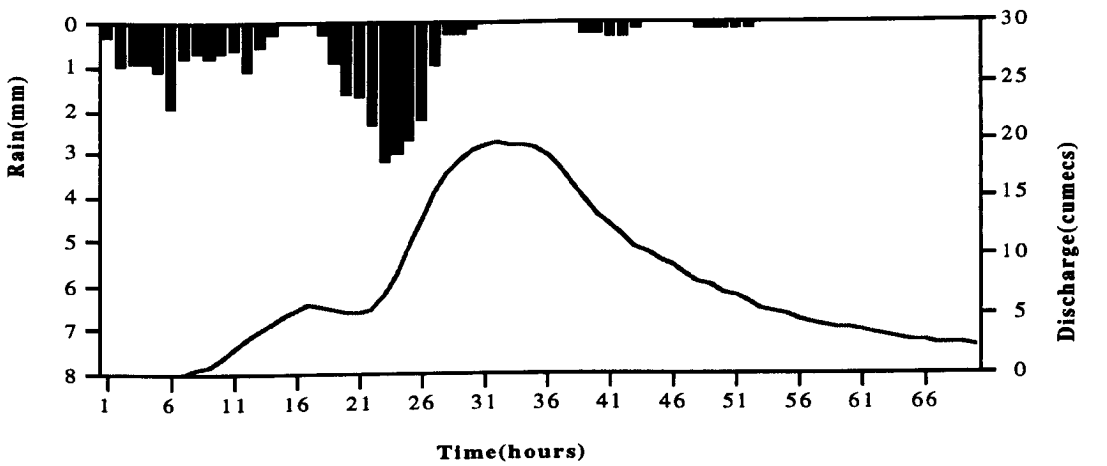

Calibration event no. 25 (19.03.78) Orgeval catchment

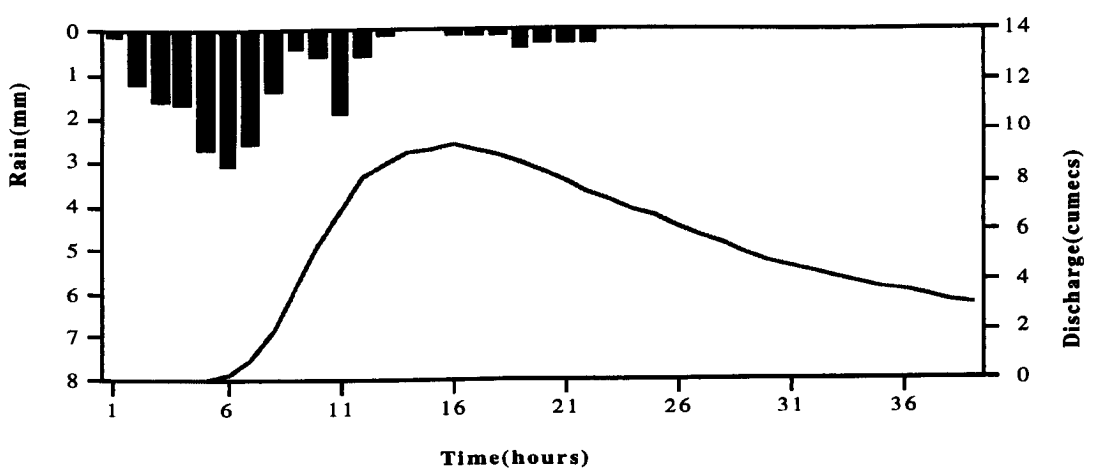

Calibration event no. 26 (29.03.78) Orgeval catchment

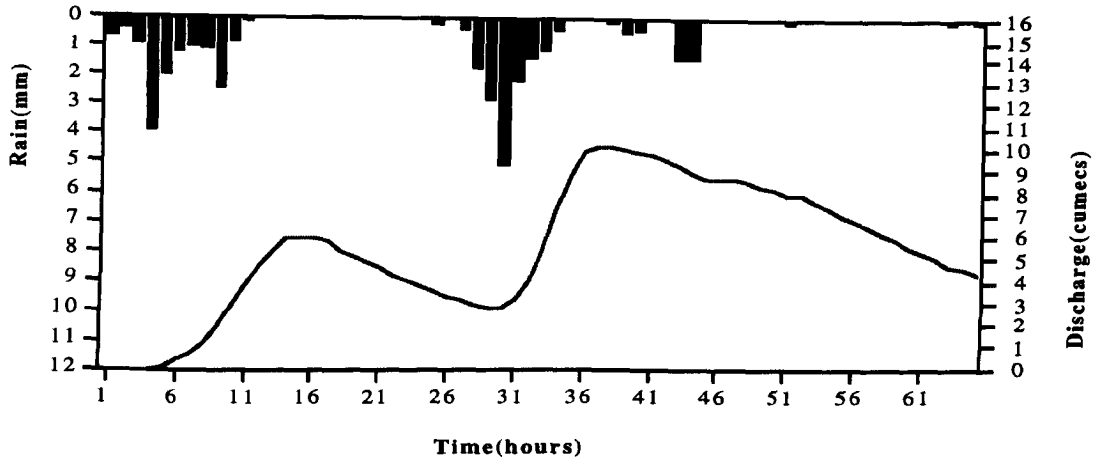

Calibration event no. 27 (19.02.77) Orgeval catchment

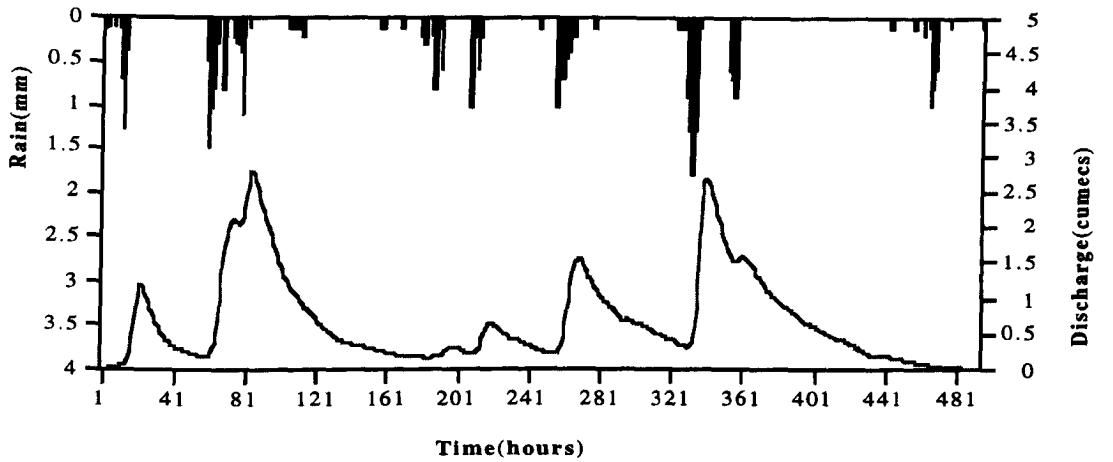

Calibration event no. 28 (19.03.75) Orgeval catchment

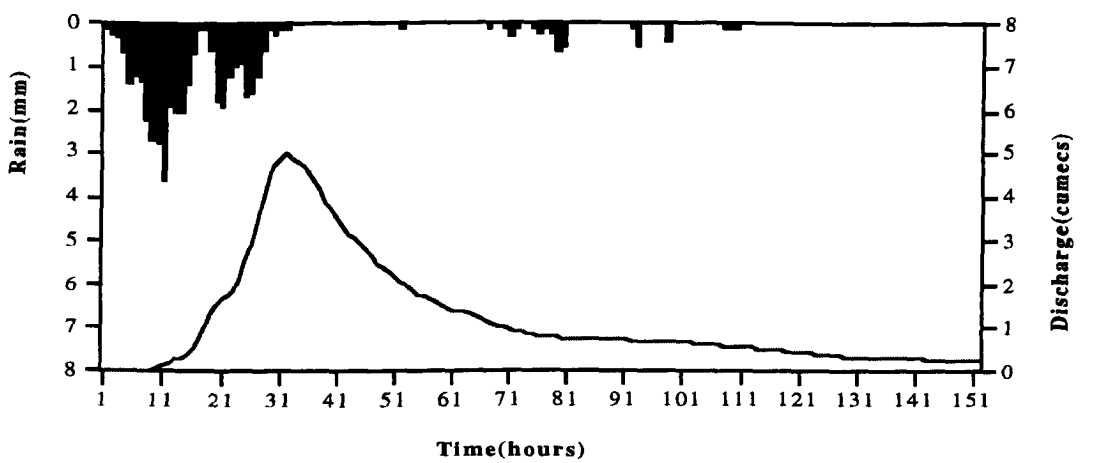

Calibration event no. 29 (6.05.75) Orgeval catchment

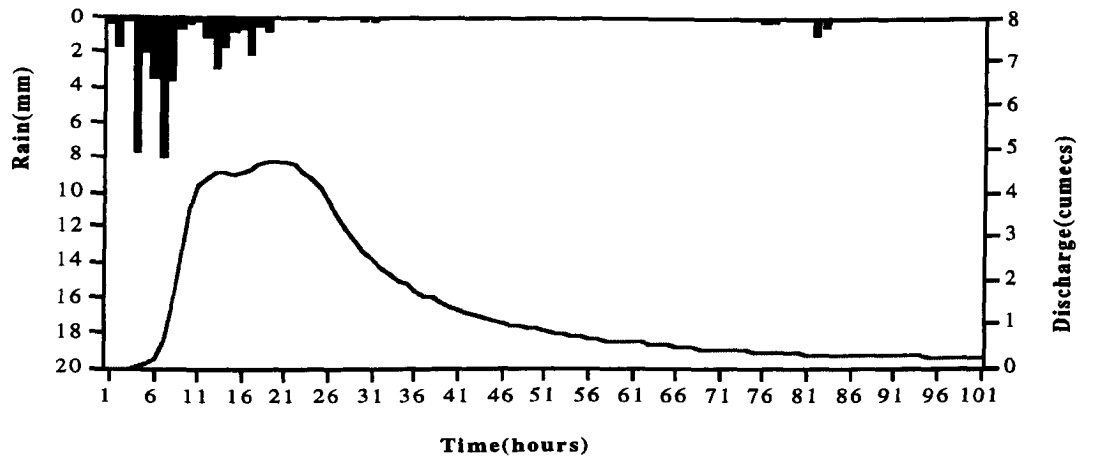

Calibration event no. 30 (29.09.75) Orgeval catchment

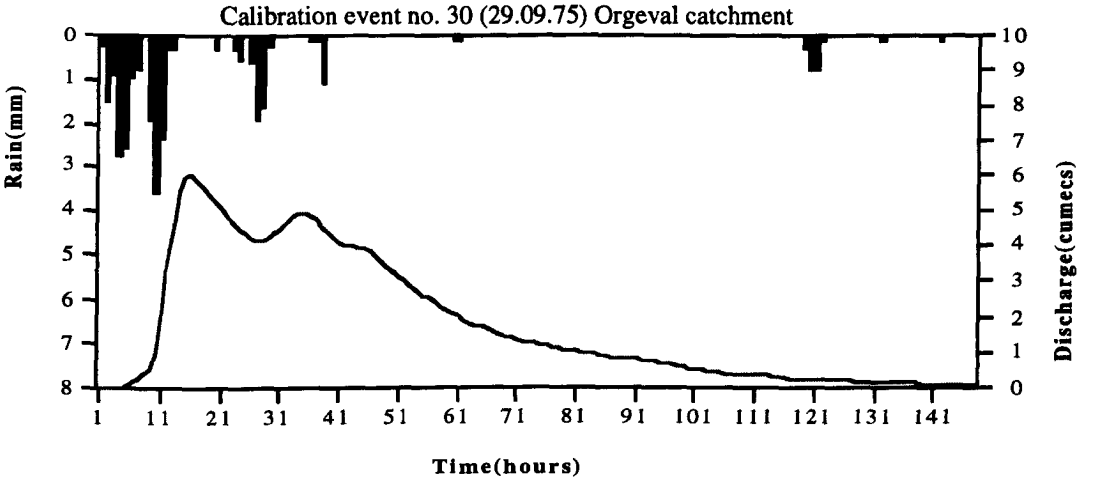

Calibration event no. 31 (2.04.77) Orgeval catchment

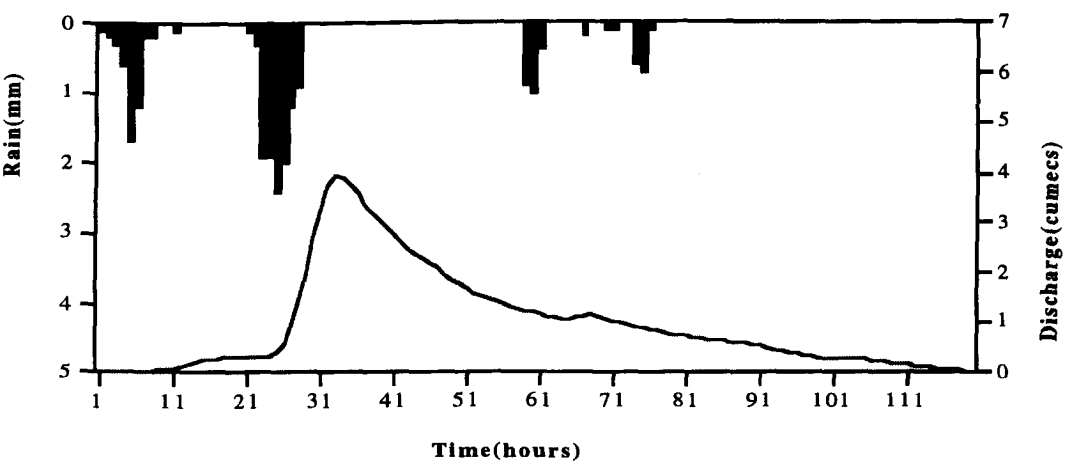

Calibration event no. 32 (9.05.77) Orgeval catchment

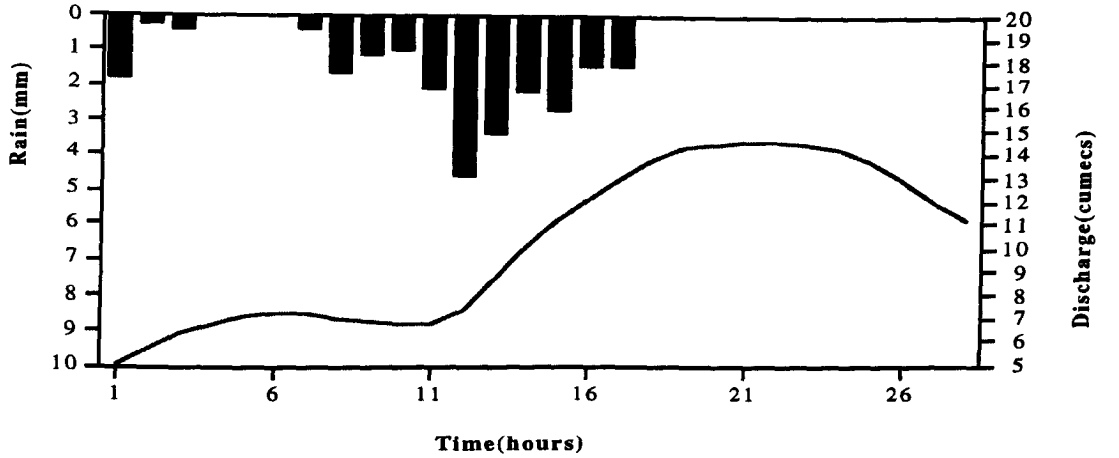

Verification event WMO 1 (31.12.78) Orgeval catchment

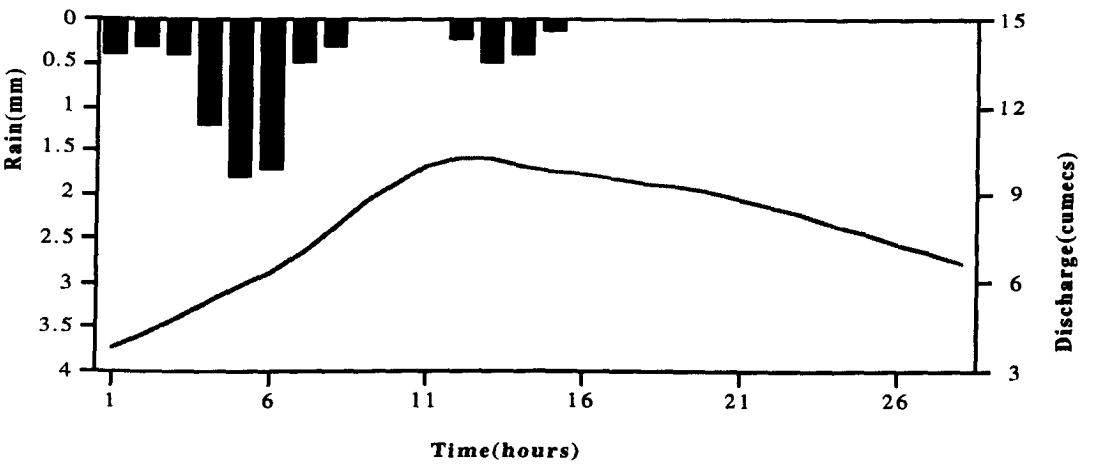

Verification event WMO 2 (2.02.79) Orgeval catchment

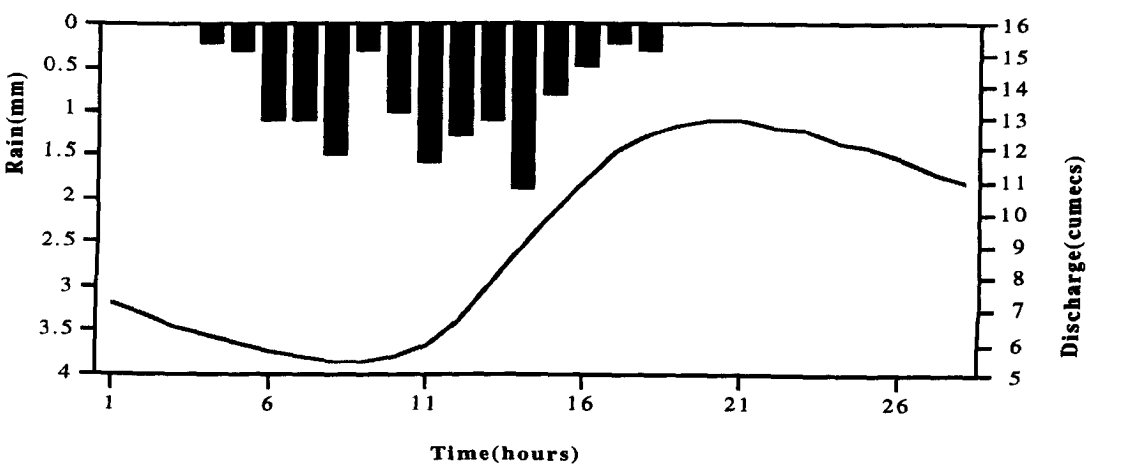

Verification event WMO 3 (10.03.79) Orgeval catchment

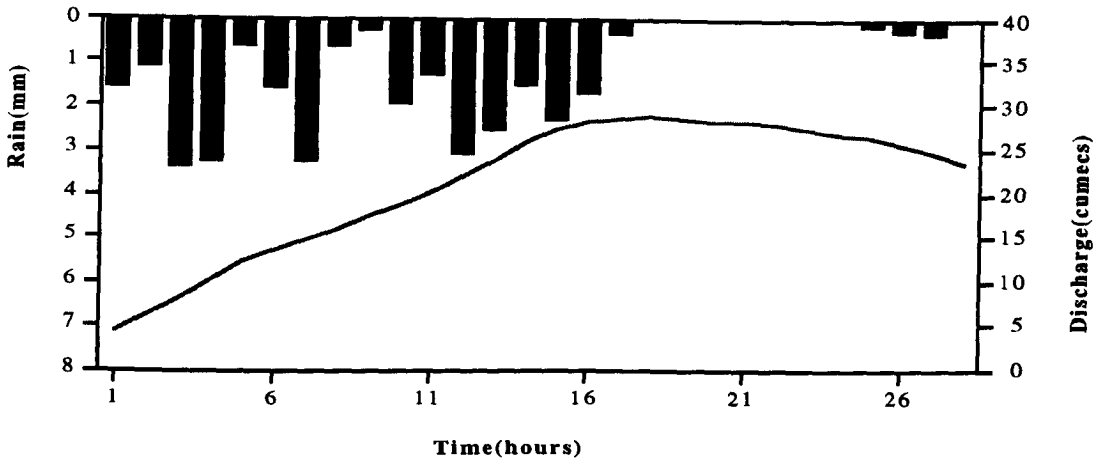

Verification event WMO 4 (13.03.80) Orgeval catchment

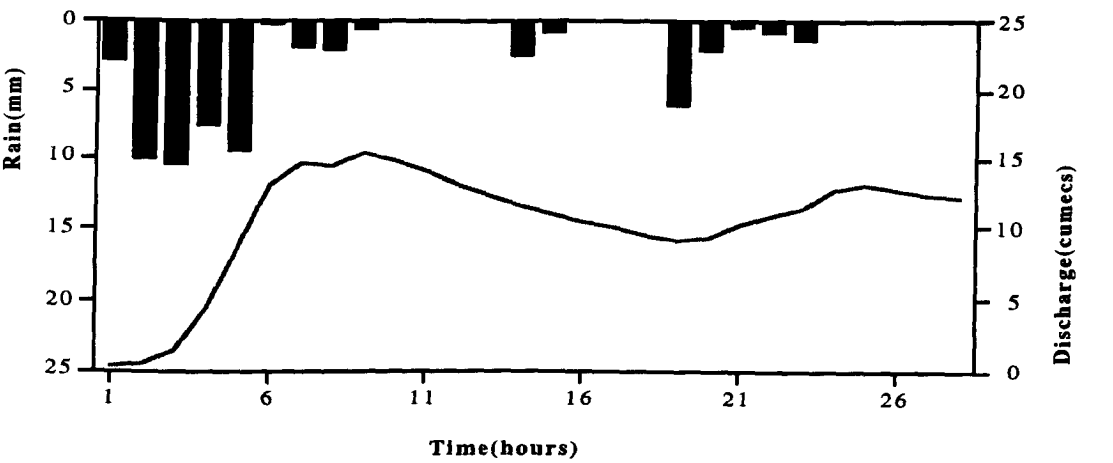

Verification event WMO 5 (13.07.80) Orgeval catchment

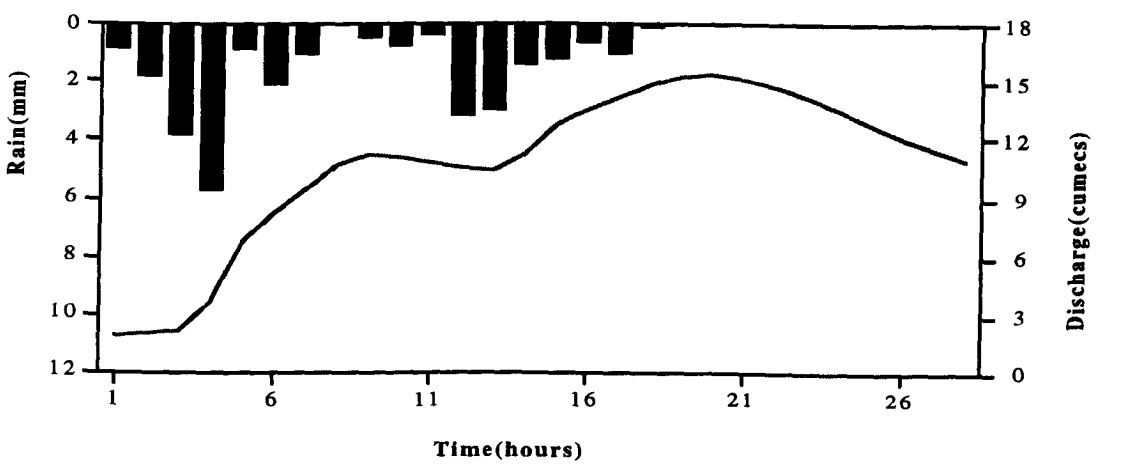

Verification event WMO 6 (20.07.80) Orgeval catchment

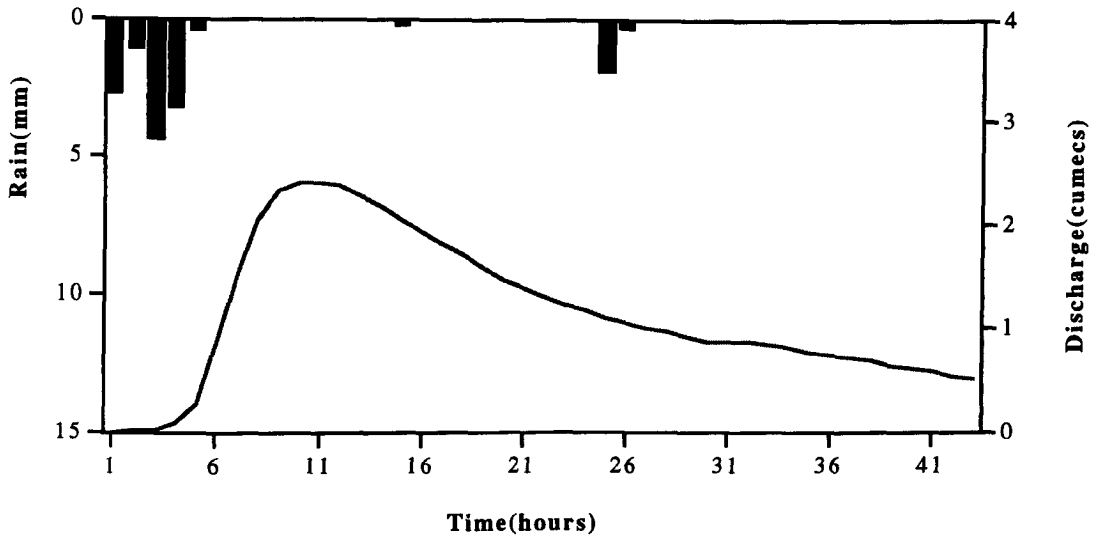

Verification event no. 7 (15.11.73) Orgeval catchment

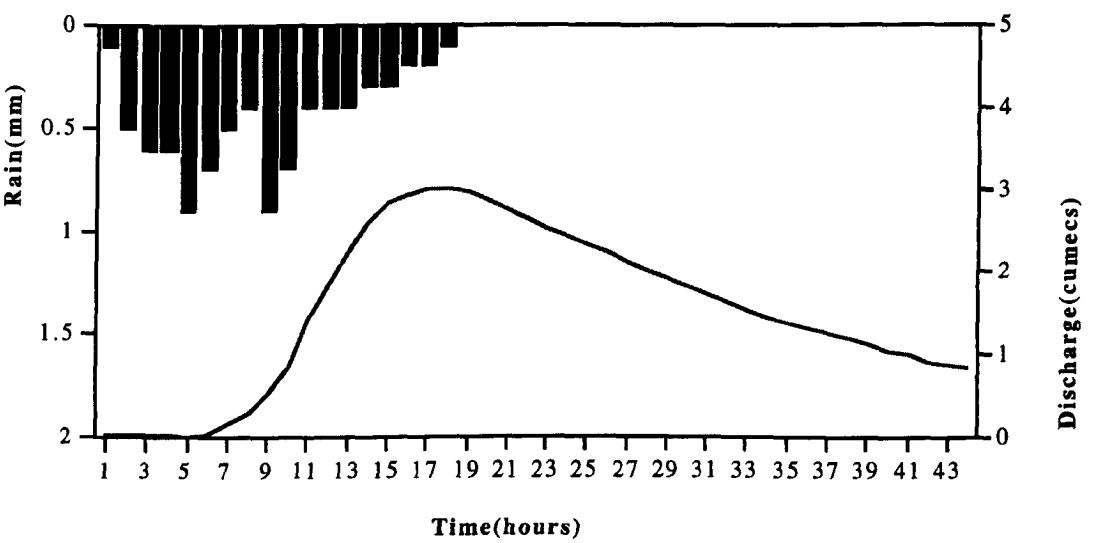

Verification event no. 8 (30.11.74) Orgeval catchment

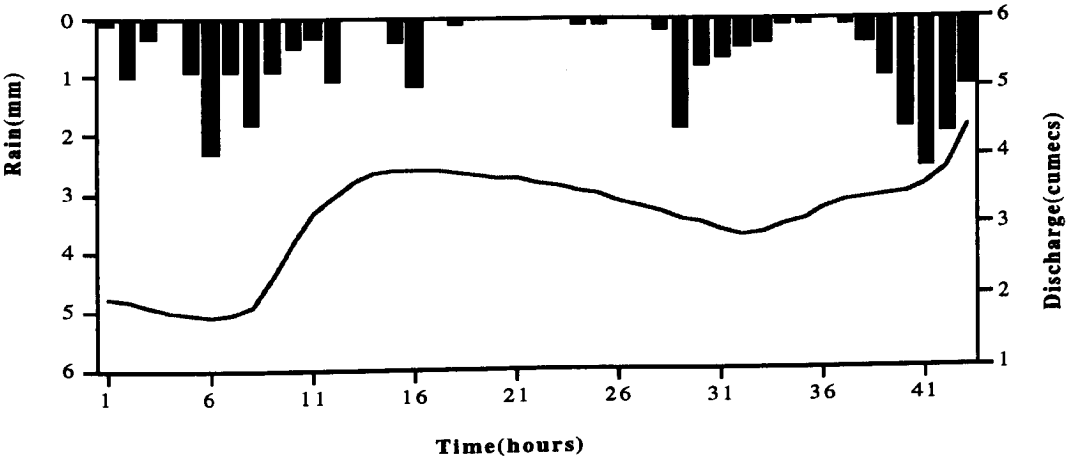

Pre-event no. 1 (29.12.78) Orgeval catchment

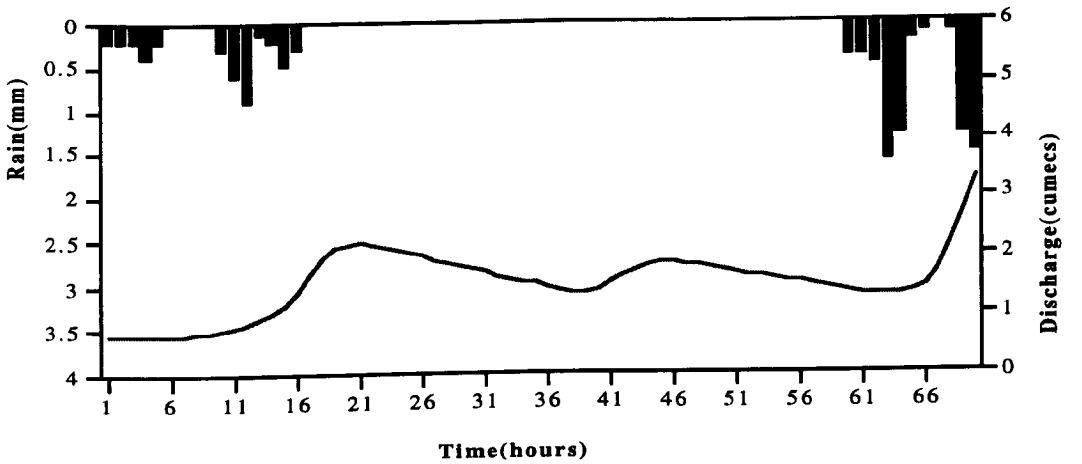

Pre-event no. 2 (30.01.79) Orgeval catchment

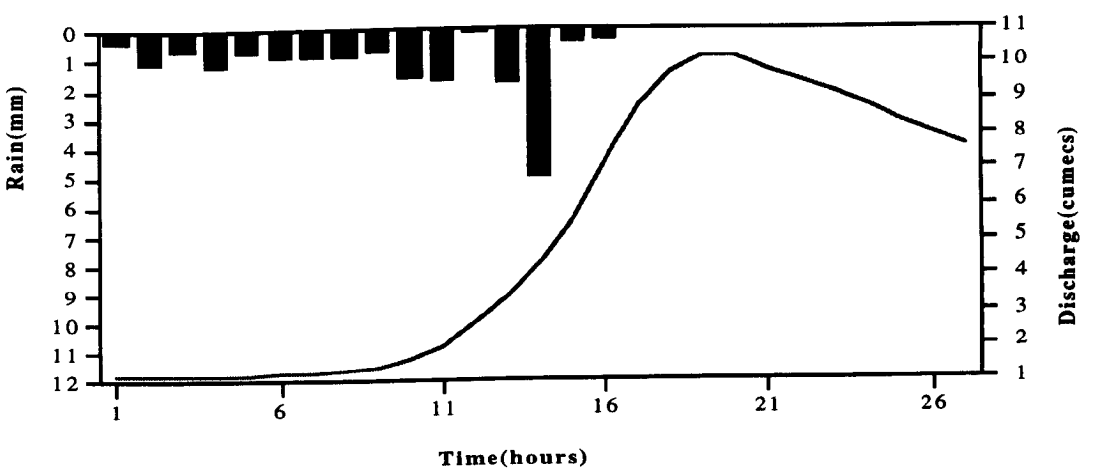

Pre-event no. 3 (8.03.79) Orgeval catchment

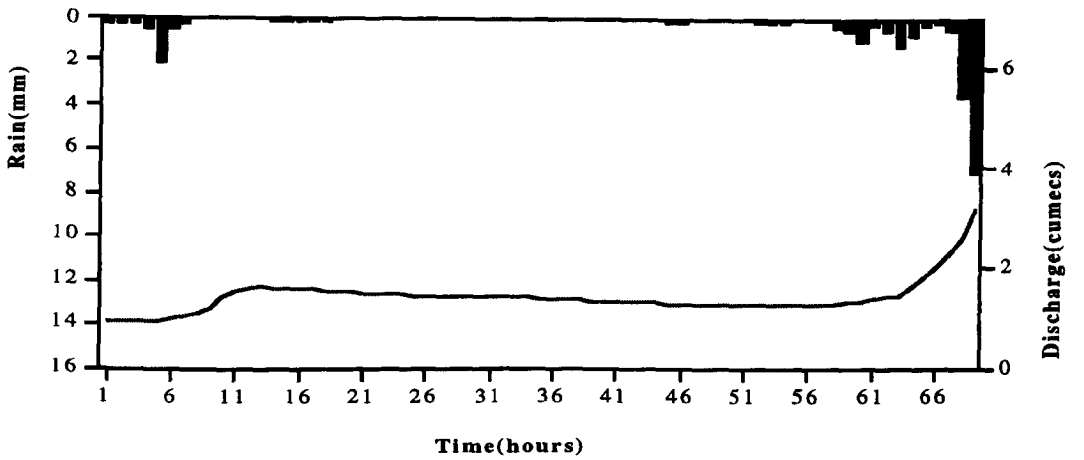

Pre-event no. 4 (10.03.80) Orgeval catchment

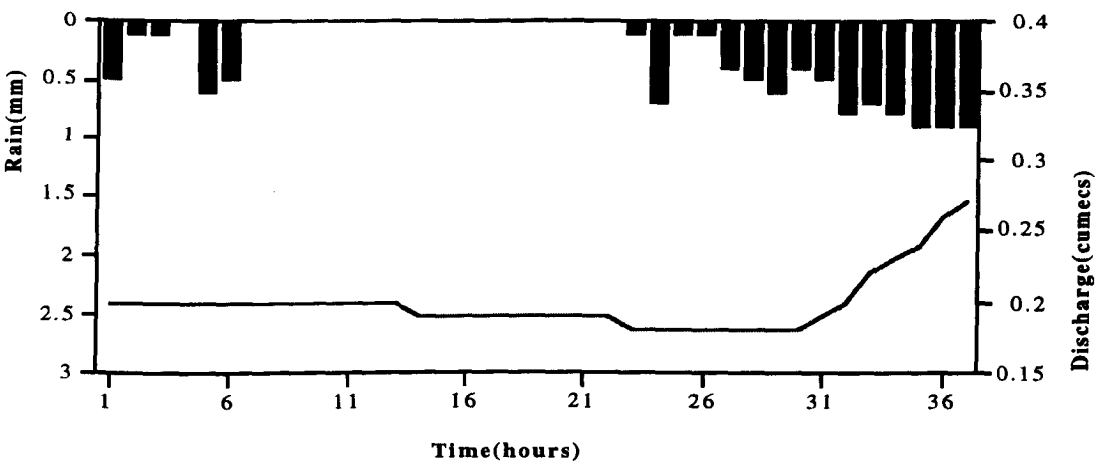

Pre-event no. 5 (11.07.80) Orgeval catchment

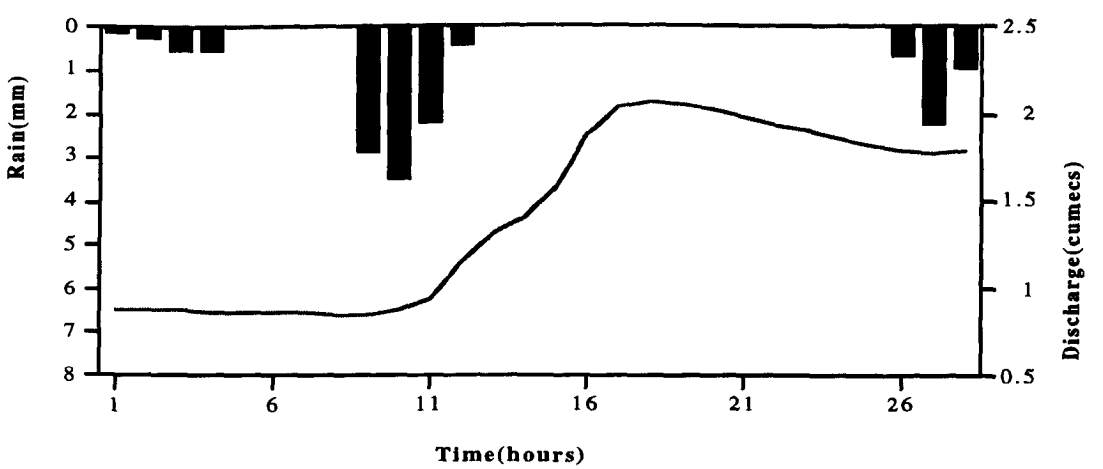

Pre-event no. 6 (18.07.80) Orgeval catchment

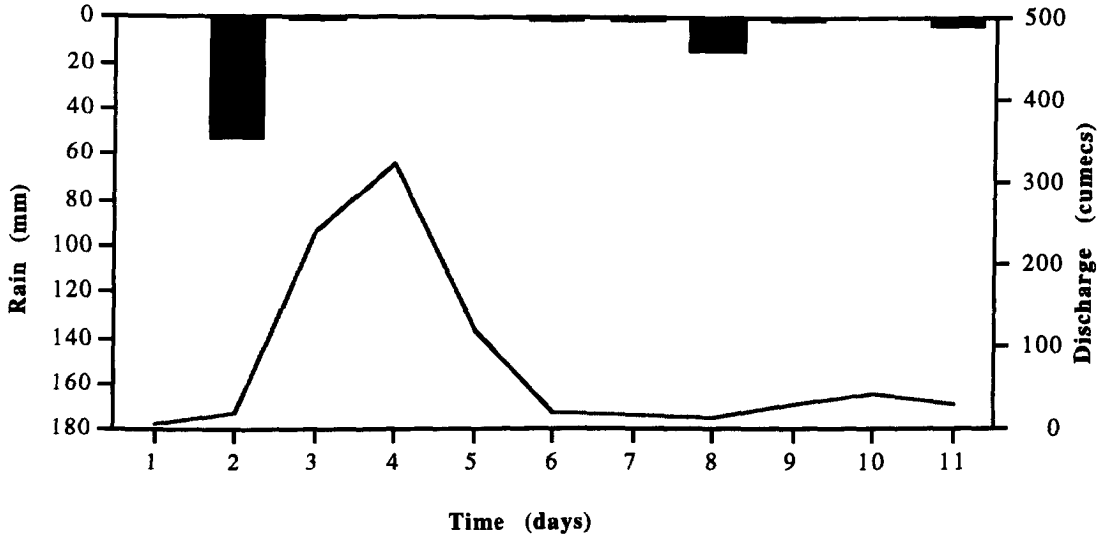

Verification event no. 1 (11.11.72) Bird Creek catchment

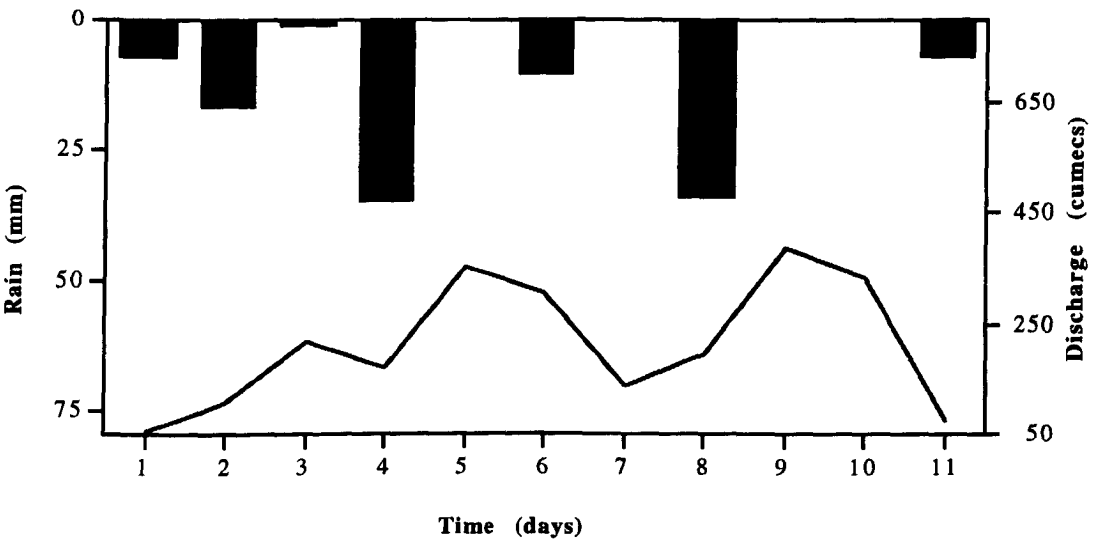

Verification event no. 2 (3.03.73) Bird Creek catchment

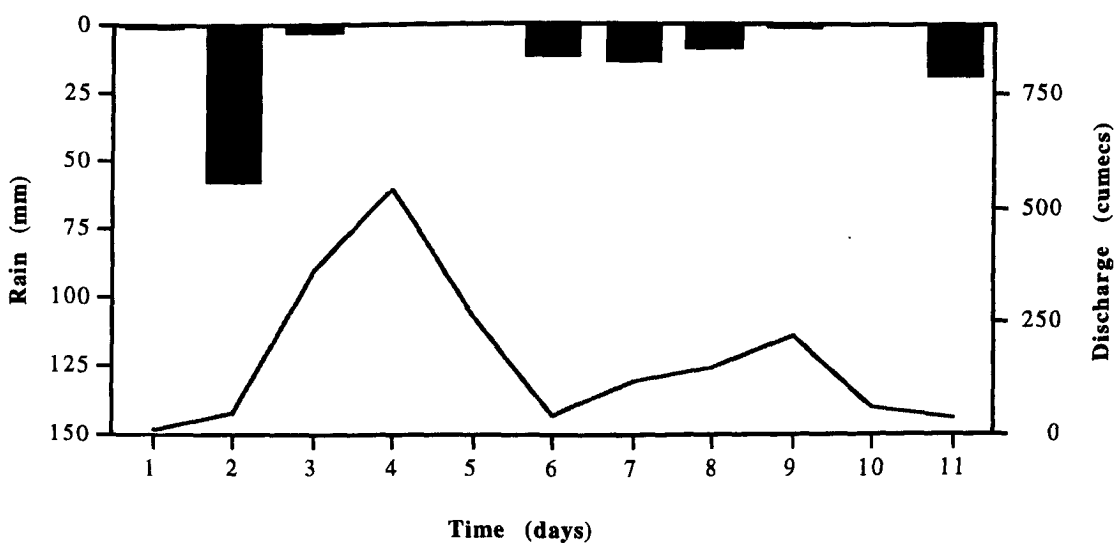

Verification event no. 3 (9.04.73) Bird Creek catchment

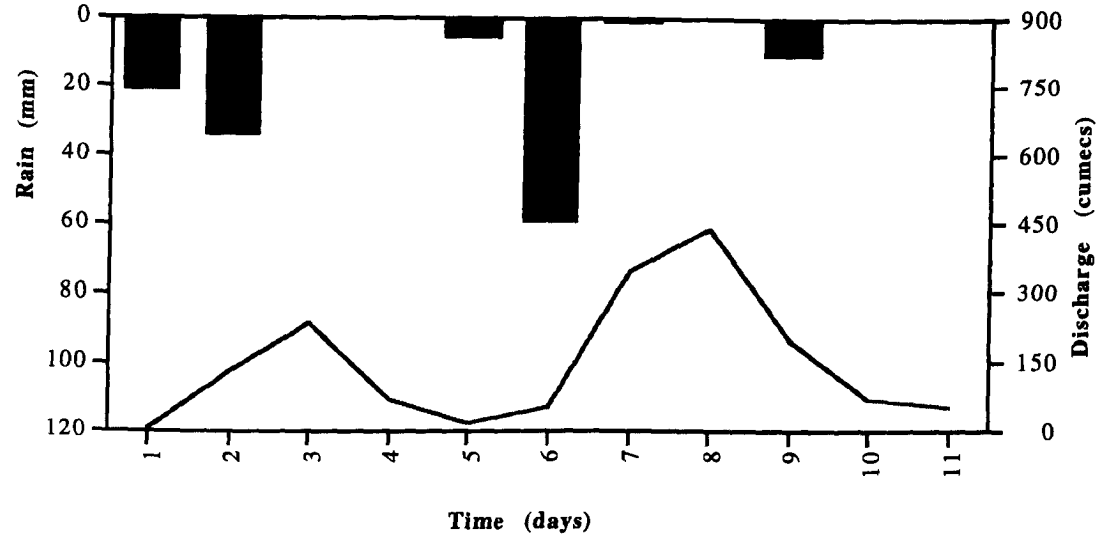

Verification event no.4 (19.11.73) Bird Creek catchment

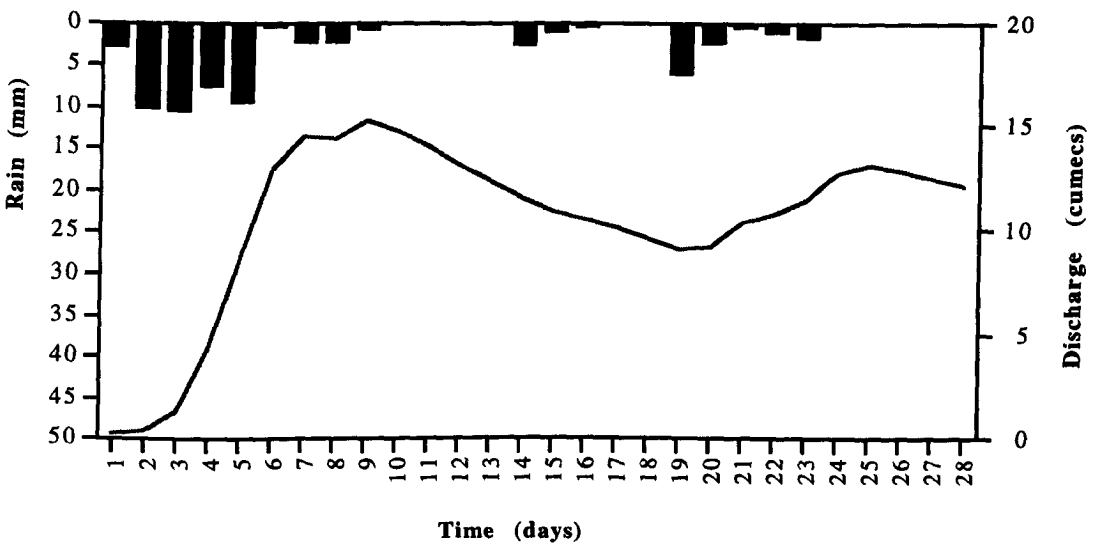

Verification event no.5 (7.03.74) Bird Creek catchment

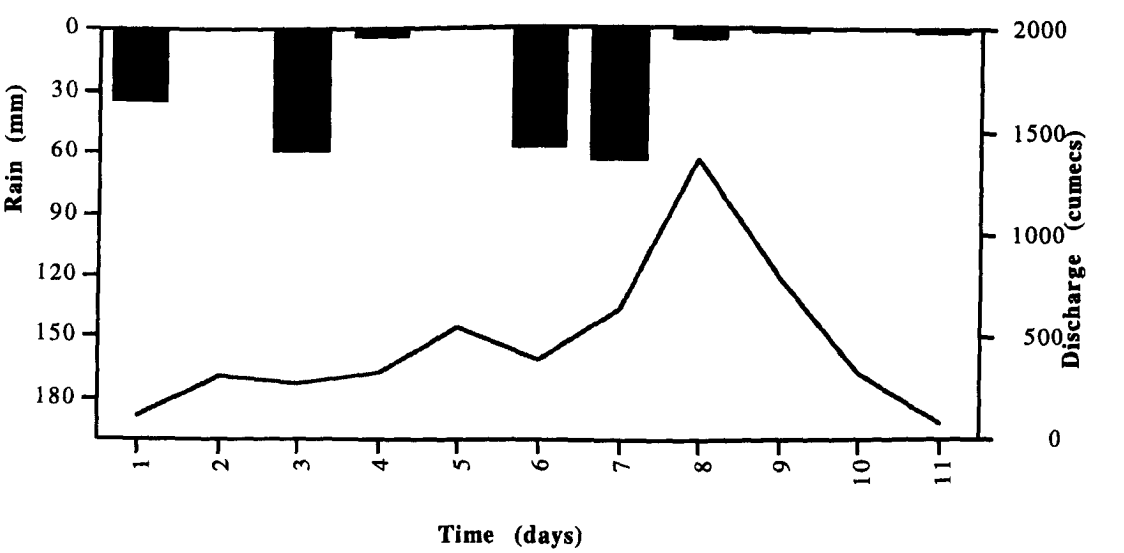

Verification event no.6 (28.10.74) Bird Creek catchment

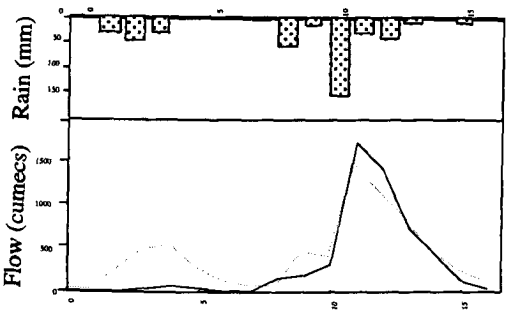

Time (days)

Event no. 1 (24.09.59)

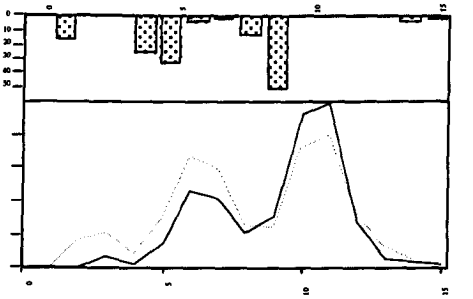

Time (days)

Event no. 2 (30.04.61)

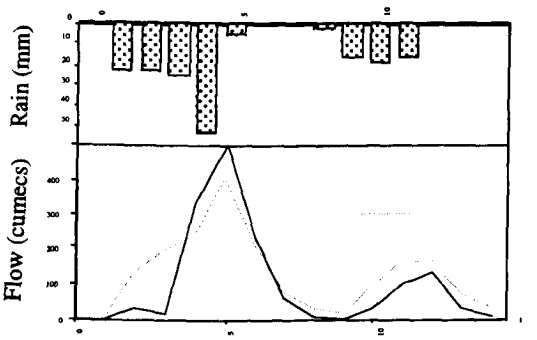

Time (days)

Event no. 3 (12.07.61)

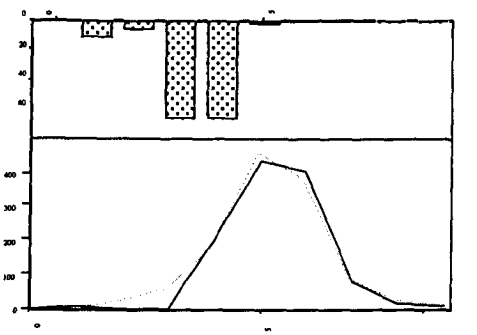

Time (days)

Event no. 4(11.08.61)

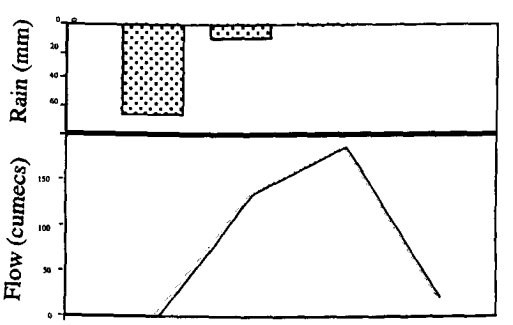

Time (days)

Event no. 5 (3.09.61)

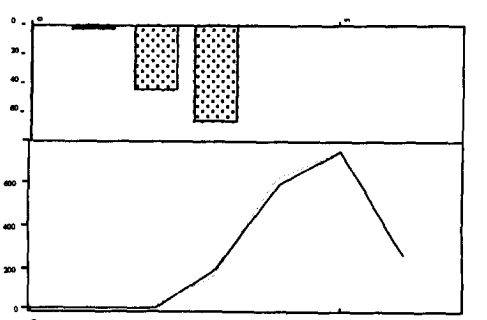

Time (days)

Event no. 6 (11.09.61)

Calibration events Bird Creek catchment

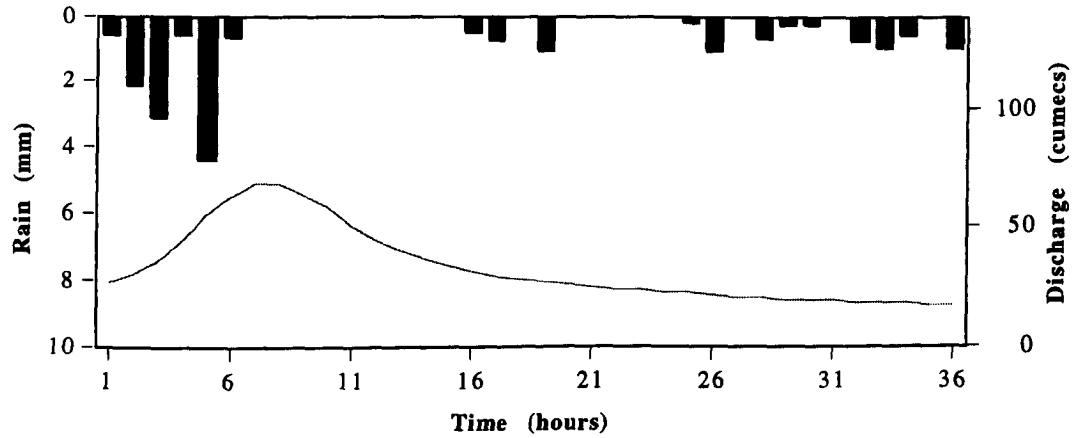

Event No 1 (16:00/03/01/82) Blackford Bridge Catchment

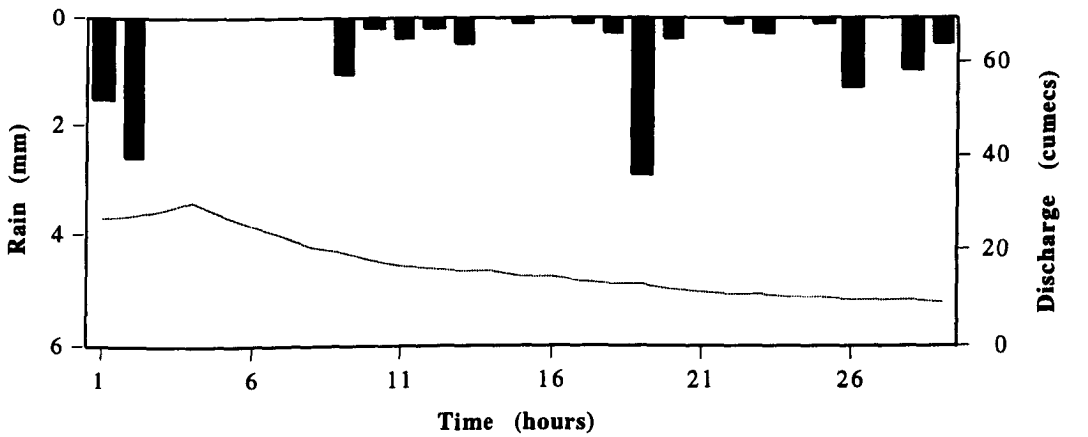

Event No 2 (05:00/10/03/82) Blackford Bridge Catchment

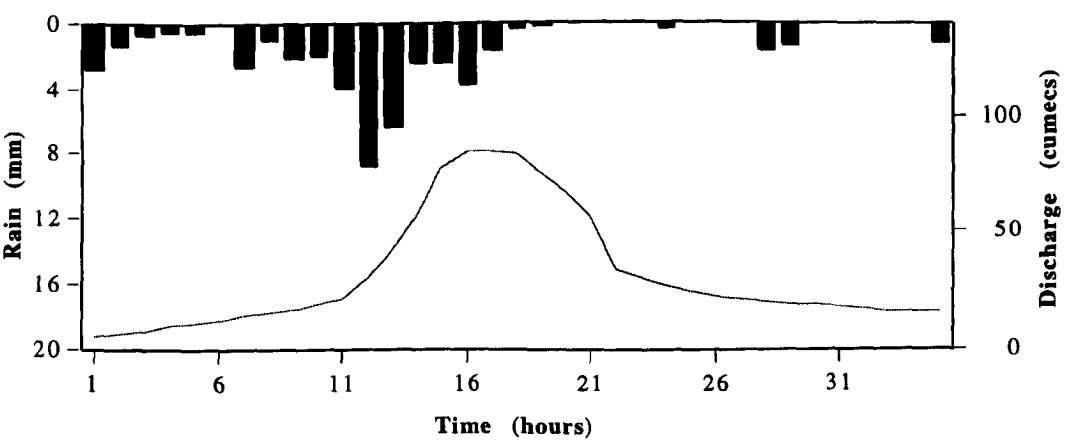

Event No 3 (24:00/08/11/83) Blackford Bridge Catchment

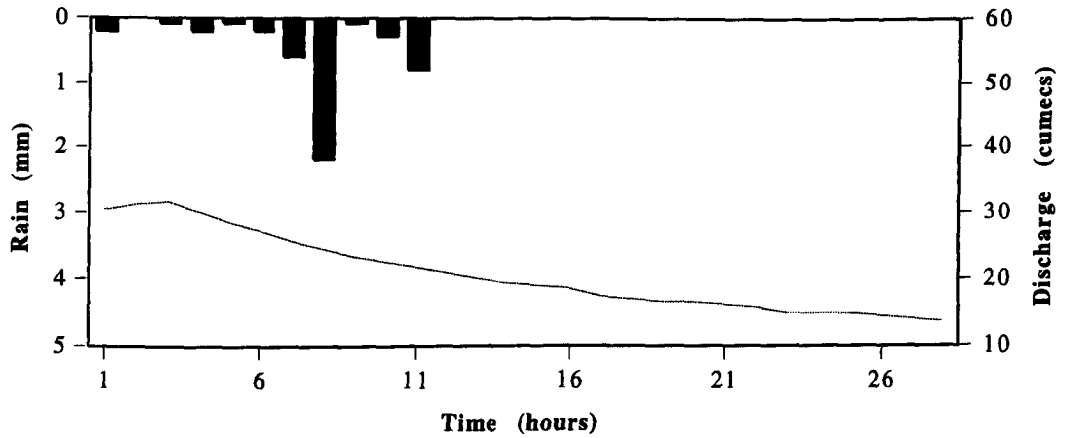

Event No 4 (20:00/06/02/84) Blackford Bridge Catchment

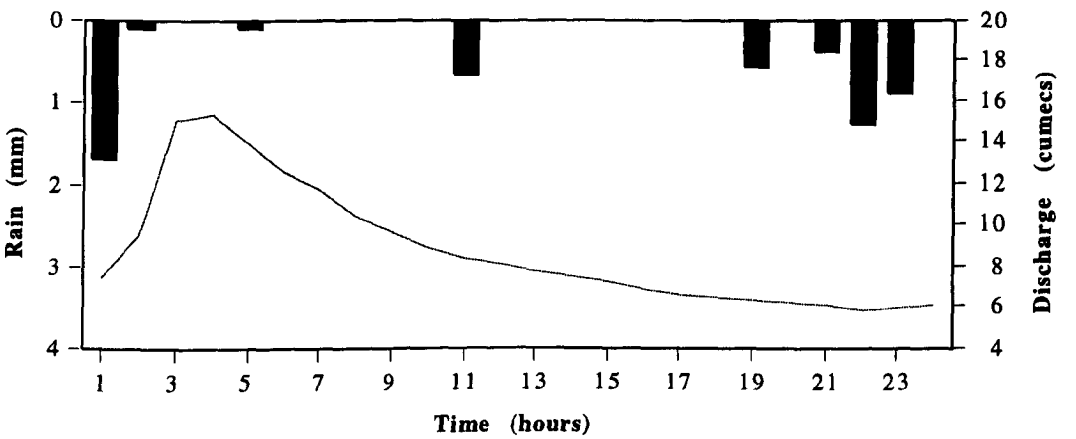

Event No 5 (01:00/30/10/86) Blackford Bridge Catchment

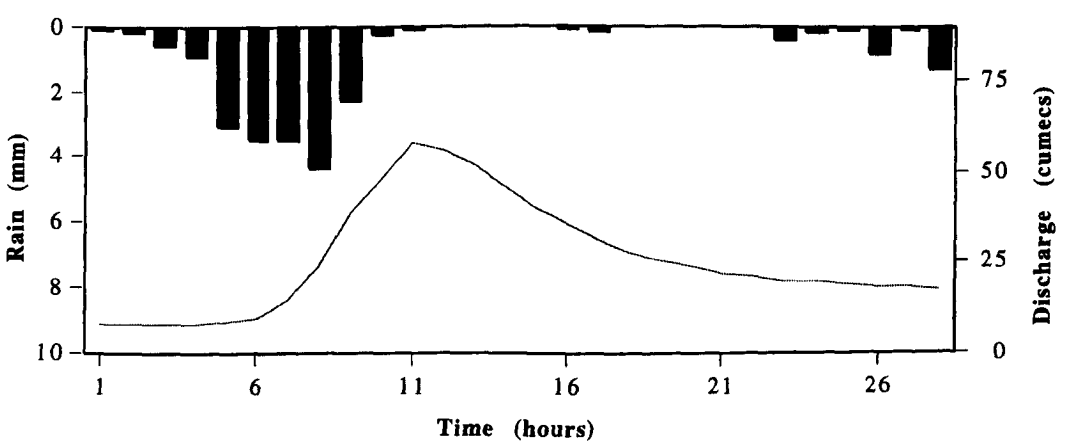

Event No 6 (02:00/01/01/87) Blackford Bridge Catchment

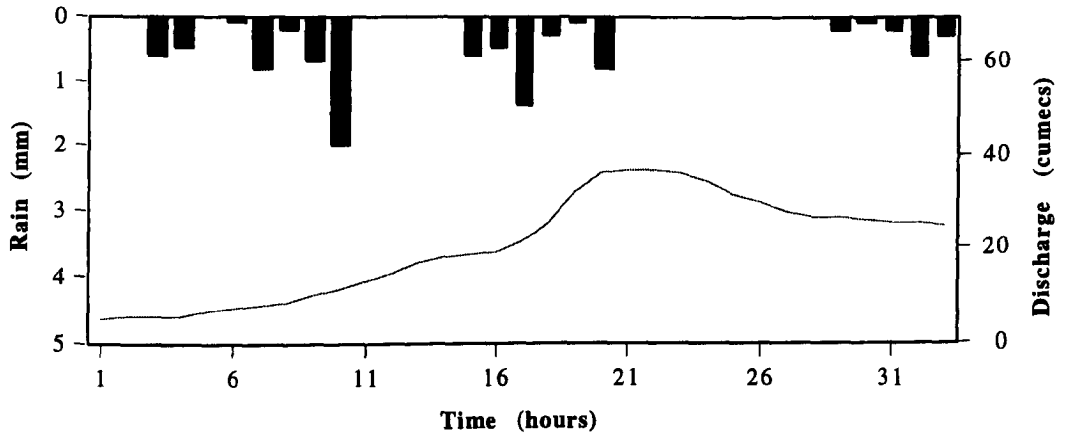

Pre-event No 1 (06:00/02/01/82) Blackford Bridge Catchment

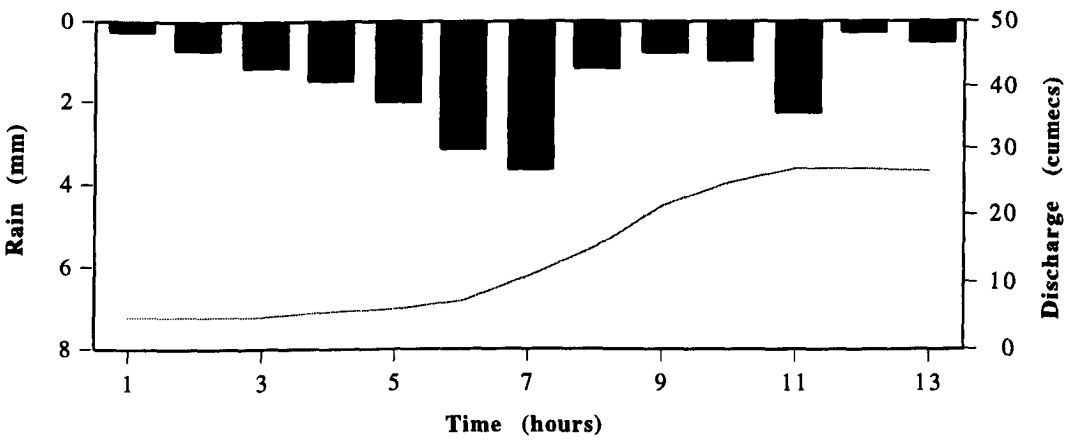

Pre-event No 2 (15:00/09/03/82) Blackford Bridge Catchment

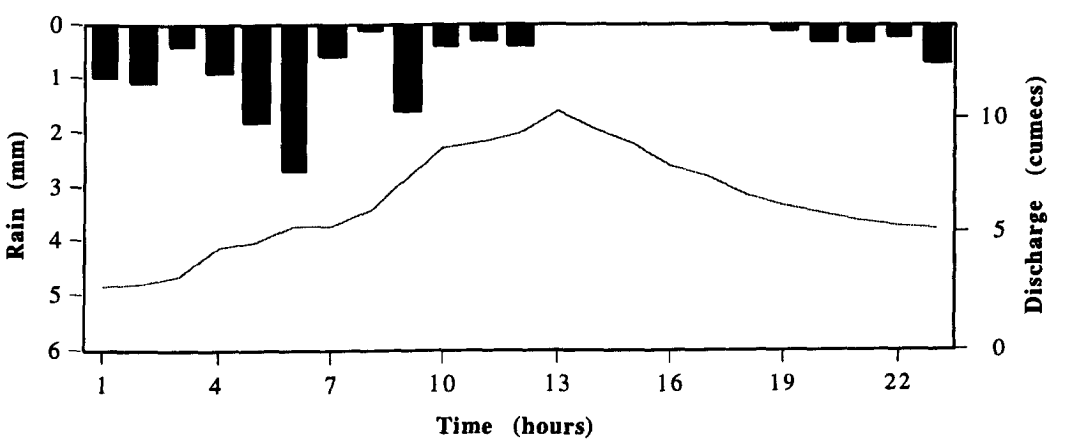

Pre-event No 3 (00:00/08/11/83) Blackford Bridge Catchment

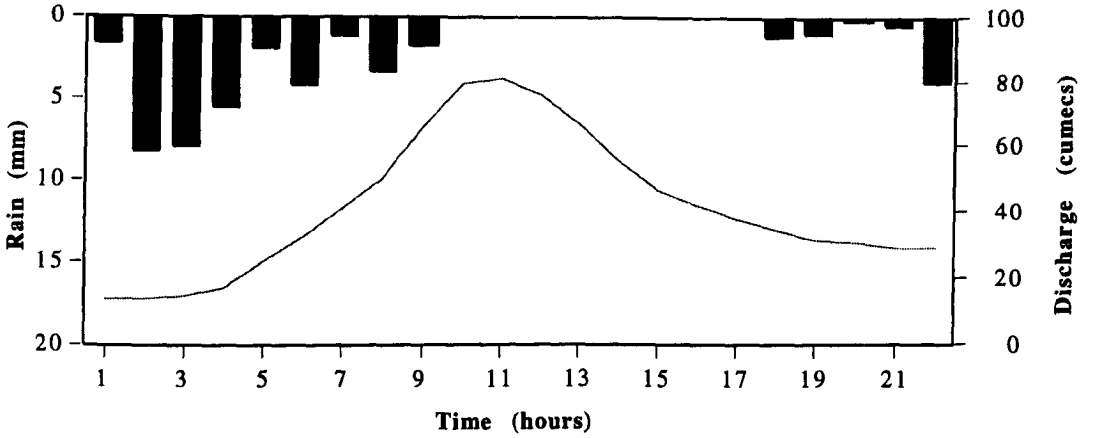

Pre-event No 4 (21:00/05/02/84) Blackford Bridge Catchment

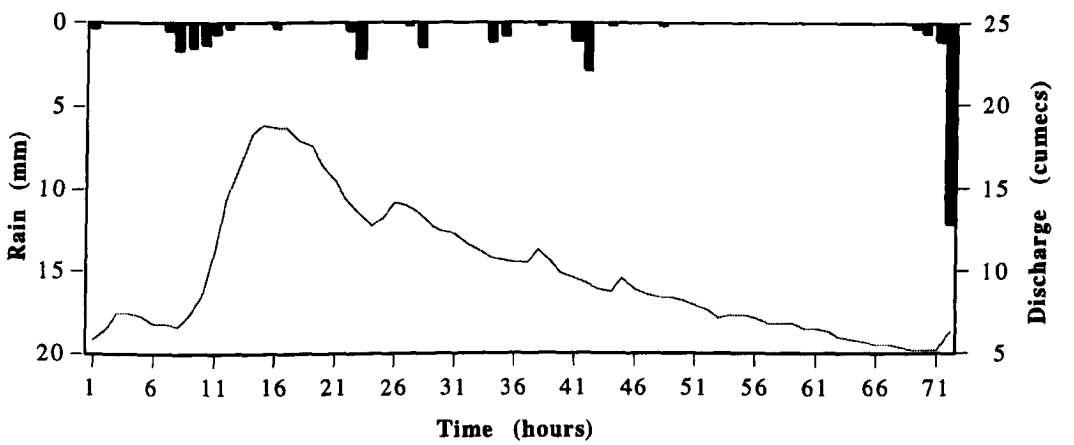

Pre-event No 5 (00:00/27/10/86) Blackford Bridge Catchment

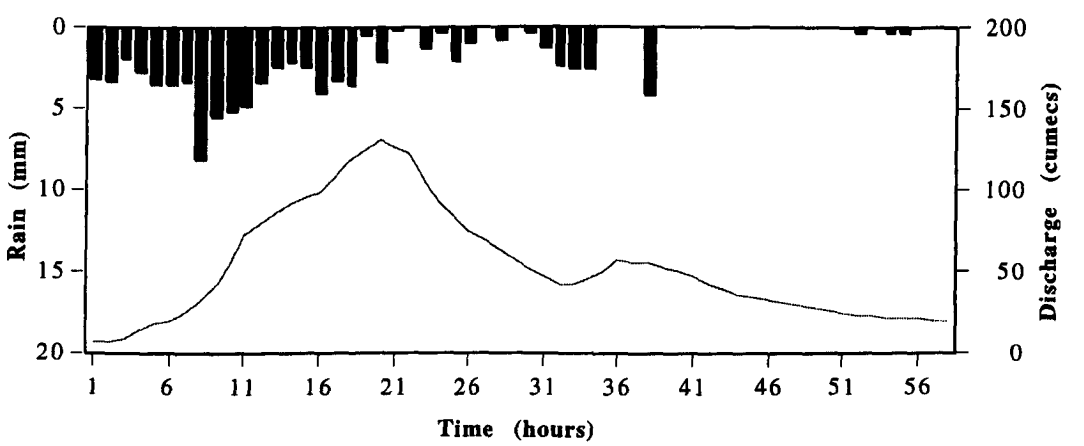

Pre-event No 6 (15:00/29/12/86) Blackford Bridge Catchment

APPENDIX 3

FLOWCHARTS AND EXAMPLES OF HGA IN PRTF MODEL

A3.1 Introduction

In this appendix flow charts of HGA for simulation of PRTF model both in real and binary numbers are presented. Furthermore, two examples of applications of HGA to the PRTF model are illustrated. The first example is related to identification of PRTF model using real number representation, and the second to binary representation. It should be emphasised that because there is not enough room to present whole generations, only a few selected generations are presented here.

A flowchart for the simulation (updating) of PRTF model using the developed HGA and real numbers is presented in figure (A3.1).

A3.2 HGA using real numbers representation

In order to illustrate the application of HGA in parameter estimation of PRTF model, one event from Bird Creek catchment is chosen. The aim is to estimate the time to peak and B_j PRTF parameters using a given rainfall hyetograph and its corresponding hydrograph. Once this has been done calculation of A_j parameters is straightforward.

Only six generations of HGA are shown here including the first five generations and the last generation. Each panel gives the full information of a single generation of the HGA: time to peak, B_j parameters, A_j parameters and corresponding fitness. Since a 2×1 order PRTF model is used, the first column is the time to peak the second and third are related to the B_j parameters the fourth and fifth are A_j parameters and the last column is related to the fitness factor. The first five generation runs are provided to show the progression of the genetic algorithm towards an optimal solution. The reader is encouraged to examine the panels successively and gain reassurance that the algorithm is systematically moving the population towards minimum fitness and hence is optimising the fitness factors.

Figure (A3.1) Flowchart for HGA in simulation of PRTF model using real numbers

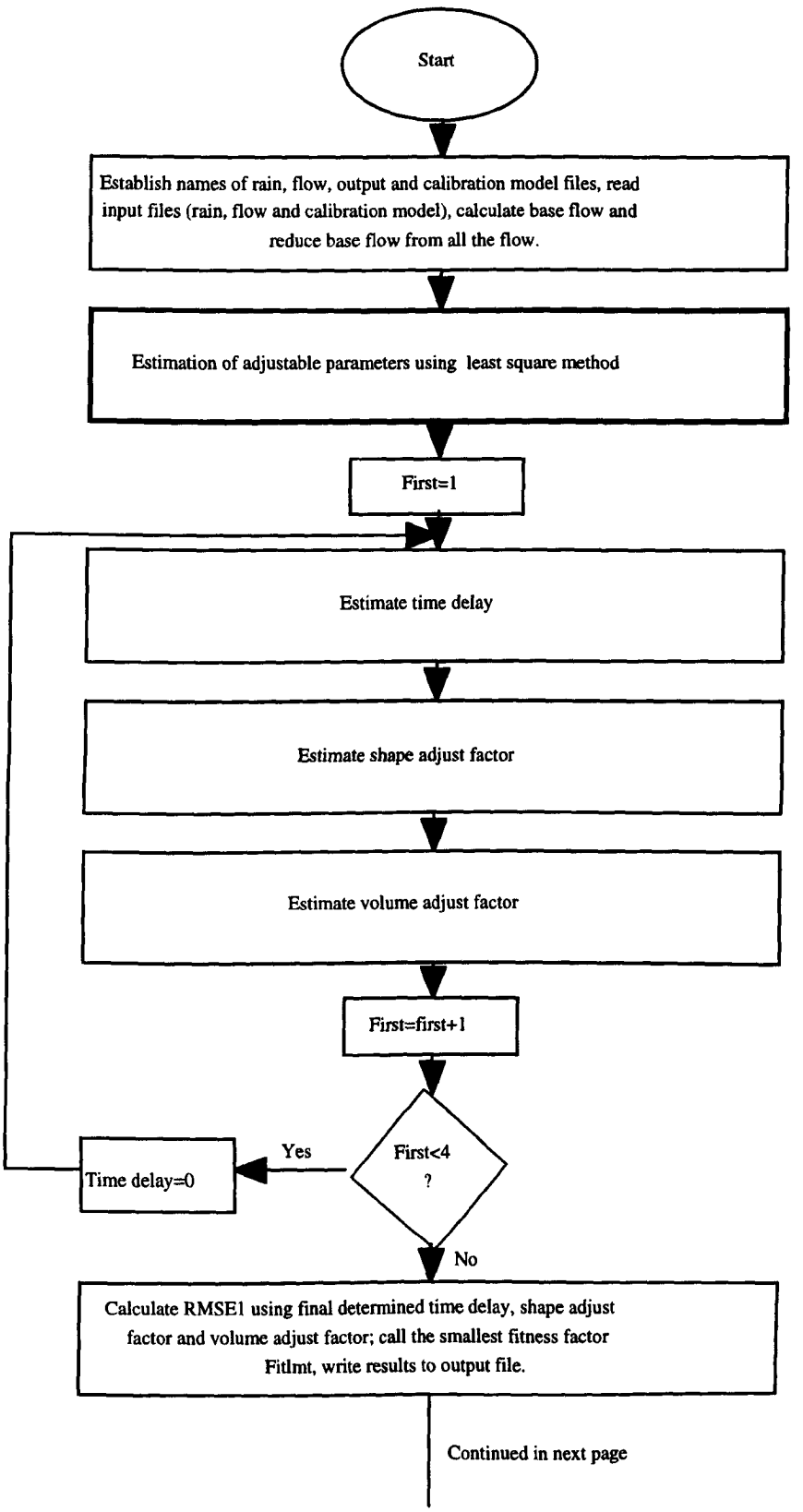

Figure (A3.1) continued

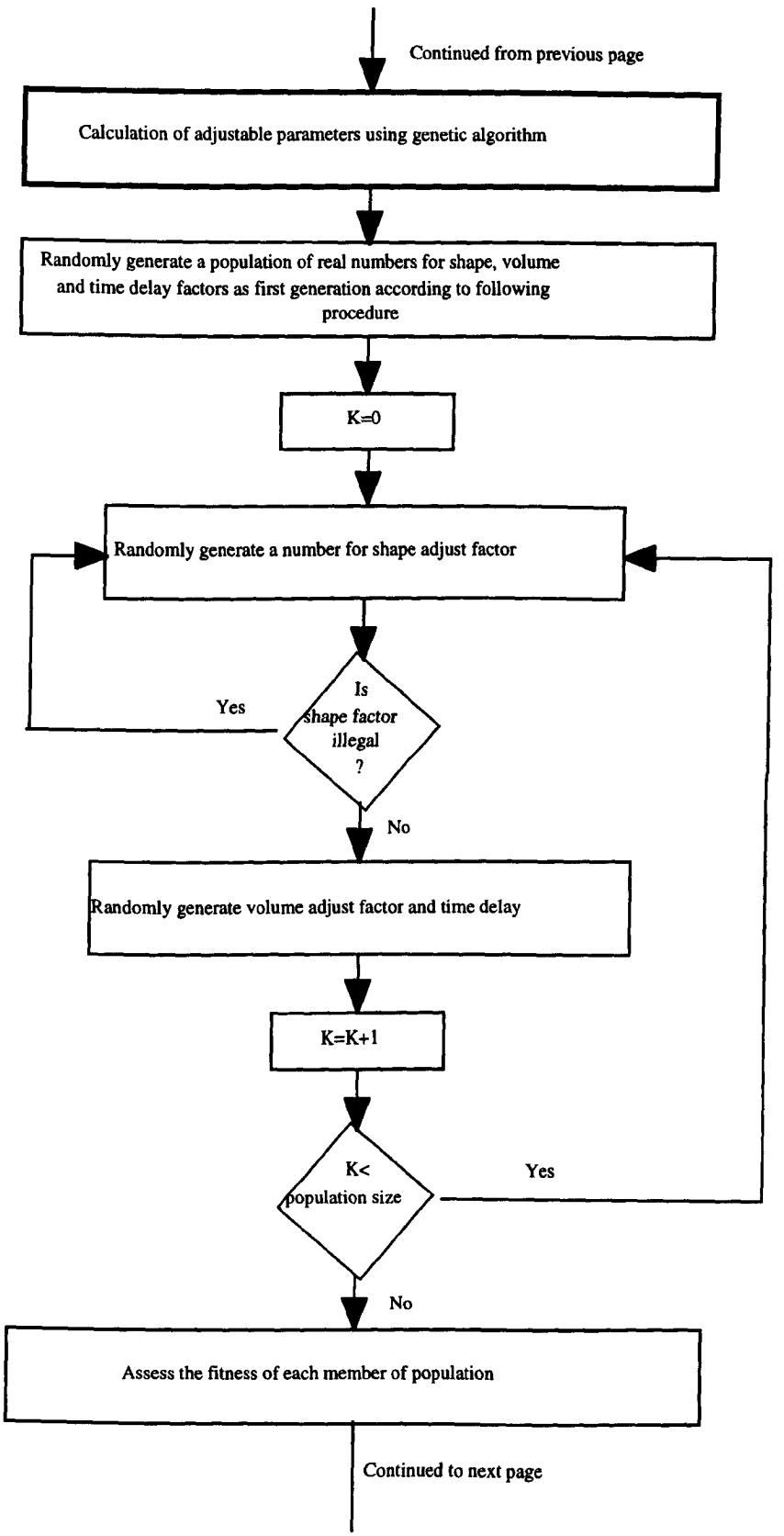

Figure (A3.1) Continued

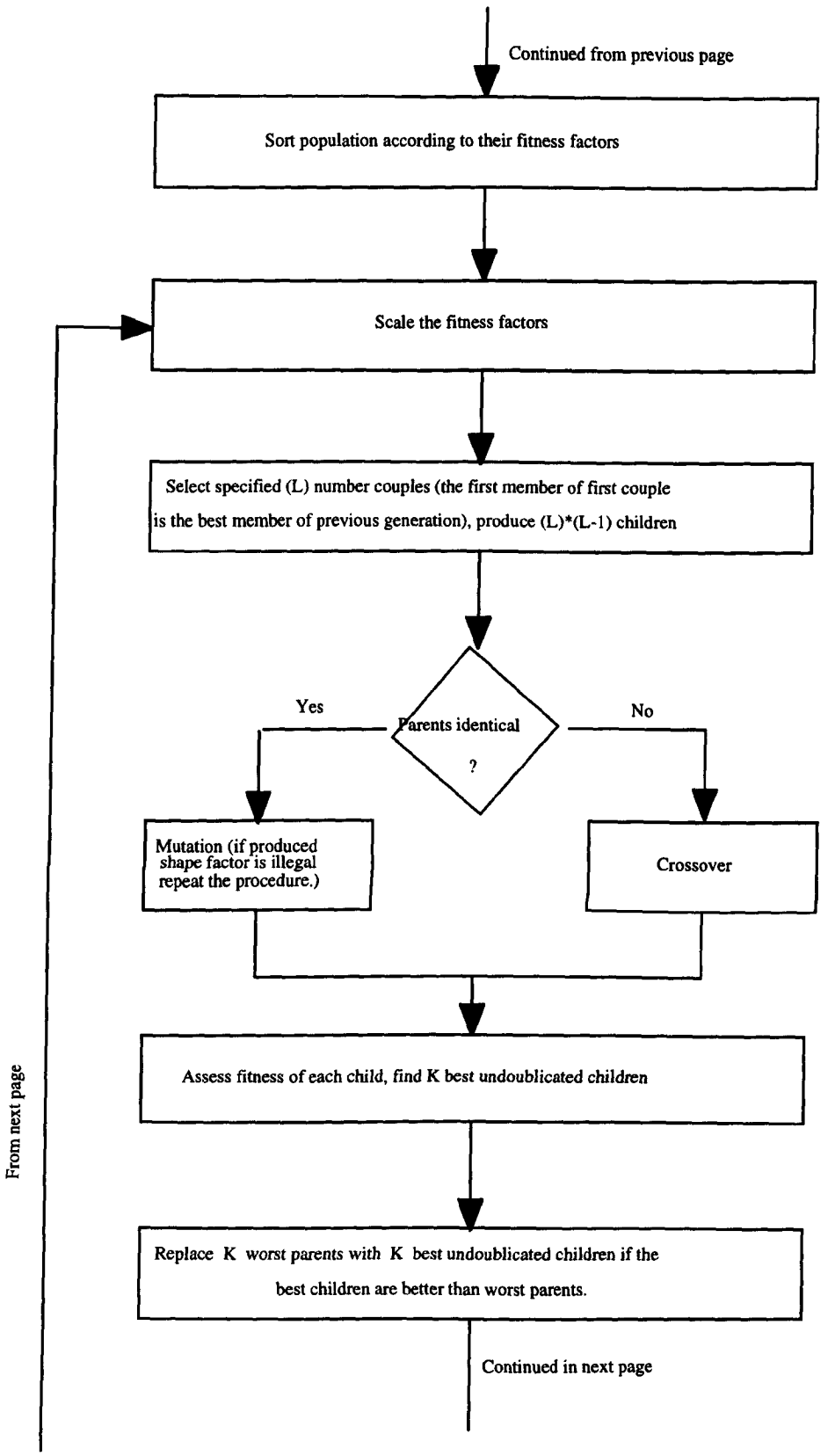

Figure (A3.1) Continued

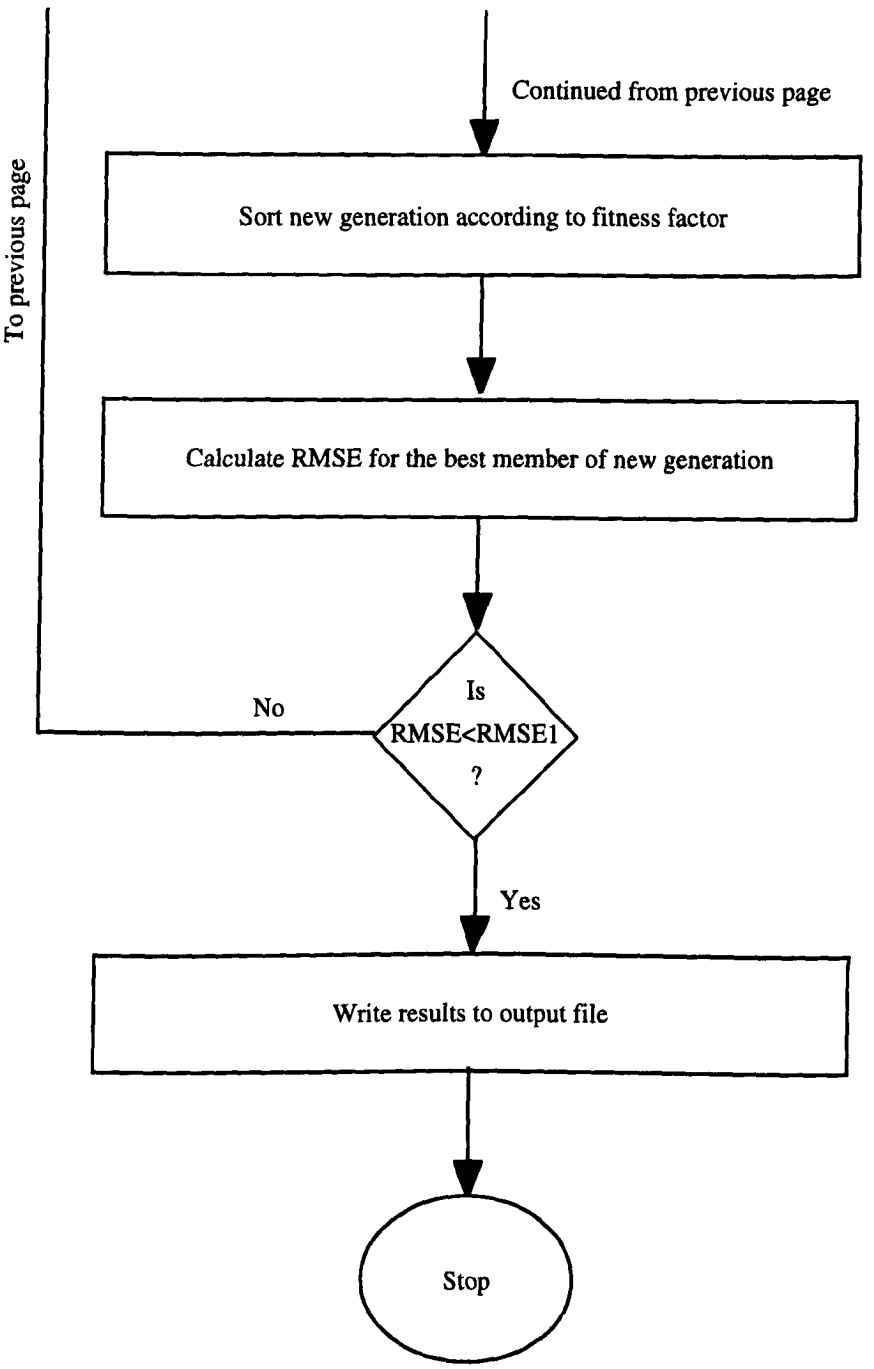

Here the population size is considered to be 10. It is also supposed that the number of selected parents in each step of algorithm to be same as population size so that in each generation 90 children are produced.

Table (A3.1a) shows the initial population for HGA. It can be seen that there is no pattern for the population because they are generated randomly.

Table (A3.1b) is related to second generation and illustrates the power of the GA. Here it is supposed that 30% of the best individuals of the previous generation remain in the next generation. Thus it can be seen that individuals 3, 5 and 6 are remain in the second generation. The second generation also shows the mutation and crossover effects. Due to the roulette wheel parent selection mechanism, members of first generation with fitness factors which are too large do not appear in the second generation.

Table (A3.1c) is related to generation 3. It shows that the average population fitness has decreased dramatically over that of generation 2. It should be noted that much of randomness of generations 1 and 2 has now gone.

Similar pattern is observed in the remaining generations and the HGA continues until a lower RMSE is obtained.

Table (A3.1) List of population evolution in some selected generation, Bird Creek catchment.

Generation	Member	Time to peak	B parameter		A parameter		Fitness factor
A3.1a Generation 1							
1	1	7.97	1.65	7.26	1.79	-0.80	112.81
1	2	3.72	0.39	8.76	1.62	-0.65	42.65
1	3	0.93	1.67	1.20	1.19	-0.35	0.34
1	4	9.50	0.08	7.52	1.82	-0.83	93.45
1	5	2.29	0.37	0.62	1.48	-0.54	0.58
1	6	1.77	0.38	3.28	1.39	-0.49	1.49
1	7	4.38	0.62	2.80	1.66	-0.69	6.81
1	8	3.26	3.46	1.00	1.58	-0.63	7.64
1	9	10.61	0.78	1.79	1.83	-0.84	11.63
1	10	2.78	5.06	8.29	1.54	-0.59	60.59
A3.1b Generation 2							
2	1	0.93	1.67	1.20	1.19	-0.35	0.34
2	2	0.93	1.67	1.20	1.19	-0.35	0.34
2	3	0.93	0.62	2.80	1.19	-0.35	0.39
2	4	1.18	2.05	1.02	1.26	-0.40	0.48
2	5	2.29	0.37	0.62	1.48	-0.54	0.58
2	6	1.77	0.62	2.80	1.39	-0.49	1.27
2	7	1.77	0.38	3.28	1.39	-0.49	1.49
2	8	1.77	0.38	3.28	1.39	-0.49	1.49
2	9	2.78	1.67	1.20	1.54	-0.59	2.12
2	10	0.93	0.08	7.52	1.19	-0.35	2.62
A3.1c Generation 3							
3	1	0.93	1.67	1.20	1.19	-0.35	0.34
3	2	0.93	1.67	1.20	1.19	-0.35	0.34
3	3	0.93	1.67	1.20	1.19	-0.35	0.34
3	4	0.93	0.62	2.80	1.19	-0.35	0.39
3	5	0.93	0.62	2.80	1.19	-0.35	0.39
3	6	0.93	0.38	3.28	1.19	-0.35	0.44
3	7	1.18	2.05	1.02	1.26	-0.40	0.48
3	8	2.29	0.37	0.62	1.48	-0.54	0.58
3	9	1.77	1.67	1.20	1.39	-0.49	0.86
3	10	1.77	0.62	2.80	1.39	-0.49	1.27

Table (A3.1) Continued

Generation	Member	Time to peak	B parameter		A parameter		Fitness factor
A3.1d Generation 4							
4	1	0.93	1.67	1.20	1.19	-0.35	0.34
4	2	0.93	1.67	1.20	1.19	-0.35	0.34
4	3	0.93	1.67	1.20	1.19	-0.35	0.34
4	4	0.93	1.67	1.20	1.19	-0.35	0.34
4	5	0.93	0.62	2.80	1.19	-0.35	0.39
4	6	0.93	0.38	3.28	1.19	-0.35	0.44
4	7	1.18	2.05	1.02	1.26	-0.40	0.48
4	8	2.76	1.61	-0.77	1.53	-0.59	0.54
4	9	2.29	0.37	0.62	1.48	-0.54	0.58
4	10	1.19	3.91	0.13	1.27	-0.40	0.86
A3.1e Generation 5							
5	1	0.93	1.67	1.20	1.19	-0.35	0.34
5	2	0.93	1.67	1.20	1.19	-0.35	0.34
5	3	0.93	1.67	1.20	1.19	-0.35	0.34
5	4	0.93	1.67	1.20	1.19	-0.35	0.34
5	5	0.93	0.62	2.80	1.19	-0.35	0.39
5	6	0.45	2.30	3.69	1.00	-0.25	0.43
5	7	0.93	0.38	3.28	1.19	-0.35	0.44
5	8	0.91	3.45	-0.60	1.19	-0.35	0.44
5	9	1.18	2.05	1.02	1.26	-0.40	0.48
5	10	2.76	1.61	-0.77	1.53	-0.59	0.54
A3.1f Generation 16 (last one)							
16	1	0.06	0.35	4.94	0.78	-0.15	0.12
16	2	0.28	0.95	3.57	0.92	-0.21	0.16
16	3	0.20	0.92	3.25	0.87	-0.19	0.16
16	4	0.20	0.23	3.11	0.87	-0.19	0.20
16	5	0.01	1.05	2.87	0.74	-0.14	0.22
16	6	0.30	1.27	2.10	0.93	-0.21	0.23
16	7	0.47	0.04	2.91	1.01	-0.26	0.23
16	8	0.35	1.50	4.04	0.96	-0.23	0.25
16	9	0.45	1.67	1.20	1.00	-0.25	0.30
16	10	0.45	2.05	1.02	1.00	-0.25	0.30

A3.3 HGA using binary representation

A flowchart for the simulation of PRTF model using the HGA and binary numbers is presented in figure (A3.2).

Here again one event from Bird Creek catchment is selected to examine the capability of HGA in the identification of a PRTF model using a given rainfall hyetograph and its related hydrograph. Details of the procedures are listed as following for a few selected generations.

In the current example, the population contains 20 chromosomes and the algorithm has been run without interview for 500 generations. Here again a 2×1 order PRTF model is used. Since the length of each gene selected is 12, and three variables- one for time to peak and two for the B parameters- has to determined, each chromosome contains 36 bits.

For the first generation a population containing 20 chromosomes was randomly generated as shown in table (A3.2a). The population of chromosomes are numbered from 1 to 20 for the 20 individuals. It should be noted that since the 0's and 1's are selected randomly, there is no special pattern in the initial generation. For each member of the population in addition to the binary representation of chromosome, equivalent encoded of chromosome is also presented. Therefore the first column of real numbers is time to peak, the second and third are related to B_i parameters, the fourth and fifth are allocated to the related A_i parameters, and the last column defines the fitness. It can be seen that member 20 is the best member of this generation and using the elitism mechanism is included to the second generation as well. To produce remaining members of the second generation, first using the roulette wheel two members of previous generation are selected then multiple crossover and random mutation is applied to them if the probability test is passed. Finally the two modified members are included in the second generation. This procedure is continued until all 20 members are obtained. The fitness of each member of the second generation is calculated and the best member (1) passes into the third generation. It should be noted that once two individuals are selected there is 80% probability for each gene (variable) of chromosome that a crossover will take place. However there is only 5% probability that each variable will be randomly mutated. The second generation is presented in table (A3.2b). The best member of third generation which (16) is included to the fourth generation.

A similar procedure is applied to generations 4-500. It is worth noting that as the procedure progresses, the average of the fitness factors falls although due to the random

mutation, some diversity is fed on to the following generations. This sometimes causes the fitness factor to be worse than that of previous generations. The members of third, fourth and fifth generation are presented in table (A3.2c), (A3.2d), and (A3.2e) respectively. Finally, the members of last generation-generation 500 is shown in table (A3.2f).

Figure (A3.2) Flowchart for HGA in simulation of PRTF model using binary numbers

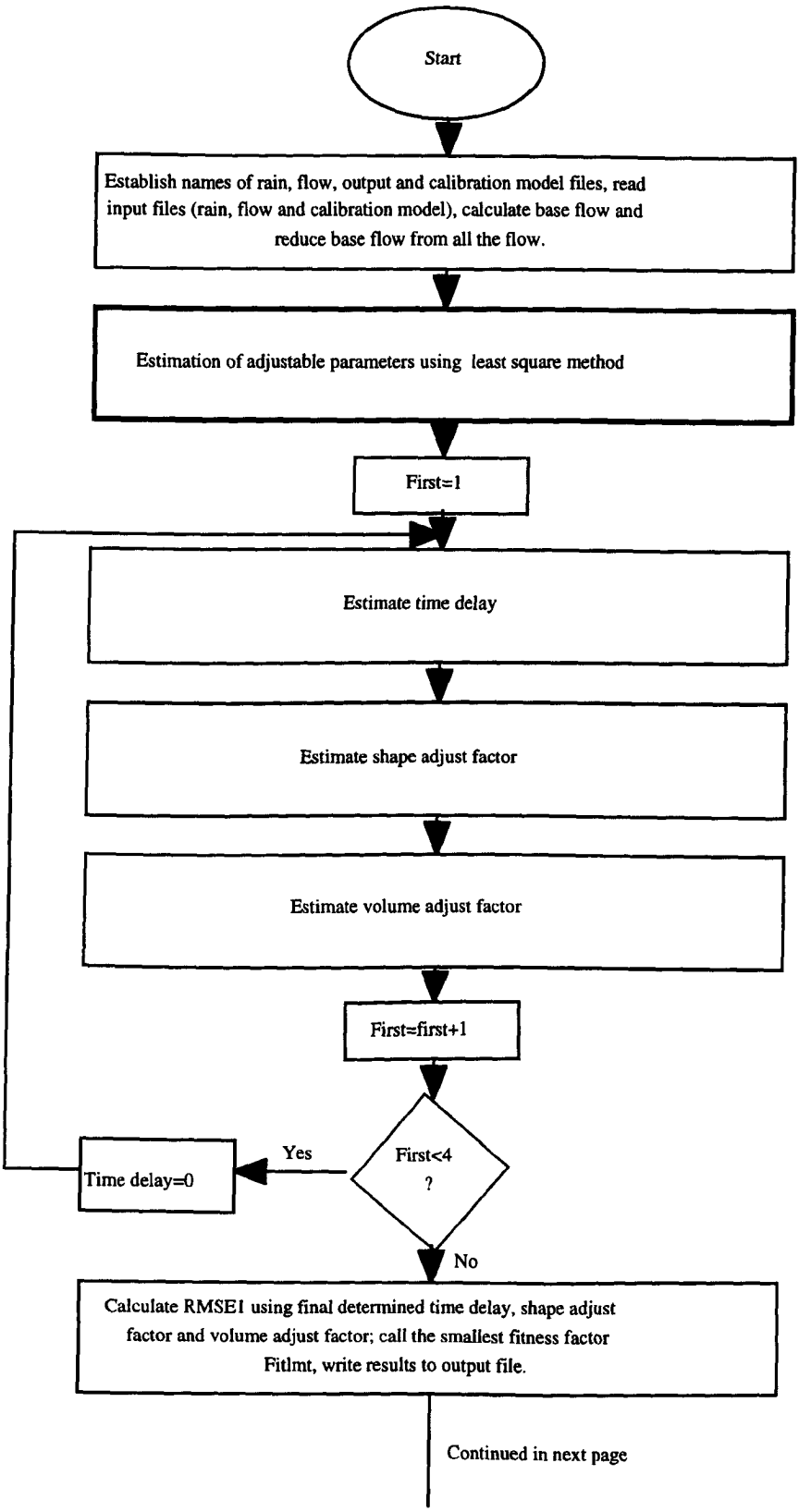

Figure (A3.2) Continued

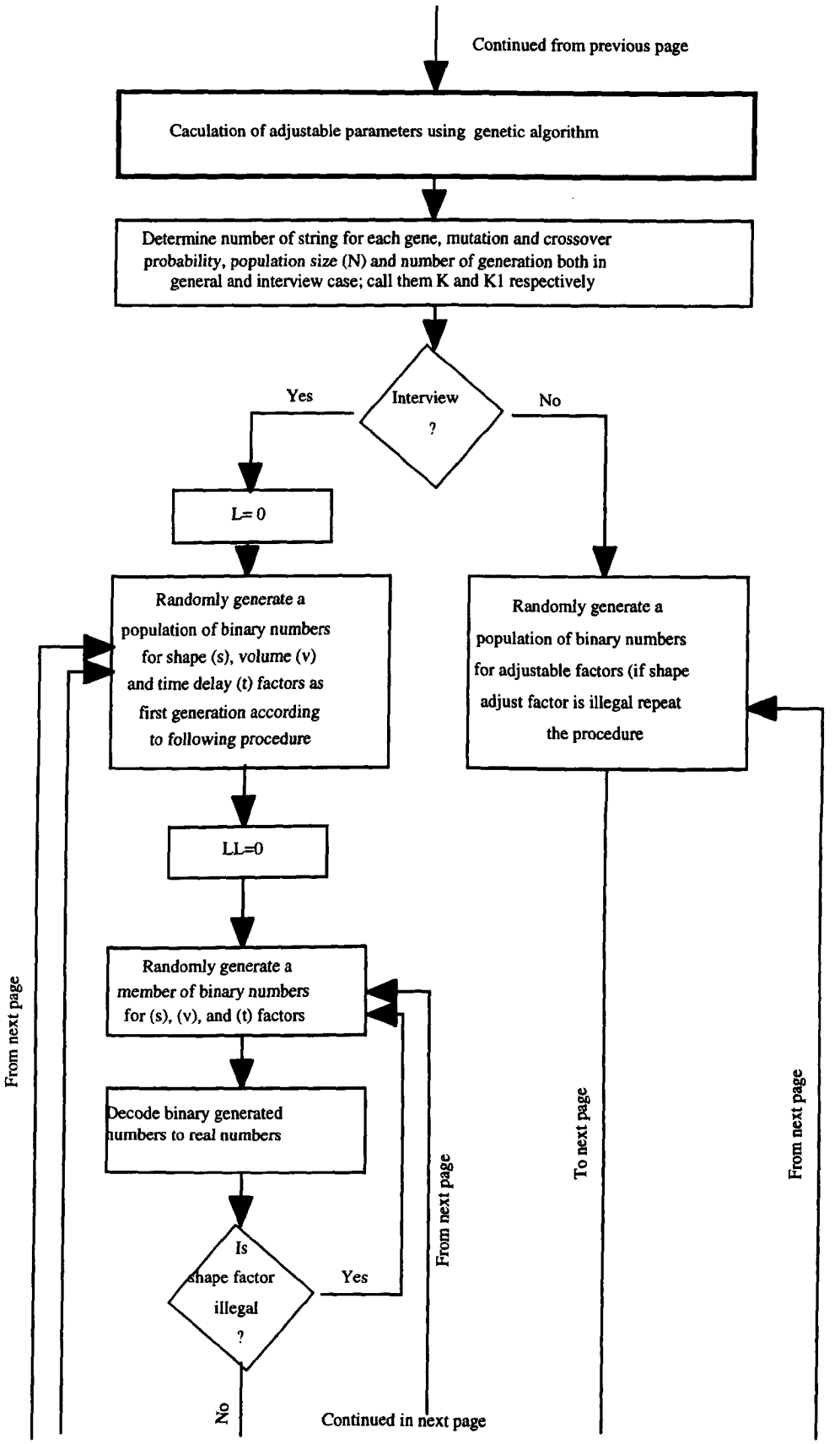

Figure (A3.2) Continued

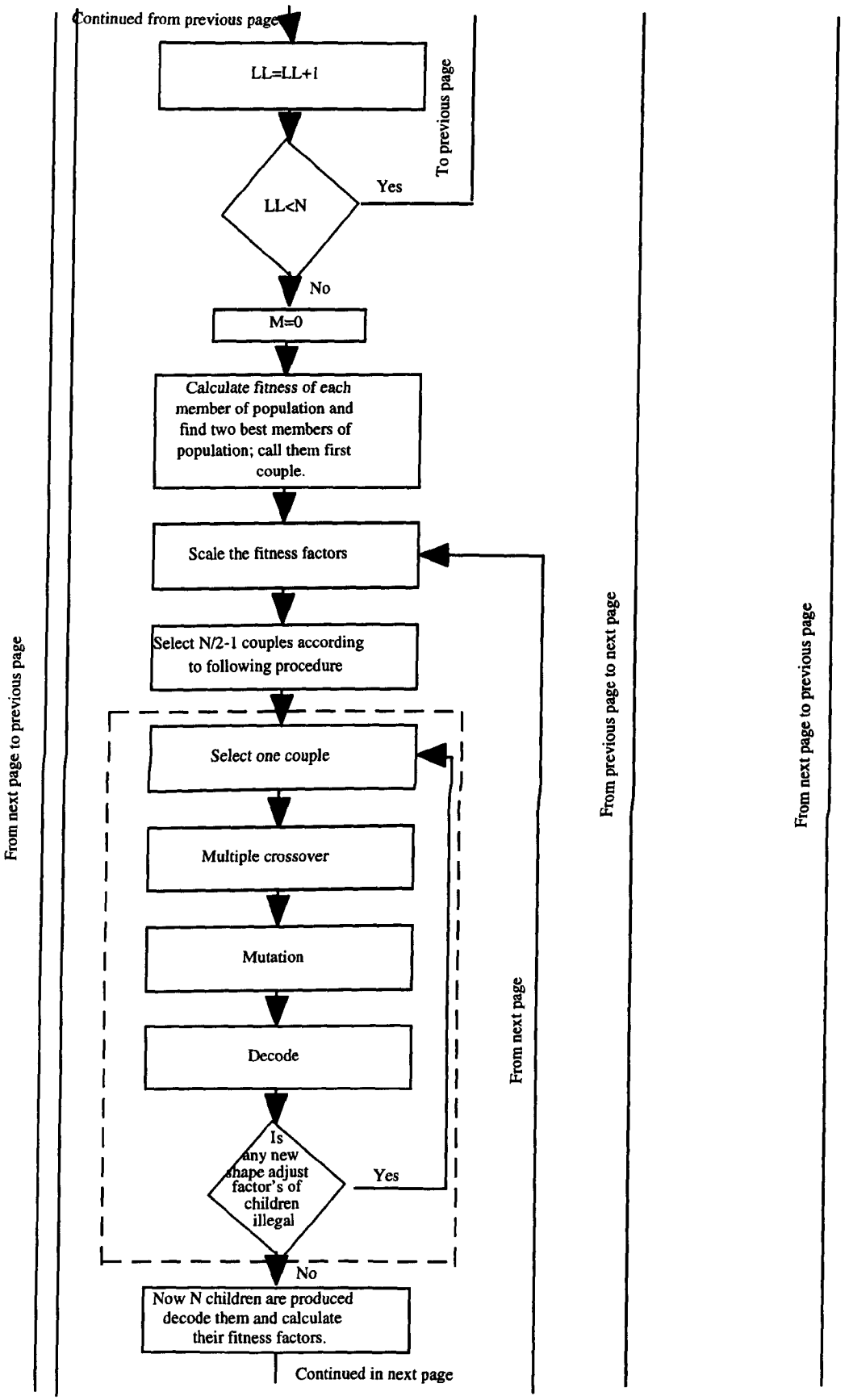

Figure (A3.2) Continued

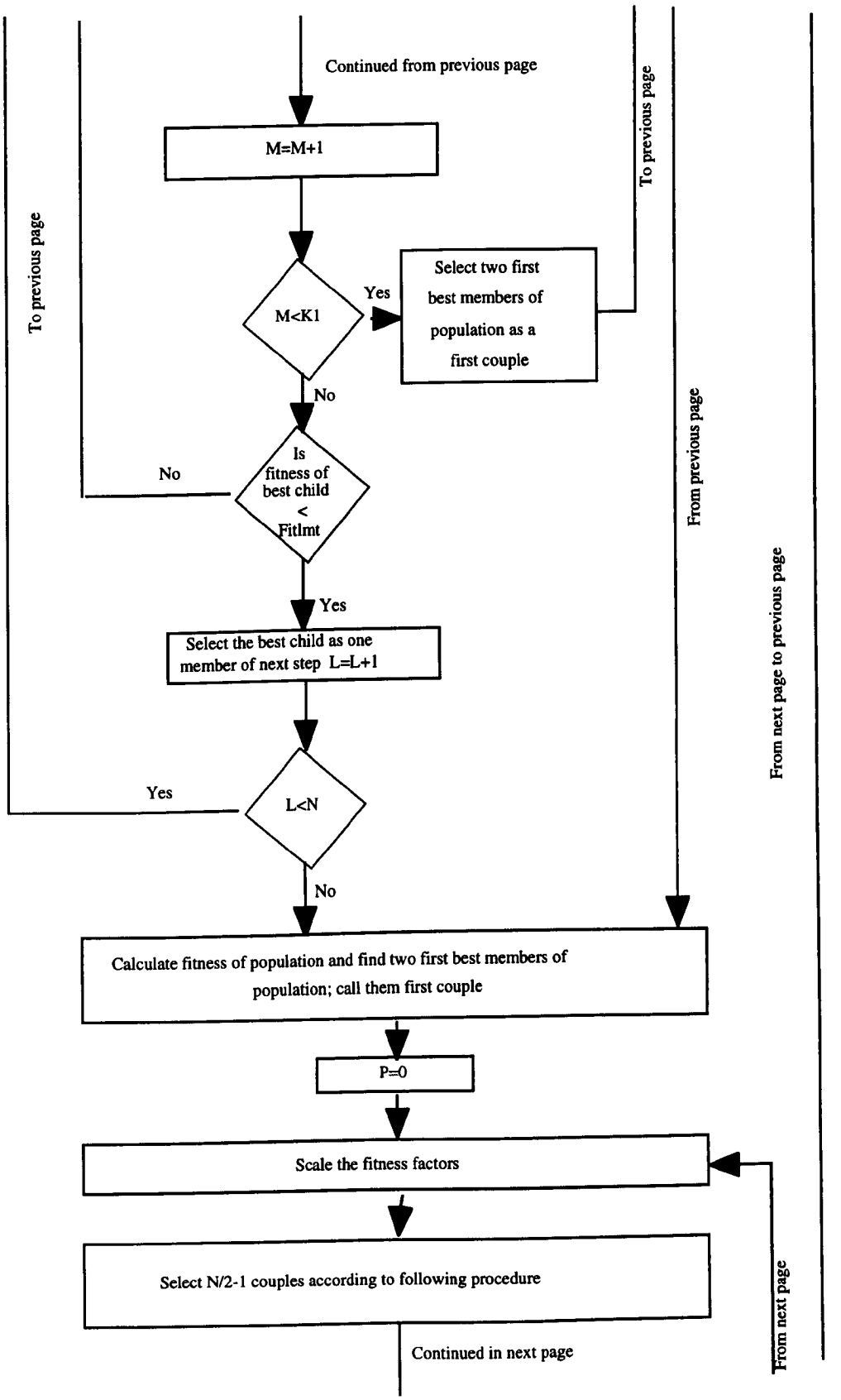

Figure (A3.2) Continued

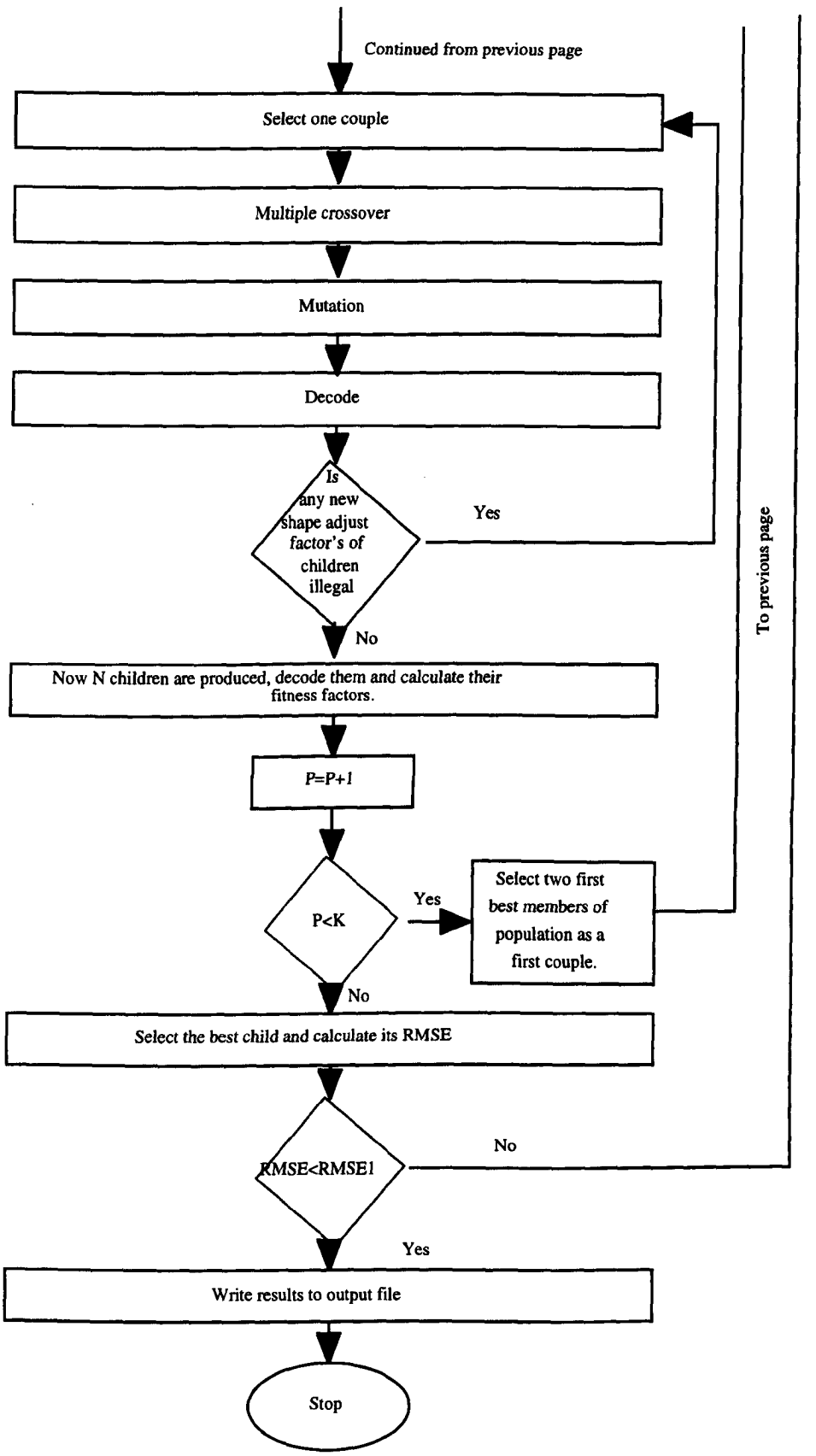

Table (A3.2) List of population evolution in some selected generation (HGA identification of PRTF model using binary numbers) Bird Creek catchment.

Generation	Member	Chromosome	Time to peak	B parameter		A parameter		Fitness Factor
A3.2a generation 1								
1	1	00010010000011101000000100000000000	1.73	4.53	-1.22	1.39	-0.48	1.19
1	2	00001001000110101101101110001010010	1.39	2.25	4.21	1.32	-0.43	3.37
1	3	11101000110110010001010001000011101	10.13	1.14	1.43	1.83	-0.84	11.46
1	4	01011100000111101011111101011111 0001	4.63	4.68	2.49	1.67	-0.70	38.20
1	5	01111100011110010010111111100110100	5.89	1.21	8.28	1.73	-0.75	89.05
1	6	10110001011111001011101000110100 1011	7.96	3.42	0.83	1.79	-0.80	27.35
1	7	11011010110011101000000011110100 0100	9.58	4.53	8.32	1.82	-0.83	297.28
1	8	11100111010111101111111001101000 0110	10.07	4.84	2.85	1.83	-0.83	115.99
1	9	01001101000110000000010110111011101	4.04	0.48	6.19	1.64	-0.67	24.87
1	10	11000101011110110100000101101010 0110	8.75	2.50	2.93	1.80	-0.81	47.25
1	11	00101111111011001000000100000101101	2.90	3.28	3.89	1.55	-0.60	17.15
1	12	00100001000011000111011110101 1100110	2.32	3.26	5.59	1.48	-0.55	18.21
1	13	01001001001011011000010010100 1101001	3.89	3.92	5.28	1.63	-0.66	47.84
1	14	10011101111110101110101010000 0100100	7.20	2.29	3.87	1.77	-0.78	48.37
1	15	11111100000111010101010000 1101101111	10.88	3.80	0.92	1.84	-0.85	47.30
1	16	00001101010011100001101101001 0010110	1.55	4.28	1.64	1.35	-0.46	3.41
1	17	01010101100001111111000011110 0101000	4.37	0.43	8.25	1.66	-0.69	48.66
1	18	00101111000101111110011011110 0101101	2.87	0.40	8.26	1.54	-0.60	24.97
1	19	00101110011111000000101011101 1001010	2.85	2.99	8.02	1.54	-0.59	41.53
1	20	01111110101010000011001100011 1110101	5.98	0.59	0.00	1.73	-0.75	0.76

Table (A3.2) Continued

Generation	Member	Chromosome	Time to peak	B parameter		A parameter		Fitness Factor
A3.2 b generation 2								
2	1	01111110101010000011001100011111 10101	5.98	0.59	0.00	1.73	-0.75	0.76
2	2	01111110101010000011001100011111 10101	5.98	0.59	0.00	1.73	-0.75	0.76
2	3	01001100000110101011101100011111 10101	4.00	2.17	0.00	1.64	-0.67	2.40
2	4	00001001000110101101111110001011 0010	1.39	2.26	4.21	1.32	-0.43	3.39
2	5	00011001000110101111101110110100 1011	2.01	2.33	5.84	1.43	-0.51	11.75
2	6	10110001011111001011010000010110010	7.96	3.42	-0.79	1.79	-0.80	10.88
2	7	01101001000110010010111011010110010	5.14	1.20	7.96	1.70	-0.72	69.21
2	8	00011100011111001101101111010 0110100	2.14	3.50	7.03	1.45	-0.53	23.22
2	9	01111100000110010010111111010111 10001	5.88	1.21	7.49	1.73	-0.75	74.29
2	10	01011100011111101011111101110 0110100	4.64	4.68	3.28	1.68	-0.70	47.42
2	11	01111100011111101100000100110 0110100	5.89	4.69	0.78	1.73	-0.75	31.69
2	12	00010010000010010010111111000000000	1.73	1.21	6.28	1.39	-0.48	7.39
2	13	10110001011110010001010001100011 1101	7.96	1.14	2.68	1.79	-0.80	19.77
2	14	11101000110111001001101000110100 1011	10.13	3.34	0.83	1.83	-0.84	34.18
2	15	11101000110110010001010001000011 1101	10.13	1.14	1.43	1.83	-0.84	11.46
2	16	01101100110110010001010001000011 1101	5.28	1.14	1.43	1.71	-0.73	5.12
2	17	00001001000111101101101110001011 0010	1.39	4.75	4.21	1.32	-0.43	7.47
2	18	00001001000110101101101110001011 0010	1.39	2.25	4.21	1.32	-0.43	3.37
2	19	10100001000111001011001100101011 0010	7.32	3.41	0.46	1.77	-0.79	20.44
2	20	00001001011110101101101010010100 1011	1.40	2.25	4.59	1.32	-0.43	3.95

Table (A3.2) Continued

Generation	Member	Chromosome	Time to peak	B parameter		A parameter		Fitness Factor
A3.2c generation 3								
3	1	01111110101010000011001100011111 10101	5.98	0.59	0.00	1.73	-0.75	0.76
3	2	01111110101010000011001100011111 10101	5.98	0.59	0.00	1.73	-0.75	0.76
3	3	01111110101010000011001110011111 10101	5.98	0.59	5.00	1.73	-0.75	30.08
3	4	01111110101010100011001100011111 10101	5.98	1.84	0.00	1.73	-0.75	3.30
3	5	01111100100010000011001100011111 10101	5.90	0.59	0.00	1.73	-0.75	0.76
3	6	01111111101110000011001100011111 10101	6.02	0.59	0.00	1.73	-0.75	0.76
3	7	01111110101010000011001100011111 10101	5.98	0.59	0.00	1.73	-0.75	0.76
3	8	01111110101010000011001100011111 10101	5.98	0.59	0.00	1.73	-0.75	0.76
3	9	01111110101010000011001110011111 10101	5.98	0.59	5.00	1.73	-0.75	30.08
3	10	01111110111010000011001100011111 10101	5.99	0.59	0.00	1.73	-0.75	0.76
3	11	01111110101010000011001100011111 10101	5.98	0.59	0.00	1.73	-0.75	0.76
3	12	01111110101010000011001100011111 10101	5.98	0.59	0.00	1.73	-0.75	0.76
3	13	01111010101010011011100100101111 1101	5.82	1.54	0.64	1.73	-0.75	4.37
3	14	01111110101010000011001100011111 10101	5.98	0.59	0.00	1.73	-0.75	0.76
3	15	01111110100010000011001100011111 10101	5.97	0.59	0.00	1.73	-0.75	0.76
3	16	00011110101010000011001100011111 10101	2.23	0.59	0.00	1.47	-0.54	0.63
3	17	01110110101010000011001100011111 10101	5.67	0.59	0.00	1.72	-0.74	0.74
3	18	01111110101010000011001100011111 10101	5.98	0.59	0.00	1.73	-0.75	0.76
3	19	01111110101010000011001100011011 10101	5.98	0.59	-0.16	1.73	-0.75	0.70
3	20	01111110101010000011001100011111 10101	5.98	0.59	0.00	1.73	-0.75	0.76

Table (A3.2) Continued

Generation	Member	Chromosome	Time to peak	B parameter		A parameter		Fitness Factor
A3.2d generation 4								
4	1	00011110101010000011001100011111 10101	2.23	0.59	0.00	1.47	-0.54	0.63
4	2	01111110101010000011001100011011 0101	5.98	0.59	-0.16	1.73	-0.75	0.70
4	3	01111110101010000011001100011111 0101	5.98	0.59	0.00	1.73	-0.75	0.76
4	4	01111110101010000011001101011111 0101	5.98	0.59	2.50	1.73	-0.75	8.76
4	5	01111110101010000011001100011111 0101	5.98	0.59	0.00	1.73	-0.75	0.76
4	6	11111110101010000011001100011111 0101	10.98	0.59	0.00	1.84	-0.85	1.05
4	7	01111110101010000011001100011111 0101	5.98	0.59	0.00	1.73	-0.75	0.76
4	8	01111110101010000011001100011111 0101	5.98	0.59	0.00	1.73	-0.75	0.76
4	9	00111110101010000011001110011111 0101	3.48	0.59	5.00	1.60	-0.64	13.41
4	10	01111110101010000011001100011111 0101	5.98	0.59	0.00	1.73	-0.75	0.76
4	11	01101011101010000011001100011111 0101	5.24	0.59	0.00	1.70	-0.73	0.72
4	12	01111110101010000011001100011111 0101	5.98	0.59	0.00	1.73	-0.75	0.76
4	13	01111110101010000011011101011111 0101	5.98	0.60	2.50	1.73	-0.75	8.82
4	14	01111110101011000011000100011111 0101	5.98	3.09	0.00	1.73	-0.75	9.78
4	15	01111011101010010011001100011111 0111	5.86	1.22	0.00	1.73	-0.75	1.50
4	16	01110110101010000011001100011111 0101	5.67	0.59	0.00	1.72	-0.74	0.74
4	17	01111110101011000011001100011111 0101	5.98	3.09	0.00	1.73	-0.75	9.82
4	18	01111110101010010011001100011111 0101	5.98	1.22	0.00	1.73	-0.75	1.53
4	19	01111110101010000011001100011111 0101	5.98	0.59	0.00	1.73	-0.75	0.76
4	20	01111110101010000011001100011111 0101	5.98	0.59	0.00	1.73	-0.75	0.76

Table (A3.2) Continued

Generation	Member	Chromosome	Time to peak	B parameter		A parameter		Fitness Factor
A3.2e generation 5								
5	1	00011110101010000011001100011111 10101	2.23	0.59	0.00	1.47	-0.54	0.63
5	2	01111110101010000011001100011011 0101	5.98	0.59	-0.16	1.73	-0.75	0.70
5	3	00111110101010000011001100011111 0101	3.48	0.59	0.00	1.60	-0.64	0.64
5	4	00011110101010100011001100011111 0101	2.23	1.84	0.00	1.47	-0.54	0.65
5	5	00011110101010000010001100011111 0101	2.23	0.55	0.00	1.47	-0.54	0.65
5	6	00011110101010000011001101011111 0101	2.23	0.59	2.50	1.47	-0.54	1.64
5	7	00011110001010000011001110011111 0101	2.21	0.59	5.00	1.46	-0.54	5.96
5	8	10011110101010000011001100011111 0101	7.23	0.59	0.00	1.77	-0.78	0.84
5	9	10010110101010000011001100011111 0101	6.92	0.59	0.00	1.76	-0.78	0.82
5	10	00011110100010000011001110111110 0101	2.22	0.59	6.21	1.47	-0.54	9.39
5	11	00011110101010000011001100011111 0101	2.23	0.59	0.00	1.47	-0.54	0.63
5	12	00111110100010000011001100011111 0101	3.47	0.59	0.00	1.60	-0.64	0.64
5	13	00011110101010000011001100011111 0101	2.23	0.59	0.00	1.47	-0.54	0.63
5	14	00111110101010000011001101011111 0111	3.48	0.59	2.51	1.60	-0.64	3.78
5	15	00011110101010000011001100011111 0101	2.23	0.59	0.00	1.47	-0.54	0.63
5	16	00011110101010000011001100011111 0101	2.23	0.59	0.00	1.47	-0.54	0.63
5	17	00011110101010000011001100011111 0101	2.23	0.59	0.00	1.47	-0.54	0.63
5	18	00011110101010000111001100011111 0101	2.23	0.75	0.00	1.47	-0.54	0.58
5	19	00111110101010000111001100011111 0101	3.48	0.75	0.00	1.60	-0.64	0.63
5	20	10111110101010001011001100011111 0101	8.48	0.90	0.00	1.80	-0.81	1.44

Table (A3.2) Continued

Generation	Member	Chromosome	Time to peak	B parameter		A parameter		Fitness Factor
A3.2f generation 500								
500	1	000000000000100011111111001111111111	1.03	1.09	1.27	1.22	-0.37	0.36
500	2	000000000000100011111111001111111111	1.03	1.09	1.27	1.22	-0.37	0.36
500	3	000001000000100011111111001110111111	1.19	1.09	1.12	1.27	-0.40	0.40
500	4	000000000000100011111111001010011111	1.03	1.09	0.41	1.22	-0.37	0.44
500	5	000000000000100011011111001111111111	1.03	1.01	1.27	1.22	-0.37	0.36
500	6	000000000000100011111111001111111111	1.03	1.09	1.27	1.22	-0.37	0.36
500	7	000000000000100011111111001111111111	1.03	1.09	1.27	1.22	-0.37	0.36
500	8	000000000000100011111111001111111111	1.03	1.09	1.27	1.22	-0.37	0.36
500	9	000000000000100011111111001111110111	1.03	1.09	1.25	1.22	-0.37	0.36
500	10	000000010000100011111111001111111111	1.07	1.09	1.27	1.23	-0.38	0.36
500	11	000100000000100011111111001111111111	1.66	1.09	1.27	1.37	-0.47	0.59
500	12	001000110000100011111111001111111111	2.40	1.09	1.27	1.49	-0.56	1.10
500	13	000000000000100011101111001111111111	1.03	1.05	1.27	1.22	-0.37	0.36
500	14	000000000000100011111111001111101011	1.03	1.09	1.23	1.22	-0.37	0.36
500	15	000000000000101011111111001111111111	1.03	2.34	1.27	1.22	-0.37	0.50
500	16	000000000000100011111111001111111111	1.03	1.09	1.27	1.22	-0.37	0.36
500	17	000000000000100011111111001110111101	1.03	1.09	1.11	1.22	-0.37	0.36
500	18	000000000000100001111111001111011111	1.03	0.78	1.20	1.22	-0.37	0.38
500	19	000000000000100011111111001111111111	1.03	1.09	1.27	1.22	-0.37	0.36
500	20	000000000000100011111111001111111111	1.03	1.09	1.27	1.22	-0.37	0.36